

**HYBRID INORGANIC-ORGANIC MATERIALS AND
NANOCOMPOSITES;
SYNTHESIS, CHARACTERIZATIONS AND CATALYTIC
APPLICATIONS
IN ORGANIC TRANSFORMATIONS**

THESIS
SUBMITTED FOR THE DEGREE OF

DOCTOR OF PHILOSOPHY
IN CHEMISTRY

TO THE
UNIVERSITY OF PUNE

BY

Research Student
Ankur Bordoloi

Research guide
Dr. S. B. Halligudi

INORGANIC CHEMISTRY AND CATALYSIS DIVISION

NATIONAL CHEMICAL LABORATORY
PUNE - 411 008, INDIA

June-2008



राष्ट्रीय रासायनिक प्रयोगशाला
(वैज्ञानिक तथा औद्योगिक अनुसंधान परिषद)
डॉ. होमी भाभा मार्ग पुणे - 411 008. भारत
NATIONAL CHEMICAL LABORATORY



(Council of Scientific & Industrial Research)
Dr. Homi Bhabha Road, Pune - 411 008. India.

CERTIFICATE

Certified that the work incorporated in the thesis entitled **“Hybrid inorganic-organic materials and nanocomposites; synthesis, characterizations and catalytic applications in organic transformations”** submitted by **Mr. Ankur Bordoloi**, for the Degree of **Doctor of Philosophy**, in **Chemistry** was carried out by the candidate under my supervision in the Inorganic Chemistry and Catalysis Division, National Chemical Laboratory, Pune - 411008, India. Materials obtained from other sources have been duly acknowledged in the thesis.

Dr. S. B. Halligudi

(Research Supervisor)

Communication
Channels

NCL Level DID : 2590
NCL Board No. : +91-20-25902000
EPABX : +91-20-25893300
+91-20-25893400



FAX

Director's Office : +91-20-25893355
COA's Office : +91-20-25893619
COS&P's Office : +91-20-25893008

WEBSITE

www.ncl-india.org

Candidate's Declaration

I hereby declare that the thesis entitled “*Hybrid inorganic-organic materials and nanocomposites; synthesis, characterizations and catalytic applications in organic transformations*” submitted by me for the degree of *Doctor of Philosophy* in *Chemistry* to the *University of Pune* is the record of work carried out by me during the period of September, 2005 to June, 2008 and has not been submitted by me for a degree to any other University or Institution. This work was carried out at Inorganic Chemistry and Catalysis Division, National Chemical Laboratory, Pune, India. Any inadvertent omissions that might have occurred due to oversight or error in judgment are regretted.

Ankur Bordoloi

June 2008
Inorganic chemistry and Catalysis Division
National Chemical Laboratory
Pune 411008, Maharashtra
India

In the hands of...

Luku mahi,

My Parents

& My Teachers



ACKNOWLEDGEMENT

It is my great pleasure to express my heartfelt gratitude to my research supervisor, Dr. S. B. Halligudi, for his unending support and invaluable guidance throughout the period of this investigation. I sincerely thank for the care and affection that I received from him and his family in the entire period.

I would like to express my profound gratitude to former Head of catalysis division, Dr. Rajiv Kumar, for providing the facilities required for my work. I would like to take the opportunity to thank Prof. F. Lefebvre for his help in NMR spectroscopy.

It gives me a great pleasure to express my deep sense of gratitude and indebtedness to Dr. Anil Kumar, Dr. Rane, Dr. Pardhy, Dr. Deshpande, Dr. Shubhangi, Dr. Singh, Dr. Dongare, Dr. Srinivas, Dr. Satyanarayana, Dr. Mirajkar, Dr. Gopinath, Dr. Joshi, Dr. Bellhekar, Dr. Selvaraj, Ms. Violet, Dr. Jacob, Dr. Nandini, Dr. Guruswami, Dr. Kalaraj, Mr. Jha, Mr. Niphadkar, Mr. Tejas, Mr. Purushothaman, Mr. Dipak, Mr. Golap, Mr. Gaikwad, Mr. Madhu, Mr. Kashinathan, Mr. Punekar and all the other scientific and non-scientific staff of NCL for their help and inspiring guidance and suggestions in carrying out the research work.

I sincerely thank my labmates Dr. Biju, Dr. Tresa, Dr. Dhanashri, Dr. Ganapati, Suman, Nevin, Suresh, Josena, Nishita, Nilesh, Amol and Palraj for their friendly help and kind cooperation during the period of my work. I also thank all my friends in the division and in NCL especially Rohit, Shraeddha, Manu, Ramakant, Atul, Lakshi, Devu, Ganesh, Sachin, Ankush, Maitri, Pallaivi, Selva, Surendran, Nagarajan, Shivram, Prashant, Sanker, Thiru, Debasish, Pranjal (both), Manas, Diganta, Sofia, Khirud, Gitali and many others for their cooperation, encouragement, invaluable help and moral support in one way or other, which made my work much easier.

I would like to thank my friends Rahul, Ujjal, Bishwa, Rupam, Santu, Shekhar, Dhiraj, Nayan Upendra, Gunin, Bishnu and Devajeet for their encouragements, love and never failing supports during my many years of studies.

I take this occasion to thank all my teachers, well-wishers, classmates & friends in various stages for their love, encouragement and kind cooperation that I received from them whose names are not mentioned here.

The words are not enough to express all my love and thankfulness towards Luku mahi, my sister, my parents and all my beloved family members for their blessings that I could reach here.

Finally, my thanks are due to Dr. S. Sivaram, Director, NCL for allowing me to carry out the research work at NCL and CSIR, New Delhi, India, for the financial support in the form of research fellowship.

(Ankur Bordoloi)



Maya blue
The first inorganic -organic
hybrid

*Never regard study as a duty, but as the enviable
opportunity to learn to know the liberating
influence of beauty in the realm of the spirit for
your own personal joy and to the profit of the
community to which your later work belongs.*

Albert Einstein

1.5.4.	Polymerization of metal containing monomer	11
1.6.	Polyoxometalates	11
1.6.1.	Heteropoly acids	11
1.6.2.	Structure of heteropoly compounds in the solid state	12
1.6.2.1	Primary structure	12
1.6.2.2	Secondary structure	13
1.6.2.3	Proton structure	13
1.6.2.4	Tertiary structure	14
1.6.3.	Synthesis	15
1.6.4.	Heterogeneous catalysis	16
1.6.5.	Transition metal substituted polyoxometalates (TMSP)	16
1.7.	Schiff base complex	18
1.8.	Mesoporous materials	19
1.8.1.	Synthesis and mechanism of formation	22
1.8.2.	Liquid Crystal Templating (LCT) Mechanism	22
1.8.3.	Generalized Liquid Crystal Templating Mechanism	23
1.8.4.	Mechanism of formation of SBA-15 molecular sieves	23
1.8.5.	Surface modification of mesoporous silica	24
1.8.5.1.	Grafting methods	25
1.8.5.1.	Co-condensation methods	26
1.8.6.	Periodic mesoporous organosilicas (PMO)	27
1.8.7.	Mesoporous Carbon	28
1.9.	Supported ionic liquid	30
1.10.	Inorganic-organic hybrid material and catalysis	31
1.11.	Mesoporous materials for preparation of inorganic-organic hybrid materials	33
1.12.	Immobilization approach	34
1.12.1.	Adsorption	34
1.12.2.	Covalent tethering	34
1.12.3.	Ion exchange (electrostatic interaction)	37
1.12.4	Entrapment/ ship in bottle	37

1.13.	References	38
2.	Physicochemical characterization	42
2.1.	X-ray diffraction	42
2.2.	Inductively coupled plasma -AES	43
2.3.	Energy dispersive X-ray spectroscopy	44
2.4.	Diffuse reflectance UV-vis spectroscopy	44
2.5.	Fourier transform infrared spectroscopy	45
2.6.	FT-Raman spectroscopy	46
2.7.	Cross-polarization magic angle spinning NMR spectroscopy	46
2.8.	Electron paramagnetic resonance spectroscopy	47
2.9.	X-ray photoelectron spectroscopy	48
2.10.	Scanning electron microscopy	49
2.11.	Transmission electron microscopy	50
2.12.	Atomic force microscope	50
2.13.	Porosity measurements by N ₂ sorption	51
2.14.	Temperature programmed reduction (TPR) and oxidation (TPO)	52
2.15.	Thermal analyses	53
2.16.	References	53
3.	Inorganic-organic hybrid materials based on polyoxometalates	
3.1.1.	Selective oxidation of anthracene using inorganic- organic hybrid materials based on Molybdovanadophosphoric acids	56
3.1.1.1.	Introduction	56
3.1.1.2.	Experimental	57
3.1.1.2.1.	Chemicals	57
3.1.1.2.2.	Catalysts preparation	57
3.1.1.3.	Results and Discussion	62
3.1.1.3.1.	Catalyst characterization	62
3.1.1.3.2.	Catalytic oxidation of anthracene by 70% aqueous TBHP	72
3.1.1.3.3.	Catalyst recycling	75
3.1.1.4.	Conclusion	77

3.1.2.	Oxyfunctionalisation of adamantane using inorganic- organic hybrid materials based on isopoly and heteropoly anions: kinetics and mechanistic study	78
3.1.2.1.	Introduction	78
3.1.2.2.	Results and Discussion	80
3.1.2.2.1.	Catalysts characterization	80
3.1.2.2.2.	Oxidation of adamantane	80
3.1.2.2.3.	Kinetic studies	82
3.1.2.2.3.a	Effect of substrate concentration	82
3.1.2.2.3.b	Effect of H ₂ O ₂ (oxidant) concentration	83
3.1.2.2.3.c	Effect of catalyst concentration	84
3.1.2.2.3.d	Effect of temperature	84
3.1.2.2.4.	Reaction mechanism and rate law	84
3.1.2.3.	Conclusion	88
3.2	Inorganic–organic hybrid materials based on functionalized silica and carbon: A comprehensive understanding toward the structural property and catalytic activity difference over mesoporous silica and carbon supports	90
3.2.1.	Introduction	90
3.2.2.	Experimental	92
3.2.2.1.	Chemicals	92
3.2.2.2.	Catalysts preparation	92
3.2.2.3.	Catalytic testing in 2-methyl naphthalene (2MN) oxidation	94
3.2.3.	Results and Discussion	95
3.2.3.1.	Catalyst characterization	95
3.2.3.2.	Catalytic oxidation of 2-methyl naphthalene by 30% aq.H ₂ O ₂	104
3.2.4.	Conclusions	107
3.3	Heteropoly acid based supported ionic liquid phase catalyst for the selective oxidation of alcohols	108
3.3.1.	Introduction	108
3.3.2.	Catalyst synthesis	109
3.3.3.	Catalyst characterization	112

	3.3.3.1.	ICP/AES analysis	112
	3.3.3.2.	Low angle XRD	112
	3.3.3.3.	Surface area	112
	3.3.3.4.	³¹ P and ⁵¹ V CP-MAS NMR	113
	3.3.3.5.	FT-IR	116
	3.3.3.6.	UV-Vis	116
	3.3.3.7.	TG-DTA	117
	3.3.4.	Catalysis	117
	3.3.4.1.	Typical procedure for the oxidation	117
	3.3.5.	Conclusion	120
	3.4.	References	121
4.	Coordination polymers		
4.1.	Organotin-oxometalate coordination polymer catalysed oxyfunctionalisation of monoterpenes		130
	4.1.1.	Introduction	130
	4.1.2.	Experimental	131
	4.1.2.1.	Materials	131
	4.1.2.2.	Catalyst preparation	131
	4.1.3.3.	Catalytic activity measurements	132
	4.1.3.	Results and discussion	132
	4.1.3.1.	Characterization	132
	4.1.3.2.	Catalytic activity	136
	4.1.3.3.	Spectral characteristics of the oxidation products of limonene	137
	4.1.3.4.	The performance of [(nBu ₃ Sn) ₂ MoO ₄] catalyst in the oxidation of monoterpenes	138
	4.1.3.5.	Effect of reaction parameters	141
	4.1.3.6.	Catalyst recycling and leaching	141
	4.1.4.	Conclusions	142
4.2.	Tungsten and molybdenum based coordination polymers catalyzed N-oxidation of primary aromatic amines with aqueous hydrogen peroxide		143

4.2.1.	Introduction	143
4.2.2.	Catalytic activity measurement	144
4.2.3.	Results and Discussion	145
4.2.4.	Conclusion	147
4.3.	Refernces	148
5.	Inorganic-organic hybrid mterials based on metal complexes	
5.1.	Immobilized CobpbH₂Cl₂2H₂O complex as heterogeneous catalyst for epoxides ring opening by amines under ambient conditions	151
5.1.1.	Introduction	151
5.1.2.	Experimental section	152
5.1.2.1.	Materials	152
5.1.2.2.	Catalysts preparation	152
5.1.2.3.	Typical procedure for epoxide ring opening	154
5.1.3.	Results and discussion	155
5.1.3.1.	Catalyst characterization	155
5.1.3.2.	Catalytic epoxide ring opening studies	159
5.1.3.3.	Catalyst stability and recyclability	160
5.1.4.	Conclusions	162
5.2.	[Ru (salen) (NO)] complex encapsulated in mesoporous SBA-16 as catalyst for hydrogenation of ketones to alcohols	163
5.2.1.	Introduction	163
5.2.2.	Experimental	164
5.2.2.1	Chemicals	164
5.2.2.2	Catalyst preparation	164
5.2.2.3.	Catalytic experiments	166
5.2.3.	Results and discussion	167
5.2.4.	Conclusions	172
5.3.	References	173
6.	Nanocomposites	
6.	Studies in structural characterization and correlation with the catalytic activity of an efficient and stable WO_x/SBA-15 nanocomposite catalyst	177
6.1.	Introduction	177

6.2.	Experimental section	178
6.2.1.	Materials	178
6.2.2.	Catalyst preparation	178
6.2.3.	Typical procedure for oxidation sulfides to sulfoxides	179
6.3.	Results and discussion	180
6.3.1.	Catalyst characterization	180
6.3.2.	Catalytic oxidation of sulfides	189
6.3.3.	Catalytic stability and recyclability	192
6.4.	Conclusions	194
6.5.	References	195
7.	Summary and Conclusions	198
7.1.	Summary	198
7.2.	Conclusions	201
7.3.	Future directions of inorganic-organic hybrid materials	203

ABBREVIATIONS

AFM	Atomic force microscopy
AN	Anthracene
AQ	Anthraquinone
BET	Brunauer-Emmett-Teller
BJH	Barret–Joyner–Halenda
CP	Cross polarization
CTAB	Cetyltrimethylammonim bromide
EDAX	Energy dispersive X-ray spectroscopy
EPR	Electron paramagnetic spectroscopy
F123	Poly-(ethylene oxide)-poly(propylene oxide)- poly(ethylene oxide) EO20PO70EO20
F127	Poly-(ethylene oxide)-poly(propylene oxide)- poly(ethylene oxide) EO106PO70EO106
FID	Flame ionized detector
FT-IR	Fourier-transform Infrared
GC	Gas Chromatography
GCMS	Gas Chromatography-Mass Spectroscopy
HPA	Heteropoly acid
HRTEM	High resolution transmission electron microscopy
HTXRD	High temperature X-ray diffraction
ICP-AES	Induced coupled plasma – Atomic emission spectroscopy
IL	Ionic liquid
IOHM	Inorganic-organic hybrid material
LCT	Liquid crystal template
MAS	Magic angle spinning
MC	Mesoporous carbon
MCM	Mobil composition of mater

2MN	2-Methylnaphthalene
2MNQ	2-Methylnaphthaquinone
MPA	Molybdophosphoric acid
MS	Mesoporous silica
NMR	Nuclear magnetic resonance
PMO	Periodic mesoporous organosilica
POM	Polyoxometalates
RTIL	Room temperature ionic liquid
SAXS	Small angle X-ray scattering
SBA	Santa Barbara Amorphous
SEM	Scanning electron microscopy
SILP	Supported ionic liquid phase
STA	Silicotungstic acid
TBHP	<i>tert</i>- Butyl hydrogen peroxide
TCD	Thermal conductivity detector
TEM	Transmission electron microscopy
TEOS	Tetraethyl orthosilicate
TG-DTA	Thermogravimetry-Differential thermal analysis
TLC	Thin layer chromatography
TMSP	Transition metal substituted heteropoly acid
TOF	Turn over frequency
TPA	Tungstophosphoric acid
TPD	Temperature programmed desorption
TPR/O	Temperature programmed reduction/oxidations
UHP	Urea hydrogen peroxide
UV-Vis	Ultra violet-visible
XPS	X-ray photoelectron spectroscopy
XRD	X-ray diffraction

Research Student	Ankur Bordoloi
Research Guide	Dr. S. B. Halligudi
Title of the thesis	<i>Hybrid inorganic-organic materials and nanocomposites; synthesis, characterizations and catalytic applications in organic transformations</i>
Registration No.	EI/191/Ph.D/2006
Date of Registration	23/09/2005
Place of work	Inorganic Chemistry and Catalysis Division, National Chemical Laboratory, Pune 411 008

Scope of the thesis

In the present work, oxidation of monoterpenes, aromatic hydrocarbons, alkane, sulfides, alcohols, amines, ring opening of epoxides and hydrogenation of ketones using heterogeneous catalysts including inorganic organic hybrid materials based on heteropoly acids and metal complexes, coordination polymers and nanocomposites has been carried out. The structural properties of the catalysts were correlated with the observed catalytic activities, wherever possible.

The following objectives were taken into consideration:

1. Preparation of inorganic organic hybrid materials based on Heteropoly acids and metal complexes, Coordination polymers and nanocomposites adopting various synthesis techniques.
2. Characterization of these catalyst systems by different techniques like elemental analysis, N₂-sorption, XRD, FT-IR, Raman, UV-vis, TEM, SEM, MAS NMR, Thermogravimetric analysis and EPR.
3. Evaluation of the above mentioned materials in different selective and controlled oxidation processes, and assessment of advantages of these catalyst systems over conventional catalyst systems with respect to substrate conversions products

selectivity, stability and reusability.

4. Correlation of the structural properties of the catalyst with the activities and product selectivity in the oxidation reaction under studies and their kinetics and mechanism studies.

Outline of the thesis

The thesis has been divided into seven chapters

CHAPTER I

Chapter I give a brief introduction of inorganic organic hybrid materials and their importance. It also gives an introduction to both industrially and synthetically important various oxidative organic transformations. It further gives an introduction to the catalysts used for oxidative transformations viz. inorganic organic hybrid materials based on Heteropoly acids and metal complexes, Coordination polymers and nanocomposites. A review of the literature to date in these areas is included. Finally, the aim of the thesis is outlined briefly.

CHAPTER II

This chapter deals with all materials used for synthesis and catalyst screening. Inorganic organic hybrid materials based on heteropoly acids and metal complexes, coordination polymers and nanocomposites were characterized by different techniques such as N₂ sorption, AAS, EDAX, XRD, TEM, SEM, FT-IR, FT-Raman and MAS NMR, H₂-TPR and EPR. For each technique, its theory and experimental procedures are described briefly.

CHAPTER III

Chapter III is divided into three sections

Section A The 1st part deals with the preparation of Inorganic – organic hybrid materials by immobilization of Molybdo Vanadophosphoric acids onto Mesoporous silicas such as MCM-41, MCM-48 and SBA-15. All catalyst materials were characterized by elemental analysis, FT-IR, N₂ sorption measurements, SAXS, UV/Vis, XPS, MAS-NMR, SEM and TEM for their structural integrity and physico-chemical properties. These inorganic-

organic hybrid materials were applied for the liquid-phase oxidation of anthracene with 70% aqueous *tert*-Butylhydroperoxide (TBHP) oxidant in benzene.

The catalysts were further screened for C-H activation reaction (oxidation of adamantane). Catalysts with different isopoly and heteropoly ions immobilized on SBA-15 were prepared and well characterized. Detailed kinetics and mechanisms were discussed for oxidation of adamantane.

Section B The 2nd part describes synthesis of inorganic–organic hybrid materials based on functionalized silica and carbon were synthesized by anchoring $H_5[PMo_{10}V_2O_{40}]\cdot 32.5H_2O$ onto ethane bridged SBA-15 and mesoporous carbon. Small angle X-ray diffraction, N_2 sorption analysis, HRTEM, SEM, FT-IR, CP-MAS NMR were used to diagnose the structural intergrowth of the materials. These materials were applied in the environmentally friendly oxidation of 2-methylnaphthalene (2MN) with 30% aqueous hydrogen peroxide.

Section C The 3rd Describes synthesis of a simple cation exchanged form of $H_5[PMo_{10}V_2O_{40}]\cdot 32.5H_2O$ supported on ionic liquid-modified SBA-15 (V2ILSBA) and its application in catalyzed aerobic oxidation of primary and secondary alcohols to corresponding aldehydes and ketones with no trace of over oxidation.

CHAPTER IV

This chapter deals with the preparation, characterization and catalytic activities of organotin-oxometalate coordination polymers $[(nBu_3Sn)_2MO_4]\cdot nH_2O$ (where, M= Mo or W) and tested in oxyfunctionalization of monoterpenes with urea hydroperoxide (UHP) as an oxidizing agent. The oxyfunctionalization of monoterpenes gave commercially important products such as epoxides, ketones and hydroxyl derivatives. The integrity of the organotin–oxometalates polymers were confirmed by X-ray diffraction, Surface analysis, FT-IR, FT-Raman, SEM, TG/DTA and MAS NMR (^{13}C , ^{119}Sn) analysis. The effects of reaction parameters on limonene conversions and product selectivities have been studied in detail using $[(nBu_3Sn)_2MoO_4]$ catalyst

The catalyst was further used for developing green protocol for N-oxidation of primary aromatic amines in the presence of 30% H₂O₂ in high yield with good recyclability.

CHAPTER V

Chapter V is divided into two sections

Section A The 1st part deals with synthesis of CobpbH₂Cl₂·2H₂O [where, bpbH₂ = 1,2-Bis(Pyridine-2-carboxamido)benzene] complex immobilized on sulfonic acid-functionalized SBA-15 molecular sieve (SBA-15-SO₃-CobpbH₂Cl₂·2H₂O). The catalyst was characterized by elemental analysis, FT-IR, N₂ sorption measurements, Small angle XRD, UV-vis, and HRTEM for their structural integrity and physicochemical properties. This catalyst system has been applied catalyst for the opening of epoxide rings by amines, and this provided an environmentally friendly method for the synthesis of β-amino alcohols under solvent free conditions.

Section B The 2nd part describes synthesis on [Ru(salen)(NO)Cl] complex, its immobilization on mesoporous SBA-16 by ship in a bottle method and detailed characterization of the catalyst material. This well characterized material has been applied for hydrogenation of ketones.

CHAPTER VI

This chapter deals with synthesis and detailed characterizations of nanocomposite material composed of tungsten oxide nanocluster and nanoporous SBA-15. This catalyst system has been applied for selective oxidation of sulfur compounds giving excellent yields at room temperature with exceptional recyclability.

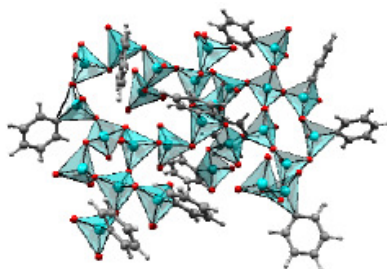
CHAPTER VII

This chapter summarizes the conclusions reached in this thesis.

CHAPTER I

Introduction

1.1.	<i>Catalysis</i>	1
1.2.	<i>Inorganic-organic hybrid materials</i>	2
1.3.	<i>Nanocomposites</i>	5
1.4.	<i>Synthetic strategies towards hybrid materials</i>	7
1.5.	<i>Coordination polymers</i>	9
1.6.	<i>Polyoxometalates</i>	11
1.7.	<i>Schiff base complex</i>	18
1.8.	<i>Mesoporous materials</i>	19
1.9.	<i>Supported ionic liquid</i>	30
1.10.	<i>Inorganic-organic hybrid materials and catalysis</i>	31
1.11.	<i>Mesoporous materials for preparation of inorganic-organic hybrid materials</i>	33
1.12.	<i>Immobilization approach</i>	34
1.13.	<i>References</i>	38



1. Introduction

1.1 Catalysis

The term “catalysis” was coined by Berzelius in 1853 and used to cover a number of physiological and chemical reactions, discovered at that time, all with the common feature that they proceeded in the presence of a further substance, which did not itself alter during the course of the reaction. A substance able to increase the rate of a chemical reaction without itself being consumed or changed by the reacting chemicals is called a catalyst and the action is called catalysis (Fig. 1.1).

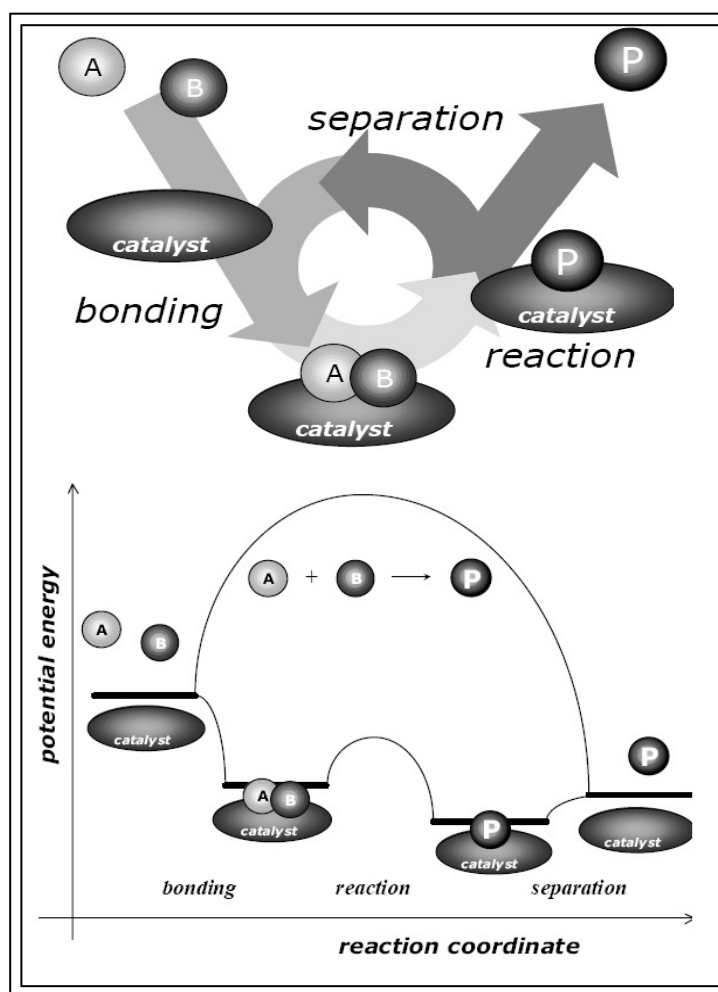


Fig 1.1. Pictorial representation of a catalysis process

Catalysts may be gases, liquids, or solids. In homogeneous catalysis, the catalyst is molecularly dispersed in the same phase (usually gaseous or liquid) as the reactants. In

heterogeneous catalysis, the reactants and the catalyst are in different phases, separated by a phase boundary.

1.2. Inorganic-organic hybrid materials

Recent technological breakthroughs and the desire for new functions generate an enormous demand for novel functional materials. Many of the well-established materials cannot fulfill all the technological requirements for various new applications. Scientists and engineers realized that the mixtures of materials can show superior properties compared with the pure counterparts. Inorganic-organic hybrid materials (IOHM) represent the natural interface between the two worlds of chemistry, each with significant contributions and characteristic properties. The advantages and limitations to their field, lead to a creative alternative for obtaining new materials with unusual features. The main idea of developing hybrid materials is to take advantages of the best properties of each component and try to decrease their drawbacks. Hence a unique advance material with potential applications results. The possibility of combining the properties of inorganic and organic compounds to get a unique material is a challenging task in recent years. Although, we do not know the original birth of hybrid materials exactly, it is clear that mixing of inorganic and organic components was carried out in ancient times. However, it was only at the end of the 20th and the beginning of the 21st century, researcher considered IOMH as innovative and advanced material having potential application in various fields including catalysis.

IOHM can be applied in many branches of materials chemistry since they are simple to process and amenable to design on the molecular scale. Currently, there are four major topics in the synthesis of inorganic-organic materials; molecular engineering, nanometer and micrometer-sized organization, the transition from functional to multifunctional hybrids and their combination with bioactive components.

The term hybrid material is used for many different systems, spanning a wide area of different materials, such as highly crystalline coordination polymers, amorphous sol-gel compounds, with and without interactions between the inorganic and organic units (Table 1.1). The most wide ranging definition is that: a hybrid material, which includes

two moieties blended on the molecular scale. Commonly, one of these compounds is inorganic and the other one is organic in nature.

Table 1.1. Possibilities of hybrid materials composition and structure

Matrix:	crystalline ↔ amorphous organic ↔ inorganic
Building blocks:	molecules ↔ macromolecules ↔ particles ↔ fibers
Interaction between components :	strong ↔ weak

According to their interface interactions, IOHM materials were divided into two classes; Class I, IOHM embedded by weak bonds, (hydrogen, Van der Waals or ionic bonds) and Class II in which the two phases (inorganic and organic) are linked together through strong chemical bonds (covalent or ionic-covalent interactions). It is natural, that the second type of IOHM materials, organic and inorganic components could also interact through the same kind of weak bonds that are mentioned in the first category (Fig.1.2).

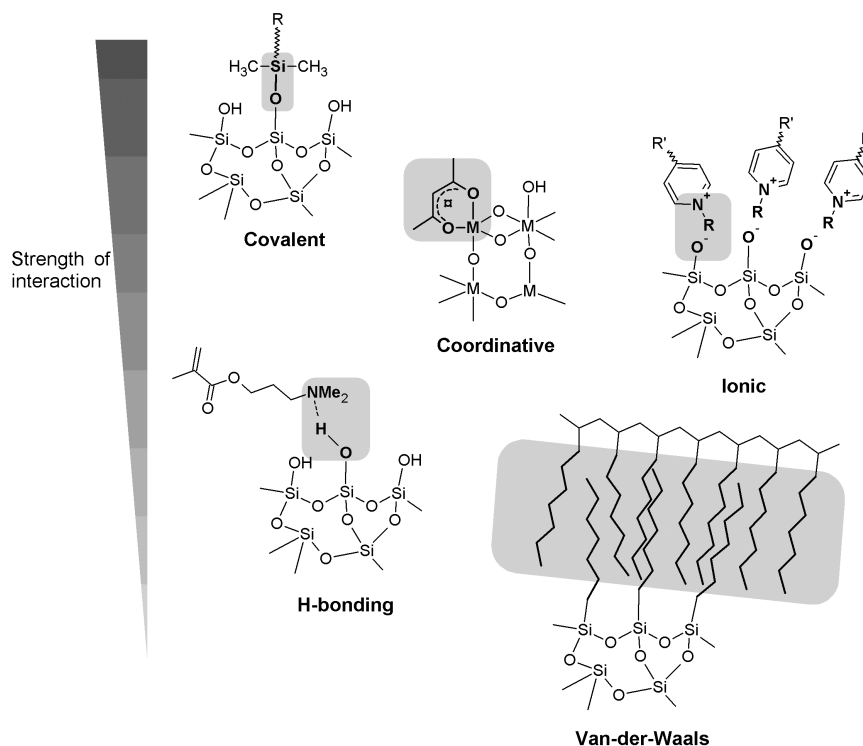


Fig 1.2. Various interactions in hybrid materials

Table 1.2. Chemical interactions and their strengths

Type of interaction	Strength [KJmol ⁻¹]	Range	Character
Van der Waals	ca. 50	short	nonselective, nondirectional
H-bonding	5-65	short	selective, directional
Coordination bonding	50-200	short	directional
Ionic	50-250 ^[a]	long	nonselective
Covalent	350	short	Predominantly irreversible

^a data are for organic media, depending on solvent and ion solution

Table 1.2 represents the energetic categorization of different chemical interactions in hybrid materials depending on their binding energies. In addition to the bonding characteristics, structural properties can also be used to distinguish between various hybrid materials and organic moiety containing a functional group that allows the attachment to an inorganic network, e.g. a trialkoxysilane group, can act as a network-modifying compound because in the final structure the inorganic moiety is only modified by the organic group. Phenyltrialkoxysilanes are example of such compounds. They modify the silica network in the sol-gel process via the reaction of the trialkoxysilane group (Fig.1.3.a) without supplying additional functional groups intended to undergo further chemical reactions to the material formed. If a reactive functional group is incorporated in the system, it is called a network functionalizer (Fig.1.3.c). However, the situation is different if two or three of such anchor groups modify an organic segment. This leads to materials in which the inorganic group becomes an integral part of the hybrid network (Fig. 1.3.b).

Blends are formed if no strong chemical interactions exist between the inorganic and organic building blocks. If an inorganic and an organic network interpenetrate each other without strong chemical interactions, interpenetrating networks (IPNs) are formed. Both materials described above belong to class I hybrids. Class II hybrids are formed, when the discrete inorganic building blocks are covalently bonded to the organic polymers or inorganic and organic polymers are covalently connected with each other (Fig.1.4).

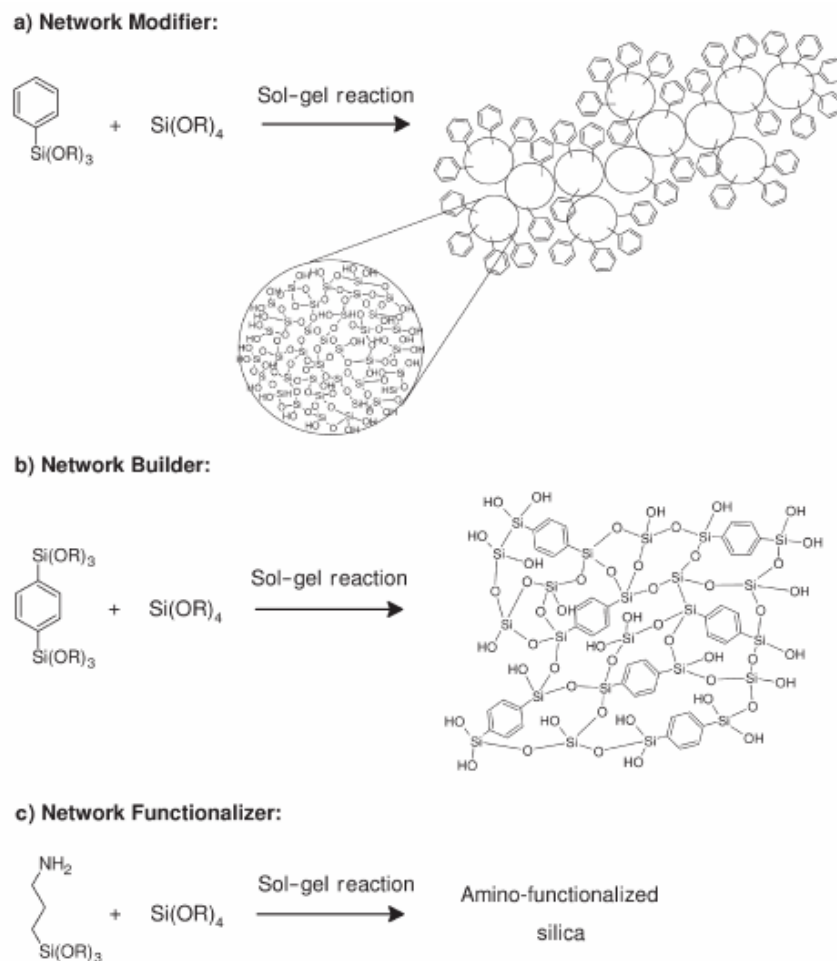


Fig 1.3. Formation routes of hybrid materials

1.3. Nanocomposites

Nanocomposites are a class of materials where two or more phases are combined with at least one of the phases having nanometer-sized particles. It can be considered solid structures with nano scale dimension along with different phases constituting the structure. These materials can either consist of an inorganic (host) solid containing an organic component (or vice-versa) or they can be of two or more inorganic/organic phases in some combinational form with the constraint that at least one of the phases or feature can be in the nanosize. Porous media, colloids, gels, and copolymers serve as examples for these materials.

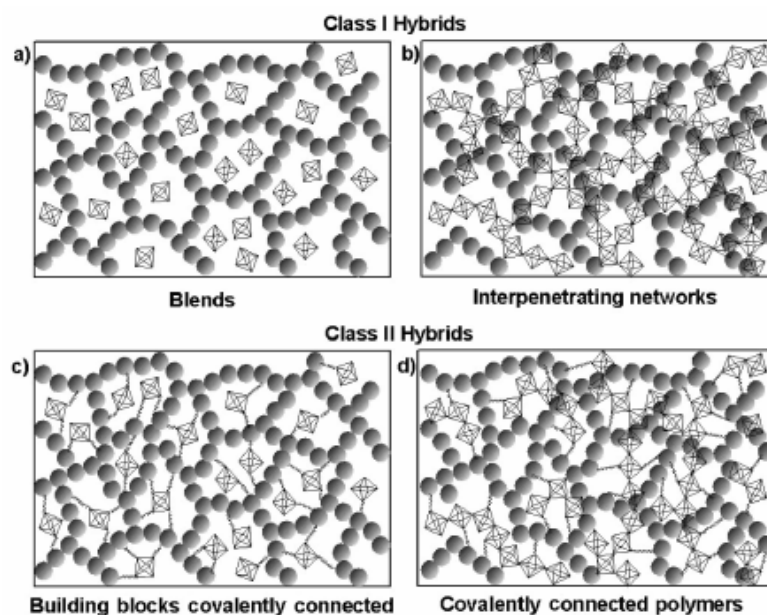


Fig 1.4. Polymer Composites

Apart from the properties of individual components in a nanocomposite, their interfaces play an important role in enhancing or limiting the overall properties of the system. This may be due to the high surface area of nanostructures, nanocomposites present in interfaces between the constituent intermixed phases. Special properties of nanocomposite materials often arise from the interaction of its phases at the interfaces.

The term nanocomposite is used if one of the structural units, either the organic or the inorganic, is in a defined size range of 1-100 nm. Therefore, there is a gradual transition between hybrid materials and nanocomposites because large molecular building blocks for hybrid materials, such as large inorganic clusters, can already be of the nanometer length scale. Commonly the term nanocomposite is applied if discrete structural units in the respective size regime are used for designing the materials. However the term hybrid materials are more often used if the inorganic units are formed in situ by molecular precursors.

1.4. Synthetic strategies towards hybrid materials

1.4.1. Building block approach

Building blocks are applied that react with each other to form the final hybrid material in which the precursors still at least keep their original integrity partially. A typical building block should consist of a well-defined molecular or nanosized structure and of a well defined size and shape, with a tailored surface structure and composition.

1.4.1.1 Inorganic building blocks

Cluster compounds of various compositions of inorganic building blocks can keep their molecular integrity but commonly pure metal clusters are not stable without surface functionalization. This functionalization can be done with groups that decrease surface energy and thus avoid coalescence to larger particles. The following two methods are used for the synthesis of such surface-functionalized molecular building blocks:

1.4.1.1. a. *Post-synthetic modification*

Post synthetic modification means that the cluster or nanoparticle is formed with well-established procedures in the first step and the functionalization with organic groups is carried out in the second step.

1.4.1.1. b. *In situ functionalization*

It deals with the functionalization of cluster and particles during synthesis.

1.4.1.2 Organic building blocks

Organic building blocks can be used for the formation of hybrid materials. The modification of inorganic networks with small molecules can be defined as the origin of hybrid materials. Organic colloids formed from physically or chemically cross linked polymers can also be used as building blocks for inorganic-organic hybrid materials and nanocomposites.

1.4.2. In situ formation of the components

One or both structural units are formed from the precursors that are transformed into a novel structure.

1.4.2.1. Sol-gel process

This process is chemically related to an organic polycondensation reaction in which small molecules form polymeric structures by the loss of substituents.

1.4.2.2. Nonhydrolytic sol-gel process

In this process the reaction between metal halides and alkoxides is used for the formation of the material. The alkoxides can be formed during the process by various reactions. Usually this process is carried out in sealed tubes at elevated temperature but it can also be employed in unsealed systems under an inert gas atmosphere.

1.4.2.3. Sol-gel reactions of non-silicates

Metal and transition metal alkoxides are generally more reactive towards hydrolysis and condensation reaction compared to silicon.

1.4.2.4. Hybrid materials by the sol-gel process

Organic molecules other than the solvent can be added to the sol and become physically entrapped in the cavities of the formed network upon gelation.

1.4.2.5. Hybrid materials derived by combining the sol-gel approach and organic polymers

Compared with other inorganic network forming reactions, the sol-gel processes show mild reaction conditions and a broad solvent compatibility. These two characteristics offer the possibility to carry out the inorganic network forming process in the presence of a preformed organic polymer or to carry out the organic polymerization before, during or after the sol-gel process. The properties of the final hybrid materials are not only determined by the properties of the inorganic and organic component, but also by the phase morphology and the interfacial region between the two components.

1.4.3. Formation of organic polymers in the presence of performed Inorganic materials

The inorganic material can either have no surface functionalization but the bare material surface; it can be modified with nonreactive organic groups; or it can contain reactive surface groups such as polymerizable functionalities.

1.5.1. Classification of polymer–metal complexes

The polymer–metal complexes may be classified into different groups according to the position occupied by the metal, which is decided by the method of preparation. The methods include complexation between a ligand function anchored on a polymer matrix and metal ion, reaction of a multifunctional ligand with metal ion and polymerization of metal containing monomers.

1.5.2. Complexation of polymeric ligand with metal ion

(a) *Pendant metal complexes*

A pendant metal complex is one in which the metal ion is attached to the polymer ligand function, which is appended on the polymer chain. Based on the chelating abilities of the ligands, pendant complexes are classified as monodentate or polydentate polymer–metal complexes.

(b) *Inter/intra-molecular bridged polymer–metal complexes*

When a polymer ligand is mixed directly with metal ion, which generally has four or six coordinate bonding sites, the polymer–metal complex formed may be of the intra-polymer chelate type or interpolymer chelate type.

1.5.3. Complexation of multifunctional ligands with a metal

A low molecular weight compound with multifunctional ligands on both ends of the molecules grows into a linear network polymer. The polymer chain is composed of coordinate bonds and the ligand is the bridging unit as per the following representation. Multifunctional ligands capable of forming this type of coordination polymers are classified into linear coordinated polymers and network-coordinated polymers (Parquet). Further linear coordinated polymers can be of two types. In one case the polymer chain is composed of bifunctional ligand and metal ion. While the other is a simple compound or ion can function as a bridging ion giving rise to a polymeric structure.

Parquet polymers are flat, netlike organic macromolecules in which a metal is completely enmeshed. This type of polymer–metal complex is formed by “template reaction” between two functional groups of the ligand induced by their coordination to metal ions, resulting in the following chelated type metal complexes.

1.5.4. Polymerization of metal containing monomer

A high molecular weight polymer formed due to polymerization of metal containing monomers, occurs by radical or ionic initiation.

1.6. Polyoxometalates

Polyoxometalates (POMs) are self-assembled nano-sized anionic metal oxide clusters. They are typically synthesized under acidic aqueous conditions and have counter ions that can be alkali metal cations, ammonium, or alkylammonium cations, etc. There are two broad classes of POMs, isopoly and heteropoly. In the heteropoly case, X is the heteroatom and is located in the center of the cluster. The element (M) that composes the framework is usually molybdenum or tungsten. The heteroatom is often P^{+5} or Si^{+4} , but there are numerous examples for over 70 different elements.

The first POM discovered was by Berzelius in 1826 which was the ammonium salt of $[PMo_{12}O_{40}]^{3-}$. Although many POMs had been reported, their structures were not fully understood until 1933 when Keggin determined the structure of $H_3PW_{12}O_{40}$ by powder diffraction.

1.6.1. Heteropoly acids

Heteropolyacids (HPAs) are hydrogen forms of heteropolyanions produced by the condensation of more than two kinds of oxoanions. HPAs have several advantages as catalysts, which make them economically and environmentally attractive. HPAs have a very strong Brønsted acidity and they are efficient oxidants under mild conditions. Also, HPAs have high solubility in polar solvents and fairly high thermal stability in the solid state. These properties render HPAs potentially promising acid, redox and bifunctional catalysts in homogeneous as well as in heterogeneous systems. HPAs are widely used as model systems for fundamental research, providing unique opportunities for mechanistic studies on the molecular level. The catalytic function of heteropoly compounds has attracted much attention in recent years and design of the catalyst is possible at atomic or molecular level. The elucidation of catalytic processes is also possible at the atomic/molecular level due to their molecular nature. Out of a large number of HPAs, the relatively inexpensive and most commonly used in catalytic applications are keggins

heteropolyacids such as tungstophosphoric acid, silicotungstic acid and phosphomolybdic acid.

1.6.2. Structure of heteropoly compounds in the solid state

In solid state, HPAs show hierarchic structure. The structure divided into three levels – primary, secondary and tertiary as exemplified.

1.6.2.1. Primary structure

The structure of a heteropolyanion or polyoxoanion molecule itself is called a primary structure. In solution, heteropolyanions are present in the unit of the primary structure, being coordinated with solvent molecules and/or protonated. Based on primary structure, different polyoxoanion structures exist.

a. Keggin structure: Keggin structures are anionic metal-oxygen cluster compounds having the molecular formula $XM_{12}O_{40}$, where “X” is a central, tetrahedrally coordinated atom connecting twelve peripheral, octahedrally coordinated “M” metal atoms. Berzelius synthesized the first Keggin structure (ammonium 12-molybdophosphate) in 1826, Marignac determined the analytical composition in 1862, and Keggin correctly deduced its geometry based on powder X-ray diffraction patterns in 1933. The acid and salt forms of the structure have proven to be industrially important; as ion-exchange materials, analytical reagents for the determination of environmental contaminant concentrations; protein precipitants and catalysts (Fig.1.6).

The ideal Keggin structure of the α type has T_d symmetry and consists of a central XO_4 tetrahedron (X = heteroatom or central atom, most commonly Si^{IV} , P^V , or Ge^{IV}) surrounded by twelve MO_6 octahedra (M = addenda atom, most commonly Mo or W). The twelve MO_6 octahedra comprise four groups of three edge-shared octahedra, the M_3O_{13} triplet, which has a common oxygen vertex connected to the central heteroatom. The oxygen atoms in this structure fall into four classes of symmetry-equivalent oxygens: $X-O_a-(M)_3$, $X-O_b-M$, connecting two M_3O_{13} units by corner sharing; $X-O_c-M$, connecting two M_3O_{13} units by edge sharing; and O_d-M , where M is the addenda atom and X is the heteroatom.

b. Lacunary Keggin anion: This is a defective derivative of a Keggin structure. In solution, several species are present in equilibrium and composition depending on the pH.

In the case of $\text{PW}_{12}\text{O}_{40}^{3-}$, the lacunary $\text{PW}_{11}\text{O}_{39}^{7-}$ is formed at $\text{pH} = 2$. The degradation of $\text{PW}_{11}\text{O}_{39}^{7-}$ to give $\text{PW}_9\text{O}_{34}^{9-}$ occurs at $\text{pH} > 8$.

c. Dawson structure: The Dawson structure, $\text{M}_2\text{X}_{18}\text{O}_{62}^{6-}$ is formed by the fusion of two lacunary Keggin anions, $\text{PW}_9\text{O}_{31}^{3-}$ units (Fig.1.6).

d. Anderson structure: This structure comprises seven edge-shared octahedra (Fig.1.6).

Keggin HPAs are the most important in catalysis due to its simple synthesis procedure compared to other structures. Besides, in contrast to HPAs with Keggin-structure, heteropolyacids of other types are thermally less stable and not capable of dehydrating at 150-200 °C and thus cannot be employed for reactions, which are conducted above 150 °C.

1.6.2.2. Secondary structure

Heteropoly compounds in the solid state are ionic crystals (sometimes amorphous) consisting of large polyanions, cations, water of crystallization, and other molecules. This three-dimensional arrangement is called the “secondary structure”. The secondary structure is variable for the group A salts. For example, $\text{H}_3\text{PW}_{12}\text{O}_{40} \cdot n\text{H}_2\text{O}$, is cubic for $n = 0-6$ and orthorhombic for $n = 21$. The crystal structures of Cs and NH_4 salts are the same as the cubic $\text{H}_3\text{PW}_{12}\text{O}_{40} \cdot 6\text{H}_2\text{O}$, with cations at the sites of $\text{H}^+(\text{H}_2\text{O})_2$ sites.

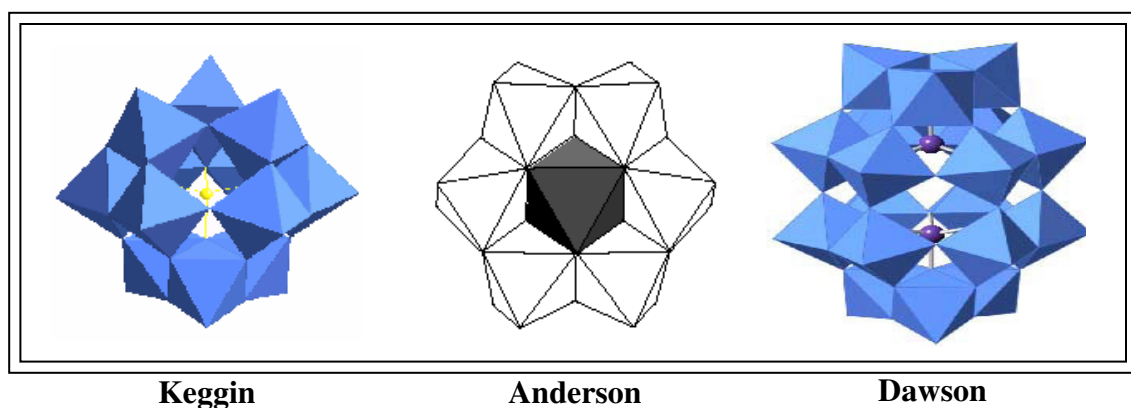


Fig 1.6. Keggin, Anderson and Dawson structure of Heteropoly acids

1.6.2.3. Proton structure

The states and dynamics of protons and water in HPAs have been studied using solid-state ^1H , ^{31}P and ^{17}O MAS NMR spectroscopies. Acidic protons are present in three forms; (a) proton attached to polyanions, (b) H_3O^+ (hydronium ion monomer) or H_2O

strongly interacting with acidic protons, and (c) H_5O_2^+ (hydronium ion dimer). H_3O^+ and H_5O_2^+ weakly interact with polyanions by hydrogen bonding (Fig.1.7).

1.6.2.4. Tertiary structure

Tertiary structure is the structure of solid heteropoly compounds as assembled. The size of the primary and secondary particles, pore structure, distribution of protons and cations, etc. is the elements of the tertiary structure (Fig.1.8). Counter cations greatly influence the tertiary structure of HPAs. The surface area of the crystalline heteropolyacids is small ($3\text{-}8\text{ m}^2\text{ g}^{-1}$), but some of their salts with appropriately large cations such as ammonium, cesium and rubidium show surface areas of the order of 100 to $200\text{ m}^2\text{ g}^{-1}$. Heteropolyacids and salts having low surface area exhibit several common properties that are in contrast with the properties of salts with high surface area, hence, a distinction is made in the literature: low surface area heteropolyacids and salts termed as “group A”, while high surface area salts termed as “group B”. Group A species are soluble in water, whereas, group B species are not; group A species decompose in the temperature range from $250\text{ }^\circ\text{C}$ to $600\text{ }^\circ\text{C}$, whereas, group B species are typically stable up to $700\text{ }^\circ\text{C}$ and above; and group A species exhibit interesting properties ascribed to a “pseudo-liquid” phase, whereas, group B species do not.

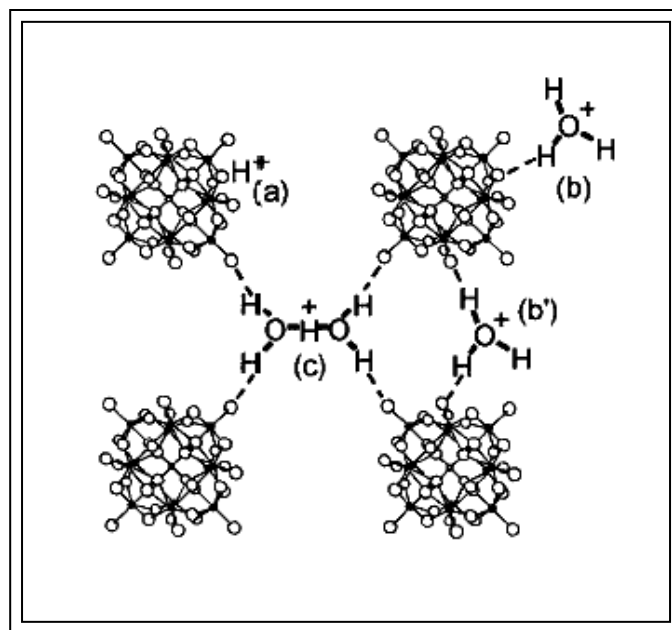


Fig 1.7. Models proposed [1] for the states of acidic protons and water in solid $\text{H}_3\text{PW}_{12}\text{O}_{40} n\text{H}_2\text{O}$ ($0 < n < 6$); two possible positions are shown for H_3O^+

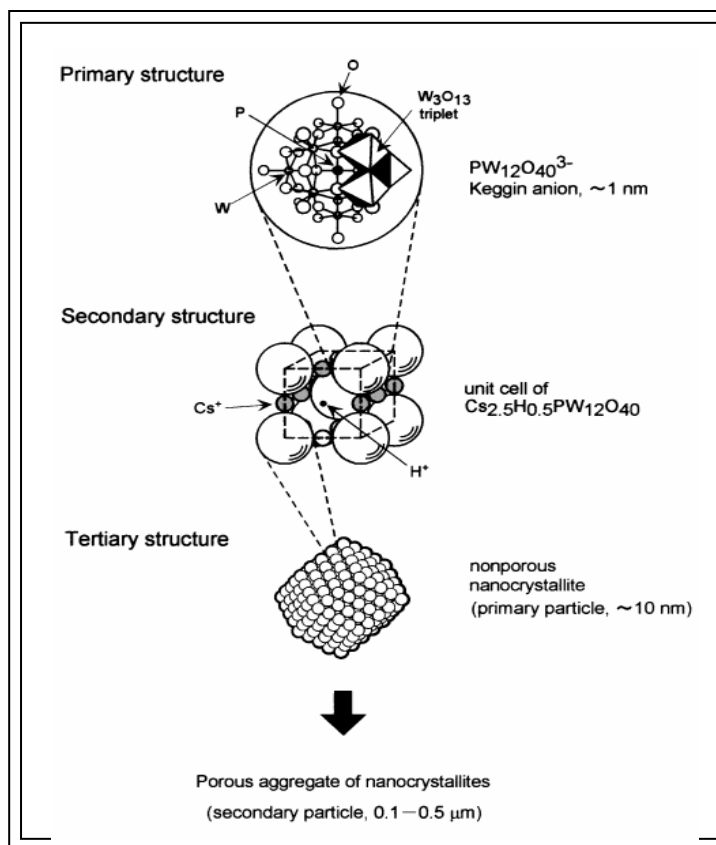
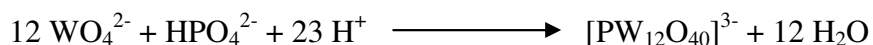


Fig 1.8. Various structures of heteropoly acids

1.6.3. Synthesis

The simplest way to prepare heteropolyanions involves the acidification of an aqueous solution containing the oxoanions and the heteroatom.



Control of the pH and X/M (central atom/addenda atom) ratio is necessary in order to obtain the desired structure, i.e., the Keggin HPA, the Wells-Dawson HPA, the Anderson HPA, a lacunary compound or the desired specific isomer. Free acids are synthesized primarily by following two methods: (1) by extraction with ether from acidified aqueous solutions and (2) by ion exchange from salts of heteropoly acids.

1.6.4. Heterogeneous catalysis

1.6.4.1 Surface-type catalysis

Surface-type catalysis is the ordinary heterogeneous catalysis, where the reactions take place on the two-dimensional surface (outer surface and pore wall) of solid catalysts. The reaction rate is proportional to the surface area in principle. For example, the rates of double-bond isomerization of olefins are proportional to the surface area of $\text{H}_3\text{PMo}_{12}\text{O}_{40}$ (Fig. 1.9).

1.6.4.2 Bulk-type catalysis

In the bulk-type (I) catalysis, e.g., acid-catalyzed reactions of polar molecules over the HPA and group A salts at relatively low temperatures, the reactant molecules are absorbed in the interpolation space of the ionic crystal and react there, and thereafter the products desorbed from the solid. Polar molecules like alcohols and amines are readily absorbed into the solid bulk by substituting for water molecules and/or by expanding the distance between polyamines. The solid behaves like a solution and the reaction field becomes three-dimensional. This is known as “pseudo liquid” catalysis first proposed in 1979 (Fig. 1.9).

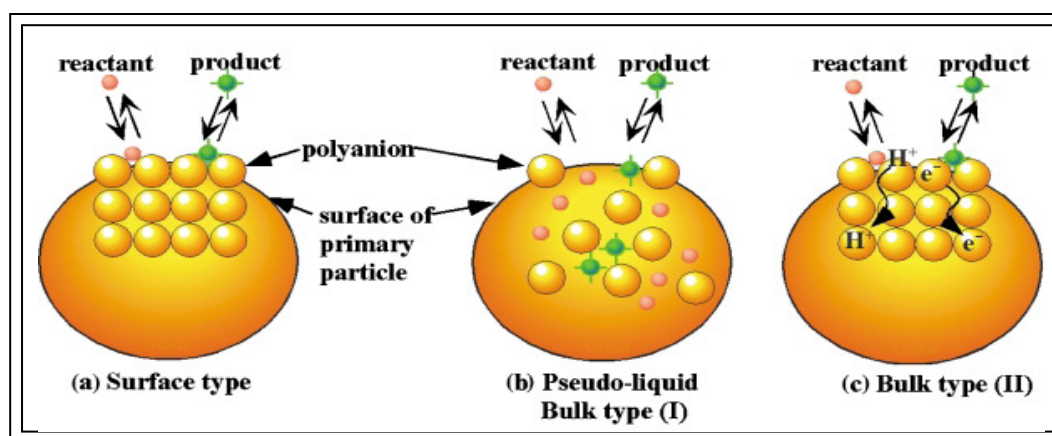


Fig 1.9. Reaction mechanism of heteropoly acids

1.6.5. Transition metal substituted polyoxometalates (TMSP)

The continuous interest in designing and making novel transition metal substituted polyoxometalates (TMSPs) has persisted because of their impressive compositional diversity and versatile applications in catalysis (similar to

metalloporphyrin), medicine and material science. The common transition metals incorporated in the framework are the first row metals. The transition metal fits into the lacunary vacancy created in the otherwise complete Keggin structural unit. The lacunary or “defect structure” is created by the loss of an MO_6 octahedra (which is equivalent to stoichiometric loss of a MO^{n+} unit resulting in the formation of $\text{XM}_{11}\text{O}_{39}^{n-}$). This involves the partial degradation of the Keggin unit by lowering the pH of the solution by the addition of a suitable buffer. The pH is dependent on the nature of the central and the addenda atom. Selecting an appropriate counter cation can control the solubility of the TMSP complexes. Usually alkali metals and tetra alkyl ammonium groups are the counter cations of choice. There are two methods for the synthesis of TMSP. The first method (method A) involves the addition of a transition metal salt to the already prepared isolated lacunary salt under appropriate synthetic conditions while the second method (method B) developed by Simmons *et al* involves the generation of *in situ* lacunary vacancy followed by the addition of the transition metal salt (Fig.1.10).

Molybdenum based heteropoly acids are better catalysts for oxidation reactions than their tungsten counterparts. The activity of these catalysts can be improved by partial substitution of vanadium for molybdenum in the Keggin structure, thus changing the stoichiometric formula from $\text{H}_3\text{PMo}_{12}\text{O}_{40}$ to $\text{H}_4\text{PMo}_{11}\text{VO}_{40}$. The higher number of charge balancing protons associated with the V-substituted material is due to the difference in formal charge between a molybdenum ion (+6) and a vanadium ion (+5). Heteropolyacids having a second vanadium atom ($\text{H}_5\text{PMo}_{10}\text{V}_2\text{O}_{40}$) are even more active in oxidation chemistry.

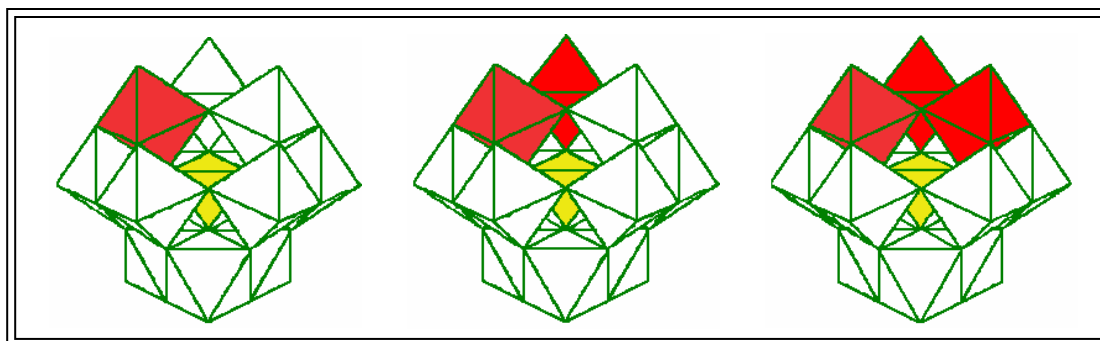


Fig 1.10. Vanadium containing heteropoly acids

1.7. Schiff base complex

Hugo Schiff described the condensation between an aldehyde and an amine leading to a Schiff base in 1864. Schiff base ligands are able to coordinate metals through imine nitrogen and another group, usually linked to the aldehyde. Modern chemists still prepare Schiff bases, and nowadays active and well-designed Schiff base ligands are considered “privileged ligands”. In fact, Schiff bases can stabilize many different metals in various oxidation states, controlling the performance of metals in a large variety of useful catalytic transformations. When two equivalents of salicylaldehyde are combined with a diamine, a particular chelating Schiff base is produced. The so-called salen ligands, with four coordinating sites and two axial sites open to ancillary ligands, are very much like porphyrins, but more easily prepared. Although the term salen was used originally only to describe the tetradentate Schiff bases derived from ethylenediamine, the more general term salen-type is used in the literature to describe the class of [O,N,N,O] tetradentate bis-Schiff base ligands (Fig. 1.11). Salen complexes are generally prepared by one of the following methods: (1) Reaction of metal ion and Schiff base in the presence of added base such as acetate or hydroxide, usually in an alcohol or aqueous alcohol solution, (2) Reaction of primary amine with bis or tris (salicylaldehyde) metal complex. The preformed salicylaldehyde complex is refluxed with a slight excess of amines in solvents such as ethanol, chloroform or dichloromethane. The crude product obtained by precipitation is then purified, (3) Template reactions: planar four coordinated complexes can be synthesized by this method.

The coordination chemistry of bispyridylamides with the general structure LH₂ has been intensively studied since the compounds were first prepared by Ojima in 1967. Metal complexes with a large variety of metal ions, including both hard high-valent and soft low-valent ions and even zerovalent metals, have been prepared. The pyridine nitrogen atoms regularly take part in coordination to the metal ion. The amide groups can be neutral or deprotonated and bispyridylamides can thus serve as neutral, mono- or dianionic ligands. Deprotonated amide groups usually coordinate via the nitrogen atom whereas coordination via oxygen is more frequent for neutral ligands. The anionic ligand is a strong σ -donor capable of stabilizing metal ions in high oxidation states. Complexes

with square planar, square pyramidal or octahedral geometry where the compound acts as a planar tetradentate N_4 ligand are common, but examples of other geometries with N_4 -, N_2O_2 - or NO-coordination exist. In addition, to monomeric complexes, dimers, trimers and oligomers with either N_4 - or N_2O_2 -coordination, and complexes with different metal to ligand ratios, are known. Although a large number of metal complexes have been characterized and their electrochemical, spectroscopic and magnetic properties as well as their ligand exchange ability were studied, it is only recently that they have found more extensive applications in catalysis. One factor, which makes the ligands attractive for catalytic applications, is the simplicity whereby the structure of the ligands can be modified by a modular approach. The electronic and steric properties can conveniently be modified by altering the diamine backbone and by the introduction of suitable substituents in the pyridine nuclei. These possibilities make the ligands attractive for catalytic applications.

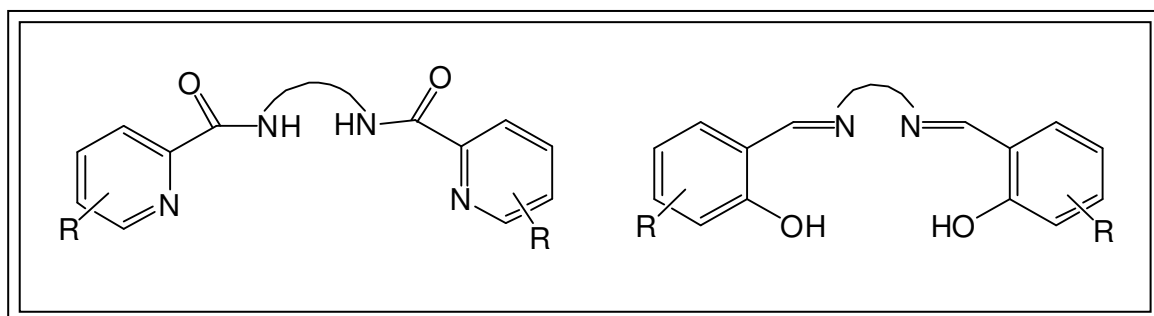
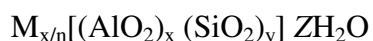


Fig 1.11. Schiff base ligands

1.8. Mesoporous materials

Zeolite [in Greek “zeos” and “lithos”, meaning “boiling stones”] group of minerals was discovered in 1756 and named by the Swedish mineralogist Baron Cronstedt. Zeolites are classified as crystalline microporous materials consisting of silicon (Si), aluminium (Al) and oxygen (O) as essential elements, in which the Si and Al are tetrahedrally coordinated by O atoms in a three-dimensional network. The crystallographic unit cell of the zeolites can be represented as:



Where M is a charge compensating cation with valency 'n'. The ratio 'y/x' may have any value ranging from one to infinity. 'Z' represents the number of water molecules, which can be reversibly adsorbed and desorbed into the zeolite micro pores.

Even though, zeolites, having pore dimensions of 5 to 7 Å, served the purpose of most of the industrial reactions by providing high surface area, the pore dimensions are not sufficient enough to accommodate broad spectrum of larger molecules. The performance of zeolite systems is limited by diffusion constraints associated with smaller pores.

With the first successful report on the mesoporous materials (M41S) by Mobil researchers, with well-defined pore sizes of 20-500Å, the pore-size constraint (15Å) of microporous zeolites was broken. The high surface area (>1000m²/g) and precise tuning of the pores are among the desirable properties of these materials. Mainly these materials used in a new synthetic approach where, instead of a single molecule as templating agent as in the case of zeolites, self-assembly of molecules aggregates or supramolecular assemblies are employed as templating agent.

The important members of the M41S mesoporous family are MCM-41, MCM-48 and MCM-50 (Fig.1.12). MCM-41 posses honeycomb arrays of nonintersecting uniformly sized channels with diameters ranging from 15 to 100 Å depending on the template used, the addition of auxiliary organics and the synthesis parameters like synthesis time, synthesis temperature or post synthesis treatments. MCM-48 is a cubic phase with *Ia3d* symmetry consisting of an enantiomeric pair of nonintersecting three-dimensional channel systems that are mutually intertwined. Among the M41S materials, the hexagonally channel oriented MCM-41 receives much attention than the cubic three dimensionally channel oriented MCM-48, due to the simple synthesis protocols. Moreover, the classical surfactants used in the synthesis of M41S related materials, like the alkyl trimethyl ammonium halides, preferentially form hexagonal or lamellar phases, which imply that the synthesis of high quality MCM-48 is subjected to a very narrow margin. However, the synthesis of MCM-48 with *Ia3d* symmetry is alluring as it has a more appealing structure and offers potential advantages than the MCM-41 material. MCM-50 posses lamellar phases and after surfactant removal the structure usually gets collapsed.

The number of research papers dealing not only with mesoporous silica, but also with other oxides, such as alumina, titania, and zirconia, has grown tremendously during the last decade. Obviously, when new types of materials such as these are discovered, an explosion of scientific and commercial development swiftly follows, and a new investigation on every conceivable aspect of their nature, the synthesis procedures and synthesis mechanisms, heteroatom insertion, characterization, adsorption, and catalytic properties, rapidly occurs.

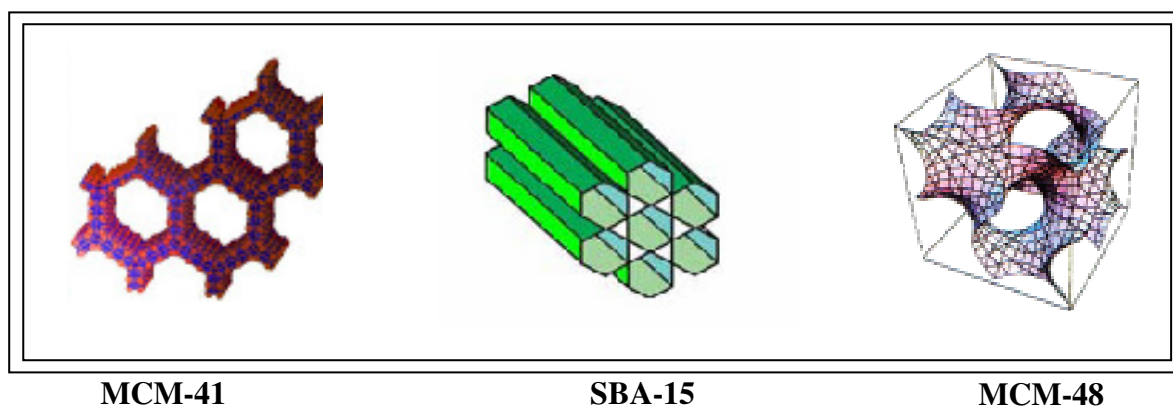


Fig 1.12. Mesoporous siliceous materials

SBA-15 has recently been synthesized by Stucky and co workers, in an acidic medium with poly(alkylene oxide) triblock copolymers, such as poly(ethylene oxide)–poly(propylene oxide)–poly(ethylene oxide) (PEO–PPO–PEO) and found to have uniform and large tubular channels up to 30 nm in diameter. Since SBA-15 also possesses thick pore walls, the hydrothermal stability is much higher than MCM-41. Such features may provide high potential as supports for catalytic applications.

The purpose and advantages of synthesizing mesoporous materials is as follows.

1. To overcome the diffusional constraints with zeolites.
2. Very high surface area ($>1000 \text{ m}^2/\text{g}$) and pore size distribution (20–100 Å).
3. Good host material for guest species (i.e. heterogenization of homogeneous species or metal complexes on the walls).
4. Easier to monitor the changes made with active species via surface area measurement and pore size distribution experiment.

1.8.1. Synthesis and mechanism of formation

Mesoporous materials such as MCM-41 are invariably synthesized by using organic structure directing agents called templates for example, cationic surfactants containing long alkyl chain with 10-20 carbons quaternary ammonium compounds often followed with addition of co-surfactants. Even though synthesis parameters such as temperature and time have a role in the formation of the materials, the surfactant or polymer template certainly plays a dominating factor for obtaining a specific structure. The surfactants have a hydrophilic head group and a long chain hydrophobic tail group, within the same molecule, and in solution they will aggregate and self-organize in such a way so as to minimize the contact between the incompatible ends. Therefore, the mechanism responsible for the formation of M41S materials from its precursors had attracted much scientific attention.

Different synthesis mechanisms have been postulated in the literature to explain the formation mechanism of mesoporous materials.

1.8.2. Liquid crystal templating (LCT) Mechanism

Mobil researchers proposed two synthesis mechanisms. In the first route, the cationic surfactant species organize into lyotropic liquid crystal phase, which can serve as template for the formation of hexagonal structure (Fig.1.13). Surfactant micelles aggregate into hexagonal array of rods, followed by the interaction of silicate anions present in the reaction mixture with the cationic head groups of the surfactant species. The condensation of the silicate species further leads to the formation of an inorganic polymeric species. The template is removed by calcination to get hexagonally arranged inorganic hollow cylinders.

In the second route, the hexagonal ordering is assumed to be initiated by the presence of silicate species in the reaction mixture (Fig.1.13). Chen *et al.* proposed that randomly distributed surfactant micelles interact with silicate oligomers by columbic interactions which results in randomly oriented surfactant micelles surrounded by two or three silica monolayers.

These species spontaneously pack into a highly ordered mesoporous phase with an energetically favorable hexagonal arrangement, accompanied by silicate condensation.

Further condensation between silicate species on adjacent rods occurs on heating and the inorganic wall continues to condense to form the stable hexagonal network.

Some other mechanisms for the formation of mesoporous silica like charge density matching mechanism by Stucky *et al.*, folded sheet mechanism by Inagaki *et al.* and silicatropic liquid crystal models by Firouzi *et al.* have also been proposed

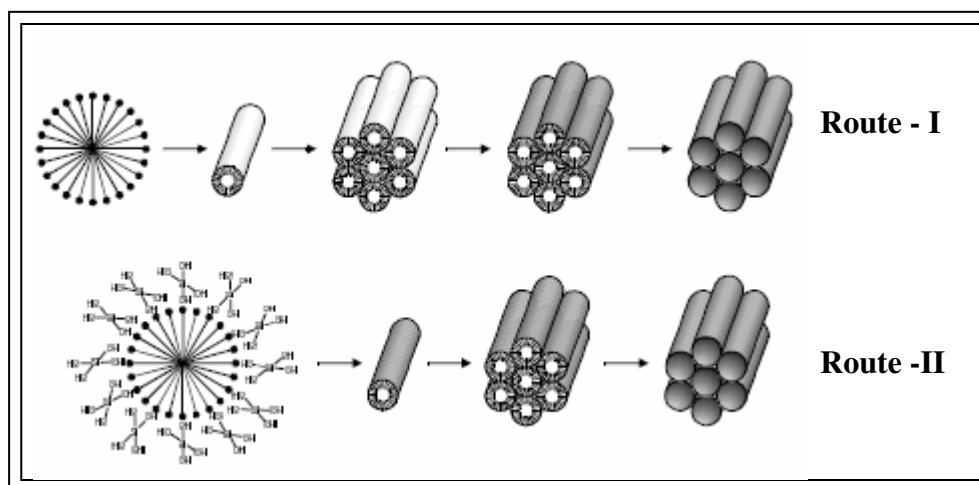


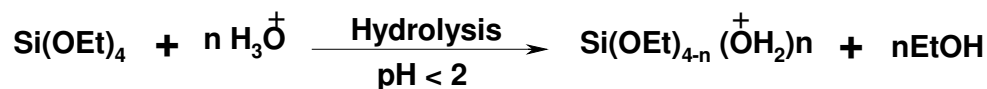
Fig 1.13. Mechanism of formation of mesoporous material

1.8.3. Generalized liquid crystal templating mechanism

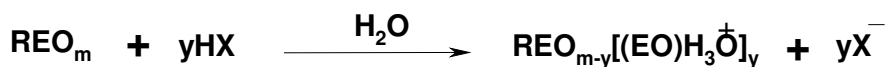
Many researchers have tried to explain the possible ways by which a surfactant species interacts with the silica species under various synthesis conditions for the development of mesoporous materials having interesting textual and structural properties :(i) Ionic Route (Electrostatic Interaction) by Huo *et al.*, (ii) Neutral Templating Route (Hydrogen bonding Interaction) by Tanev and Pinnavaia and (iii) Ligand-Assisted Templating Route (Covalent Interaction) by Antonelli and Ying.

1.8.4. Mechanism of formation of SBA-15 molecular sieves

Monnier *et al.* and Tanev showed that the assembly of mesoporous materials can also be driven by hydrogen bonds in the case of neutral templates such as nonionic poly (ethylene oxide) (PEO) surfactants and inorganic precursors. The assembly of the mesoporous silica organized by non-ionic alkyl-ethylene oxide(alkene oxide) triblock copolymer species in acid media occurs through an (S^0H^+) (XI^+) path way. First, alkoxy silane species are hydrolyzed at a pH less than 2.



This is followed by partial oligomerisation of the silica. The EO moieties of the surfactant in strong acid media associating with hydronium ions



Where R = alkyl, poly (propylene oxide) and X⁻ = Cl⁻, Br⁻, I⁻, NO₃⁻, H_ySO₄^{-2+y}, H_yPO₄^{-3+y}

Zhao et al. proposed that the formation of SBA-15 occurs through a scheme where the silica source is first hydrolyzed at low pH to form Si(OMe)_{4-n}(OH₂⁺)_n species and the PEO moieties of the block copolymer associate with hydronium ions. Then, the charged PEO units and the cationic silica species are assembled together, via Cl⁻, by a combination of electrostatic, hydrogen bonding and Van der Waals interactions to form REO^{m-y}[(EOH₃O⁺)_y...yX⁻...I⁺], which can be designated as (S⁰H⁺)(X⁻I⁺). Coordination sphere expansion around the silicon atom by anion (e.g. Cl⁻) coordination of the form X⁻·Si⁺OH₂⁺ may play an important role. Further condensation of the silica species and the organization of the surfactant and inorganic species result in the formation of the lowest energy silica-surfactant mesophase structure by the solidifying inorganic network. Furthermore, the time required for silica mesopore precipitation depends on the acid anion and is found to be the shortest in the presence of Cl⁻ anion when used in the form of hydrochloric acid. It was shown that the EO-length determines which mesostructure is formed. The length of the hydrophilic EO-block determines the silica mesostructure and influences the wall thickness of SBA-15. The hydrophobic PO-block affects the pore diameter and further, the PO-block length influences the templating ability as a longer PO-block results in more highly ordered domains and better defined particles.

1.8.5. Surface modifications of mesoporous silica

The applications of siliceous mesoporous materials itself is restricted because of the limitations in the active sites and have to be modified according to the requirements. Hence, in order to utilize the unique properties of the mesoporous material for specific applications in catalysis, sorption, sensing, ion exchange, etc. Introduction of reactive organic functional groups, by the incorporation of organic components as part of the silicate walls or trapped within the channels to form organic-inorganic hybrid materials

remains the key issues. The advantages of organic-inorganic hybrid materials arise from the fact that inorganic components can provide mechanical, thermal or structural stability, while the organic features can be readily modified for various specific applications.

1.8.5.1. Grafting methods

Grafting refers to post synthesis modification of the inner surface of a prefabricated mesoporous support, where the organic functional groups are introduced as the terminal groups of an organic monolayer, usually after surfactant removal. Mesoporous silica possesses surface silanol groups (Si-OH) in high concentration and, like in amorphous silica, it can act as convenient anchoring points for organic functionalization (Fig.1.14). Silylation generally occurs on free ($\equiv\text{Si-OH}$) and geminal silanol ($=\text{Si}(\text{OH})_2$) groups, while hydrogen-bonded silanol groups are less accessible to modification because they form hydrophilic networks among themselves. If a high surface coverage of organic functional groups is required, it is important to maintain a large number of surface silanol groups, after the removal of surfactants.

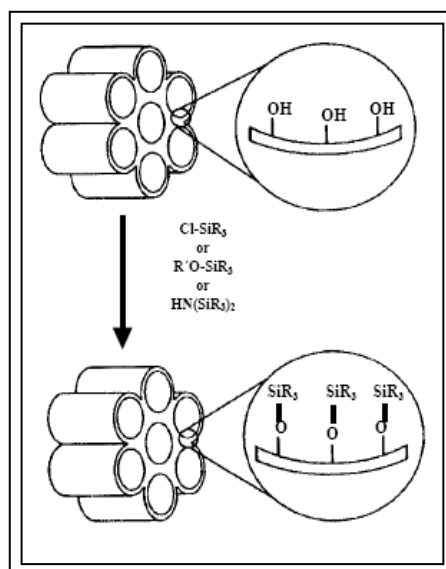


Fig 1.14. Grafting in mesoporous materials

Surfactant removal is usually carried out either by calcination or by appropriate solvent extraction methods. Since calcinations at higher temperatures can lead to the condensation of silanol groups, a decrease in the density of silanol groups is often obtained than the solvent extraction process (*e.g.*, with acid/alcohol mixtures for cationic surfactants or with alcohols for neutral surfactants).

1.8.5.1.1. Grafting with passive surface groups

Organic functional groups with lower reactivity could be grafted to enhance the hydrophobicity of the surface and protecting the material towards hydrolysis. Further, the pore diameter of mesoporous materials can also be adjusted by varying the alkyl chain length of the silylating agent or by increasing the quantity of the silylating agent.

1.8.5.1.1. Grafting with reactive surface groups

Grafting of the mesoporous silica surfaces with organic units containing reactive functional groups like olefin, cyanide, thiol, amide, halide, *etc* permits further functionalization of the surface as their terminal end contains a reactive functional group. After, modification of these materials with the desired functionalities, catalytically active homogenous transition metal complexes as well as organometallic complexes can be anchored over these organic-inorganic hybrid materials.

1.8.5.1.1. Site-Selective grafting

The external surface silanols of the mesoporous materials are kinetically more accessible than the internal surface silanols. Hence, in order to minimize the grafting of reactive surface sites on the external surface and thereby to utilize the inner pore channels, it is necessary to passivate the external silanol groups before functionalizing on the internal surfaces.

1.8.5.2. Co-condensation methods

Organic-inorganic hybrid mesoporous materials can be also prepared at room temperature or at higher temperatures by the one-step co-condensation method between tetraalkoxy silanes ($\text{Si}(\text{OR}')_4$, $\text{R}' = \text{Et}, \text{Me}$) with one or more organoalkoxy silanes ($\text{RSi}(\text{OR}')_3$, $\text{R}' = \text{Et}, \text{Me}$), through the sol-gel process in presence of a structure orientor. Depending on the nature of the R groups, a variety of organofunctionalized mesoporous materials attached covalently with the silica surface can be synthesized. Solvent extraction of the as-synthesized materials in an acidic-alcohol mixture helps to remove the occluded surfactants from the pore channels and to obtain the organofunctionalized ordered mesoporous material (Fig.1.15).

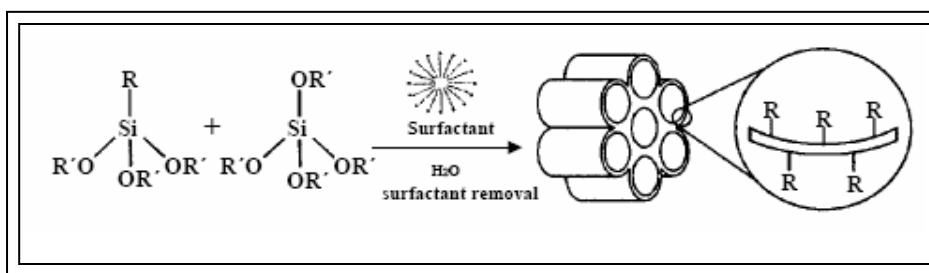


Fig 1.15. Organofunctionalization of mesoporous material

1.8.6. Periodic mesoporous organosilicas (PMO)

The combination of organic and inorganic fragments inside the structure of porous materials, which are self-assembled into architectures with dimensions spanning multiple length scales, can give rise to new materials preserving the unique characteristic of both organic and inorganic materials. Thus, an alternative strategy in the synthesis of organic-inorganic hybrid mesoporous materials is to replace one or more of the siloxane links with organic groups. Since the organic groups integrated inside the channel walls is the carrier of the desired property, it finds interesting to tailor the properties of these materials by the replacement of the bridging oxygen group by bridging organic groups in the wall channels.

Inagaki *et al.* have first reported the synthesis of 'periodic mesoporous organosilica' (PMO) with organic functional groups uniformly incorporated in the mesoporous walls, using 1,2-bis(triethoxysilyl)ethane as the framework precursor and octadecyl trimethylammonium chloride as the surfactant. Asefa *et al.* and Melde *et al.* have also described the co-condensation of either 1,2-bis(triethoxysilyl)ethane or 1,2-bis(triethoxysilyl)ethylene with silica precursors to synthesize hexagonal hybrid framework materials, under basic reaction conditions. Thus the co-condensation of silsesquioxane precursors of the type, $(R'O)_3SiRSi(OR')_3$, where $R = -(CH_2)_x-$, $-C_6H_5-$, $-CH=CH-$, *etc.*, and their self assembly over an organized surfactant species can create organic-inorganic hybrid materials having long-range ordering and organic moiety as component of the solid network. Organic groups like ethylene, phenyl and biphenyl in the framework exhibit crystalline wall channels and thus the discovery of PMO is considered as a major breakthrough in the field of materials science. The crystal-like ordering of the wall structures is thought to form through self-organization of the precursor molecules as a result of hydrophobic hydrophilic interaction of hydrolyzed $(OH)_3Si-R-Si(OH)_3$ species

or π - π interactions of aromatic groups. Now, a wide range of synthetic routes to mesoporous organosilicas with different mesophases and morphologies has been reported including the use of cationic, neutral and non-ionic surfactants and surfactant mixtures under basic, acidic and neutral conditions (Fig.1.16).

The important advantages of the PMO materials over the conventional organic-inorganic hybrid mesoporous materials are due to: (i) organic moieties in PMO are homogeneously dispersed inside the wall channels with a maximum loading of 100%, which are not achievable with the organic pendant groups grafted, (ii) bridging organics inside the channel walls do not block the pores, (iii) the soft organic groups integrated within the channel walls impart interesting physical and mechanical properties of the host and (iv) the organic groups integrated inside the channel walls can be varied to produce a wide range of materials with potentially interesting characteristics.

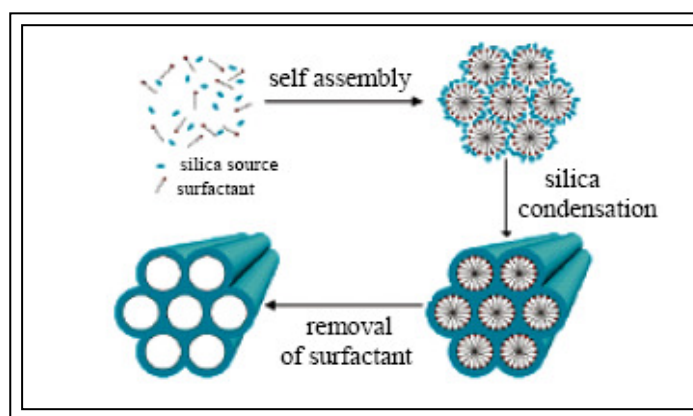


Fig 1.16. Synthesis of organic-inorganic hybrid mesoporous materials having organic groups in the frame wall positions. Silica source: Bridged Silsesquioxanes, $(R'O)_3SiRSi(OR')_3$, where $R = -(CH_2)_x-$, $-C_6H_5-$, $-CH=CH-$

1.8.7. Mesoporous Carbon

Porous carbon materials are ubiquitous and indispensable in many modern-day scientific applications. They are used extensively as electrode materials for batteries, fuel cells, and super capacitors, as sorbents for separation processes and gas storage, and as supports for many important catalytic processes. Their use in such diverse applications is directly related not only to their superior physical and chemical properties, such as

electric conductivity, thermal conductivity, chemical stability, and low density, but also to their wide availability. Porous carbon materials can be classified according to their pore diameters as microporous (pore size < 2 nm), mesoporous (2 nm < pore size < 50 nm), and/or macroporous (pore size > 50 nm). Conventional porous carbon materials, such as activated carbon and carbon molecular sieves, are synthesized by pyrolysis of physical or chemical activation of organic precursors, such as coal, wood, fruit shell, or polymers, at elevated temperatures. These carbon materials normally have relatively broad pore-size distributions in both micropore and mesopore ranges. Two methods have been used for synthesis of mesoporous carbon materials with well-controlled mesopores in recent years.

(i) Hard-template synthesis method: Synthesis involving the use of presynthesized organic or inorganic templates is called a hard-template synthesis method. The templates mainly serve as molds for replication of mesoporous carbon materials, and no significant chemical interactions take place between templates and carbon precursors.

(ii) Soft-template synthesis method: Synthesis involving amphiphilic molecules, such as surfactants and block copolymers (soft templates) are called a soft-template synthesis method, which generate the nanostructures through self-assembly of organic molecules (Fig. 1.17). The corresponding pore structures are determined by synthetic conditions. They differ from hard-template synthesis by the self-assembly of organic templates, in which molecules or moieties are manipulated at the molecular level and spatially organized in nanospaces by hydrogen bonding, hydrophobic/hydrophilic interactions, ion pairing, and/or dative interactions.

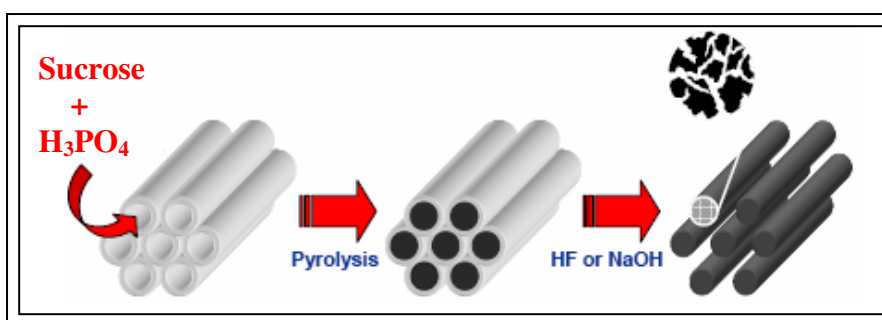


Fig 1.17. Synthesis of mesoporous carbon

1.9. Supported ionic liquid

ILs (Ionic Liquids) are composed of a bulky and organic cation as well as organic or inorganic anions and are liquid at room temperature, mainly due to the large asymmetrical cations preventing close packing of the ions, which can cause their low melting points (Room Temperature Ionic Liquids, RTILs). The most commonly used ionic liquids are based on imidazolium, pyridinium, pyrrolidinium, phosphonium cations and metal halide anions such as BF_4^- , PF_6^- , NO_3^- , SO_3^- , $(\text{CF}_3\text{SO}_2)_2\text{N}^-$. Making changes to the cation or anion of ILs can result in significant changes in their properties, such as solubility, density, refractive index and viscosity to suit the needs for a specific application. They have attracted lots of attention since their discovery as a reaction media for catalytic reactions in industry due to their some important features such as environmentally safe and non-corrosive reaction media.

One of the key challenges in the application research of ionic liquids has been the availability and cost issue. Although a multitude of recipes has been published to carry out the synthesis of ionic liquids, not all laboratories focused on applied research have the expertise, work practices and equipment necessary to carry out synthesis work. Also, to prepare pure, dried RTILs or to execute post synthesis purification steps are often challenging. ILs can't be used in fixed bed continuous flow reactor. Therefore, the concept of immobilized ionic liquids entrapped, for instance, on the surface and pores of various porous solid materials offers an attractive alternative to study the performance of ILs cost effectively. Also, due to the higher relative viscosity of many RTILs, compared to that of classical molecular solvents, the established thin ionic liquid layer is an advantage, facilitating more rapid diffusion and mass transfer (Fig.1.18(A) & (B)).

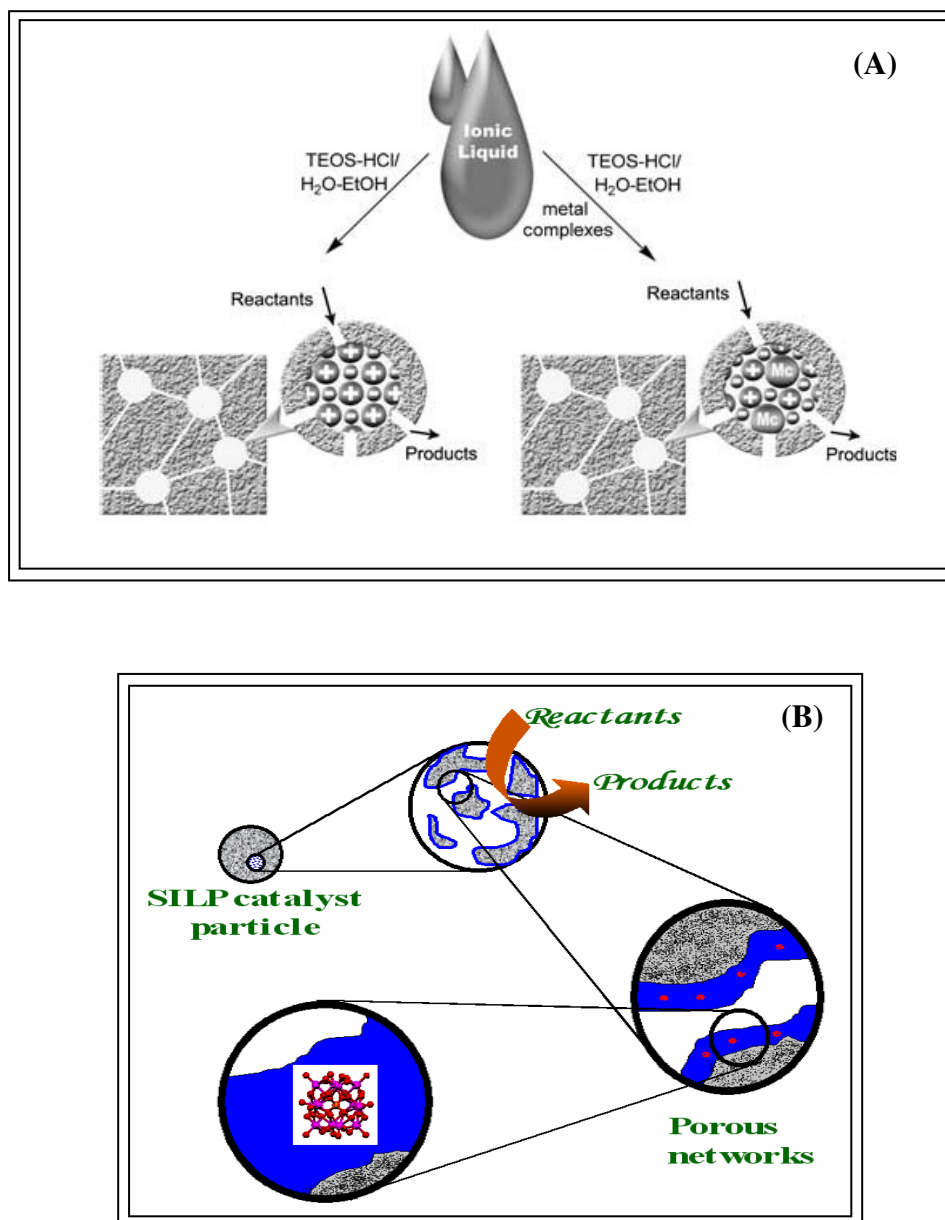


Fig 1.18(A & B). Pictorial representation of a supported ionic liquid phase catalysts

1.10. Inorganic-organic hybrid material and catalysis

Catalysts played a major role in establishing the economic strength of the chemical industry in the first half of the 20th century. As we approach the first half of the 21st century increasingly demanding environmental legislation, public and corporate pressure and the resulting drive towards clean technology in the industry will provide

new opportunities for catalysis and catalytic processes. Some of the major goals of 'Green Chemistry' are to increase process selectivity, to maximize the use of starting materials (aiming for 100% atom efficiency), to replace stoichiometric reagents with catalysts and to facilitate easy separation of the final reaction mixture including the efficient recovery of the catalyst. The use of efficient solid catalysts can go a long way towards achieving these goals. These features can lead to improve processing steps, better process economics, and environmentally friendly industrial manufacturing. Thus, the motivating factors for creating recoverable catalysts are large. Traditional heterogeneous catalysts are rather limited in the nature of their active sites and thus the scope of reactions that they can accomplish. Soluble organic catalysts can catalyze a much larger variety of reaction types than traditional solid catalysts but suffer from their inability (or high degree of difficulty) to be recycled. Since much is known about organic catalysts, the immobilization of these entities onto solids to create organic-inorganic hybrid catalysts can be accomplished with some aspects of design. The goal is to utilize the organic moiety as the active site and the solid to provide avenues to recovery and possibly recyclability of the organic active site.

Oxidation reactions are among the most important reactions in nature; they are responsible for the activation of molecular oxygen in living species on the earth's surface and are being used in chemical industry to prepare variety of oxygenated organic compounds useful either directly or as intermediates for other value added chemicals. Catalytic oxidation is a key technology for converting petroleum-based feedstock to useful fine and bulk chemicals, as building blocks for the preparation of variety of products. Millions of tons of these compounds are annually produced worldwide and find applications in all areas of chemical industries, ranging from pharmaceutical to large-scale commodities. The industrial use of oxidation reaction for the production of bulk chemicals is primarily based on heterogeneous catalyst with molecular O₂ in the form of air as the terminal oxidant, while homogeneous catalysis is mainly used for the preparation of fine chemicals with a variety of different terminal oxidants Immobilization of metal ions, metal complexes and polyoxometalates on inorganic matrices has opened many tracks to more practical fine chemicals processes. A serious caveat is, however, needed regarding the true heterogeneity of several of these new catalytic materials.

Accurate control of pore shapes and dimensions along with surface functionalization is needed to precisely control the environment of the active site. Moreover, it is clear that for such aims microporous and ordered mesoporous molecular sieves offer much better perspectives. It seems that many successful catalysts have resulted from the fortuitous combination of a metal, a ligand, a polyoxometallate, a support and reaction conditions. Designing a true heterogeneous catalyst system for organic transformations is real challenging task in present decade. It is because of the catalyst recycling and recovering drawbacks of homogeneous catalyst systems. The disadvantages of homogeneous catalyst systems are; deactivation due to the formation of μ -oxo dimer or oligomers and most of the organic ligands undergo oxidative destruction under oxidizing conditions. On the other hand, a heterogeneous catalyst system suffers from leaching, which is due to the use or generation of polar molecules during oxidation reaction. These polar molecules hydrolyze the bonds between catalyst and support. One of the major hurdles for many metal catalysts, however, is excessive, unproductive decomposition of oxidants. Keeping the above points in mind, we propose to synthesize new catalyst (IOHM), which would solve the problems associated with the conventional homogeneous catalysts. These discrepancies can be minimized by IOHM based on polyoxometalates and transition metal complexes, coordination polymers and nanocomposites.

1.11. Mesoporous materials for preparation of inorganic-organic hybrid materials

One of the strategies followed for the preparation of IHOM has been immobilization of molecular homogeneous catalyst in heterogeneous inorganic matrixes.

The ordered mesoporous materials possess narrow and controlled pore size distribution and large pore openings, which has stimulated fundamental research in inclusion of metal, polyoxometalates and metal complexes inside the mesoporous channels. The reactivity of the internal surfaces of mesoporous silica has been widely exploited by anchoring of several organic functional groups on the channel walls. These functional groups can act as anchor to hold metal complexes and polyoxometalates. Since the mesoporous surfaces are inert towards abrasion, biodegradation and mechanical resistance of the solids, these inorganic particles are less prone to attrition due to stirring

and solvent attack during their use in a chemical reactor under continuous operation, so several strategies were developed for the incorporation of active species into the mesoporous channels.

1.12. Immobilization approach

The literature reports on immobilized active species into/onto inorganic supports in four main categories depending on the support-complex interaction: (1) adsorption (2) encapsulation within the cages inorganic matrixes using a methodology generally known as “ship in a bottle” (SIB) synthesis, the resulting active species becoming mechanically immobilized; (3) immobilization by weak dipolar or strong coulombic interactions, where in the latter case the active species is adsorbed onto the support by ion-pairing with an anionic or cationic solid; and (4) connection by covalent bond of the ligand and the support, which requires the necessary functionalization of the complex to allow the immobilization (Fig .1.19).

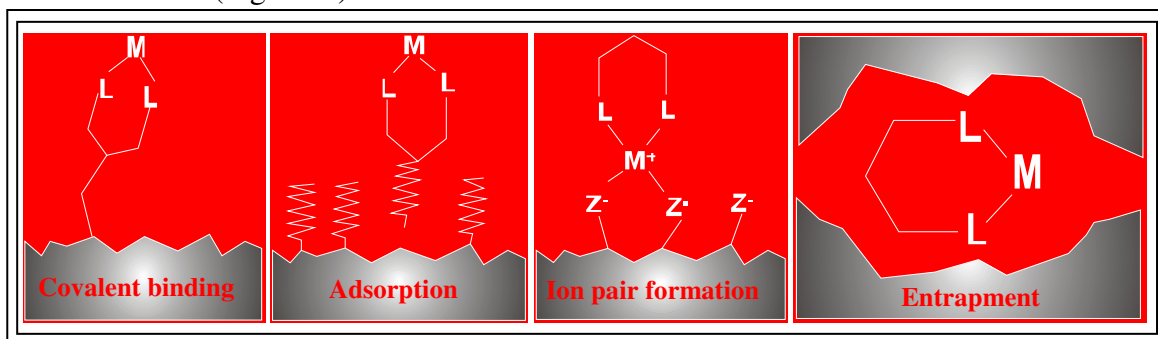


Fig 1.19. Immobilization of active species into/onto inorganic supports

1.12.1 Adsorption

Ligands containing a sulfonic acid functional group can be adsorbed onto silica surfaces through hydrogen bonding interactions with the surface silanol groups.

1.12.2. Covalent tethering

(a) Formation of an Apical Coordinative Bond with the Metal

The surface of the inorganic solids can be easily functionalized by introducing a variety of different organic functional groups that can enhance the interaction of the inorganic oxide with the active species. Silica materials are often used as supports for the

heterogenization of catalysts. Besides classical impregnation (e.g. with metal cations) the silanol groups on the surface can react with silane compounds with leaving groups. Since the character of the silica surface changes due to these reactions this process is referred to as functionalization. Often used leaving groups for surface functionalization are chlorides (Cl^-), silazanes (N-SiR_3) and alkoxy groups (OR^-) (Fig.1.20). Chlorosilane and disilazane compounds are very reactive. Therefore, water has to be excluded during functionalization reactions with these compounds. That makes these reactions synthetically rather demanding. Furthermore, adsorbed water on the surface of silica materials has to be removed prior to functionalization. Often this is done under high vacuum at elevated temperatures ($100\text{ }^\circ\text{C} - 400\text{ }^\circ\text{C}$). Under these severe conditions not only physisorbed water is removed from the silica surface but also neighboring silanol groups condense and form siloxane bridges (Fig.1.21). Therefore, the number of reactive silanol groups is reduced during this treatment, which leads to a low loading of functional groups after the functionalization reaction.

The surface of silica materials can be functionalized with various organic groups by treatment with the respective silane component. This methodology is often referred to as grafting. Silanol groups react thereby with chloro- or alkoxyorganosilanes. Silanes with one, two or three leaving groups are common. In this study, silanes with three alkoxy leaving groups were mostly used. The possible modes of surface modification are depicted in Figure 6.1. The availability of the silanol groups on the surface determines whether the grafted silicon atom is bound via one, two or three silicon-oxygen bonds. It is still not clear which is the predominant mode under a certain condition. The grafted silicon atoms are denoted as T1 (RSi(OSi)(OR')_2), T2 ($\text{RSi(OSi)}_2(\text{OR}')$) and T3 (RSi(OSi)_3) sites, respectively, where R is the organic moiety and R' is an alkyl-group or a H atom. Depending on the silane, the specific surface area of the silica and the available number of surface silanol groups organic loadings of 0.2-5 mmol/g of solid can be obtained. Because many silanes are commercially available silica surfaces can be functionalized with a broad variety of organic groups. If ordered mesoporous silica materials as M41S or SBA-15 are used for functionalization by grafting of silanes both the average pore diameter and the specific surface are decreased during this process. To a certain extent this effect is expected because the walls of the materials become thicker.

An organic group, which is often used for functionalization is 3-aminopropyl. A primary amine is a good ligand for metal ions and can therefore serve as sorbent in waste water treatment or can immobilize catalytically active transition metal ions and poly oxometallates. Furthermore, the nucleophilic primary amine can be used as linker between the silica surface and any organic species with a leaving group for a nucleophilic substitution reaction or serve as solid base catalyst. Mesoporous materials functionalized with 3-aminopropyl groups can either be prepared by co-condensation of 3-aminopropyl-trialkoxysilane with a silica precursor (typically TEOS) or by post synthetic grafting on the surface of a mesoporous silica support. An important advantage of post synthetic grafting is that the mesoporous silica can be calcined to remove all templates. The calcinations stabilize the silica framework. Moreover, the synthesis of the support and the functionalization are independent, which allows more flexibility in both procedures.

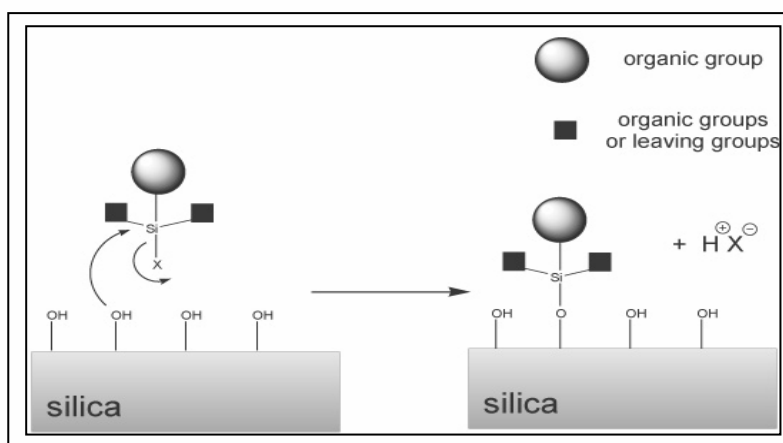


Fig 1.20. Post synthetic grafting on the surface of mesoporous silica

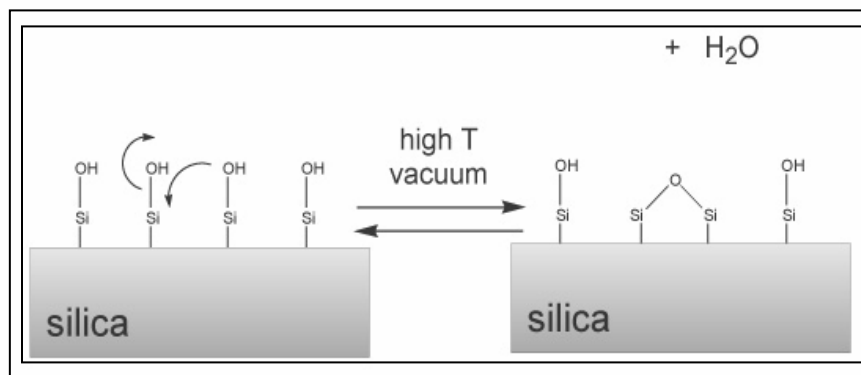


Fig 1.21. Elimination of water in grafting process

(b) Covalent Binding of the Ligand to the Support

This methodology deals with the immobilization of active species by covalent anchoring to the support through the ligand. This is accomplished by reacting complementary functional groups, one located in the solid and the other at the active species.

1.12.3. Ion exchange (electrostatic interaction)

In this methodology, one possibility to achieve the immobilization of the active species on the support is by electrostatic interaction between the surface of the inorganic solid and an electrically charged homogeneous species, either unmodified or suitably functionalized

1.12.4. Entrapment/ ship in bottle

The ship in bottle approach alludes to a methodology to immobilize homogeneous complexes in which the host-guest interaction is not chemical (neither ionic nor covalent bonding), but physical. The ship in bottle concept refers to the similarity of the resulting complex imprisoned within the porous framework to the artistic bottles containing a ship larger than the bottleneck.

A number of literature reports have been found in current date of applying immobilization strategy to design hybrid materials. This gives an immense opportunity for designing of heterogeneous catalyst system for pharmaceutical to large-scale commodities. A number of research groups studied extensively various base catalyzed reaction such as Knoevenagel condensation, epoxidation, aldol, Michael addition, transesterification and synthesis of chromenes and coumarins by synthesizing hybrid inorganic-organic materials by grafting primary, secondary amines in various supports. After proof of usefulness of homogeneous asymmetric catalysis in a number of industrial applications; due to economic and environmental considerations various research groups try to make them heterogeneous by immobilizing them in solid supports. As a result of that we now get a number of metal complex immobilized systems (hybrid system) for various asymmetric transformations in current literature. Heteropoly acid is an important class of compound in catalysis but compared to metal complexes less importance has been given to immobilization them due to their complex nature. A few reports could be

seen in literature immobilization of heteropoly acids in solid supports for various organic transformations.

1.13. References

Hybrid materials and nanocomposites

1. G. Kickelbick (Ed.) Hybrid Materials. Synthesis, Characterization, and Applications. Wiley-VCH, Weinheim, 2007.
2. P. Gómez-Romero, C. Sanchez (Eds.) J. Mater. Chem.15 (2005) 3543.
3. P. Gómez-Romero, C. Sanchez (Eds.) Functional Hybrid Materials, Wiley-VCH, Weinheim, 2004.
4. G. Schottner, Chem. Mater. 13 (2001) 3422.
5. G. Kickelbick, U. Schubert, Monatsh. Chem. 132 (2001) 13.
6. K.-H. Haas, Adv. Eng. Mater. 2 (2000) 571.
7. C. Sanchez, F. Ribot, B. Lebeau, J. Mater. Chem. 9 (1999) 35.
8. K.G. Sharp, Adv. Mater. 10 (1998) 1243.
9. P. Judeinstein, C. Sanchez, J. Mater. Chem. 6 (1996) 511.
10. P. M. Forster, A.K. Cheetham, Topics in Catalysis 24 (2003)1.
11. Special issue of J. Nanosci. and Nanotechn. 6 (2006) 265.
12. A. Usuki, N. Hasegawa, M. Kato, Adv. Polym. Sci. 79 (2005)135.
13. C. Sanchez, B. Julian, P. Belleville, M. Popall, J. Mater. Chem. 15 (2005) 3559.
14. (a) G. Kickelbick, Progr. Polym. Sci. 28 (2003) 83, (b) Special issue of Chem. Mater. 13 (2001) 3059.
15. J-L. Shi, Z.-L. Hua, L.-X. Zhang, J. Mater. Chem. 14 (2004) 795.
16. J. Wen, G.L. Wilkes, L. Garth Chem. Mater. 8 (1996)1667.
17. J.W. Kriesel, T.D. Tilley, Adv. Mater. 13 (2001) 1645.
18. R.W.J. Scott, O.M. Wilson, R.M. Crooks, J. Phys. Chem. B 109 (2005) 692.

Coordination polymers

19. S.R. Batten Current Opinion in Solid State and Materials Science 5 (2001) 107.
20. T. Kaliyappan, P. Kannan, Prog. Polym. Sci. 25 (2000) 343.

Polyoxometalates

21. M. Misono, Chem. Commun. (2001) 1141.

22. T. Okuhara, N. Mizuno, M. Misono, *Adv. Catal.* 41 (1996) 113.
23. N. Mizuno, M. Misono, *Chem. Rev.* 98 (1998) 199.
24. T. Okuhara, *Chem. Rev.* 102 (2002) 3641.
25. I.V. Kozhevnikov, *Chem. Rev.* 98 (1998) 171.
26. M.T. Pope, *Heteropoly and Isopoly Oxometalates*. Springer-Verlag, Berlin, 1983.
27. M.T. Pope, A. Muller, *Angew. Chem. Int. Ed. Engl.* 30 (1991) 34.
28. M.T. Pope, A. Muller, (Eds.) *Polyoxometalates: From Platonic Solids to Anti-Retroviral Activity*, Kluwer, Dordrecht, (1994).
29. J.F. Keggin, *Nature (London)* 131 (1933) 908.
30. L. Pettersson, I. Anderson, L.O. Ohman, *Inorg. Chem.* 25 (1986) 4726.
31. B. Dawson, *Acta Crystallogr.* 6 (1953) 113.
32. J.S. Anderson, *Nature* 140 (1937) 850.
33. B. Gruttner, and G. Jander, in *Handbook of Preparative Inorganic Chemistry*, 2nd Ed. (G. Brauer, Ed.), Academic Press, New York, 2 (1976) 1716.
34. F. Cavani, *Catal. Today* 41 (1998) 73.

Schiff base complexes

35. P.G. Cozzi, *Chem. Soc. Rev.* 33 (2004) 410.
36. O. Belda, C. Moberg, *Coord. Chem. Rev.* 249 (2005) 727.
37. **Mesoporous materials**
38. D.W. Breck, *Zeolite Molecular Sieves*, Wiley, New York, 1974.
39. (a) R. M. Barrer, *Hydrothermal Chemistry of Zeolites*, Academic Press, New York, (1982), (b) R. Szostak, *Molecular Sieves: Principles of Synthesis and Identification*, Van Nostrand Reinhold, New York, 1989, (c) M. E. Davis, *Acc. Chem. Res.* 26 (1993) 111. (d) P.G. Schultz, *Angew. Chem. Int. Ed.* 28 (1989) 1283, (e) A. Corma, *Chem. Rev.* 95 (1995) 559, (f) I.W.C.E. Arends, R.A.S., M. Wallau, U. Schuchardt, *Angew. Chem. Int. Ed.* 36 (1997) 1144, (g) J.M. Thomas, *Angew. Chem. Int. Ed.* 38 (1999) 3588.
40. (a) C.T. Kresge, M.E. Leonowicz, W.J. Roth, J.C. Vartuli, J.S. Beck, *Nature* 359 (1992) 710, (b) J.S. Beck, J.C. Vartuli, W.J. Roth, M.E. Leonowicz, C.T. Kresge, K.D. Schmitt, C.T.-W. Chu, D.H. Olson, E.W. Sheppard, S.B. McCullen, J.B. Higgins, J.L. Schlenker, *J. Am. Chem. Soc.* 114 (1992) 10834, (c) T. Yanagisawa,

- T. Shimizu, K. Kuroda, Bull. Chem. Soc. Jpn. 63 (1990) 988, (d) S. Inagaki, Y. Fukushima, K. Kuroda, J. Chem. Soc., Chem. Commun. (1993) 680.
J.M. Thomas, Angew. Chem. Int. Ed. 38 (1999) 3588.
41. A. Taguchi, F. Schuth, Micropor. Mesopor. Mat. 77 (2005) 1.
 42. J.A. Melero, R.V. Grieken, G. Morales, Chem. Rev. 106 (2006) 3790.
 43. P.J. Langley, J. Hulliger, Chem. Soc. Rev. 28 (1999) 279.
 44. D. Zhao, J. Feng, Q. Huo, N. Melosh, G.H. Fredrickson, B.F. Chmelka, G.D. Stucky, Science 279 (1998) 548.
 45. D. Zhao, Q. Huo, J. Feng, B.F. Chmelka, G.D. Stucky, J. Am. Chem. Soc. 120 (1998) 6024.
 46. C.Y. Chen, S.L. Burkett, H.X. Li, M.E. Davis, Microporous Mater. 2 (1993) 27.
 47. A. Monnier, F. Schuth, Q. Huo, D. Kumar, D. Margolese, R.S. Maxwell, G. Stucky, M. Krishnamurty, P. Petroff, A. Firouzi, M. Janicke, B. Chmelka, Science 261 (1993) 1299.
 48. P.T. Tanev, T.J. Pinnavaia, Science 267 (1995) 865.
 49. D.H. Olson, G.D. Stucky, J.C. Vartuli, U.S. Patent, 5, 364, 79 (1994).
 50. A. Firouzi, F. Atef, A.G. Oertli, G.D. Stucky, B.F. Chmelka, J. Am. Chem. Soc. 119 (1997) 3596.
 51. P. Kipkemboi, A. Fogden, V. Alfredsson, K. Flodstrom, Langmuir 17 (2001) 5398.
 52. A. Stein, B. J. Melde, R.C. Schroden, Adv. Mater. 12 (2000) 1403.
 53. (a) S. Inagaki, S. Guan, Y. Fukushima, T. Ohsuma, O. Terasaki, J. Am. Chem. Soc. 121 (1999) 9611, (b) S. Guan, S. Inagaki, T. Ohsuma, O. Terasaki, J. Am. Chem. Soc. 122 (2000) 5660, (c) T. Asefa, M.J. McLachlan, N. Coombs, G.A. Ozin, Nature, 402 (1999) 867, (d) B.J. Melde, B.T. Holland, C.F. Blanford, A. Stein, Chem. Mater. 11 (1999) 3302.

Mesoporous carbon

54. C. Liang, Z. Li, S. Dai, Angew. Chem. Int. Ed. 47 (2008) 2.

Supported Ionic liquids phase catalyst

55. M. Fremantle, Chem. Eng. News 76(1998) 32.
56. C.M. Gordon, J.D. Holbery, A.R. Kennedy, K.R. Seddon, J. Mater. Chem. 8 (1998) 2627.

57. C.P. Mehnert Chem. Eur. J. 11 (2005) 50.
58. A. Riisagera, R. Fehrmann, M. Haumann, P. Wasserscheid, Top. in Catal. 40 (2006) 91.

Catalysis and oxidation reactions

59. Encyclopedia Britannica 2004.
60. G. Centi, F. Cavani, F. Tifiro, Selective oxidation by heterogeneous catalysis, Kulwar Academic, Plenum Publishers, New York, 2001.
61. J. Backvall (Ed), Modern Oxidation Methods, Wiley-VCH, Weinheim, 2004.
62. R.A. Sheldon, R.A. van Saten (Eds), Catalytic Oxidation, Principles and Applications, World Scientific Publishing, Singapore, 1995.

Hybrid materials and catalysis

63. A. P. Wight, M.E. Davis, Chem. Rev. 102 (2002) 3589.
64. (a) K.J. Balkus Jr., A.G. Gabrielov, Journal of inclusion Phenomena and Molecular Recognition in Chemistry 21 (1995) 159, (b) C. Baleiza, H. Garcia, Chem. Rev. 106 (2006) 3987, (c) M. Heitbaum, F. Glorius, I. Escher, Angew. Chem. Int. Ed. 45 (2006) 4732, (d) C.E. Song, S. Lee, Chem. Rev. 102 (2002) 3495, (e) A. Corma, H. Garcia, Chem. Rev. 102 (2002) 3837, (f) P. McMorn, G.J. Hutchings, Chem. Soc. Rev. 33 (2004) 108, (g) D.E. De Vos, M. Dams, B.F. Sels, P.A. Jacobs, Chem. Rev. 102 (2002) 3615.
65. J.A.F. Gamelas, D.V. Evtuguin, A.P. Esculcas, Trans. Metal Chem. 32 (2007) 1061
66. C.N. Kato, A. Tanabe, S. Negishi, K. Goto, K. Nomiya, Chem. Lett. 34 (2005) 2.
67. (a) O.A. Kholdeeva, M.P. Vanina, M.N. Timofeeva, R.I. Maksimovskaya, T.A. Trubitsina, M.S. Melgunov, E.B. Burgina, J. Mrowiec-Bialon, A.B. Jarzebski, C.L. Hill, J. Catal. 226 (2004) 363, (b) A.M. Khenkin, R. Neumann, A.B. Sorokin, A. Tuel, Catal. Lett. 63 (1999) 189, (c) N.K. Kala Raj, S.S. Deshpande, R.H. Ingle, T. Raja, P. Manikandan, Catal. Lett. 98 (2004) 217.
68. W. Kaleta, K. Nowinska, Chem. Commun. (2001) 535.
69. B.J.S. Johnson, A. Stein, Inorg. Chem. 40 (2001) 801.
70. B. Karimi, M.G. Nezhad, J.H. Clark, Org. Lett. 7 (2005) 4.

CHAPTER II

Physicochemical characterization

2.1.	<i>X-ray diffraction</i>	42
2.2.	<i>Inductively coupled plasma – atomic emission spectroscopy</i>	43
2.3.	<i>Energy dispersive X-ray spectroscopy</i>	44
2.4.	<i>Diffuse reflectance UV-Vis spectroscopy</i>	44
2.5.	<i>Fourier transform infrared spectroscopy</i>	45
2.6.	<i>FT-Raman spectroscopy</i>	46
2.7.	<i>Cross-polarization magic angle spinning NMR spectroscopy</i>	46
2.8.	<i>Electron paramagnetic resonance spectroscopy</i>	47
2.9.	<i>X-ray photoelectron spectroscopy</i>	48
2.10.	<i>Scanning electron microscopy</i>	49
2.11.	<i>Transmission electron microscopy</i>	50
2.12.	<i>Atomic force microscope</i>	50
2.13.	<i>Porosity measurements by N₂ sorption</i>	51
2.14.	<i>Temperature programmed reduction (TPR) and oxidation (TPO)</i>	52
2.15.	<i>Thermal analyses</i>	53
2.16.	<i>References</i>	53



2. Physicochemical characterization

The inorganic–organic hybrid materials can be characterized by various techniques, which provide important information about different physicochemical features of the materials. The most extensively used techniques can be categorized into the following.

1. Diffraction techniques

Powder X-ray diffraction (XRD)

2. Spectroscopic techniques

(a) Induced coupled plasma – Atomic emission spectroscopy (ICP-AES), (b) Energy dispersive X-ray spectroscopy (EDAX). (c) Ultraviolet-visible (UV-Vis) spectroscopy, (d) FT-Raman spectroscopy (e) Fourier transform infrared (FT-IR) spectroscopy, (f) Solid state nuclear magnetic resonance (NMR) spectroscopy, (g) Electron paramagnetic resonance (EPR) and (h) X-ray photoelectron spectroscopy (XPS).

3. Microscopic techniques

(a) Scanning electron microscopy (SEM), (b) Transmission electron microscopy (TEM), and (c) Atomic force microscopy (AFM)

4. Volumetric techniques

(a) Porosity measurements by nitrogen (N₂) adsorption (BET method) and (b) Temperature Programmed Reduction (TPR) and Oxidation (TPO)

5. Gravimetric techniques

(a) Thermo gravimetric analyses (TGA) and (b) Differential thermal analysis (DTA)

2.1. X-ray diffraction

It is well recognized that X-ray diffraction, based on wide-angle elastic scattering of X-rays, has been the single most important tool to determine the structure of the materials characterized by long-range ordering. The X-ray diffraction patterns are obtained by measurement of the angles at which an X-ray beam is diffracted by the sample. Bragg's equation relates the distance between two hkl planes (d) and the angle of diffraction (2θ) as: $n\lambda = 2d\sin\theta$, where λ = wavelength of X-rays, n = an integer known as the order of reflection (h , k and l represent Miller indices of the respective planes). From the diffraction patterns, the uniqueness of mesoporous structure, phase purity,

degree of crystallinity and unit cell parameters of the semicrystalline hybrid materials can be determined.

The identification of phase is based on the comparison of the set of reflections of the sample with that of pure reference phases distributed by International Center for Diffraction Data (ICDD). Unit cell parameter (a_0) of a cubic lattice can be determined by the following equation: $a_0 = d_{hkl} \sqrt{h^2 + k^2 + l^2}$, where d = distance between two consecutive parallel lattice planes having Miller indices h , k and l . The average crystallites size of the nanoparticles can be estimated using the Debye-Scherrer equation: $D = k\lambda / \beta \cos\theta$, where D = thickness of the nanocrystal, k is a constant, λ = wavelength of X-rays, β = width at half maxima of (111) reflection at Bragg's angle 2θ [1-4].

SAXS patterns of the samples were obtained in reflection mode with a Philips X'Pert Pro 3040/60 diffractometer using $\text{CoK}\alpha$ radiation ($\lambda = 0.17890$ nm), an iron filter, and an X'celerator as a detector. XRD pattern of the samples at wide-angle region was measured on Rigaku Model D/MAXIII VC, Japan, $\lambda = 1.5418$ Å with Ni filtered Cu-K α radiation.

2.2. Inductively coupled plasma – atomic emission spectroscopy

ICP-AES is an emission spectrophotometric technique, exploiting the fact that excited electrons emit energy at a given wavelength as they return to ground state. The fundamental characteristic of this process is that each element emits energy at specific wavelengths peculiar to its chemical character. Although each element emits energy at multiple wavelengths, in the ICP-AES technique it is most common to select a single wavelength (or a very few) for a given element. The intensity of the energy emitted at the chosen wavelength is proportional to the amount (concentration) of that element in the analyzed sample. Thus, by determining which wavelengths are emitted by a sample and by determining their intensities, the analyst can quantify the elemental composition of the given sample relative to a reference standard. ICP-OES, is one method of optical emission spectrometry. When plasma energy is given to an analysis sample from outside, the component elements (atoms) are excited. When the excited atoms return to low energy position, emission rays (spectrum rays) are released and the emission rays that correspond to the photon wavelength are measured. The element type is determined

based on the position of the photon rays, and the content of each element is determined based on the ray's intensity. ICP-OES analysis was done on Perkin-Elmer Optima 2000 DV with Winlab software instrument. Standard solutions were used for calibration. This instrument can analyze aqueous solutions for metals with either a Radial or an axial plasma configuration. In Axial mode, you can generally achieve a 5-10 ppb detection limit, depending upon the element [5].

2.3. Energy dispersive X-ray spectroscopy

Energy dispersive X-ray spectroscopy (EDS or EDX) is an analytical technique used for the elemental analysis or chemical characterization of a sample. As a type of spectroscopy, it relies on the investigation of a sample through interactions between electromagnetic radiation and matter, analyzing X-rays emitted by the matter in response to being hit with the electromagnetic radiation. Its characterization capabilities are due in large part to the fundamental principle that each element has a unique atomic structure allowing X-rays that are characteristic of an element's atomic structure to be identified uniquely from each other [6].

For microstructural analyses a modern Leica Stereoscan-440 SEM equipped with Phoenix EDAX, is used. A high stability of the electron beam was achieved by a Schottky field emission gun. The producer indicates a resolution of 1 nm (at 20 kV).

2.4. Diffuse reflectance UV-Vis spectroscopy

UV-Vis spectroscopy deals with the study of electronic transitions between orbitals or bands of atoms, ions or molecules in gaseous, liquid and solid state. In the case of transition metal ions or atoms, any change in their coordination sphere may affect their optical properties and therefore can be characterized by UV-Vis. For solid substances like transition metal containing mesoporous materials, diffuse reflectance UV-Vis spectroscopy (DRUV-Vis) is applied to determine the ligand field symmetry and oxidation state of the metal inside the solid matrices. Thus DRUV-Vis is a sensitive probe to examine the type of the sites, framework or extra-framework, in which that metal ion or cluster exist. DRS is also a suitable technique for studying the speciation of

supported metal complexes and heteropoly acids because it measures both their d-d transitions and charge transfer bands.

Diffuse reflectance spectroscopy (DRS) is a spectroscopic technique based on the reflection of light in the ultraviolet (UV), visible (VIS) and near-infrared (NIR) region by a powdered sample. In a DRS spectrum, the ratio of the light scattered from an “infinitely thick” closely packed catalyst layer and the scattered light from an infinitely thick layer of an ideal non-absorbing (white) reference sample is measured as a function of the wavelength λ . The scattered radiation, emanating from the sample, is collected in an integration sphere and detected. The most popular continuum theory describing diffuse reflectance effect is Schuster-Kubelka-Munk (SKM) theory. If the sample is infinitely thick, the diffuse reflection of the sample (R_∞) is related to an apparent absorption (K) and apparent scattering coefficient (S) by the SKM equation [7, 8]:

$$F(R_\infty) = (1-R_\infty)^2 / 2R_\infty = K/S \quad (2.1)$$

At low concentrations of supported transition metal ions (TMI), this equation is a good representation of the absorbing spectrum and allows a quantitative determination of the TMI.

$$F(R_\infty) = (1-R_\infty)^2 / 2R_\infty = K/S = \alpha C_{\text{TMI}} / S = k C_{\text{TMI}} \quad (2.2)$$

At a given wavelength λ , S is constant, the above equation gives a linear relation between $F(R_\infty)$ and the TMI concentration, C_{TMI} . The coefficients α and k are proportionality constants.

Diffuse reflectance UV-Vis (DRUV-vis) spectra of catalyst samples were obtained using a Shimadzu UV-2101 PC spectrometer equipped with a diffuse-reflectance attachment, with BaSO_4 as the reference. The reflectance spectra were converted into the Kubelka-Munk function, $F(R)$, which is proportional to the absorption coefficient for low values of $F(R)$. The spectra were measured in the range of 200-800 nm in air at room temperature.

2.5. Fourier transform infrared spectroscopy

Fourier transform infrared (FT-IR) spectroscopy deals with the vibration of chemical bonds in a molecule at various frequencies depending on the elements and types

of bonds. After absorbing electromagnetic radiation the frequency of vibration of a bond increases leading to transition between ground state and several excited states. The energy corresponding to these transitions corresponds to the infrared region (4000–400 cm^{-1}) of the electromagnetic spectrum. The term Fourier transform (FT) refers to a recent development in the manner in which the data are collected and converted from an interference pattern to an infrared absorption spectrum that is like a molecular "fingerprint"[9]. FT-IR and diffuse reflectance IR (DRIFT) experiment has been performed using Shimadzu FT-IR-8201PC equipment.

2.6. FT-Raman spectroscopy

Raman spectroscopy is based on the inelastic scattering of photons, which lose energy by exciting vibrations in the sample. A vibration is Raman active if it changes the polarizability of the molecule. Raman and infrared spectroscopy complement each other, in particular for highly symmetrical molecules.

The Raman spectrometer (The Brücker FRA106) is equipped with a Nd: YAG (Neodymium: Yttrium Aluminium Garnet) Laser that is frequency doubled to 532 nm. The laser was operated at a power level of 20 mW measured at the sample with a power meter. The spectra have been collected at room temperature in the wavelength range from 0 to 4000 cm^{-1} . The spectral resolution of the spectrometer is 5 cm^{-1} . Sampling times were between 20 to 25 min. The electrons are generated by thermionic emission from a metal filament, and accelerated to ~25 keV. A system of electrical and magnetic field 'optics' is used to focus the beam to a spot ~10 nm in diameter on the sample surface.

2.7. Cross-polarization magic angle spinning NMR spectroscopy

Nuclear magnetic resonance (NMR) spectroscopy is one of the most powerful tools to investigate structure and dynamics of a molecular system in liquid phase. Atomic nuclei consisting of odd number of protons and/or neutrons possessing a nuclear spin $I \neq 0$ and consequently a magnetic moment $\mu = \gamma \hbar I$ ($\gamma =$ gyromagnetic ratio), when placed in a magnetic field of strength B_0 , Zeeman interaction results in quantized orientations of the nuclear magnetic moments. The nucleus can adopt $2I + 1$ Eigen states with energies $E(m)$

$= -m\gamma\hbar B_0$, where $m = (I, I-1, \dots, -I)$. Transitions between neighboring energy states ($\Delta m = \pm 1$) can be induced by electromagnetic radiation (energy $E = h\nu$) of frequency $\nu_0 = \gamma B_0/2\pi$. The chemical shift interaction arises from secondary local magnetic fields induced by the interaction of the electrons surrounding the nucleus. The induced local field opposes B_0 and hence shields the nucleus under observation. The shielding is spatially anisotropic due to the nonspherical electron distribution around the nucleus.

In solid-state NMR, the line shape is determined by dipolar and quadrupolar interactions. The lines are usually broader because the rigid structure of the solid phase prevents the averaging of the dipolar interaction by motions. Since, the first order quadrupolar and dipolar interactions are proportional to $(3 \cos^2\theta - 1)$, where, θ is the angle between an internuclear vector and the magnetic field, these interactions can be removed, to a first order approximation, by spinning the sample around the so-called magic angle β with respect to the external magnetic field, for which $3 \cos^2\beta - 1 = 0$, i.e. $\beta = 54.74^\circ$. This technique is known as Magic Angle Spinning (MAS) [10, 11].

Cross-polarization (CP) involves indirect excitation of the less abundant nucleus through magnetization transfer from an abundant spin system (e.g. ^1H). [12, 13]. i.e., the signal to noise ratio (SNR) of the spectra of nuclei with low natural abundance (e.g. ^{13}C , ^{29}Si , ^{31}P etc.), and to monitor the spatial proximity of nuclei. CP technique does not affect the line width of the spectra, but is applied to improve the sensitivity.

^{31}P CP-MAS, ^1H MAS NMR and ^{51}V MAS NMR has been performed on Bruker DSX-300 MHz spectrometer and ^{29}Si -MAS NMR on Bruker DRX-500 MHz spectrometer. ^{31}P CP-MAS NMR was recorded at 121.5 MHz with high power decoupling with a Bruker 4 mm probehead. The spinning rate was 10 kHz and the delay between two pulses was varied between 1 and 30 s to ensure that a complete relaxation of the ^{31}P nuclei occurred. The chemical shifts are given relative to external 85% H_3PO_4 .

2.8. Electron paramagnetic resonance spectroscopy

Electron Paramagnetic Resonance (EPR), often called Electron Spin Resonance (ESR), is a branch of spectroscopy in which electromagnetic radiation (usually of microwave frequency) is absorbed by molecules, ions, or atoms possessing electrons with

unpaired spins, *i.e.* electronic spin $S > 0$. EPR is similar to Nuclear Magnetic Resonance (NMR). In both EPR and NMR, the sample material is immersed in a strong static magnetic field and exposed to an orthogonal low- amplitude high-frequency field. ESR usually requires microwave-frequency radiation (GHz), while NMR is observed at lower radio frequencies (MHz). With ESR, energy is absorbed by the sample when the frequency of the radiation is appropriate to the energy difference between two states of the electrons in the sample, but only if the transition satisfies the appropriate selection rules. In EPR, because of the interaction of the unpaired electron spin moment (given by two projections, $m_s = \pm 1/2$, for a free electron) with the magnetic field, the so-called Zeeman effect, there are different projections of the spin gain different energies.

$$E_{ms} = gm_B B_0 m_s \quad (2.3)$$

Here, B_0 is the field strength of the external magnetic field. The SI units for magnetic field is tesla, T, but, historically in EPR, gauss (1 G = 0.0001 T) is still used. Other terms in Eq.(2.3): m_s - is a spin projection on the field ($m_s = \pm 1/2$ for a free electron), m_B is the Bohr magneton.[14,15]

EPR spectra were recorded on a Bruker EMX spectrometer operating at X band frequency and 100-kHz field modulation. Measurements at variable temperatures were done using a Bruker BVT 3000 temperature controller.

2.9. X-ray photoelectron spectroscopy

X-ray photoelectron spectroscopy (XPS) is widely used for probing the electronic structure of atoms, molecules and condensed matter. When an X-ray photon of energy $h\nu$ is incident on a solid matter, the kinetic energy (E_k) and the binding energy (E_b) of the ejected photoelectrons can be related as follows: $E_k = h\nu - E_b$.

This kinetic energy distribution of the photoelectrons is fabricated by a series of discrete bands, which symbolizes for the electronic structure of the sample. The core level binding energies of all the elements (other than H and He) in all different oxidation states are unique, which provides instant detection of the chemical composition of the sample after a full range scan. However, to account for the multiplet splitting and

satellites accompanying the photoemission peaks, the photoelectron spectra should be interpreted in terms of many-electron states of the final ionized state of the sample, rather than the occupied one-electron states of the neutral species [16,17].

XPS spectra were recorded on a VG Microtech Multilab-ESCA 3000 spectrometer equipped with a twin anode of Al and Mg. All measurements were carried out using Mg-KP X-ray at room temperature. Base pressure in the analysis chamber was 4×10^{-10} Torr. Multichannel detection system with nine channels was employed to collect the data. The overall energy resolution of the instrument was better than 0.7 eV, determined from the full width at half maximum of the $4f_{7/2}$ core level of gold surface. The errors in all the B.E. values were within ± 0.1 eV. The binding energy correction was performed using the C_{1s} peak of carbon at 284.9 eV as the reference.

2.10. Scanning electron microscopy

Scanning electron microscopy (SEM) is an important tool for morphological characterization of mesoporous molecular sieve materials. A scanning electron microscope can generate an electron beam scanning back and forth over a solid sample. The interaction between the beam and the sample produces different types of signals providing detailed information about the surface structure and morphology of the sample. When an electron from the beam encounters a nucleus in the sample, the resultant Coulombic attraction leads to a deflection in the electron's path, known as Rutherford elastic scattering. A fraction of these electrons will be completely backscattered, reemerging from the incident surface of the sample. Since the scattering angle depends on the atomic number of the nucleus, the primary electrons arriving at a given detector position can be used to produce images containing topological and compositional information [18,19].

The high-energy incident electrons can also interact with the loosely bound conduction band electrons in the sample. However, the amount of energy given to these secondary electrons as a result of the interactions is small, and so they have a very limited range in the sample. Hence, only those secondary electrons that are produced within a very short distance from the surface are able to escape from the sample. As a result, high-resolution topographical images can be obtained in this detection mode.

The morphology of the catalytic material was determined by JEOL-JSM-5200 SEM with a resolution of 5.5 nm.

2.11. Transmission electron microscopy

Transmission electron microscopy (TEM) is typically used for high resolution imaging of thin films of a solid sample for microstructural and compositional analysis. The technique involves: (i) irradiation of a very thin sample by a high-energy electron beam, which is diffracted by the lattices of a crystalline or semicrystalline material and propagated along different directions, (ii) imaging and angular distribution analysis of the forward-scattered electrons (unlike SEM where backscattered electrons are detected), and (iii) energy analysis of the emitted X-rays. The topographic information obtained by TEM in the vicinity of atomic resolution can be utilized for structural characterization and identification of various phases of mesoporous materials, *viz.*, hexagonal, cubic or lamellar. TEM also provides real space image on the atomic distribution in the bulk and surface of a nanocrystal [20, 21].

Formation of mesoporous materials was detected by TEM (JEOL Model 1200 EX instrument operated at an accelerating voltage at 120 kV). Samples were prepared by placing droplets of a suspension in isopropanol on a polymer microgrid supported on a Cu grid for TEM measurements.

2.12. Atomic force microscope

The atomic force microscope (AFM) or scanning force microscope (SFM) is a very high-resolution type of scanning probe microscope, with demonstrated resolution of fractions of a nanometer, more than 1000 times better than the optical diffraction limit. The AFM is one of the foremost tools for imaging, measuring and manipulating matter at the nanoscale [22].

The agglomerate-like morphology of the material was studied by AFM in the contact mode on a VEECO Digital instruments multimode scanning probe microscope equipped with a nanoscope IV controller. According to the interaction of the tip and the

sample surface, the AFM can be classified as repulsive or Contact mode and attractive or Non-contact mode.

2.13. Porosity measurements by N₂ sorption

Despite of some theoretical limitations, the Brunauer-Emmett-Teller (BET) method continues to be the most widely used method for the evaluation of surface area, pore volumes and pore size distributions of porous solids from N₂ physisorption isotherm data. The BET equation can be represented as follows:

$$\frac{p}{v(p_0 - p)} = \frac{1}{v_m c} + \frac{c - 1}{v_m c} \frac{p}{p_0}$$

where, v = volume of N₂ adsorbed by the sample under pressure p , p_0 = saturated vapor pressure at the same temperature, v_m = volume of N₂ adsorbed when the surface is covered with a unimolecular layer, and c = constant for a given adsorbate.

The equation suggests that the plot of $\frac{p}{v(p_0 - p)}$ versus $\frac{p}{p_0}$ should be linear, and

from the intercept $\frac{1}{v_m c}$ and slope $\frac{c - 1}{v_m c}$, the values of v_m and c can be determined as

follows: $v_m = (\text{slope} + \text{intercept})^{-1}$.

Thus the specific surface area (S) of a sample can be determined as follows:

$S = \frac{N_0 v_m A}{22414m}$, where N_0 = Avogadro number, m = amount of solid adsorbent, A = cross-section of the gas molecules (16.2 Å² for N₂), and S is expressed in cm² g⁻¹ unit.

Several computational procedures are available for the derivation of pore size distribution of mesoporous samples from physisorption isotherms. Most popular among them is the Barrett-Joyner-Halenda (BJH) model, which is based on speculative emptying of the pores by a stepwise reduction of p/p_0 , and allowance being made for the contraction of the multilayer in those pores already emptied by the condensate. The mesopores size distribution is usually expressed as a plot of $\Delta V_p/\Delta r_p$ versus r_p , where V_p = mesopore volume, and r_p = pore radius. It is assumed that the mesopores volume is completely filled at high p/p_0 .

The BET surface area of samples were measured with an Omnisorb 100CX (Coulter, USA) system under liquid N₂ temperature, using N₂ as an adsorbent. Sample was outgassed at 523 K for 2-3 h under helium before subjecting the sample for N₂-adsorption. The isotherms were analyzed in a conventional manner in the region of the relative pressure, $p/p_0 = 0.05$ to 0.3. The BJH method was used to determine the area of the pore walls and uses the Kelvin equation to correlate the partial pressure of nitrogen in equilibrium with the porous solid to the size of the pores where capillary condensation takes place. The pore size distribution is obtained by analysis of the desorption isotherm [23, 24].

2.14. Temperature programmed reduction (TPR) and oxidation (TPO)

Temperature-programmed reduction (TPR) has proved a powerful tool to analyze the reduction kinetics of oxidic catalyst precursors. This technique consists of heating the catalyst with a linear temperature ramp in a flow of hydrogen while monitoring the hydrogen consumption. Similarly, the oxidation behavior of a catalyst can be studied by temperature-programmed oxidation (TPO) experiments. The advantage of this method which uses oxygen as reactant is that it allows one to monitor the oxygen uptake directly. TPR experiments are sometimes complemented with TPO experiments in order to study the reversibility of reduction/reoxidation cycles. However, structural changes of the catalyst which may occur when heating to elevated temperatures in a hydrogen atmosphere have to be avoided.

The reducibility of the calcined catalysts was measured by TPR method with Micromeritics AutoChem 2910 instrument. About 300 mg of the catalyst was mounted in a quartz tube and calcined in argon flow at 500 °C for 1 h (temperature-programmed rate of 10 °C min⁻¹) with the aim to remove the substances physisorbed. It is then cooled to ambient temperature in argon prior to the reduction by a mixing gas of hydrogen and helium (5% H₂ in volume percentage). In the H₂-TPR analysis, the heating rate was 10 °C min⁻¹ and the gas flow was 10 ml min⁻¹. The cold trap consisted of liquid nitrogen and 2-propanol. The hydrogen consumed during the reduction was detected by a thermal conductivity detector [25].

2.15. Thermal analyses

Thermo analytical techniques involve the measurement of the response of the solid under study (energy or mass released or consumed) as a function of temperature (or time) dynamically by the application of a linear temperature program. Thermogravimetry (TG) is a technique, which measures the variation in mass of a sample when it undergoes temperature scanning in a controlled atmosphere. Differential thermal analysis (DTA) is a technique, which measures the difference in temperature between a sample and a reference (a thermally inert material) as a function of time or temperature, when they undergo temperature scanning in a controlled atmosphere. DTA method enables any transformation to be detected for all the categories of materials, providing information on exothermic and endothermic reactions taking place in the sample, which include phase transitions, dehydration, decomposition, redox, or solid-state reactions. In catalysis, these techniques are used to study the genesis of catalytic materials via solid-state reactions. Differential thermal analysis (DTA) measurements of samples were performed on a Pyris Diamond TG-DTA apparatus from room temperature to 1000 °C in flowing dry oxygen (ca. 50 ml min⁻¹), using α -Al₂O₃ as reference. In each experiment, 5-8 mg of the sample was used with a heating rate of 20 °C min⁻¹ [26].

2.16. References

1. W.H. Bragg, W.L. Bragg, *The Crystalline State*, Vol. 1, McMillan, New York, 1949.
2. S. Biz, M. Occelli, *Catal. Rev. Sci. Eng.*, 40(1998) 329.
3. G. Bergeret, *Handbook of Heterogeneous Catalysis*. Vol. 2, Eds: G. Ertl, H. Knozinger, J. Weitkamp, Wiley-VCH, Weinheim, 1997.
4. R.C. Rau *Advances in X-Ray Analysis*, Vol. 5, Ed: W.M. Mueller, Sir Isaac Pitman and Sons Ltd., London, 1962.
5. A. Montaser, D.W. Golightly, (eds). *Inductively Coupled Plasmas in Analytical Atomic Spectrometry*, VCH Publishers, Inc., New York, 1992.
6. Garratt-Reed, A.J. Bell, *Energy Dispersive X-ray Analysis in the Electron*

- Microscope, Edi 1, BIOS scientific publisher, 2003.
7. B.M. Weckhuysen, R.A. Schoonheydt, *Catal. Today* 49 (1999) 441.
 8. R.A. Schoonheydt, *Diffuse Reflectance Spectroscopy*, Chapter 4, *Characterization of Heterogeneous Catalysts*, F. Delannay (Ed.), Marcel Dekker, New York, 1984.
 9. P.R. Griffiths, J.A. De Haseth, *Fourier Transform Infrared Spectrometry*, John Wiley and Sons Inc., New York, 1986.
 10. W.W. Paudler, *Nuclear Magnetic Resonance: General Concepts and Applications*, John Wiley and Sons Inc., New York, 1987.
 11. M. Mehring, *High Resolution NMR Spectroscopy in Solids*, Springer-Verlag, Berlin, 1976.
 12. G. Engelhardt, D. Michel, *High-Resolution Solid-State NMR of Silicates and Zeolites*, John Wiley and Sons Ltd., Chichester, 1987.
 13. G. Engelhardt, *Handbook of Heterogeneous Catalysis*, Vol. 2, Eds: G. Ertl, H. Knozinger, J. Weitkamp, Wiley-VCH, Weinheim, 1997.
 14. S.A. Altshuler, B.M. Kozirev, *Electron Paramagnetic Resonance*. Academic, New York, 1964
 15. J.E. Wertz, J.R. Bolton, *Electron Spin Resonance: Elementary Theory and Practical Applications*. McGraw-Hill, New York, 1972
 16. C.S. Fadley, *Electron Spectroscopy: Theory, Techniques and Applications*, Vol. 2, Eds: C.R. Brundle, A. D. Baker, Academic Press, New York, 1978.
 17. W.N. Delgass, T.R. Hughes, C.S. Fadley, *Catal. Rev.* 4 (1970) 179.
 18. G. Lawes, *Scanning Electron Microscopy And X-Ray Microanalysis*, John Wiley and Sons Ltd., Chichester, 1987.
 19. D.E. Newbury, D.C. Joy, P. Echlin, C.E. Fiori, J.I. Goldstein, *Advanced Scanning Electron Microscopy and X-Ray Microanalysis*, Plenum Press, New York, 1986.
 20. J.R. Fryer, *Chemical Applications of Transmission Electron Microscopy*, Academic Press, San Diego, 1979.
 21. (a) J.M. Thomas, O. Terasaki, P.L. Gai, W. Zhou, J. Gonzalez-Calbet, *Acc. Chem. Res.* 34 (2001) 583. (b) V. Alfredsson, M. Keung, A. Monnier, G.D. Stucky, K.K. Unger, F. Schuth, *J. Chem. Soc., Chem. Commun.* (1994) 921
 22. S.J. Hill (Ed.) *Inductively Coupled Plasma Spectrometry and its Applications*, Edi.

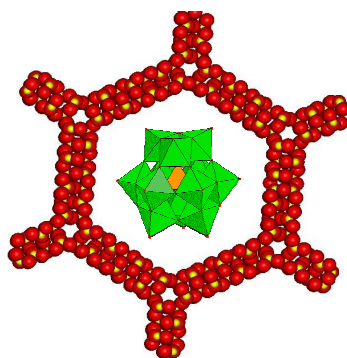
- 2, Wiley-Blackwell 2007.
23. S. Brunauer, P.H. Emmett, E. Teller, J. Am. Chem. Soc. 60 (1938) 309.
24. E.P. Barrett, L.G. Joyner, P.P. Halenda, J. Am. Chem. Soc. 73 (1951) 373.
25. J.J. Spivey, Catalysis, R.S.C. Vol 16, 2002.
26. P. Gabbott (Ed.) Principles and Applications of Thermal analysis, Wiley-Blackwell, 2007.

CHAPTER III

Inorganic-organic hybrid materials based on Polyoxometalates

This chapter features the following sections:

3.1.1.	<i>Section A1</i>	56
3.1.2.	<i>Section A2</i>	78
3.2.	<i>Section B</i>	90
3.3.	<i>Section C</i>	108



3.1. Section A1

3.1.1. Selective oxidation of anthracene using inorganic-organic hybrid materials based on molybdovanadophosphoric acids

3.1.1.1. Introduction

Immobilization and encapsulation of metal complexes or polyoxometalates (POMs) in mesoporous solids are the approaches to designing and fabricating catalyst systems that give nearly 100% selectivity to the desired product without sacrificing activity and while using less energy [1]. In constrained environments, the active POMs lose some of the degrees of freedom that they had in the bulk state, adopt a particular geometry, hook onto the functional groups available on the support surfaces, change their coordination sphere geometry, and relax or restrict their sphere of influence, depending on whether or not they reside inside the channels of the mesoporous supports. Thus, they exhibit improved reactivity so as to promote the reaction in sterically controlled pathways [2]. Recent reports have described the immobilization of POMs and transition metal substituted POMs on various supports, including silica, carbon, mesoporous silica MCM-41, and SBA-15, through an organic linker, and explored their use in various organic transformations [3–14].

Intense interest has been focused on the anthraquinone (AQ) derivatives due to their potential utility in cancer chemotherapy as antioxidants and antitumor agents. 9,10-Anthraquinone is the most important quinone derivative of anthracene (AN) [15–24]; its most widespread use is as a H₂ carrier in the industrial production of H₂O₂ [25,26]. It is commercially produced in several ways, including oxidation of AN with chromic acid [27], condensation of benzene with phthalic anhydride, and through the Diels–Alder reaction [28]. Vapor-phase oxidation of AN by air has been carried out over a supported iron vanadate–potassium catalyst at 390 °C [27]. Consequently, there is a need to develop cost-effective liquid-phase oxidation catalysts for selective oxidation of AN to AQ. AQ is the parent substance of a large class of dyes and pigments [29]. It is also used in the paper industry, and molecular switches have been synthesized for use in the electronic devices [30–36].

Over the last two decades, a number of homogeneous catalyst systems have been used for the oxidation of AN. Because of the drawbacks of homogeneous catalyst systems, polymeric metal chelates, immobilized enzymes, and supported vanadium POM ($\text{H}_5\text{PV}_2\text{Mo}_{10}\text{O}_{40}\cdot 32.5\text{H}_2\text{O}$) have been studied for the oxidation of AN. Here we report our results on immobilized catalyst systems that are atom-efficient and eco-friendly for the oxidation of AN to AQ. The impulsion for this research is twofold: (1) to investigate the effect of the immobilization of POMs on mesoporous inorganic supports through an organic linker for functioning as heterogeneous catalyst and (2) to develop a catalyst system for the selective oxidation of AN to AQ.

3.1.1.2. Experimental

3.1.1.2.1. Chemicals

Adamantane, TEOS, P123 block copolymer (poly(ethyleneglycol)-poly(propylene glycol)-poly(ethylene glycol), average molecular mass 5800 and fumed silica were procured from Aldrich. Sodium hydrogen phosphate, sodium metavanadate, sodium molybdate (dehydrated), sulfuric acid, hydrochloric acid, sodium hydroxide, anthracene, anthroquinone, anthrone and oxanthrone were obtained from Merck (India) Ltd., Mumbai. CTAB was purchased from Loba Chemie and SD Fine chemicals Ltd. respectively. 70% aqueous TBHP has procured from Acros organics. Sodium hydrogen phosphate, sodium tungstate, sodium metavanadate, sodium molybdate (dehydrated), sulfuric acid, hydrochloric acid, were procured from Loba Chemie. Pvt.Ltd, molybdophosphoric acid ($\text{H}_3\text{Mo}_{12}\text{O}_{40}\text{P}\cdot x\text{H}_2\text{O}$), silicotungstic acid ($\text{H}_3\text{W}_{12}\text{O}_{40}\text{Si}\cdot x\text{H}_2\text{O}$), tungstophosphoric acid ($\text{H}_3\text{W}_{12}\text{O}_{40}\text{P}\cdot x\text{H}_2\text{O}$) were purchased from S.D. Fine Chemical.Ltd. –Mumbai-India, and 30% aq. H_2O_2 has been procured from Ranbaxy. All chemicals used were of research grade and used as received without further purification.

3.1.1.2.2. Catalysts preparation

3.1.1.2.2.1. MCM-41 (Mobil Composition of Mater): The pure siliceous MCM-41 material was prepared as described in the literature [2]. The gel composition used for preparing Si-MCM-41 material was 10 SiO_2 : 5.4 $\text{C}_n\text{H}_{2n+1}(\text{CH}_3)_3\text{NBr}$: 4.25 Na_2O : 1.3 H_2SO_4 : 480 H_2O . C_{16} -MCM-41 is prepared using CTABr (32.0 g) and 115 g of water and this mixture was stirred for 30 min at room temperature. Sodium silicate solution (37.4 g) was added drop wise to the surfactant solution under vigorous stirring for another 30 min.

Then 2.4 g of H₂SO₄ in 10 g of water was added to the above mixture and the stirring was continued for another 30 min. The resulting gel was transferred into a polypropylene bottle and kept in an oven at 373 K for 24 h. After cooling to room temperature, the resultant solid was recovered by filtration, washed with distilled water and dried in an oven at 373 K for 6 h. Finally the material was calcined in a muffle furnace at 813 K for 10 h to give MCM-41 [37].

3.1.1.2.2.2. MCM-48: MCM-48 was synthesized by the conventional hydrothermal pathway by following the procedure described in literature [3,4]. The molar composition of the gel was 1 TEOS: 0.25 Na₂O: 0.65 C₁₆H₃₃(CH₃)₃NBr: 0.62 H₂O. CTABr (31.2 g) was dissolved in (93.6 g) deionized water at 318 K and stirred for 40 min. Then TEOS (30 g) followed by sodium hydroxide (69 g, 1 M) solution were added to the above mixture and the stirring was continued for another 1 h at room temperature. The resulting gel was transferred into a polypropylene bottle and kept in an oven at 373 K for 72 h under static condition. After cooling to room temperature, the solid was recovered by filtration, washed with ethanol followed by distilled water and dried in an air oven at 373 K for 6 h. Finally, the material was calcined in a muffle furnace at 813 K for 10 h to give MCM-48 [37].

3.1.1.2.2.3. SBA-15 (Santa Barbara Amorphous): SBA-15 was synthesised with a gel composition of 4 g Polymer: 0.041 TEOS: 0.24 HCl: 6.67 H₂O as per literature procedure [5,6]. In a typical synthesis, amphiphilic triblock copolymer poly(ethylene glycol)-block-poly(propylene glycol)-block-poly(ethylene glycol), average molecular weight = 5800 (4 g) was dispersed in 30 g of water and stirred for 4 h. Then, 120 g of 2 M HCl solution was added and stirred for 2 h. To this homogeneous solution, 8.54 g of TEOS was added under stirring. The resulting gel was aged at 313 K for 24 h and finally heated to 373 K for 48 h. After synthesis, the solid was filtered, washed with distilled water and dried in an air oven at 373 K for 5 h followed by calcination at 813 K to remove the triblock-copolymer and obtain a white powder [38].

3.1.1.2.2.4. Synthesis of 11-Molybdo-1-Vanadophosphoric acid, H₄[PMO₁₁VO₄₀] 32.5H₂O: NaHPO₄, 7.1 g, was dissolved in 100 mL of water and mixed with 6.1 g of sodium metavanadate that had been dissolved by boiling in 100 mL of water. The mixture was cooled and acidified to a red color with 5 mL of concentrated sulfuric acid.

To this mixture was added a solution of 133 g of $\text{Na}_2\text{MoO}_4 \cdot 2\text{H}_2\text{O}$ dissolved in 200 mL of water. Finally, 85 mL of concentrated sulfuric acid was added slowly with vigorous stirring of the solution. With this addition the dark red color changed to a lighter red. The heteropoly acid was then extracted with 400 mL of ethyl ether after the water solution was cooled. In this extraction, the heteropoly etherate was present as a middle layer; the bottom layer (water) was yellow and probably contained vanadyl species. After separation, a stream of air was passed through the heteropoly etherate layer to free it of ether. The orange solid that remained was dissolved in 50 mL of water, concentrated to the first appearance of crystals in a vacuum dessicator over concentrated sulfuric acid, and then allowed to crystallize further. The orange crystals that formed were filtered, washed with water and air-dried. The crystalline acid effloresces slowly at room temperature; thus the amount of water of crystallization varied slightly from sample to sample. The yield was 27 g. Analytical cal: P: 1.31; Mo: 44.52; V: 2.65:H₂O (based on Mo) 24.82.

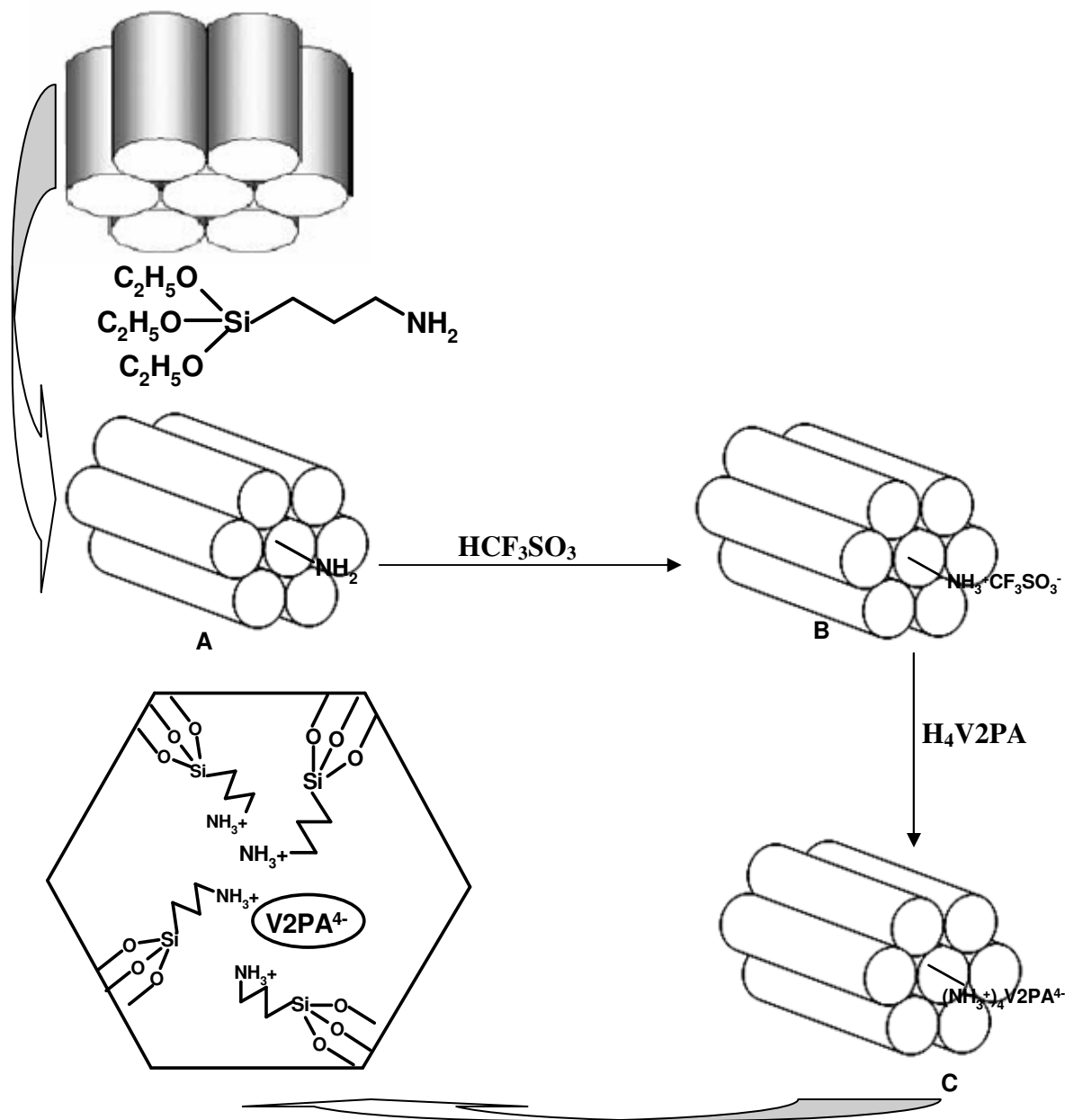
3.1.1.2.2.5. Synthesis of 10-Molybdo-2-Vanadophosphoric acid, $\text{H}_5[\text{PMo}_{10}\text{V}_2\text{O}_{40}] \cdot 32.5\text{H}_2\text{O}$: Sodium metavanadate, 24.4 g, was dissolved by boiling in 100 mL of water and then mixed with 7.1 g of Na_2HPO_4 in 100 mL of water. After the solution was cooled, 5 mL of concentrated sulfuric acid was added, and the solution developed a red color. Then addition of 121 g of $\text{Na}_2\text{MoO}_4 \cdot 2\text{H}_2\text{O}$ dissolved in 200 mL of water was added to the above solution. While the solution was vigorously stirred, 85 mL of concentrated sulfuric acid was added slowly, and the hot solution was allowed to cool to room temperature. The 10-molybdo-2-vanadophosphoric acid was then extracted with 500 mL of ethyl ether. Air was passed through the heteropoly etherate (bottom layer) to free it of ether. The solid remaining behind was dissolved in water, concentrated to first crystal formation, as already described, and then allowed to crystallize further. The large red crystals that formed were filtered, washed with water, and air-dried. The yield was 34 g. analytical cal: P:1.32; Mo:40.62; V:4.67. H₂O (based on Mo) 26.28.

3.1.1.2.2.6. Synthesis of 9-Molybdo-3-Vanadophosphoric acid, $\text{H}_6[\text{PMo}_9\text{V}_3\text{O}_{40}] \cdot 34\text{H}_2\text{O}$: Na_2HPO_4 , 7.1 g, was dissolved in 50 mL of water and mixed with 36.6 g of sodium metavanadate that had been dissolved by heating in 200 mL of water. After 5 mL of concentrated sulfuric acid and added to the cooled mixture, it attained a cherry red

color. This solution was mixed with 54.5 g of $\text{Na}_2\text{MoO}_4 \cdot 2\text{H}_2\text{O}$ dissolved in 150 mL of water, and while it was being vigorously stirred, 85 mL of concentrated sulfuric acid was then slowly added. The hot solution was allowed to cool to room temperature. The free acid was extracted with 400 mL of ethyl ether, the heteropoly etherate being the middle layer. The etherate was freed of ether when a stream of air was passed through the solution. The red solid remaining was dissolved in 40 mL of water and concentrated to crystal formation in a vacuum desiccator over concentrated sulfuric acid. The red crystals were filtered and washed with water. The yield was 6.9 g. The solid effloresces slowly at room temperature. Analytical cal: P:1.34; Mo:38.72; V:5.51. H_2O (based on Mo) 7.11 [39].

3.1.1.2.2.7. Amine-functionalized SBA-15: Surface modification of SBA-15 by (3-aminopropyl) triethoxysilane (APTES) was carried out using a grafting method following the reported procedure [58]. In a typical preparation, freshly activated SBA-15 (2 g) was refluxed with 50 mL of toluene (distilled over sodium and dried) to remove occluded moisture azeotropically for 4 h. To this APTES (1 g) in 10 mL of toluene was added and stirred under reflux condition for 4 h. After distilling off solvent, solid was filtered, washed in a Soxhlet apparatus with dichloromethane, and then dried at room temperature. Product is designated as $\text{NH}_2\text{-SBA-15}$. Nitrogen elemental analysis estimated showed the content of 2.2 mmol of NH_2 per gram of $\text{NH}_2\text{-SBA-15}$.

3.1.1.2.2.8. Triflic acid treated amine-functionalized SBA-15: Amine-functionalized SBA-15 was treated with triflic acid to minimize leaching and to enhance POM loading. Acidification was carried out by adding 6 mol equivalent of triflic acid per mole of V2PA to amine-functionalized SBA-15. The more positively charged NH_3^+ groups on the support, the stronger the electrostatic binding of V2PA to the support. Triflic acid was added to the amine-functionalized SBA-15 in acetonitrile, stirred, and filtered to get the acid-treated aminefunctionalized SBA-15 solid. The filtrate acetonitrile was neutral, demonstrating the complete binding of protons to the support.



Scheme 3.1.1. Immobilization process of V₂PA on OSBA-15

3.1.1.2.2.9. Immobilization of Molybdo vanadophosphoric to acid treated NH_3^+ -SBA-15: A 50-cm³ sample of methanol solution containing 0.3 g of V₂PA was added to 0.7 g of freshly activated NH_3^+ -SBA-15 and refluxed for 3 h. It was then filtered and Soxhleted using methanol solvent for 12 h and dried at 100 °C under vacuum. This was designated as V₂PA- NH_3^+ -SBA-15. Vanadium content estimated by ICP-AES was

12.86 ppm. Scheme 3.1.1. shows pictorial representation of process of immobilization. SBA-15WO_x (30), SBA-15MoO_x (30), and SBA-15VO_x (30) were prepared by treating NH₃⁺-SBA-15 with sodium tungstate, sodium molybdate and sodium metavanadate respectively. SBA-15TPA (30), SBA-15STA (30), SBA-15MPA (30), SBA-15V1(30) and SBA-15V3(30) were prepared following the above procedure. The values in the bracket corresponds the loading of TPA (tungstophosphoric acid), STA (tilicotungstic acid) and MPA (molybdophosphoric acid).

3.1.1.2.3. Catalyst reactivity in anthracene oxidation: Liquid-phase catalytic oxidation of anthracene (AN) to give mainly AQ was conducted at atmospheric air in a 50 cm³ round bottom flask equipped with a magnetic stirrer and immersed in a thermostated oil bath. In a typical experiment, a reaction mixture consisting of known amount of catalyst, AN, oxidant were mixed in benzene solvent and flask was heated to 80 °C for 12 h. Reaction samples withdrawn periodically were analyzed by gas chromatography (GC) with a capillary column (cross-linked 5% ME silicone, 30 m × 0.53 × 1.5 μm film thickness) coupled with flame ionization detector. Products were confirmed by GC-Mass spectroscopy (GC-MS), GC-IR by comparing with the authentic samples. Conversions of AN and product selectivities were calculated based on GC analysis.

3.1.1.3. Results and Discussion

3.1.1. 3.1 Catalyst characterization

3.1.1.3.1.1 SAXS and XRD: Powder small angle X-ray scattering (SAXS) patterns of SBA-15, NH₃⁺-SBA-15 and V2PA-NH₃⁺-SBA-15 are depicted in Fig.3.1.1.(a). SBA-15 showed an intense peak assigned to reflections at (100) and two low intensity peaks at (110) and (200), indicating a significant degree of long-range ordering in structure and well-formed hexagonal lattice. The amino propyl triethoxy silane (APTS)-modified sample (NH₃⁺-SBA-15) showed decreased intensities of all peaks, with a marginal shift towards lower 2θ values, indicating silylation inside the mesopores of SBA-15. While in SAXS patterns of V2PA-NH₃⁺-SBA-15 modified with 30 wt. % V2PA, peak intensities at (100), (110) and (200) reflections were further decreased indicating induction of a relatively high number of polyoxometalate anions inside SBA-15 channels. However, the

mesoporous structure of support remained intact under the conditions used for immobilization. XRD of V2PA–NH₃⁺–SBA-15 (Fig. 3.1.1.(a), inset picture) shows peaks in higher 2θ region indicating the presence of V2PA. XRD of pure, amine functionalized and V2PA modified MCM-41 and MCM-48 (Fig.3.1.1.b and Fig.3.1.1.c) show similar diffraction patterns as that of SBA-15.

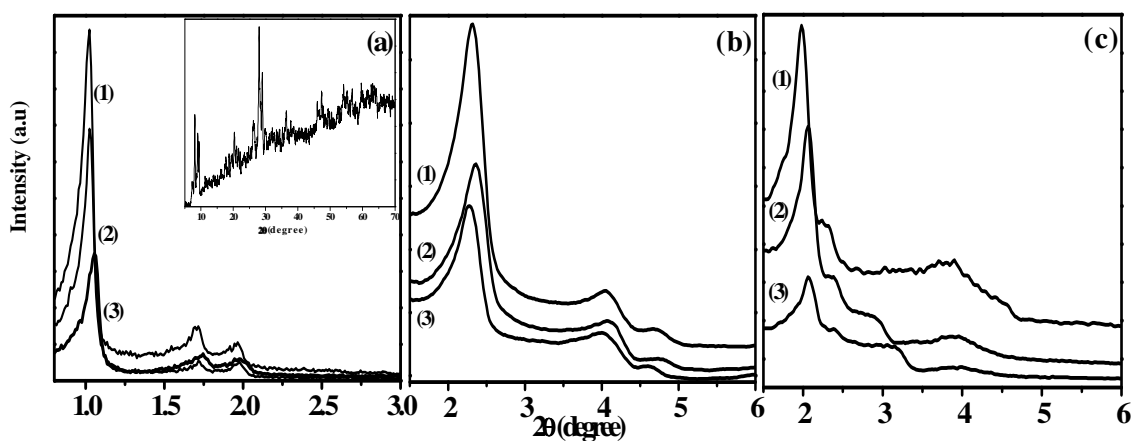


Fig. 3.1.1. Powder SAXS patterns of (a) (1) SBA-15, (2) NH₃⁺-SBA-15, (3) V2PA–NH₃⁺–SBA-15 ; Inset picture in Fig. 1(a) XRD of V2PA–NH₃⁺–SBA-15, (b) (1) MCM-41, (2) NH₃⁺-MCM-41, (3) V2PA –NH₃⁺-MCM-41, (c) (1) MCM-48, (2) NH₃⁺-MCM-48, and (3) V2PA –NH₃⁺-MCM-48.

3.1.1.3.1.2. N₂ sorption study: Specific surface area, pore volume and pore diameters (estimated from N₂ adsorption–desorption isotherms) of organo-functionalized SBA-15 material with and without PMO are presented in Table 3.1.1. BET surface areas and BJH pore distributions were calculated using N₂ adsorption at 77 K. Aminosilylation and introduction of PMO anions affected the surface area and pore distribution of modified samples significantly (Fig.3.1.2). Samples displayed a type IV isotherm with H1 hysteresis and a sharp increase in pore volume adsorbed above P/P0 ~ 0.7 cm³/g, which is characteristic of highly ordered mesoporous materials. Textural properties of SBA-15 substantially maintained over amine functionalization and on subsequent anchoring of vanadium-modified PMOs [40,41]. Parent SBA-15 sample shows a maximum pore diameter (9.1nm) and surface area (970 m²/g), respectively (Table 3.1.1.). Aminosilylation of mesoporous silica results in a shift of pore maximum to smaller diameters and a decrease in surface area (*ca.* 422 m²/g). Introduction of polyoxometalate

anions led to a further decrease in surface area and pore volume. Taking into consideration pore diameter of SBA-15 modified with APTS (Fig. 3.1.2.), and diameter of Keggin unit (12 Å) of polyoxometalate, monolayer coverage could be expected at polyoxometalates loading of *ca.* of 30 wt.% (one Keggin unit may be located along NH_3^+ -SBA-15 channels) [42, 43].

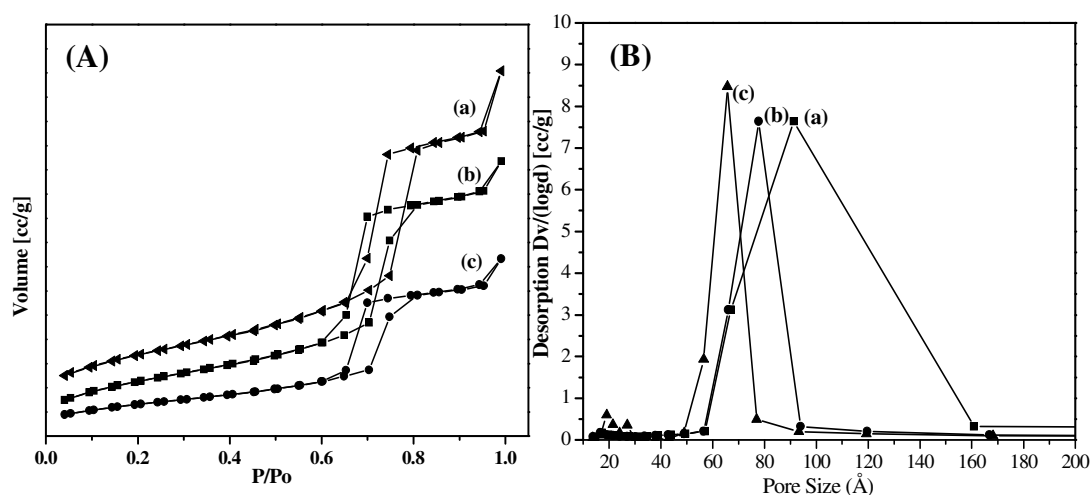


Fig. 3.1.2. (A) N_2 adsorption and desorption isotherms of nitrogen of samples (a) SBA-15, (b) NH_3^+ -SBA-15, (c) V2PA- NH_3^+ -SBA-15, (B) Pore size distribution of (a) SBA-15, (b) NH_3^+ -SBA-15, (c) V2PA- NH_3^+ -SBA-15

3.1.1.3.1.3. TEM and SEM: Fig.3.1.3 represents TEM micrographs of (a) SBA-15, (b) V2PA- NH_3^+ -SBA-15, (c) V2PA- NH_3^+ -MCM-41 and (d) V2PA- NH_3^+ -MCM-48 samples. The TEM images of parent SBA-15 (Fig.3.1.3.a) and of grafted samples provided strong evidence of retainment of mesoporous structure of supports. The characteristic hexagonal silicate structures revealed from TEM supports observations made by SAXS. Fig.3.1.4 represents the SEM micrographs of (a) SBA-15, (b) SBA-15V2 (30) samples. The SEM image of the SBA-15V2 (30) (Fig.3.1.4.b) sample revealed well distributed hexagonal particles organized into rope-like structures. This observation suggests that the mesoporous matrices retained their morphological integrity (shape and size) after functionalization by organic groups, but small agglomeration occurred in the case of immobilization of SBA-15V2 (30) [44-46].

Table 3.1.1. Physicochemical properties of the materials

Materials	V mmol/g	Mo mmol/g	Surface area (m ² /g)	Pore volume (cm ³ /g)	Average pore diameter (nm)
SiO ₂ (Amp)	-	-	110	-	-
MCM-41	-	-	1093	0.88	3.2
MCM-48	-	-	983	0.75	2.7
SBA-15	-	-	970	1.4	9.1
NH ₃ ⁺ -SiO ₂	-	-	105	-	-
NH ₃ ⁺ -MCM-41	-	-	681	0.57	2.4
NH ₃ ⁺ -MCM-48	-	-	556	0.51	2.0
NH ₃ ⁺ -SBA-15	-	-	572	1.2	7.8
SiO ₂ V2 (30)	1.98	11.68	101	-	-
MCM-41 V2 (30)	2.49	12.87	441	0.28	1.9
MCM-48 V2(30)	2.45	12.86	430	0.23	1.7
SBA-15 V2(30)	2.48	12.89	422	0.89	6.5

Legend: SiO₂V2(30) = 30wt.% V2PA loaded on NH₃⁺-SiO₂, MCM-41V2(30) = 30wt.% V2PA loaded on NH₃⁺-MCM-41, MCM48V2(30) = 30wt.%V2PA loaded on NH₃⁺-MCM-48, SBA15V2(30)=30wt.%V2PA loaded on NH₃⁺-SBA-15, V1PA=H₄[PMo₁₁VO₄₀]32.5H₂O, V2PA = H₅[PMo₁₀V₂O₄₀] 32.5H₂O, and V3PA = H₆[PMo₉V₃O₄₀] 34H₂O; Amp : amorphous

3.1.1.3.1.4. XPS: Confirmatory evidence for successful anchoring of V2PA to mesoporous matrices was obtained by XPS analysis. The XPS of NH₃⁺ –SBA-15 exhibited a N core-level peak at a binding energy of 403 eV, which is consistent with 1s of nitrogen. In case of immobilized complex, a shift in binding energy of N core level to 406 eV was observed, possibly which could be due to the coordination environment surrounding nitrogen of V2PA-NH₃⁺-SBA-15 catalyst.

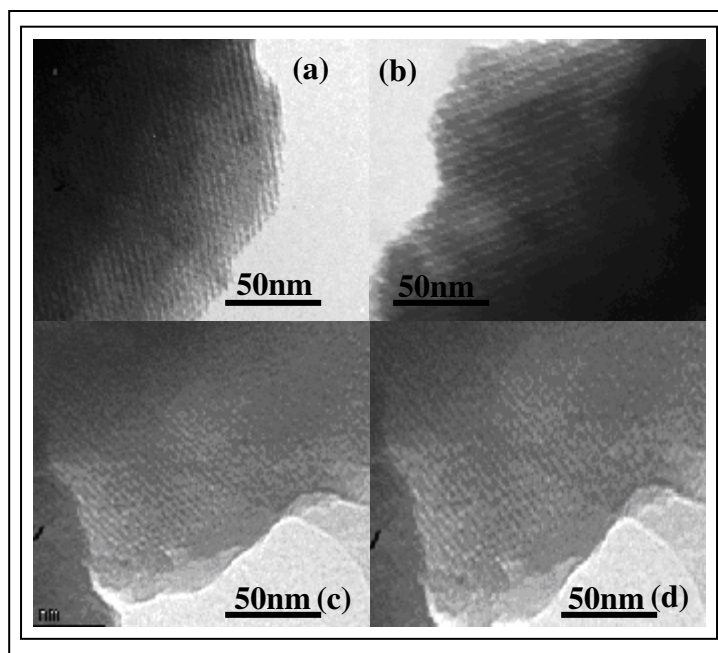


Fig.3.1.3. TEM photographs of (a) SBA-15, (b) V2PA-NH₃⁺-SBA-15 (c) V2PA - NH₃⁺-MCM-41 (d) V2PA - NH₃⁺-MCM-48

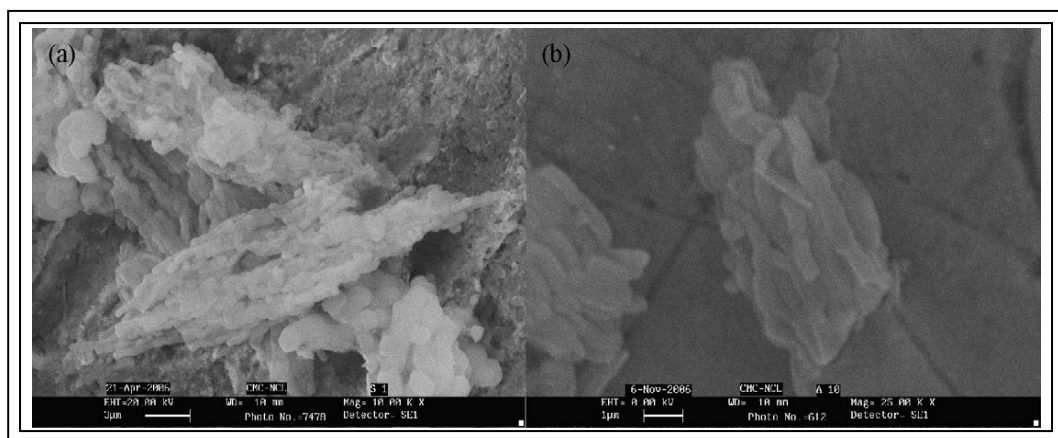


Fig 3.1.4. SEM photographs of (a) SBA-15, (b) SBA-15V2(30).

3.1.1.3.1.5. CP-MAS NMR: A good method for examining evidence for anchoring of vanadium substituted polyoxometalates onto amine-functionalized SBA-15 is by ³¹P, ⁵¹V, ²⁹Si and ¹³C NMR. The ³¹P NMR spectra of (a) V1PA-NH₃⁺-SBA-15, (b) V2PA-NH₃⁺-SBA-15, and (c) V3PA-NH₃⁺-SBA-15 are depicted in Fig 3.1.5. There is a marginal shift in ³¹P NMR peaks of anchored samples compared to corresponding neat

polyoxometalates as reported in literature [43]. ^{31}P NMR peaks corresponding to V1 (+4.05 ppm), V2 (+3.09 ppm), and V3 (+1.68 ppm) peak positions as per literature, shifted to +2 ppm, +1.5 ppm and +1 ppm, (Fig.3.1.5a, Fig.3.1.5b and Fig 3.1.5c.), respectively, which could be either due to the interaction of PMOs with mesoporous silica support or because of differences in degree of hydration of PMOs upon immobilization. These NMR results supported that the structure of PMO is retained upon immobilization onto mesoporous supports [47-50]. Wide-line spectra suffer a severe limitation; it generally is not easy to extract any accurate information about isotropic chemical shifts of the vanadium species. Fortunately, this kind of information may be obtained from magic-angle spinning samples. A small variation in the spinning speed allows accurate determination of the unshifted lines, which correspond to the isotropic chemical shifts of the various species. The ^{51}V NMR spectra of neat V2PA and its anchored form V2PA $-\text{NH}_3^+$ -SBA-15 are depicted in Fig 3.1.6. Vanadium spectra showed the presence of numerous spinning side bands envelope centered around -400 ppm attributed to various possible stereoisomers present. In fact from ^{51}V NMR spectra, we can not make a clear distinction between different isomers but could see that vanadium was in octahedrally distorted in the anchored form and was interacting with the support in Refs. [43, 51, 52]. V was in V_2O_5 coordination, as would be expected for POMs containing vanadium. In contrast to supported V_2O_5 , in this case the vanadium species were isolated from one another, because there were no V-O-V bonds between polyanions; however, no information about the dispersion of the polyanions on the surface can be deduced from these findings. Fig.3.1.7 (a & b) showed ^{29}Si MAS NMR spectra of modified SBA-15 samples with aminopropyl groups. ^{29}Si MAS NMR spectra of parent SBA-15 exhibit a broad peak and was dominated by an intense peak at -110 ppm assigned to $\text{Si}(\text{OSi})_4$ and two shoulder peaks at -100 and -90 ppm due to $\text{Si}(\text{OSi})_3\text{OH}$ (Q_3) and $\text{Si}(\text{OSi})_2(\text{OH})_2$ (Q_2) structural units present in SBA-15. Upon incorporation of aminopropyl groups, in addition to above three peaks, two more peaks at -56 and -67 ppm appeared and their intensities were greatly enhanced by ^1H cross-polarization. No peak appeared at -45 ppm corresponding to the chemical shift of silicon in liquid (3-aminopropyl) trialkoxysilane indicating the absence of free silane molecules physically adsorbed on SBA-15 surface. A peak at -67 ppm indicates formation of new

siloxane linkages (Si–O–Si) of aminopropylsilane to surface silicon atoms of SBA-15 via three siloxane bonds, $(-O-)_3\text{Si-CH}_2\text{CH}_2\text{CH}_2\text{NH}_2$ (T_3) and peak at -56 ppm via two siloxane bonds, $(-O-)_2\text{Si-CH}_2\text{CH}_2\text{CH}_2\text{NH}_2$ (T_2). Similar spectral observations have been made for heteropoly acids anchored to SBA-15 in literature [53].

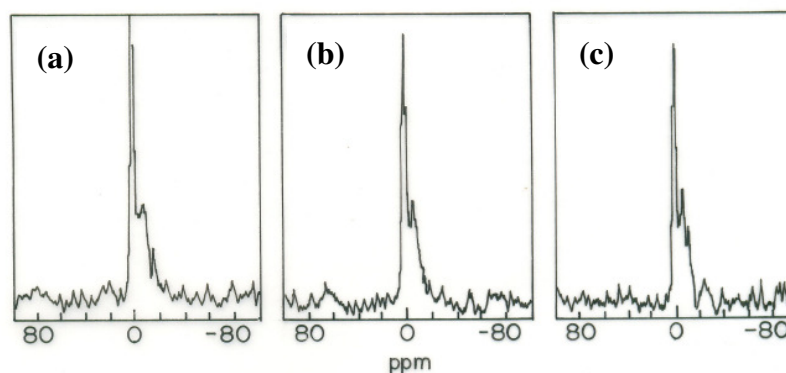


Fig. 3.1.5. ^{31}P MAS NMR profile of (a) V1PA- NH_3^+ -SBA-15, (b) V2PA- NH_3^+ -SBA-15, (c) V3PA- NH_3^+ -SBA-15

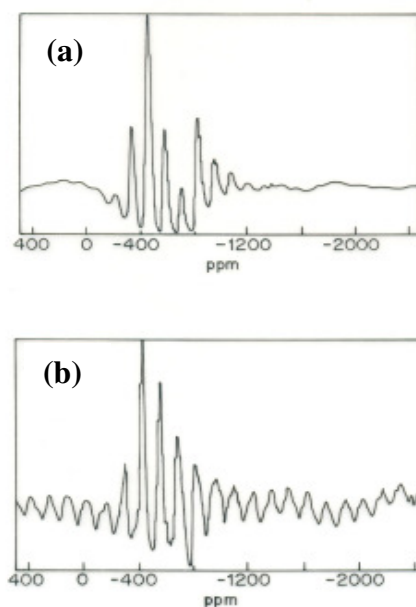


Fig. 3.1.6. ^{51}V MAS NMR profile of (a) V2PA, (b) V2PA- NH_3^+ -SBA-15

^{13}C MAS NMR spectra shown in Fig. 3.1.7.(c&d) provided useful information on nature of incorporated aminopropyl groups on internal surface of SBA-15. Three well-

resolved peaks at -8.7, 22 and 42 ppm observed, have been assigned to C1, C2 and C3 carbons of incorporated aminopropyl groups, $(-O)_3SiCH_2(1)CH_2(2)CH_2(3)NH_2$, respectively. Structure of aminopropyl groups remains intact during incorporation process. Broad peak at 25 ppm indicates the existence of some protonated aminopropyl groups in presence of extra surface hydroxyl groups or moisture. Absence of peaks due to residual ethoxy carbons (18 and 60 ppm) in spectra suggests that hydrolysis and/or condensation of (3-aminopropyl) triethoxysilane molecules inside internal surface of SBA-15 is virtually complete.

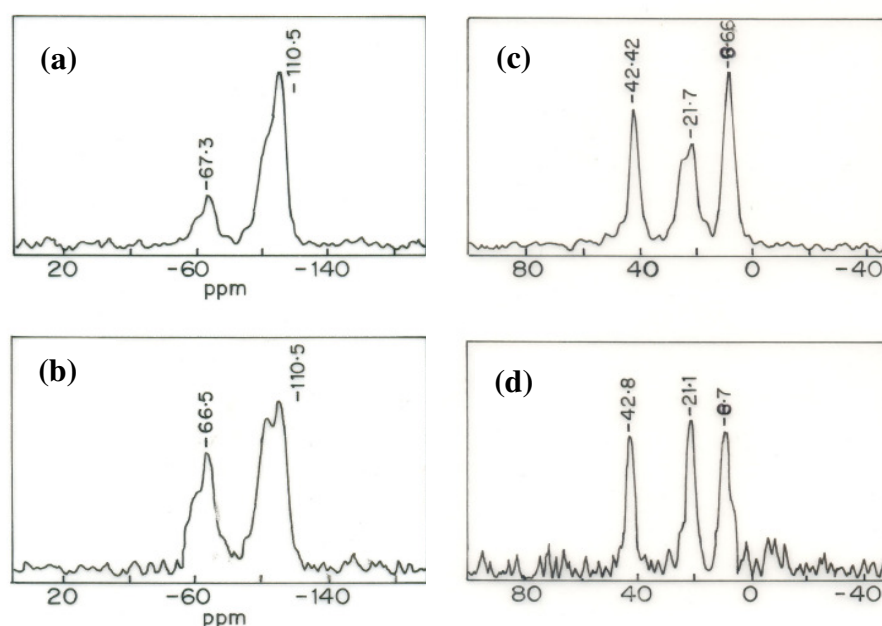


Fig. 3.1.7. ^{29}Si MAS NMR profile of (a) NH_3^+ -SBA-15, (b) V2PA- NH_3^+ -SBA-15, and ^{13}C CP- MAS NMR profile of (c) NH_3^+ -SBA-15, (d) V2PA- NH_3^+ -SBA-15

Similar spectral observations have been made for polyoxometalates anchored to SBA-15 [53]. From NMR study, we can conclude that there are no structural changes occurred in anchored moiety and silica matrix upon immobilization of polyoxometalates onto mesoporous support.

3.1.1.3.1.6. FT-IR: FT-IR spectra of V2PA, NH_3^+ -SBA-15 and V2PA- NH_3^+ -SBA-15 are shown in Fig. 3.1.8 (A). FT-IR study has been performed to identify the presence of V2PA in V2PA- NH_3^+ -SBA-15. FT-IR spectrum of V2PA- NH_3^+ -SBA-15 is compared

with that of NH_3^+ -SBA-15 and neat V2PA. In the region $400\text{--}1300\text{ cm}^{-1}$, neat V2PA showed four peaks characteristic of V2PA. Most of IR bands of pure NH_3^+ -SBA-15 (1073 , 951 , 870 , 795 and 489 cm^{-1}) overlapped with that of neat V2PA (characteristics bands of heteropoly anion, 1050 , 959 , 882 and 792 cm^{-1}) thus, these bands are not clearly seen in IR spectrum of V2PA- NH_3^+ -SBA-15. However, increase in intensity of IR bands at 795 , 951 and 1073 cm^{-1} and appearance of a new band at 870 cm^{-1} in V2PA- NH_3^+ -SBA-15 corresponding to NH_3^+ -SBA-15 may be considered an indication of presence of V2PA in mesopores of NH_3^+ -SBA-15 [54].

3.1.1.3.1.7. UV-Vis: UV-Vis spectra of V2PA and V2PA- NH_3^+ -SBA-15 are shown in Fig.3.1.8(B). Because V2PA exhibits characteristic absorption bands in UV-vis region, their structures are often characterized by diffuse-reflectance UV-vis spectroscopy. However, SBA-15 and NH_3^+ -SBA-15 do not show any characteristic absorption bands in UV-vis region. V2PA- NH_3^+ -SBA-15 exhibits certain features of LMCT; these bands are compared with the characteristic bands of neat V2PA at around 234 and 279 nm . On anchoring of V2PA onto NH_3^+ -SBA-15, these bands shifted slightly, and broad bands

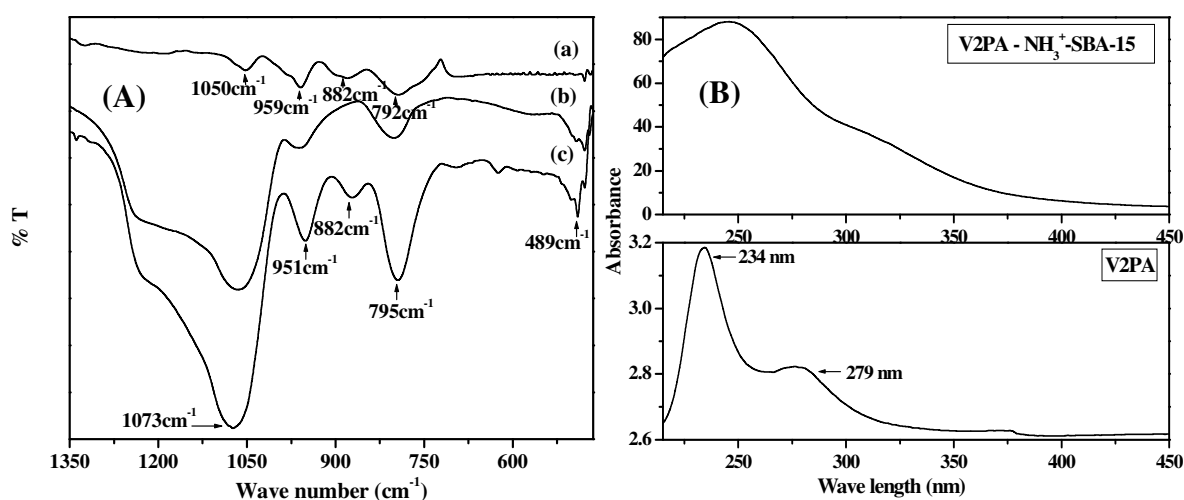


Fig. 3.1.8. (A) FT-IR spectra of (a) V2PA, (b) SBA-15 (c) V2PA- NH_3^+ -SBA-15 and (B) Diffuse reflectance UV-Vis spectra of V2PA and V2PA - NH_3^+ -SBA-15

appeared. Because some of these bands are weak due to low concentration of V2PA in the immobilized sample, they are shown in expanded scale for clarity. The presence of these bands indicates the presence of V2PA in the SBA-15 channels, and these bands exhibit small shifts in wavelength. The broadness of POM after immobilization may be

due to different reasons. We believe that definite interactions exist between POM and mesoporous silica and that POMs are under the constraint environment of mesoporous silica after immobilization. The broadness also may result from the difference in the polarization powers of H^+ ions in pure POM and propyl cations in immobilized.

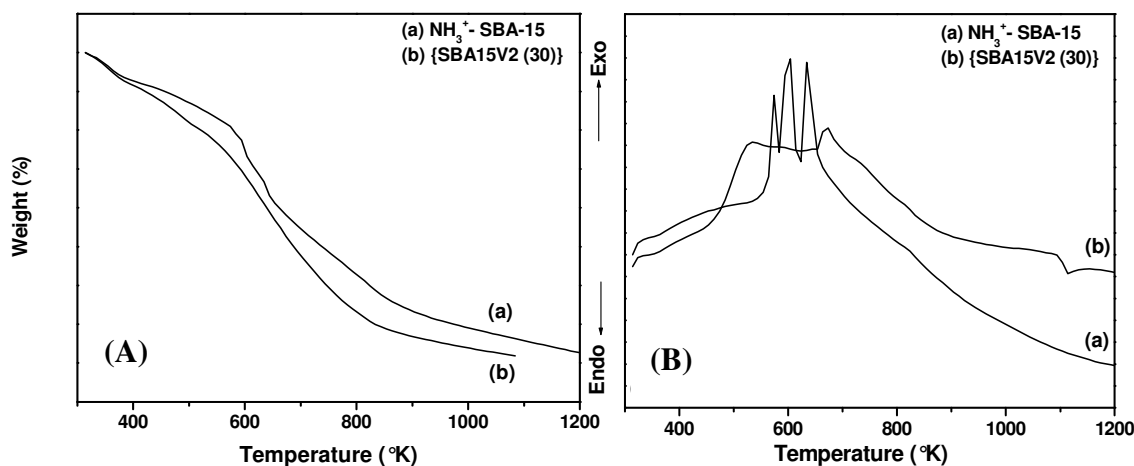
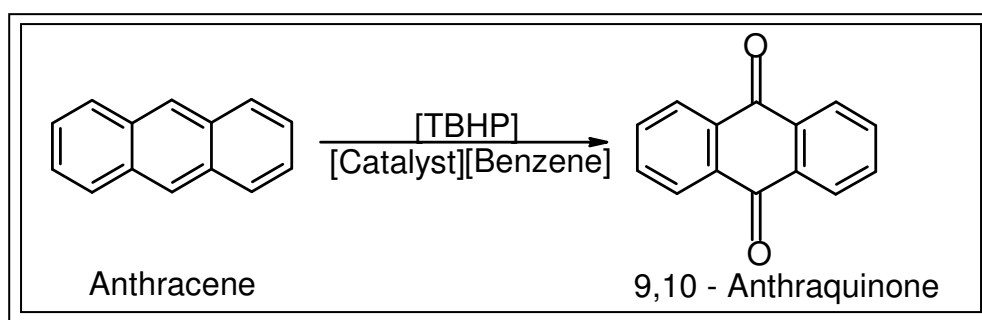


Fig 3.1.9. (A) TG and (B) DTA of (a) NH_3^+ -SBA-15 and (b) SBA-15V2(30).

3.1.1.3.1.8. Thermal Analysis: TG and DTA of NH_3^+ -SBA-15 and {SBA15V2(30)} were depicted in the Fig 3.1.9 (A & B) respectively, where curve (a) represents NH_3^+ -SBA-15 and curve (b) represents {SBA15V2(30)}. Heteropoly acids crystallize with a large number of water molecules. TG and DTA can distinguish two types of water molecule in these solids; crystallization and 'constitutional' water. There is a weight loss observed in TG curve before 430K, which is due to the loss of water of crystallization of heteropoly ion. Another weight loss was observed in the range 570-800 K corresponding to the crystallization of oxides arising from the decomposition of the heteropoly anion. Two endothermic peaks in the DTA curve were observed in curve (b); the first one (430 K) is due to the loss of 'constitutional' water molecules, *i.e.* the protons bound to the polyanion external oxygens are lost and the other one at 630 K is due to the decomposition of organic moiety (aminopropyltriethoxysilane) present in NH_3^+ -SBA-15. There is an endothermic peak in DTA curve (b) observed at 1180 K, which is due to decomposition of V_2O_5 and MoO_3 [55].

3.1.1. 3.2. Catalytic oxidation of anthracene by 70% aqueous TBHP

The liquid-phase catalytic oxidation of AN was conducted at atmospheric air, as explained previously. In a typical experiment, a reaction mixture containing 0.013 mmol of catalyst (0.1 g), 56 mmol of AN (1 g), 3 cm³ of benzene, and 280 mmol of TBHP (2.5 g) was heated to 80 °C and kept at this temperature for 12 h with constant stirring. The molar ratios of AN/catalyst and TBHP/AN were maintained at 430 and 5, respectively, in this reaction. Scheme 3.1.2 schematically represents the oxidation of AN to give mainly AQ. A blank experiment carried out without catalyst (with the same composition of the reaction mixture as earlier) showed no oxidation of AN, demonstrating that a catalyst is needed for the reaction.



Scheme 3.1.2. Oxidation of Anthracene

The catalytic activities of different catalysts, including neat and immobilized, gave mainly AQ as the product in the oxidation of AN by TBHP. The reaction conditions used for the oxidation are specified in Table 3.1.2. A comparison of the activities of both homogeneous (neat) and immobilized catalysts in AN oxidation with TBHP oxidant shows that the different catalysts were used in such amounts as to all have the same vanadium concentration. Under the reaction conditions studied, the homogeneous catalysts (V1PA, V2PA, and V3PA) gave AQ (selectivity in the range 66–72%) and the remaining anthrone and oxanthrone as the oxidation products of AN. As can be seen from the results in Table 2, conversion of AN was nearly the same (58%) for V2PA and V3PA, whereas it was 50% for V1PA. The lower activity of V1PA could be due to lower reduction potential or variable vanadium isomer content [55]. Thus, the immobilized catalysts were prepared using the more active V2PA and mesoporous silica supports like

MCM-41, MCM-48, and SBA-15, and their performance in AN oxidation were studied. It can be seen from the catalytic activity data in Table 3.1.2 that the immobilized catalysts were quite active, and the AN conversions were comparable to those of neat catalysts; however, the product selectivities differed. The selectivity for AQ with neat catalysts was in the range 66–72% (Table 3.1.2, entries 1–3); interestingly, it was 100% with immobilized catalysts, which is the most important function of these catalysts. Among the immobilized catalysts, although SiO₂V₂(30)-amorphous silica exhibited good AN conversion (59%), it had poor selectivity for AQ (69%).

Table 3.1.2. Catalytic activity data on the oxidation of anthracene

No.	Catalyst	Convsn. of AN (mol%)	TOF	Selectivity of products (%)		
				AQ	anthrone	oxanthrone
1	V1PA (neat)	50	17	66	22	12
2	V2PA (neat)	58	20	72	15	13
3	V3PA(neat)	57	20	70	16	14
4	SiO ₂ -V ₂ (30)	59	11	69	16	15
5	MCM41V ₂ (30)	50	17	100	0	0
6	MCM48V ₂ (30)	49	17	100	-	-
7	SBAV ₂ (10)	30	10	100	-	-
8.	SBAV ₂ (20)	46	16	100	-	-
9.	SBAV ₂ (30)	60	21	100	-	-
10.	SBAV ₂ (40)	55	19	100	-	-

Legend: SiO₂V₂(30) = 30wt.% V₂PA loaded on SiO₂-NH₃⁺, MCM-41V₂(30) = 30wt.% V₂PA loaded on NH₃⁺-MCM-41, MCM48V₂(30) = 30wt.% V₂PA loaded on NH₃⁺-MCM-48, SBAV₂(10 to 30) = 10 to 30wt.% V₂PA loaded on NH₃⁺-SBA-15, V1PA=H₄[PMo₁₁VO₄₀]32.5H₂O, V2PA = H₅[PMo₁₀V₂O₄₀] 32.5H₂O, and V3PA = H₆[PMo₉V₃O₄₀] 34H₂O. AN= Anthracene and AQ = 9,10-Anthroquinone

Reaction conditions: 0.013 mmole catalyst (0.1g), 56 mmole of substrate (1g), 280 mmole TBHP (2.5 g), 3 ml Benzene, 80 °C and 12 h. Substrate/catalyst mole ratio 430 and TBHP/ substrate mole ratio 5.

The immobilized catalysts retained the activities (TOFs) of their homogeneous analogues (neat) and selectively formed a clean product AQ (100%) in AN oxidation, which was attributed to the diffusional constraints toward the reactants and products in a mesoporous environment. Experiments done with a VPA salt of *n*-propylamine (prepared by the addition of *n*-propylamine in a methanolic solution of vanadium POM) as the catalyst found an anthracene conversion of 50% with an AQ selectivity of 60%. The reaction was homogeneous in nature.

To investigate the effect of V2PA loading on AN oxidation, immobilized catalysts were prepared with various V2PA loadings (10–40%) on SBA-15 and tested in AN oxidation; the results are presented in Table 3.1.2 (entries 7–10). With an increase in V2PA loading, AN conversion increased from 30 to 60%, forming a clean product AQ. At higher V2PA loading (40%), AN conversion decreased, possibly due to changes in the morphology of the support (mesopore diameter and volume). Moreover, higher loadings might have acted as an inhibitor rather than as a catalyst by capturing active radicals [57]. SBAV2(30) exhibited the highest activity (AN conversion of 60%), along with 100% AQ selectivity, because of the ease of diffusion constraints [52]; thus, this was used for further studies. Because the immobilized catalysts consist of both molybdenum and vanadium metal centers in POMs, understanding the role of these in the oxidation of AN by TBHP is crucial. Therefore, an experiment was carried out with phosphomolybdic acid under homogeneous conditions; this gave negligible AN conversion (<1%) in a reaction conducted under identical conditions. This observation confirms that vanadium, not molybdenum, is the essential active center in the oxidation of AN.

The effect of reaction parameters such as solvent, oxidant, and temperature on the rate of oxidation of AN to AQ were studied using V2PA–NH₃⁺–SBA-15 catalyst, which had the best performance of the immobilized catalysts (Table 3.1.3). The activity of the catalyst was found to depend on the nature of the solvents used in the oxidation reaction. The results (Table 3.1.3, entries 1–3) showed higher activity in the case of benzene (TOF = 21), followed by toluene and THF (TOF = 18 and 11, respectively) with 70% aqueous TBHP oxidant, but lower selectivity toward AQ in toluene and THF. The higher catalytic activity in benzene is due to its lower dielectric constant ($\epsilon = 2.28$) compared with toluene ($\epsilon = 2.38$) and THF ($\epsilon = 7.58$). Thus, benzene was used as the solvent for the oxidation of AN by TBHP in other experiments. With the intention of verifying the hydroxylation of benzene competing with AN oxidation, the same reaction was carried out with benzene and TBHP only, without AN; negligible conversion of benzene to phenol was found, and thus the possibility of hydroxylation of benzene under the reaction conditions of AN oxidation was ruled out.

To evaluate the effect of oxidants on the conversion of AN, 70% aqueous TBHP, hydrogen peroxide (30% H₂O₂), and urea hydrogen peroxide (UHP) were used in the

catalytic oxidation of AN to AQ in solvent benzene catalyzed by V2PA–NH₃⁺–SBA-15. The results, given in Table 3.1.3, show that H₂O₂ and UHP in benzene solvent had poor activity to AQ compared with TBHP (entries 4–6); thus, TBHP was used as an oxidant in further studies.

A couple of experiments were also conducted to confirm that oxygen atoms of AQ originate from TBHP. In the first experiment, the reaction was carried out at 6.8 atm air pressures (without TBHP) at 80 °C in a Parr autoclave with the active catalyst in benzene solvent. No reaction between AN and molecular oxygen of air was seen. In the next experiment, an excess amount of TBHP (substrate/oxidant:1:15) was used in argon atmosphere (with the reaction mixture extensively degassed by applying vacuum and purged a few times with argon); conversion of AN increased (66%), and the catalyst turned yellow, indicating a +5 oxidation state of vanadium. The third experiment used less TBHP (substrate/oxidant:1:3) in argon atmosphere (with the reaction mixture extensively degassed by applying vacuum and purged a few times with argon). AN conversion decreased (45%) and the catalyst turned green, indicating the mixed valance states (+4 and +5) of vanadium due to the nonavailability of oxygen (oxidant). From the above observations, we can conclude that the generation of free *tert*-butoxyl radicals was responsible for the transfer of oxygen atoms to form AQ, not from molecular oxygen (air) under the reaction conditions studied.

The results on the effect of temperature on AN conversion are presented in Table 3.1.3. AN conversion increased with increasing temperature to 60–80 °C (TOF = 10–21), due to the slow formation of *tert*-butoxyl radicals of TBHP. Further increases in temperature (to 90 °C) produced no change in AN conversion (TOF = 21). Although the AN/TBHP molar ratio was 1:5 (excess oxidant), AN conversion did not increase, because of the rapid formation of *tert*-butoxyl radicals (confirmed independently) at 90 °C and their nonavailability with time for the oxidation reaction. Thus, we can conclude that maximum conversion can be obtained at 80 °C. However, the selectivity for AQ was 100% at all temperatures studied.

3.1.1. 3.3. Catalyst recycling

One of the main advantages of using solid catalysts in a liquid-phase reaction is the ease of separation and reuse in catalytic cycles. V2PA–NH₃⁺–SBA-15 [SBAV2(30)] was used

repeatedly under the following conditions: 0.1 g of catalyst, 56 mmol (1 g) of AN, 3 cm³ of benzene, an AN/catalyst molar ratio of 430, an AN/TBHP molar ratio of 5, 80 °C, for 12 h); the first cycle gave 60% AN conversion with 100% selectivity to AQ. The catalyst was separated by filtration, washed with benzene, dried in an oven (100 °C) for 1 h, and then reused in second cycle with fresh reaction mixture. This procedure was repeated for four cycles. The results demonstrate that the AN conversion was nearly the same in all four cycles, with essentially constant (100%) AQ selectivity, suggesting that V2PA–NH₃⁺–SBA-15 [SBAV2(30)] can be used in repeated cycles without any loss of activity. A marginal decrease in conversion occurred after each cycle, possibly due to handling losses, not to leaching of active catalyst into the reaction medium.

Table 3.1.3. Reaction parameters in oxidation of Anthracene

No.	Temp. (°C)	Oxidant	Solvent	AN Convn. (mol%)	TOF	AQ, Selectivity (%)
1.	80	TBHP	Benzene	60	21	100
2.	80	TBHP	Toluene	50	17	64
3.	80	TBHP	THF	30	10	28
4.	80	TBHP	Benzene	60	21	100
5.	80	H ₂ O ₂	Benzene	10	3	100
6.	80	UHP	Benzene	9	3	100
7.	60	TBHP	Benzene	30	10	100
8.	70	TBHP	Benzene	50	17	100
9.	80	TBHP	Benzene	60	21	100
10.	90	TBHP	Benzene	60	21	100

Legend: TBHP = 70% aqueous *tert*-butyl hydroperoxide, THF = Tetrahydrofuran, UHP = Urea hydro peroxide, AN = Anthracene, Reaction condition: catalyst: V2PA-NH₃⁺-SBA-15 (SBAV2 (30)) catalyzed, AN: Oxidant (molar ratio); 1: 5, catalyst wt.: 0.1 g, time : 12 h

To confirm the absence of leaching of V2PA ions from the immobilized system into the reaction medium during the reaction, catalyzing the AN oxidation as a homogeneous system, the reaction was carried out at 80 °C for 3 h (the same conditions

used in the recycling study), after which the catalyst was removed by filtration at high temperature. The conversion of AN to AQ was 25%. The reaction was continued for another 3 h with

the filtrate only; the results are shown in Fig. 3.1.10. AN conversion remained the same after 3 h. We can conclude that the oxidation of AN is catalyzed by immobilized catalyst and is not due to leaching of V2PA ions into the medium during the reaction.

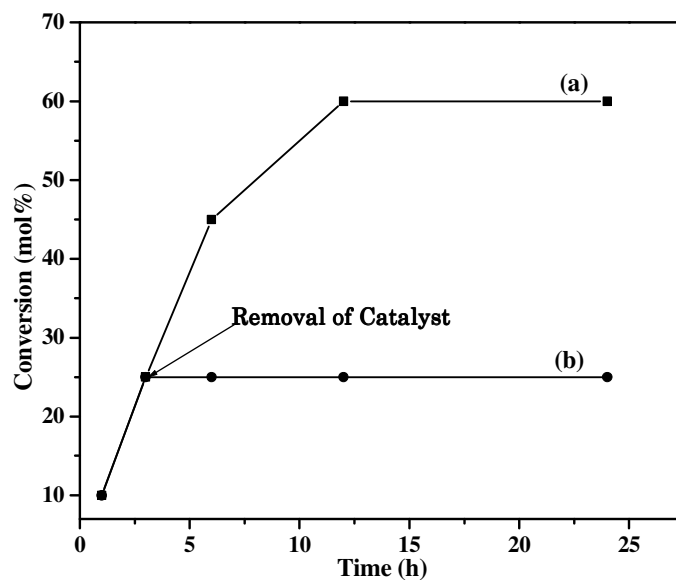


Fig 3.1.10. Catalyst recyclability study

3.1.1.4. Conclusions

We have successfully prepared molybdovanadophosphoric acid immobilized onto amine-functionalized MCM-41, MCM- 48, and SBA-15 mesoporous silica and evaluated them by different techniques, including SAXS and TEM analysis, revealing the structural integrity of the immobilized catalysts. The immobilized catalysts were active in AN oxidation with TBHP in benzene solvent to give 100% AQ selectivity. Our investigation demonstrates that molybdovanadophosphoric acid immobilized on mesoporous silica can be used for selective oxidation of AN to AQ under milder liquid phase oxidation conditions.

Section A 2

Oxyfunctionalisation of adamantane using inorganic - organic hybrid materials based on isopoly and heteropoly anions: kinetics and mechanistic study

3.1.2.1. Introduction

Activation of carbon-hydrogen bond of an alkane is considerably more difficult due to its kinetic stability. The energy required to overcome the kinetic stability of alkanes leads to deep oxidation rather than selective oxidation. [58-62]. Adamantane has been used as a model compound by numerous researchers to investigate C–H bond activation because the substituted adamantane derivatives, especially mono- or di-substituted ones, are used as important precursors for photo resistants and medicines [63,64]. It is difficult to obtain tertiary mono- and di-oxygenated products of adamantane. Conventionally 1-adamantanol and 1, 3-adamantanediol are obtained by bromination of adamantane with molecular bromine, followed by hydrolysis of the corresponding brominated derivatives, while 2-adamantanol is obtained by the rearrangement of tertiary hydroxylated adamantanes using concentrated H₂SO₄. Due to number of side products and harmful reagents, conventional techniques are unacceptable for their preparation. Therefore, there is a challenge to develop an ecological and economical process for adamantane oxidation.

In recent years, demands for replacing the oxidation methods to cleaner ones are increasing, and aerobic oxidations of alkanes leading to alcohol and carbonyl compounds are becoming important processes. During last two decades, oxidation of adamantane by molecular oxygen has been investigated using metal complexes or polyoxometalate as the molecular catalysts. These catalysts are, however, deactivated with time during reactions because of the known conventional draw backs associated with the homogeneous catalyst systems [65-72].

Isopoly and heteropoly anions have attracted much attention as oxidation catalysts because of their unique ensemble of properties, including metal oxide-like structure,

thermal and hydrolytic stability, tunable acidities, redox potentials and alterable solubilities in various media, etc [73-75]. Heterogenization of isopoly and heteropoly anions by means of synthesizing inorganic–organic hybrid materials has been an attractive strategy to overcome the difficulties involved in the separation and recyclability of homogeneous catalysts. Many methods have been adopted in the literature to synthesize inorganic–organic hybrid materials. Traditionally they are immobilized on polymeric organic materials such as resins, supported on inert porous solids such as alumina and silica or encapsulated in the pores and cavities of microporous and mesoporous materials such as zeolites, MCM-41 and SBA-15. Compared to polymeric supports porous inorganic material supports are structurally stable and more resistant to organic chemicals and solvents and provide many advantages for applications. Encapsulation of the homogeneous catalysts inside channels of porous materials also leads to partial leaching of catalysts depending on the reaction medium and conditions of reaction. Moreover, controlling the amount of loading of active catalyst is limited when encapsulation technique is adopted [76-86].

Various efforts have been made to overcome the leaching and increasing the loading of active catalyst problems to date. One of the approaches is to synthesize inorganic–organic hybrid materials by immobilizing the active catalyst on a functionalized silica surface, e.g.; microporous and mesoporous materials with organic chain containing terminal functional groups like amine, phosphine, sulfide, etc [87]. Anchoring of the isopoly and heteropoly anions onto these functionalized materials is proven to be effective in reduction of the leaching and catalyst loading problem [88]. These inorganic–organic hybrid composite materials are more versatile than polymeric supports as pore dimensions; specific surface area and mesoporous structure of these can be controlled to a large extent. A great deal of research work has been done on X- and Y-type zeolites and M41 based mesoporous materials. Amongst mesoporous materials SBA type support materials are more attractive due to their better hydrothermal stability, large pores and thick walls [38].

Keeping in view of the above facts we report here, the preparation and characterization of different isopoly and heteropoly anion solids immobilization both onto amine-modified mesoporous silica surface ($\text{NH}_2\text{-SBA-15}$) catalysts and their

catalytic activities in the oxidation of adamantane in butyronitrile solvent. We have addressed in this study, questions of which metal centre of the heteropoly and isopoly ion are responsible for effecting selective oxidation of adamantane (C–H bond activation) and minimizing catalyst leaching, which frequently limits the success of the catalytic reactions.

3.1.2.2. Results and Discussion

3.1.2.2.1. Catalysts characterization

The specific surface area, pore volume and pore diameters (estimated from N₂ adsorption–desorption isotherms) of the organo-functionalized SBA-15 material with and without polyoxometalates are presented in Table 3.1.4.

Table 3.1.4. Physicochemical properties of the catalysts

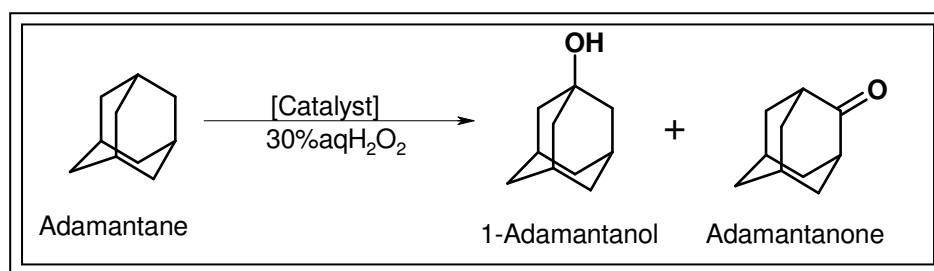
Catalysts	V mmol/g	Mo mmol/g	Surface area (m ² /g)	Pore volume (cm ³ /g)	Average pore diameter (nm)
SBA-15	-	-	970	1.4	9.1
NH ₃ ⁺ -SBA-15	-	-	572	1.2	7.8
SBA-15WO _x (30)	-	-	543	0.98	7.1
SBA-15MO _x (30)	-	13.36	517	0.92	7.3
SBA-15VO _x (30)	2.68	-	532	0.97	7.0
SBA-15TPA(30)	-	-	415	0.85	6.8
SBA-15STA(30)	-	-	409	0.88	6.3
SBA-15MPA(30)	-	-	418	0.81	6.6
SBA-15V1(30)	1.92	13.24	427	0.84	6.9
SBA-15V2(30)	2.48	12.86	422	0.89	6.5
SBA-15V3(30)	2.76	11.51	409	0.87	6.2

Legend: SBA-15V2(30) = 30wt.% H₅[PMo₁₀V₂O₄₀] 32.5H₂O loaded on NH₃⁺-SBA-15, V1=H₄[PMo₁₁VO₄₀]32.5H₂O, and V3 = H₆[PMo₉V₃O₄₀] 34H₂O, STA = silicotungstic acid, TPA = tungstophosphoric acid and MPA = molybdophosphoric acid. WO_x = sodium tungstate, MoO_x = sodium molybdate and VO_x = sodium metavanadate.

3.1.2.2.2. Oxidation of adamantane

The liquid-phase catalytic oxidation of adamantane to give mainly adamantanol and adamantanone was conducted at atmospheric air in a 50 ml round bottom flask equipped with a magnetic stirrer and immersed in a thermostated oil bath (Scheme 3.1.3). In a typical experiment, a reaction mixture consisting of known amounts of catalyst, adamantane, solvent butyronitrile (10mL) and 30% aq. H₂O₂ (oxidant) were placed in the

flask, which was heated to 358 K for 12 h. The oxidation of adamantane was carried out with different catalysts at 358 K with 30% aq H_2O_2 oxidant and the results are summarized in Table 3.1.5 along with the reaction conditions. The oxidation did not proceed in the absence of catalyst. Butyronitrile has been chosen as the solvent for the reaction study due to better solubility of adamantane compared to other solvents. The major product of oxidation was tertiary C–H bond oxygenated 1-adamantanol. It is seen from the results that the vanadium containing catalysts exhibited higher catalytic activities compared to others, which shows that vanadium centers are an essential component of the catalysts to get higher yields of oxygenated products. As seen from the results (Table 3.1.5, entry 1,2,4,5,6), it is clear that the catalysts consisting of isopoly and heteropoly acids having no vanadium content in it are inactive in the catalytic oxidation of adamantane by 30% aq H_2O_2 . Vanadium containing SBA-15VO_x (30) and vanadium substituted {SBA-15V1(30)}, {SBA-15V2 (30)}, {SBA-15V3 (30)}, respectively (Table 3.1.5 entry 3,7,8,9) have shown good activities in the oxidation of adamantane (conversion of adamantane in the range 46 – 65%. Among these, {SBA-15V2(30)} has shown the highest activity with adamantane conversion. (65%). The lower activity of {SBA-15V1(30)} could be due to the lower reduction potential or variable vanadium isomers content in it. So, we could say that vanadium is the indispensable species for this reaction and rest of the keggin ion enhances the catalytic activity.



Scheme 3.1.3. Oxyfunctionalisation of adamantane

Table 3.1.5. Catalytic data on the oxidation of adamantane

No.	Catalyst	Convsn. of adamantane (mol%)	Selectivity for products (%)	
			adamantanol	adamantanone
1	SBA-15WO _x (30)	no conversion	-	-
2	SBA-15MoO _x (30)	no conversion	-	-
3	SBA-15VO _x (30)	46	82	18
4	SBA-15TPA(30)	no conversion	-	-
5	SBA-15STA(30)	no conversion	-	-
6	SBA-15MPA(30)	no conversion	-	-
7	SBA-15V1(30)	49	81	19
8	SBA-15V2(30)	65	80	20
9	SBA-15V3(30)	61	76	24

Reaction conditions: 0.02 M of adamantane, 0.02 M of oxidant (30% aq. H₂O₂); catalyst, 2.6x10⁻⁵ M, 10 cm³ butyronitrile ((10 mL, solvent), 358K and 12 h. (M = mol)

3.1.2.2.3. Kinetic studies

Oxyfunctionalisation of adamantane catalyzed by SBA-15V2 (30) under the reaction conditions studied gave adamantanol and adamantanone. Hence, kinetic investigations of this reaction were carried out to establish the dependence of rate of oxidation with respect to the variations in the concentrations of the reactants involved in the system in excess butyronitrile solvent. The total volume of the reaction mixture in all kinetic experiments was adjusted to 10 ml by the addition of butyronitrile solvent. Rates of oxyfunctionalisation of adamantane were calculated from the plots of moles of adamantane consumed versus time using initial rate approach concept and kinetics has been interpreted.

3.1.2.2.3. a Effect of substrate concentration

Experiments on oxyfunctionalisation of adamantane were carried out at 358 K by varying the concentrations of the substrate adamantane (0.01 – 0.04 M), while keeping the concentrations of 30% aq. H₂O₂ (0.04 M) and catalyst (1.3x10⁻⁵ M) constant. The effect of substrate concentration on the rate of oxyfunctionalisation of adamantane is shown in Fig.3.1.11. (A), as a plot of rate versus concentration of adamantane. It was found that the rate of oxyfunctionalisation of adamantane showed first-order dependence with respect to substrate concentration. (where M= mol)

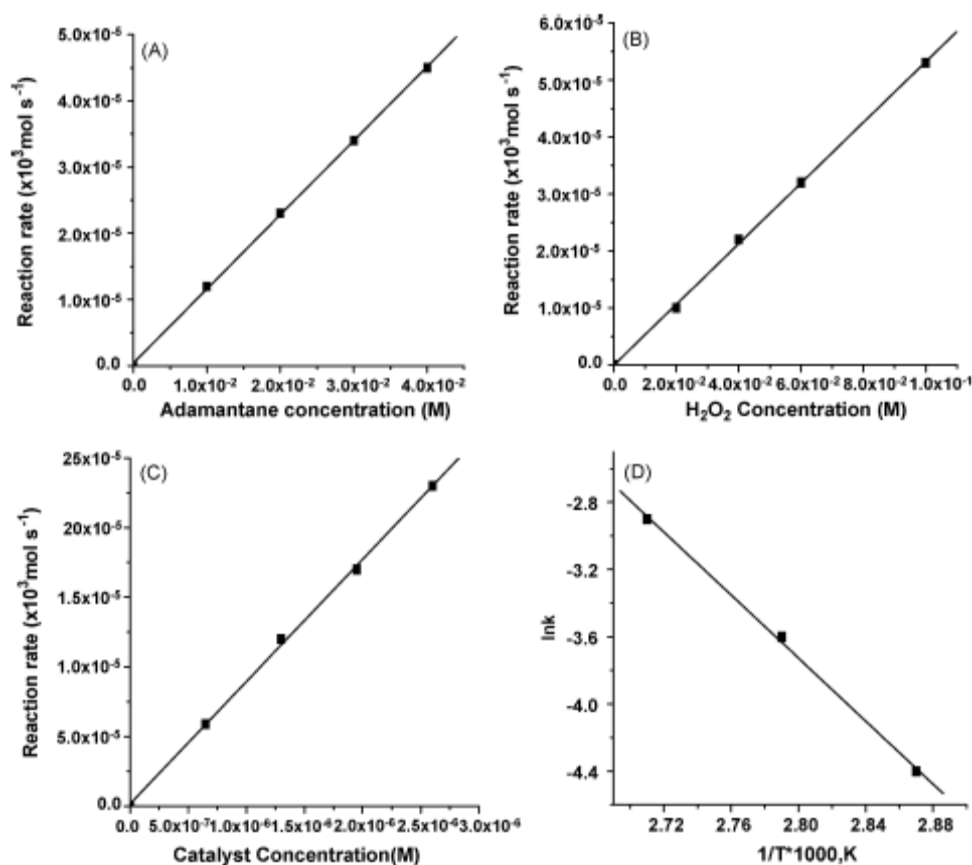


Fig.3.1.11. (A) Effect of substrate concentration: Substrate adamantane (0.01–0.04M), concentration of H_2O_2 (0.04 M) and catalyst (1.3×10^{-5} M), Temp 358 K. **(B) Effect of 30% aq. H_2O_2 (oxidant) concentration:** Substrate 0.02 M, catalyst, 1.3×10^{-5} M, Temp.358 K the 30% aq. H_2O_2 concentration (0.02 and 0.1 M). **(C) Effect of Catalyst concentration:** Catalyst concentration (0.65 and 2.6×10^{-5} M), substrate, 0.02 M, oxidant, 0.04M, temp. 358 K. **(D) Arrhenius plot:** substrate, 0.02 M. oxidant, 0.02M, catalyst, 2.6×10^{-5} M, Temp. (348 - 368 K). (M= mol)

3.1.2.2.3. b Effect of H_2O_2 (oxidant) concentration

Keeping substrate as 0.02 M, catalyst, 1.3×10^{-5} M and temperature, 358K constant, the 30% aq. H_2O_2 concentration was varied in the range 0.02 and 0.1 M. The graph of rate of oxyfunctionalisation versus $[\text{H}_2\text{O}_2]$ (Fig. 3.1.11(B)) is linear and showed a first-order dependence with respect to oxidant concentration.

3.1.2.2.3. c. Effect of catalyst concentration

Catalyst concentration was varied between 0.65 and 2.6×10^{-5} M at substrate, 0.02 M, oxidant, 0.04 M and temperature 358 K. Fig. 3.1.11.(C) shows the graph of rate of oxyfunctionalisation versus catalyst concentration and it is seen from the graph that the rate of oxyfunctionalisation has linear first-order dependence with respect to catalyst concentration.

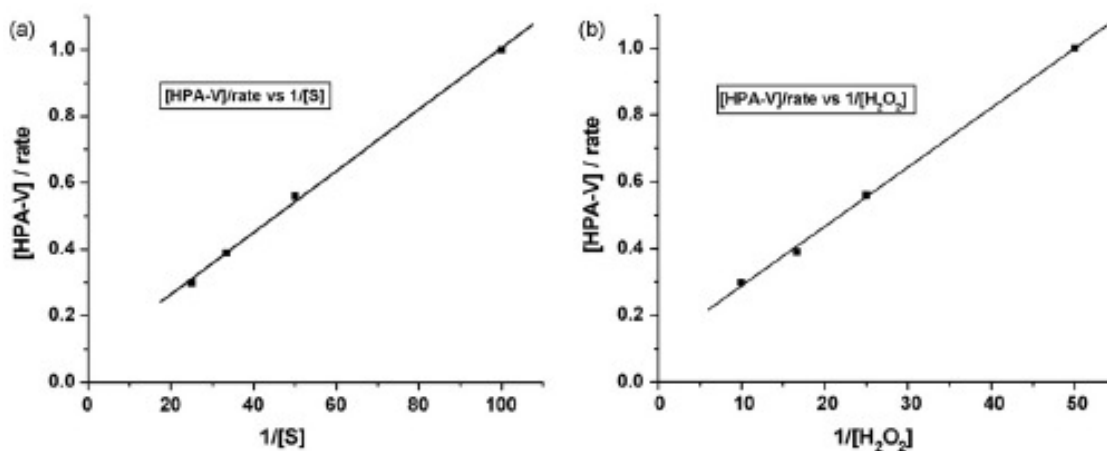


Fig. 3.1.12. Plots of (a) $[\text{HPA-V}]_{\text{T}}/\text{rate}$ vs. $1/[\text{S}]$ and (b) $[\text{HPA-V}]_{\text{T}}/\text{rate}$ vs. $1/[\text{H}_2\text{O}_2]$

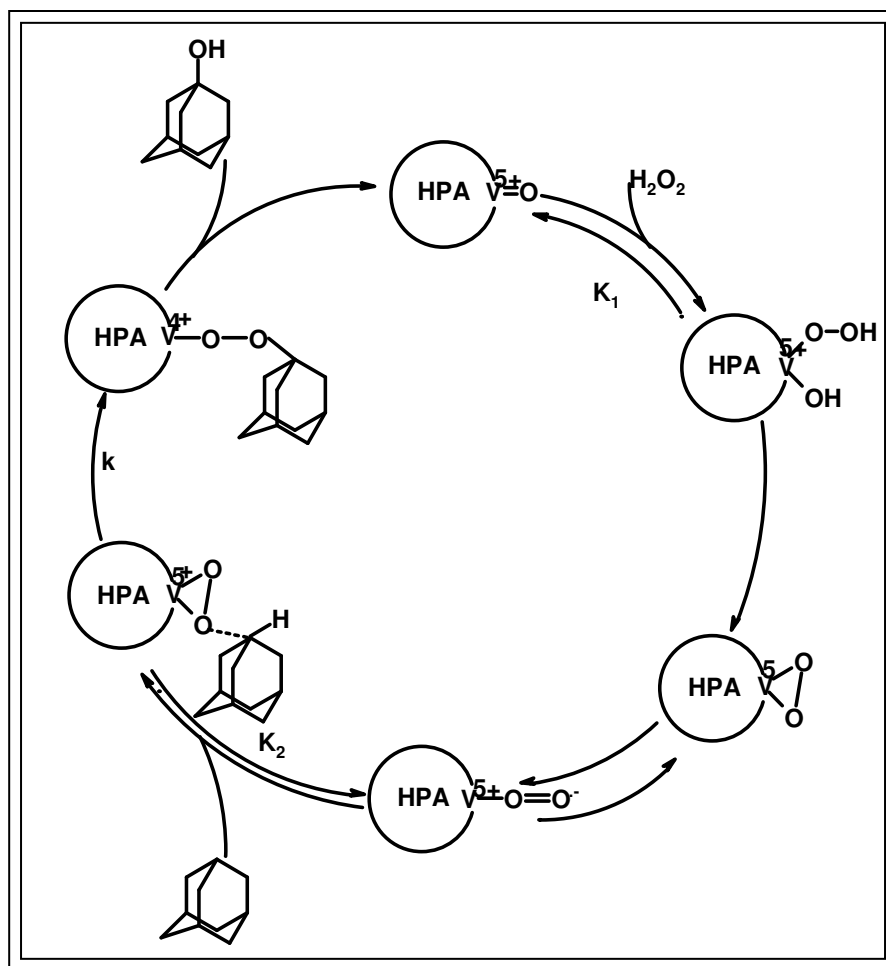
3.1.2.2.3. d. Effect of temperature

Effect of temperature on the rate of oxyfunctionalisation of adamantane was studied by varying the temperature between 348 and 368 K, while other parameters were kept constant as substrate, 0.02 M, oxidant, 0.02M and catalyst, 2.6×10^{-5} M. From Arrhenius plot of $\ln k$ versus $1/T$ shown in Fig. 3.1.11. (D), the activation energy E_a evaluated was 20 kcal mol^{-1} .

3.1.2.2.4. Reaction mechanism and rate law

Vanadium-substituted phosphomolybdic acid anchored to amine functionalized SBA-15 gave 1-adamantanol as the major product of oxidation. To understand the reaction mechanism, we made an attempt to look into the reaction intermediates by conducting EPR. experiments Representative spectrums of EPR experiments are shown in Fig. 3.1.13. The spectrum in Fig. 3.1.13a is of pure catalyst at room-temperature while exhibits isotropic ^{51}V hyperfine lines due to the presence of trace amounts of $\text{V}(4+)$ species in the

catalyst. The EPR spectrum contains eight hyperfine lines pattern due to the interaction of paramagnetic electron of V(4+) with its nucleus ($I = 7/2$). The Hamiltonian parameters of this species based on the computer simulation are: $g_{\text{iso}} = 1.92$ and $A_{\text{iso}} = 158$ G. A small difference among the lines is noticed due to the second-order hyperfine effect. In an experiment, a mixture containing catalyst and 30% aq.H₂O₂ was heated at 358 K and an EPR spectra was recorded. This shows the disappearance of the V(4+) species indicating the oxidation of V(4+)–V(5+) as seen in Fig. 3.1.13.b. This species interacts with H₂O₂, forming a superoxo radical bound to V(5+), which may be partly in equilibrium with V(5+)-peroxo species (Scheme 3.1.4). The V(5+)-superoxo species might have formed via unstable vanadium (V) hydroxy–hydroperoxy species [89]. As can be seen in Fig. 3.1.13.c, a slightly different spectra V(4+) is observed, which could be attributed to metalloperoxy adamantine intermediate species, which is formed by the interaction of vanadium–superoxo species with adamantane molecule. The minor product adamantanone might have formed by secondary oxidation, where a portion of adamantanol might have converted to adamantanone.



Scheme 3.1.4. Mechanism for the oxidation of adamantane catalyzed by SBA-15V2 (30) in the presence of 30% aq. H₂O₂

Based on the Scheme 3.1.4 and kinetic rate dependence studies, the rate law for SBA-15V2(30) catalyzed oxidation of adamantane could be written as:

$$\text{rate} = kK_1K_2[\text{HPA-V}][\text{S}][\text{H}_2\text{O}_2] \text{-----}(3.1.2.1)$$

where, k is the rate constant of the reaction of the rate controlling step shown in Scheme – 3.1.4, K_1 and K_2 are preequilibrium constants as shown in Scheme 3.1.4, $[\text{HPA-V}]$ is the SBA-15V2(30) catalyst concentration, $[\text{S}]$ the adamantane concentration and $[\text{H}_2\text{O}_2]$ is the hydrogen peroxide concentration. By applying steady state reaction conditions and the total concentration of catalyst present in different forms is expressed as $[\text{HPA-V}]_T$, the modified rate law can be written as:

$$\text{rate} = \frac{kK_1K_2[\text{HPA-V}]_T[\text{S}][\text{H}_2\text{O}_2]}{1 + K_1[\text{H}_2\text{O}_2] + K_1K_2[\text{S}][\text{H}_2\text{O}_2]} \quad (3.1.2.2)$$

To evaluate equilibrium and kinetic constants graphically, Eq. (3.1.2.2) could be rearranged in a slope and intercept form in the following two ways:

$$\frac{[\text{HPA-V}]_T}{\text{rate}} = \frac{1}{[\text{S}]} \left(\frac{1}{kK_1K_2[\text{H}_2\text{O}_2]} + \frac{1}{kK_2} \right) + \frac{1}{k} \quad (3.1.3.3)$$

$$\frac{[\text{HPA-V}]_T}{\text{rate}} = \frac{1}{[\text{H}_2\text{O}_2]} \left(\frac{1}{kK_1K_2[\text{S}]} \right) + \frac{1}{k} \left(1 + \frac{1}{K_2[\text{S}]} \right) \quad (3.1.2.4)$$

From Eq. (3.1.2.3), a plot of $[\text{HPA-V}]_T/\text{rate}$ versus $1/[\text{S}]$ gives a straight line (Fig.3.1.12(a)) with an intercept from which, the value of rate constant k of the rate controlling step was calculated. Similarly from Eq. (3.1.2.4), a plot of $[\text{HPA-V}]_T/\text{rate}$ versus $1/[\text{H}_2\text{O}_2]$ gives (Fig.3.1.12(b)) a straight line with slope = $(1/kK_1K_2[\text{S}])$ and intercept = $1/k(1+1/K_2[\text{S}])$. Substituting the value of k , in the intercept $1/k(1+1/K_2[\text{S}])$, the value of preequilibrium constant K_2 is obtained. Similarly, substituting the values of k , K_2 and $[\text{S}]$ in the slope $(1/kK_1K_2[\text{S}])$, the preequilibrium constant K_1 is obtained. Thus, the values of k , K_1 , K_2 for the oxyfunctionalisation of adamantane catalyzed by SBA-15V2(30) at 358 K were found to be as $k = 12.6 \text{ min}^{-1}$ (it is a first order rate constant with respect to the rate controlling step shown in the Scheme 3.1.4.), $K_1 = 4.2 \text{ M}^{-1}$ and $K_2 = 52 \text{ M}^{-1}$, respectively. From the temperature dependence study carried out on the oxyfunctionalization of adamantane, thermodynamic activation parameters, such as, energy of activation E_a , enthalpy of activation (ΔH^\ddagger), entropy of activation (ΔS^\ddagger) and free energy of activation (ΔG^\ddagger) were calculated from standard thermodynamic equations. These values are $\Delta H^\ddagger = 24 \text{ KJmol}^{-1}$, $\Delta S^\ddagger = 81.7 \text{ Jmol}^{-1}\text{K}^{-1}$ and $\Delta G^\ddagger = -0.51 \text{ KJmol}^{-1}$. This low value of ΔG^\ddagger shows that the reaction is possible. The energy of activation for reaction was found as $E_a = 20 \text{ KJmol}^{-1}$. This value suggests that there were no external mass transfer and intra-particle diffusion resistances [90].

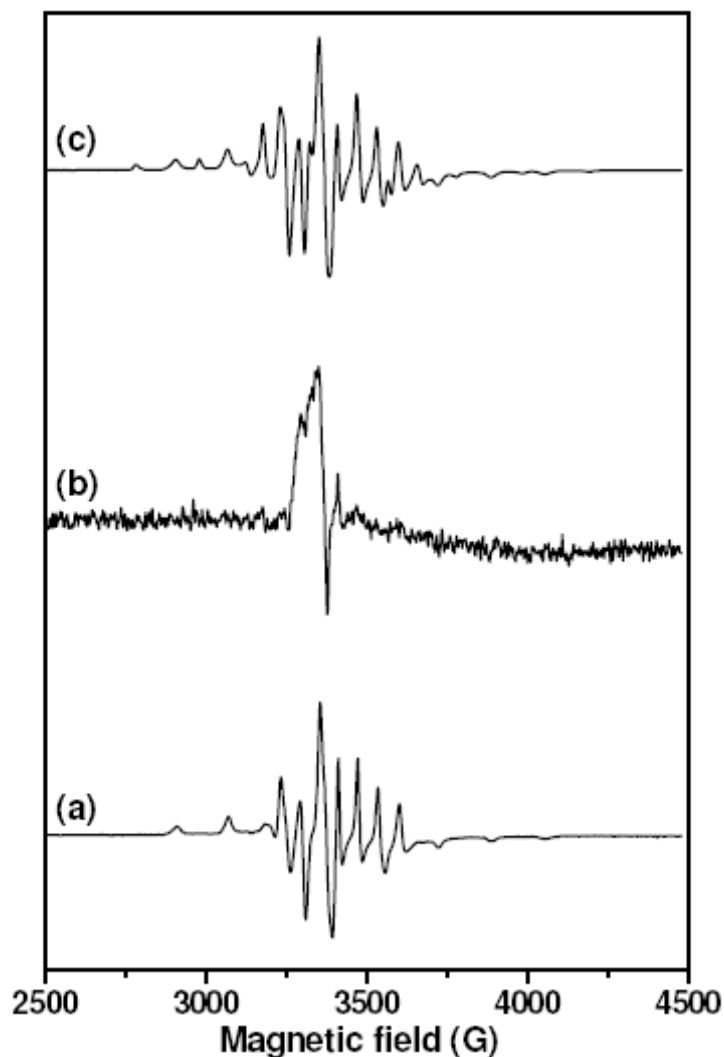


Fig: 3.1.13. EPR spectra of (a) SBA-15V2 (30) in butyronitrile, (b) SBA-15V2 (30) + 30% aq. H_2O_2 in acetonitrile and (c) the reaction mixture at 0.5 h

3.1.2.3. Conclusions

Although adamantane is one of the most stable organic compounds, we found that it can be oxidized to 1-adamantanol, and 2-adamantanone using molybdovanadophosphoric acid immobilized on amine-functionalized SBA-15. The reaction is interesting from a viewpoint of organic syntheses, especially, in connection with green chemistry, because the stable compound can be converted to the hydroxylated derivatives using hydrogen peroxide as the green oxygen sources. The synthesized materials were well characterized by various characterization techniques, which provided

evidence for the structural integrity of the amine-functionalized SBA even after immobilizing with molybdovanadophosphoric acid. The reaction was promoted mainly by the vanadium species, and rest of the keggion enhances the activity. The catalyst generates adamantyl radicals by the abstraction of one electron from adamantane. The oxidation is believed to proceed through the reactive intermediates, V (5+)-peroxo and V (4+)-superoxo species. We provide, for the first time, EPR spectroscopic evidence for participation of V(4+)-superoxo species in selective oxidations over vanadium substituted molybdovanadophosphoric acid immobilized on amine-functionalized SBA-15. The catalyst part can be separated after the reaction and can be reused for few cycles without losing its activity

Section B

3.2. Inorganic–organic hybrid materials based on functionalized silica and carbon: A comprehensive understanding toward the structural property and catalytic activity difference over mesoporous silica and carbon supports

3.2.1. Introduction

Inorganic-organic hybrid materials are in the natural interface between two different chemical worlds by forming a new material with improved property [91]. An important method of synthesizing inorganic organic hybrid materials is the incorporation of organic components, either on the inorganic solids surface or trapping inside the channels if they have. The organic functionalization of the inorganic solids permits fine-tuning of the surface properties such as hydrophilicity, hydrophobicity, and guest-host interactions of the materials. It is apparent that the structural order of porous materials is directly related to their ability to perform the desired function in a selected application. Highly ordered mesoporous materials with large pores have been recently attracted particular interest from the viewpoint of the immobilization and encapsulation of large molecules to make these as functional materials [92].

Vanadium containing polyoxometalates are excellent oxidation catalysts due to their variable redox behavior; however, their limiting applicability is because of their low surface area [93]. Immobilization of vanadium containing polyoxometalates in mesoporous solids (mesoporous silica, organosilica and carbon) not only increases the surface area of the catalysts, but also helps in design an inorganic-organic hybrid material for catalytic applications. In constrained environments, the polyoxometalates lose some of their degrees of freedom and thus exhibit improved reactivity so as to promote reaction in sterically controlled pathway [94]. There are several reports on immobilization of polyoxometalates and transition metal substituted polyoxometalates on various supports like mesoporous carbon, mesoporous silica such as MCM-41 and SBA-15 and their use in varieties of organic transformations [94-96]. To broaden the scope of ethane-bridged

organosilicas and mesoporous carbon and exploit their potential applications, we are reporting here the synthesis, surface functionalization, and fabrication of nanostructured catalytic materials within the channels of large pore ethane-bridged organosilicas and mesoporous carbon [97-100].

2-MNQ (menadione, vitamin K3), is one of the important compounds produced by the oxidation of arenes and used as a supplement for vitamins K1 and K2 in veterinary medicine. Ever since the Vitamin K3 (menadione) was found to be more active than Vitamin K1 and Vitamin K2 as antihemorrhagic agent [101], many methods have been reported for the controlled oxidation of 2MN using a series of oxidizing agents in presence of various catalyst systems [56,102–108]. Stoichiometric oxidation of 2MN using sulfuric acid and chromic acid, about 18 kg of chromium is produced per kilo gram product (30–60% yield), causing environmentally hazardous chromium containing waste water [56,109]. The use of acetic acid, hydrogen peroxide and methyl trioxorhenium, as well as Pd-polystyrene sulphonic acid resin catalyst systems gave higher conversion of 2MN with a poor selectivity for 2MNQ [110-114]. Metalloporphyrin along with potassium monopersulphate and zeolites catalyzed oxidation of 2MN have also been reported [115,116]. The best result till now for the selective oxidation of 2MN was achieved in glacial acetic acid as solvent, sulfuric acid as catalyst and acetic anhydride as the dehydration reagent to get about 80% yield for 2MNQ [117].

To improve the product selectivities of 2MN and its derivatives under neutral environment by developing heterogeneous catalysts systems using 30% aq. hydrogen peroxide is still a significant and demanding goal. Our earlier report shows that vanadium-containing polyoxometalates immobilized onto SBA-15 are an active catalyst in liquid-phase oxidation reactions using TBHP (*tert*-butyl hydrogen peroxide) as an oxidant [118]. In the present study vanadium containing polyoxometalates immobilized onto mesoporous silica, organosilica and carbon supports and their influence on catalytic activities and 2MNQ selectivities have been reported in the oxidation of 2MN. Special attention has been made to establish the role of hydrophilic–hydrophobic interactions in the heterogeneous catalyst systems in this study.

3.2.2. Experimental

3.2.2.1. Chemicals

All the solvents procured from Merck, India (A R grade) were distilled and dried prior to their use. The other chemicals purchased from Aldrich were used as received.

3.2.2.2. Catalysts preparation

3.2.2.2.1. *Organo SBA-15 (OSBA-15)*

In a typical synthesis, 1.2 g of Pluronic123 polymer and 3.5 g of NaCl were dissolved in 10 g of water and 30 g of 2.0 M HCl solution was added to it and the resulting mixture was stirred at 40 °C. To this homogeneous solution, 1.6 g of 1,2-bis-(trimethoxysilyl)ethane (BTME) was added and then the mixture was stirred for 24 h at 40 °C. Subsequently, the resulting mixture was transferred into a Teflon-lined autoclave and heated at 80 °C for an additional 24 h under static conditions (molar composition of the gel was 0.5 BTME/0.017 P123/ 5.07 HCl/5.07 NaCl/178 H₂O). The solid product obtained was then collected by filtration, washed thoroughly with water, and air-dried at room temperature. The surfactant was removed by stirring 1.0 g of as-synthesized sample in 150 mL of ethanol with 3.8 g of 36% HCl aqueous solution at 50 °C for 6 h. The resulting solid was recovered by filtration, washed with ethanol, and dried in air. This extraction procedure was repeated to remove the surfactant completely to get OSBA-15 [119].

3.2.2.2.2. *Amine-functionalized organo SBA-15 (NH₂-OSBA-15)*

Surface modification of organo OSBA-15 by 3-aminopropyl triethoxysilane (APTES) was carried out using grafting method. In a typical preparation, freshly activated OSBA-15 (2 g) was refluxed with 50 mL of toluene (distilled over sodium and dried) to remove occluded moisture azeotropically for 4 h. To this, 1.0 g APTES in 10 mL of toluene was added and stirred under reflux condition for 4 h. After distilling off the solvent, solid was filtered, washed in a soxhlet apparatus with dichloromethane, and then dried at room temperature to get a product designated as NH₂-OSBA-15. Nitrogen elemental analysis estimated showed the content as 2.1 mmole of NH₂ per gram of NH₂-OSBA-15 [120].

3.2.2.2.3. *Triflic acid treated amine-functionalized (NH₃⁺-OSBA-15)*

Amine-functionalized (NH₂-OSBA-15) was treated with triflic acid (trifluorosulphonic acid) to minimize leaching and to enhance loading of polyoxometalates. Acidification was carried out by adding 6 mol equivalent of triflic acid per mole of molybdo vanadophosphoric V2PA to NH₂-OSBA-15. Electrostatic binding of V2PA to the support will be stronger if there are more positively charged NH₃⁺ groups on it. Triflic acid is added to NH₂-OSBA-15 in acetonitrile, stirred and filtered to get acid treated amine-functionalized NH₃⁺-OSBA-15 solid. Filtrate acetonitrile was neutral, which showed complete binding of protons to the support.

3.2.2.2.4. *Immobilization of molybdo vanadophosphoric to NH₃⁺-OSBA-15 (V2OSBA)*

50 mL of methanol solution containing 0.3 g of molybdovanadophosphoric acid (V2PA) was added to freshly activated NH₃⁺-OSBA-15 (0.7 g) and refluxed for 3 h. It is then filtered and soxhleted using methanol for 12 h and dried at 100 °C under vacuum to get V2OSBA. Vanadium content estimated by ICP-AES was found to be 12.77 ppm.

3.2.2.2.5. *Mesoporous carbon*

To synthesize mesoporous carbon (MC), 2.08 g of tetraethyl orthosilicate (TEOS) was pretreated at 60°C for 4 h in acidic ethanol/water solution. The molar ratio of TEOS:water:ethanol:HCl was maintained at 1:6:6:0.01. The pre-reacted sol was then mixed with 0.9 g of sucrose, 2 g of H₂O and 8.94 g of H₃PO₄, stirred for 1 h and dried at room temperature to form transparent brown nanocomposite. The molar ratio of phosphoric acid to TEOS (P/Si) used was 0.43. The nanocomposite was then carbonized at 900°C under nitrogen for 4 h and washed with 20% HF and deionized water to remove all silica and phosphoric components. The complete removal of silica and phosphate was confirmed by X-ray energy dispersive spectroscopy (EDS) analyses [121].

3.2.2.2.6. *Mesoporous carbon oxidation*

Mesoporous carbon (MC) refluxed with 5 M nitric acid solution for 6 h (1 g/30 mL), washed with deionised water until pH 6–7 and then dried in an oven at 110 °C for 12 h under vacuum [122].

3.2.2.2.7. Reaction of mesoporous carbon with thionyl chloride (SOCl₂)

Oxidized carbon (12.0 g) was refluxed with 40 mL of a 5% (v/v) solution of thionyl chloride in toluene for 5 h, extensively washed with toluene, and then purified by Soxhlet extraction with toluene for 2 h, and finally dried in an oven at 150 °C for 12 h under vacuum [122].

3.2.2.2.8. Functionalisation of thio modified mesoporous carbon with bis(3-aminopropyl)amine (Trien)

Carbon (3.0 g) was refluxed with a solution containing 390 µmol of bis(3-aminopropyl)amine (trien) in 40 mL of dry toluene for 4 h, then filtered and extensively washed with toluene. The material was Soxhlet extracted for 2 h with toluene and dried in an oven at 150 °C for 12 h under vacuum [122].

3.2.2.2.9. Immobilization of 10-molybdo-2-vanadophosphoric acid V2PA onto the trien modified mesoporous carbon (V2MC)

The activated carbon functionalized with trien (0.60 g) was added to 100 mL of a solution of 10-molybdo-2-vanadophosphoric acid in dry methanol (119 µmol), and the mixture was refluxed for 9 h; during reflux, a progressive disappearance of the yellow color of the solution was observed. The resulting material was extensively washed with methanol and then purified by Soxhlet extraction with toluene for 7 h, and dried in an oven at 150 °C for 12 h under vacuum to get the material V2MC [123].

3.2.2.3. Catalytic testing in 2-methyl naphthalene (2MN) oxidation

The liquid-phase catalytic oxidation of 2MN by 30% aqueous H₂O₂ as oxidant to give mainly 2MNQ was conducted at atmospheric air in a 50 mL round bottom flask equipped with a magnetic stirrer and immersed in a thermostated oil bath. In a typical experiment, a reaction mixture consisting of known amounts of catalyst, 2MN and oxidant was mixed with solvent acetonitrile and the flask was kept at 80 °C for 10 h. The reaction samples withdrawn periodically were analyzed by gas chromatography (GC) with a capillary column (cross-linked 5% ME silicone, 30 m × 0.53 × 1.5 µm film thickness) coupled with a flame ionization detector. The products were confirmed by GC-Mass spectroscopy (GC-MS), GC-IR and compared with authentic samples. Conversions of 2MN and product selectivities were calculated based on the GC analysis.

3.2.3. Results and Discussion

3.2.3.1. Catalyst characterization

3.2.3.1.1. Low angle X-ray diffraction

Low-angle X-ray diffraction (XRD) patterns of OSBA-15, NH_3^+ -OSBA-15 and V2OSBA-15 materials are shown in Fig. 3.2.1. The OSBA-15 sample exhibits three well resolved peaks (Fig.3.2.1a) that can be indexed as the (100), (110) and (200) reflections of $p6mm$ hexagonal symmetry. After modification, the XRD patterns of NH_3^+ -OSBA-15 and V2OSBA-15 (Fig.3.2.1b & 1c) shows that the ordered hexagonal ($p6mm$) pore structures are well preserved and almost identical as that of OSBA-15. The low angle XRD peaks of the patterns of V2OSBA-15 (Fig.3.2.1c) modified with 30 wt% V2PA, were significantly lower in intensity compared with samples OSBA-15 and NH_3^+ -OSBA-15 displayed a complete absence of long-order reflections. This feature can be explained in terms of the presence of molybdovanadophosphoric acid, which could partially disturb the assembly of the mesophase, although a higher contrast matching effect arising from the higher size of the organic moiety should not be ruled out. A shift of the (100) peak to higher angles is seen, which could be due to the contraction of the silicate framework because of the condensation of silanol groups to form siloxane bonds during the process of modification [39,119].

3.2.3.1.2. Nitrogen sorption studies

The N_2 adsorption isotherm (Fig. 3.2.2. A) of the ethanesilicas (OSBA-15) at 77 K are of type IV with a clear H1-type hysteresis loop at high relative pressures, which is characteristic of large-pore mesoporous materials with 1D cylindrical channels and a high degree of pore size uniformity. Quantitative analysis of OSBA-15 showd that the Brunauer-Emmett-Teller (BET) surface area of $894 \text{ m}^2\text{g}^{-1}$ and the most probable pore diameter of 5.8 nm (BJH model) [119,120]. Textural data of the samples are provided in Table 3.2.1. Fig. 3.2.2.B shows the N_2 sorption isotherms of the mesoporous carbon prepared using TEOS as the silica source. The mesoporous carbons prepared using sucrose exhibit isotherms with high surface areas and pore volumes (Table 3.2.1). The pore diameters calculated using the same BJH model was 9.2 nm.

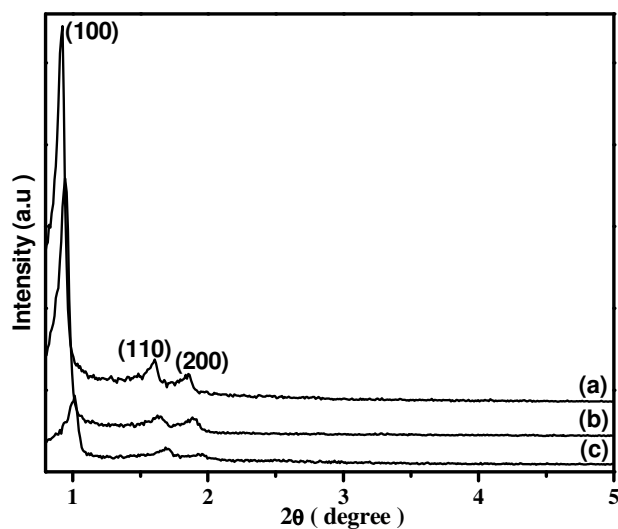


Fig. 3.2.1. Low angle Powder XRD patterns of (a) OSBA-15, (b) NH_3^+ -OSBA-15, and (c) V2OSBA

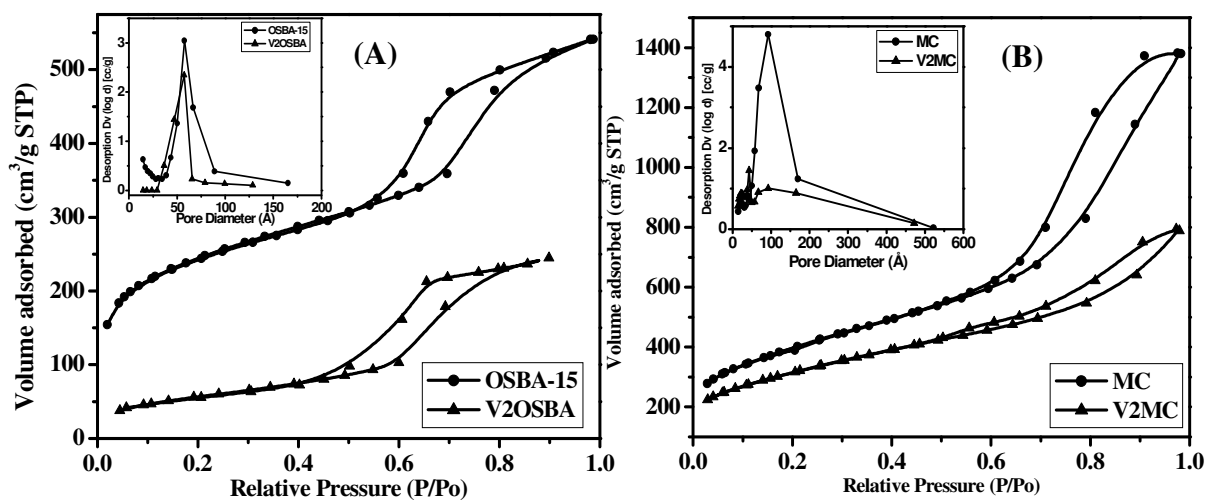


Fig. 3.2.2. (A) N_2 sorption isotherms of samples OSBA-15 and V2OSBA
(B) MC and V2MC

Aminolation and introduction of polyoxometallate (POM) anions into OSBA-15 and mesoporous carbon resulted in a decrease in surface area. The samples also displayed a type IV isotherm with H1 hysteresis, which is a characteristic of highly ordered

mesoporous materials. The textural properties of OSBA-15 and MC were substantially maintained over amine functionalization and on subsequent anchoring of vanadium containing polyoxometalates [121].

Table 3.2.1. Physicochemical properties and catalytic data of the oxidation of 2MN

No.	Materials	V mmol/g	Mo mmol/g	Surface area (m ² /g)	BJH pore diameter (nm)	Convsn. (mol%)	Selectivity (%)
1	V2PA	2.51	13.01	-	-	40	59
2	SBA	-	-	970	9.1	0	0
3	V2SBA	2.48	12.89	422	6.5	33	99
4	OSBA	-	-	894	5.8	0	0
5	V2OSBA	2.49	12.92	209	5.7	38	99
6	MC	-	-	1432	9.3	0	0
7	V2MC	2.45	12.84	1133	4.3	24	99

Legends : V2PA= H₅[PMo₁₀V₂O₄₀] 32.5H₂O , SBA = SBA-15 , V2SBA = 30wt.% V2PA loaded on NH₃⁺-SBA-15, OSBA = Organo SBA-15 , V2OSBA = 30wt.% V2PA loaded on NH₃⁺-OSBA-15, MC = Mesoporous carbon, V2MC = 30wt.% V2PA loaded on MC .

Reaction condition: 0.1g (0.7 mmol) of 2MN, 0.24g (7 mmol) of oxidant (30% aq.H₂O₂); catalyst 0.1g (0.013 mmol), acetonitrile 10 mL (solvent), 353K and 10 h

3.2.3.1.3. Nuclear magnetic resonance

An excellent method for examining the evidence for the anchoring of vanadium-substituted POMs onto amine-functionalized OSBA-15 and MC is by ³¹P, ⁵¹V, ²⁹Si, and ¹³C NMR. The ³¹P NMR spectra of (a) V2OSBA-15 and (b) V2MC are depicted in Fig. 3.2.3. There is a marginal shift in ³¹P NMR peaks of anchored samples compared with corresponding neat POMs (-4 ppm) as reported in the literature [124]. ³¹P NMR peak corresponding to V2OSBA-15 (2.2 ppm), peak position as per the literature shifted to either due to interaction of the POMs with the mesoporous silica support or the differences in the degree of hydration of POMs on immobilization.

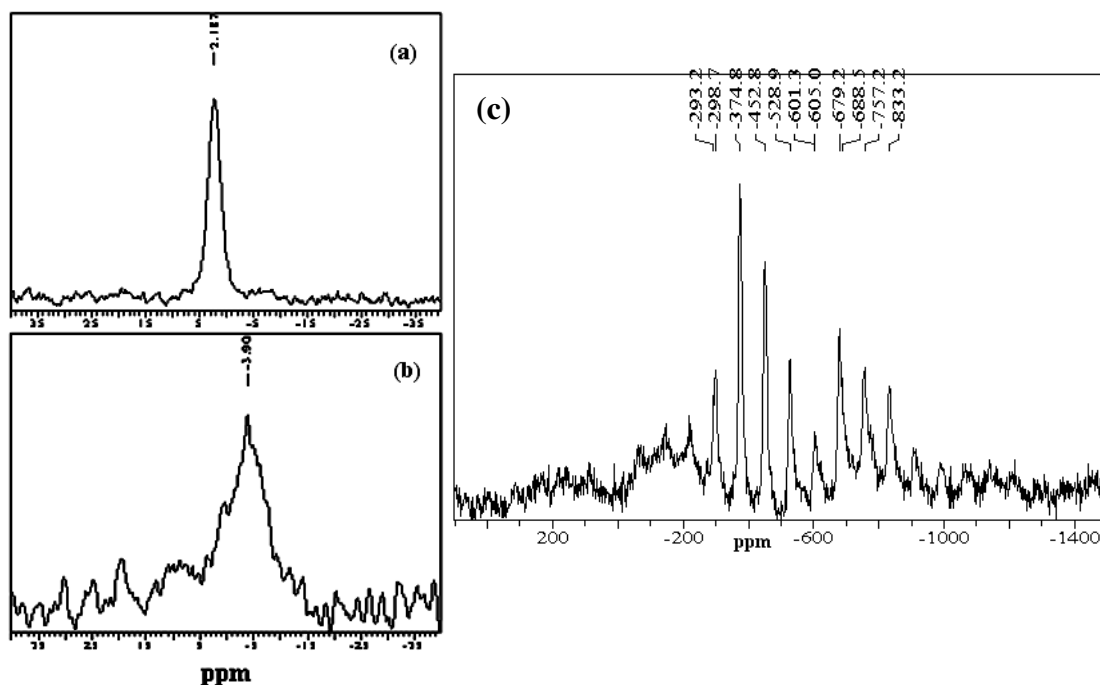


Fig. 3.2.3. ^{31}P MAS NMR profile of (a) V2OSBA and (b) V2MC

(c) ^{51}V MAS NMR profile of V2OSBA

A little broad ^{31}P NMR peak of V2MC was observed at -3.9 ppm, which could be due to the nature of the carbon. Such solids have some conducting properties, which lead to heterogeneities of the magnetic field and then to very broad spectra. The NMR results supported the fact that the structure of POM was retained on immobilization onto mesoporous supports [125–128]. Wide-line spectra suffered a severe limitation; it is generally not easy to obtain any accurate information about isotropic chemical shifts of the vanadium species. Fortunately, this kind of information may be obtained from magic-angle spinning samples. A small variation in the spinning speed allows accurate determination of the unshifted lines, which correspond to the isotropic chemical shifts of the various species. From the broad ^{51}V NMR spectra (Fig 3.2.3 (c)), we could not be able to make a clear distinction between different isomers, but could see that vanadium was octahedrally distorted in the anchored form and was interacting with the support, as reported in the literature [124,129,130].

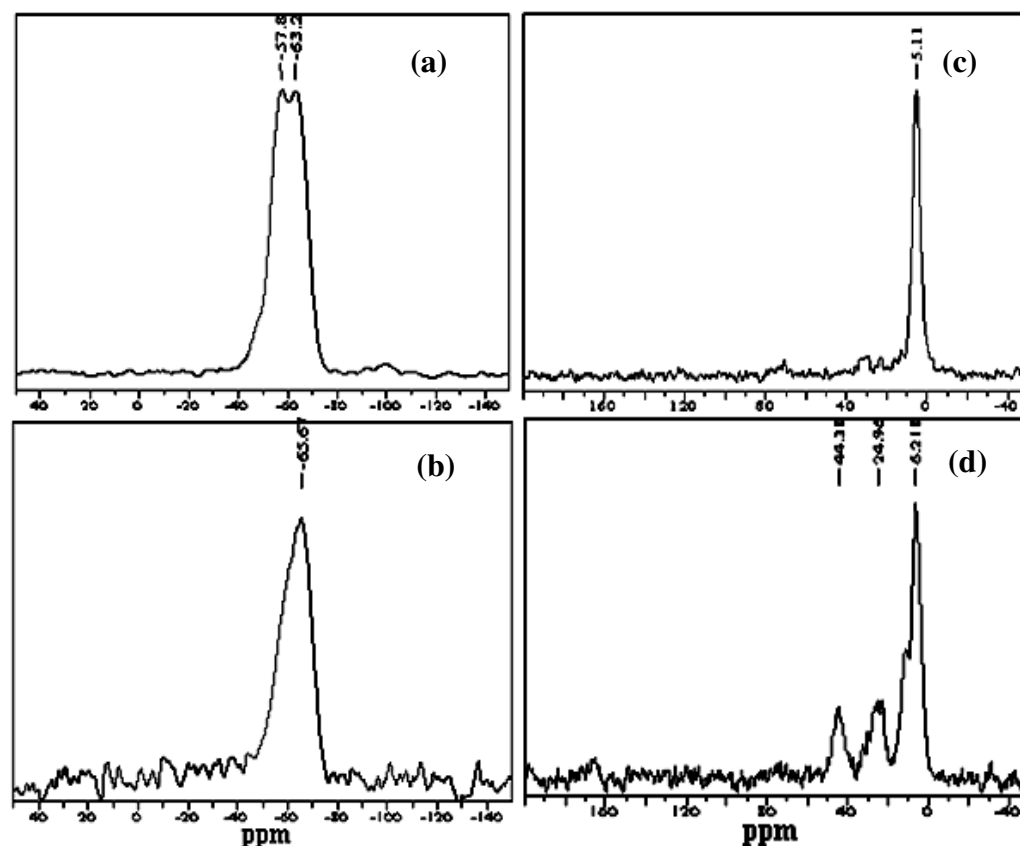


Fig. 3.2.4. ^{29}Si MAS NMR profile of (a) V2OSBA , (b) OSBA-15 and ^{13}C CP- MAS NMR profile of (c) OSBA-15, (d) V2OSBA

Fig. 3.2.4 (a & b) shows ^{29}Si MAS NMR spectra of OSBA-15 and modified OSBA-15 samples with aminopropyl groups. ^{29}Si MAS NMR resonances appear for parent OSBA-15 at -65 ppm of T type organosilica species $[(T_n) \text{RSi}(\text{OSi})_n(\text{OH})_{3-n}]$. A clear absence of Q units $[(Q_n) \text{Si}(\text{OSi})_n(\text{OH})_{4-n}]$ below -100 ppm confirms there is negligible hydrolytic Si-C bond cleavage and the bridge-bonded organic group is maintained intact in the silica framework under the synthetic conditions. On incorporation of the aminopropyl groups, two peaks at -53 and -63 ppm appeared, merging with the parent OSBA-15 peak. (Fig. 3.2.4). When looking at ^{29}Si MAS NMR spectrum of aminopropyl modified OSBA-15 and comparing it with that of OSBA, it is clear that most of the hydroxyl groups of the $(\text{SiO})_2\text{Si}(\text{OH})\text{R}$ and $(\text{SiO})\text{Si}(\text{OH})_2\text{R}$ species

have reacted. No peak appeared at -45 ppm, corresponding to the chemical shift of silicon in liquid (3-aminopropyl) trialkoxysilane, indicating the absence of free silane molecules physically adsorbed on the SBA-15 surface. A peak at -63 ppm indicates the formation of linkages (Si–O–Si) of aminopropylsilane to the surface silicon atoms of the SBA-15 via three siloxane bonds, $(-O-)_3\text{Si}-\text{CH}_2\text{CH}_2\text{CH}_2\text{NH}_2$ (T_3), and a peak at -57 ppm via two siloxane bonds, $(-O-)_2\text{Si}-\text{CH}_2\text{CH}_2\text{CH}_2\text{NH}_2$ (T_2), which indicates that the Si–C bonds remained intact under the synthesis and subsequent processing of conditions. Similar spectral observations have been reported for POMs anchored to SBA-15 [120,131].

The ^{13}C MAS NMR spectrum shown in Fig.3.2.4 (c & d) provides useful information about the presence of organo functionalities and the nature of the incorporated aminopropyl groups onto the internal surface of the OSBA-15. ^{13}C CP MAS NMR shows the presence of a single, sharp peak at 5.1 ppm for the ethane fragments ($-\text{CH}_2-\text{CH}_2-$) integrated in the wall channels of the hybrid materials. Moreover, carbon NMR shows the absence of peaks in the range $10-60$ ppm of the surfactant species. This observation indicates that the surfactant groups can be removed from the pores of the hybrid sample by employing extraction procedures. Three well resolved peaks at 6.2 , 24 , and 44 ppm were assigned to C1, C2, and C3 carbons of the incorporated aminopropyl group, $(-O-)_3\text{SiCH}_2(1)\text{CH}_2(2)\text{CH}_2(3)\text{NH}_2$, respectively. The peak at -6.2 ppm seems to be a merged peak of two peaks, C1 of aminopropyl group and ethane fragments ($-\text{CH}_2-\text{CH}_2-$) of OSBA. The structure of the aminopropyl groups remained intact during the incorporation process. The absence of peaks due to residual ethoxy carbons (18 and 60 ppm) in the spectra suggests that the hydrolysis and/or condensation of the APTES molecules inside the internal surface of OSBA-15 were virtually complete. From the NMR studies, we can conclude that no structural changes in anchored moiety and silica matrix occurred on immobilization of POMs onto mesoporous support [120,132].

3.2.3.1.4. Scanning electron microscopy

Scanning electron microscopy (SEM) images showed that the OSBA-15 and V2OSBA-15 samples shown in Fig. 3.2.5, revealed well distributed hexagonal particles organized into rope-like structures [120]. This observation suggests that the mesoporous

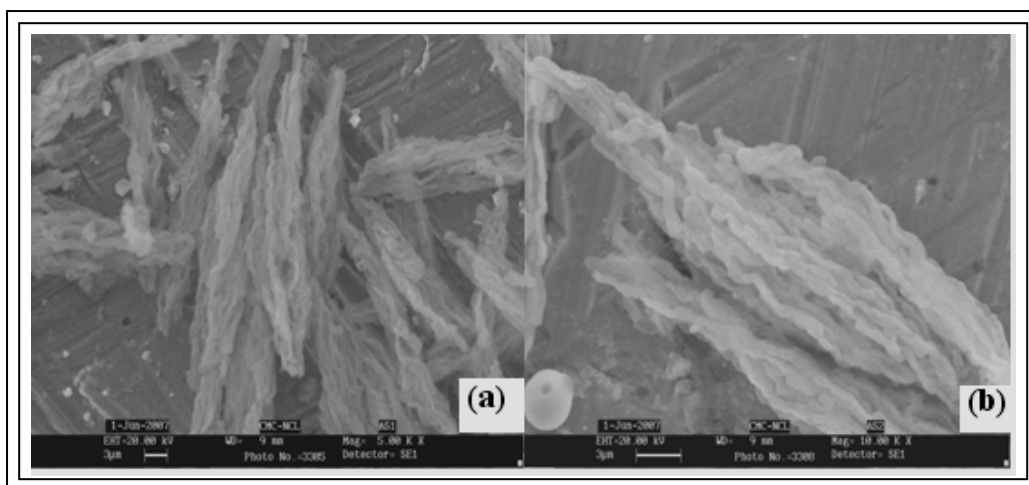


Fig. 3.2.5. SEM photographs of (a) OSBA (b) V2OSBA

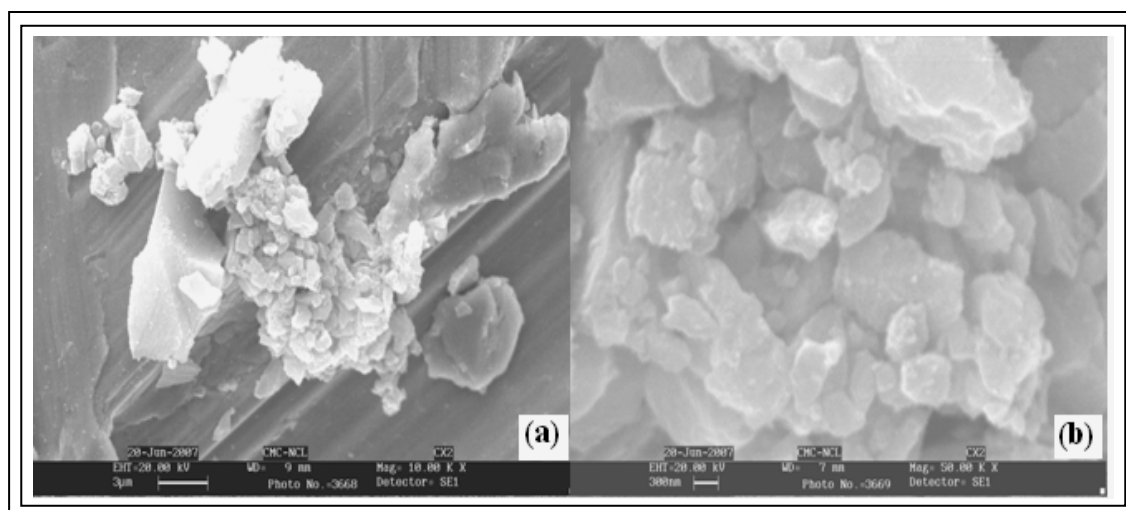


Fig. 3.2.6. SEM photographs of (a) MC (b) V2MC

matrices retained their morphological integrity (shape and size) after functionalization by organic groups. The representative SEM images of the nanoporous carbons are shown in Fig. 3.2.6. Since the samples were ground before washing with HF to remove silica, the largely granular morphology with particle size in micrometer scale is obtained [121].

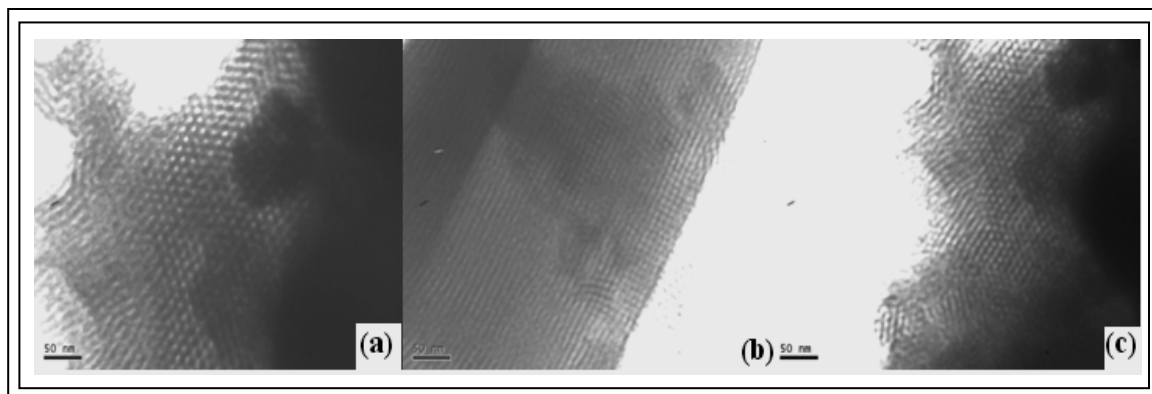


Fig 3.2.7. TEM photographs of (a) OSBA-15, (b) OSBA-15 and (c) V2OSBA

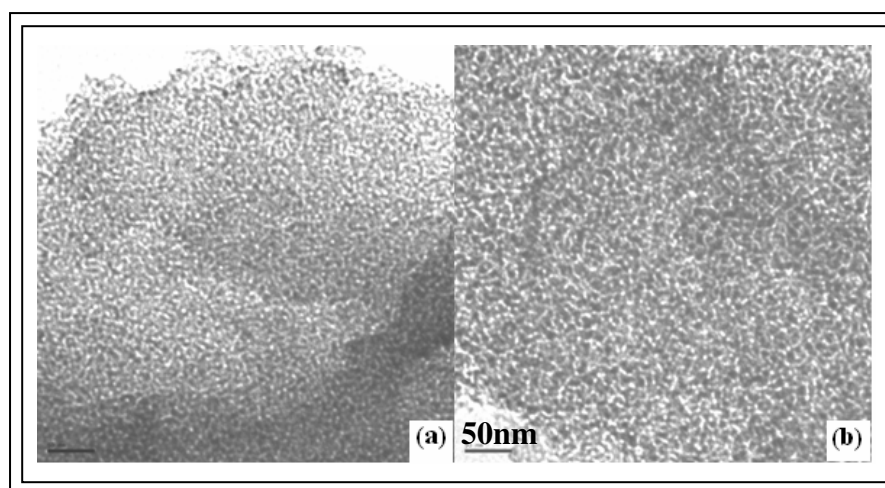


Fig. 3.2.8. HRTEM photographs of (a) MC and (b) V2MC

3.2.3.1.5. Transmission electron microscopy

Transmission electron microscopy (TEM) analysis confirms the well-ordered hexagonal arrays of 1D mesoporous channels in the OSBA-15 material (Fig.3.2.7). The TEM images of the sample OSBA-15 show a clear hexagonal arrangement of pores with uniform size (Fig 3.2.7 a), while well-aligned channels running parallel to organosilica rods are also observed (Fig 3.2.7 b). Despite the large pore size, this high degree of order is maintained over extensive regions of observation. These observations confirm that the pore structure consists of a hexagonal array of uniform 1D channel for the 2D-hexagonal sample. The TEM images of the parent V2OSBA-15 (Fig. 3.2.7a) and grafted samples

provide strong evidence that the mesoporous structure of supports is retained [31]. The characteristic hexagonal silicate structures shown on TEM support the observations made by low angle XRD. Fig. 3.2.8 (a) and (b) shows the representative HRTEM images of the mesoporous carbons and polyoxometalates modified mesoporous carbons. Both the pictures shows disordered, uniform-sized, worm-like pores structure, which is consistent with the results, reported literature [121]. The HRTEM image of the mesoporous carbon shows the presence of larger pores uniformly distributed within the mesoporous carbon framework.

3.2.3.1.6. FT-IR spectroscopy

The incorporation of amine groups in the OSBA-15 and mesoporous carbon frameworks can be qualitatively confirmed by the FT-IR data shown in Fig. 3.2.9. FT-IR showing the appearance of an absorption band assigned to (CH₂-Si) stretching 625cm⁻¹, while the another broad absorption in the range 1000-1300 cm⁻¹(Si-O-Si) indicates the formation of siloxane bonds and residual silanol groups are evidenced by (Si-OH) stretching vibration at 780 cm⁻¹. The C-N stretching vibration is normally observed in the range 1000-1200 cm⁻¹. However, this peak was not resolved due to the overlapping with the IR absorptions bands of Si-O-Si in the range 1000-1200 cm⁻¹ and of Si-CH₂-R in the range 1200-1300 cm⁻¹. Nevertheless, the peak in this region for the APTES-modified OSBA-15 sample is broader, indicating possible overlap of peaks. The peak due to bending N-H bonds at 670 cm⁻¹ is merging with the broad band of (CH₂-Si) stretching and the symmetrical NH₃⁺ bending at 1560 cm⁻¹, indicating the existence of amine groups. In addition, the peak at 1640 cm⁻¹, which can be assigned to N-H deformation band, is very intense for the APTES-modified sample, indicating the presence of N-H groups. Three strong peaks at 3400, 2940, and 2895 cm⁻¹ are seen in Fig.3.2.9. The peak at 3400 cm⁻¹ is due to silanol groups, while the other two peaks are due to adsorbed or hydrogen-bonded water molecule. The material itself was extremely hygroscopic; therefore, the significant peaks were covered by a broad -OH peak. The width of this broad peak at 3400 cm⁻¹ for APTES-functionalized sample slightly increased.

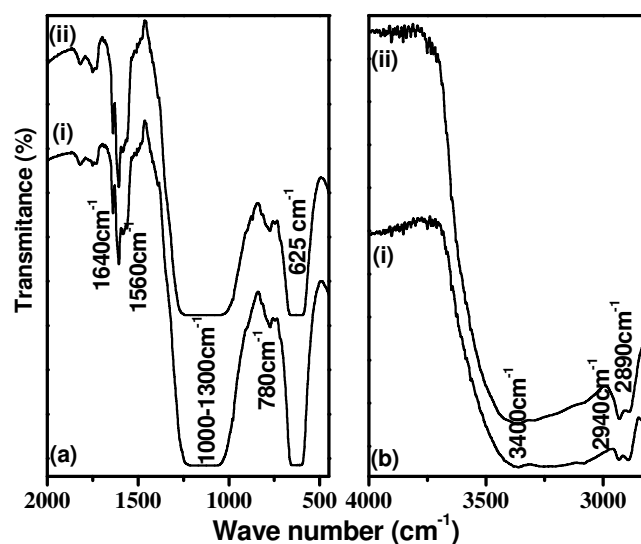


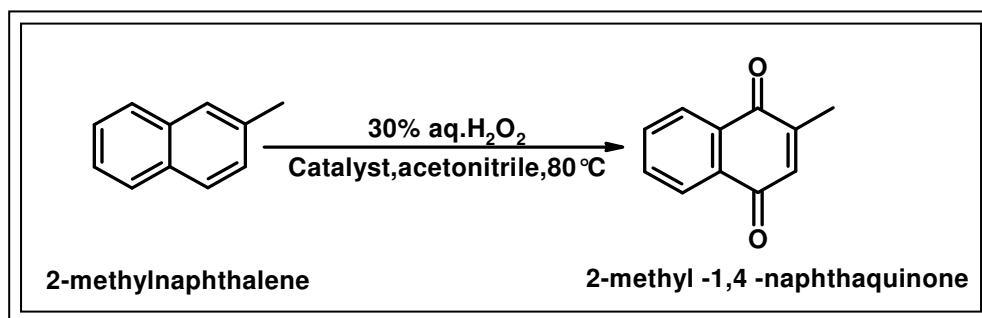
Fig. 3.2.9. FT-IR spectra of (i) NH_3^+ -OSBA-15 and (ii) V2OSBA

This widening of the peak may be due to the symmetric stretching of N-H. The N-H stretching was reported around 3345 cm^{-1} for free amine and around 3300 cm^{-1} for terminal amine groups, respectively, which are cross-linked with the silanol group [133].

3.2.3.2. Catalytic oxidation of 2-methyl naphthalene by 30% aq. H_2O_2

The liquid-phase catalytic oxidation of 2-methyl naphthalene (2MN) was conducted at atmospheric air as explained in previous text. In a typical experiment, a reaction mixture containing 0.013 mmol catalyst, 0.7 mmol of 2-methyl naphthalene (2MN), 10 mL acetonitrile and 30% aq. H_2O_2 (7 mmol) was kept in a thermostatic oil bath at $80\text{ }^\circ\text{C}$ for 10 h with constant stirring. The mole ratios of 2MN/catalyst and $\text{H}_2\text{O}_2/2\text{MN}$ were kept as 54 and 10, respectively in this reaction. Scheme 3.2.1 shows the schematic representation of the oxidation of 2MN to give mainly 2-Methy-1,4-naphthoquinone. A blank experiment carried out without catalyst (composition of the reaction mixture is the same as above) did not show any oxidation of 2MN and hence role of catalyst is authenticated for the reaction. The results on the catalytic activities of different catalysts like neat and immobilized in the oxidation of 2MN by 30% aq. H_2O_2 to

give mainly 2-Methyl-1,4-naphthoquinone as the product and the reaction conditions used for the oxidation are presented in Table 3.2.2.



Scheme 3.2.1. Oxidation of 2-methylnaphthalene

To compare the activities of both homogeneous (neat) and immobilized catalysts in 2MN oxidation with 30% aq. H₂O₂ oxidant, the amount of different catalysts were used in such a way that they all had the same concentrations of vanadium content. In our earlier report, we observed that the 30% polyoxometalates loading onto the mesoporous support, was optimum loading to perform as highly effective catalyst system and hence the same loading was used in the present studies. Under the reaction conditions studied, homogeneous catalyst V2PA showed a conversion of 2MN 40% and 2-methyl-1,4-naphthoquinone selectivity 59% as seen from the results (Table 3.2.2). The remaining products are 2-methyl-1-naphthone and 2-naphthoic acid.

Hence, the immobilized catalysts were prepared using the V2PA and mesoporous silica supports like mesoporous silica (SBA-15), mesoporous organosilica (OSBA-15) and mesoporous carbon (MC) and their performance in 2MN oxidation was studied. It could be seen from the catalytic activity data (Table 3.2.2) that the immobilized catalysts are quite active and 2MN conversions are comparable to that of neat catalysts. However, these differ in product selectivities. The selectivity for 2-Methyl-1,4-naphthoquinone with neat catalyst are in the range 59% (entry, 1-3, Table 3.2.2) and interestingly, it is 99% with immobilized catalysts, which is the most important achievement of our functionalized mesoporous catalysts. Among the immobilized catalysts, V2SBA-15 gave 2MN conversion (33%), with good selectivity for 2-methyl-1,4-naphthoquinone (99%). V2OSBA exhibited better activity (38% 2MN conversion) than V2SBA and similar selectivity (99%). This improved catalytic activity of the material V2OSBA could be

attributed to the hydrophobicity of the material. V2MC showed little lower activity, 24% 2MN conversion and 99% keone selectivity in the oxidation of 2MN, which could be due to blocking of the channels by polyoxometalates loaded onto the mesoporus carbon material. However surface area has been seen from the results presented in Table 3.2.2 that the pore size of MC is comparatively lower than that of SBA-15 and OSBA-15. The immobilized catalyst, V2OSBA retained the activity of the homogeneous analogue (neat) and gave a clean product 2-methyl-1,4-naphthoquinone (99%) in 2MN oxidation.

Table 3.2.2. Effects of different parameters on V2OSBA catalyzed oxidation of 2MN

No.	H ₂ O ₂ /2MN mole ratio	Reaction time (h)	Reaction Temperature (°C)	Conversion of 2MN (%)
(A)Effect of reaction temperature				
1	10:1	10	60	19
2	10:1	10	70	26
3	10:1	10	80	32
4	10:1	10	90	38
(B)Effect of H ₂ O ₂ /2MN mole ratio				
5	10:1	10	80	38
6	7:1	10	80	29
7	4:1	10	80	17
(C) Effect of reaction timeH ₂ O ₂ /2MN				
8	10:1	3	80	13
9	10:1	6	80	27
10	10:1	10	80	38

Reaction condition: catalyst 0.1 g (0.013 mmol), acetonitrile 10mL (solvent)

The effect of temperature, reactant molar ratios and reaction time on 2MN conversion was studied for the catalyst system V2OSBA (Table 3.2.2.).The reaction was studied in the range of temperatures from 60 to 90 °C for 10 h using the catalyst amount 0.1g (0.013 mmol). At 60 °C, 2MN conversion was 19% and increased to 38% at 80 °C. Further increase in reaction temperature to 90 °C had no appreciable effect on 2MN conversion. The effect of molar ratio on 2MN conversion was studied at 80°C with H₂O₂/2MN molar ratio 4, 7 and 10. As the H₂O₂/2MN molar ratio decreased from 10 to 6, 2MN conversion decreased from 38% to 17%. The effect of time on stream was studied at 80 °C using H₂O₂/2MN molar ratio of 10 up to 10 h. The conversion of 2MN increased from 13% at 3 h to 38% at 10 h.

3.2.4. Conclusions

In conclusion, the present study demonstrates the synthesis, characterization and catalytic applications of inorganic-organic hybrid material based on molybdovanadophosphoric acid containing mesoporous silica, mesoporous organosilica and mesoporous carbon materials. The diagnostic techniques such as small angle XRD, N₂ sorption studies, SEM, HRTEM together provided an evidence for the structural integrity of the newly synthesized catalysts systems. The new materials are truly heterogeneous and are efficient for synthesis of 2-Methy-1,4-naphthoquinone (menadione, vitamin K3 precursor). Compared to the conventional preparation of Vitamin K3, this method could be economical and environmentally benign as the use of mineral acid and chromium salts are avoided.

Section C

3.3 Heteropoly acid based supported ionic liquid phase catalyst for the selective oxidation of alcohols

3.3.1. Introduction

The use of heterogeneous catalysts in the liquid phase offers several advantages over homogeneous ones, such as ease of recovery and recycling, atom utility, and enhanced stability [134]. For the improvement, insoluble bulk materials [135], impregnation of homogeneous catalysts onto inert solid supports such as metal hydroxides [136] and polymers [137] and attachment of active species through covalent or ionic bonds with supports have been utilized [138]. However, these systems also suffer from various disadvantages such as decrease in activity, leaching of active species into the reaction medium, early decomposition of the oxidant due to support interaction and poor accessibility of substrate and oxidant either due to hydrophilicity or low surface area of the supports [139]. The use of ionic liquids, composed entirely of ions with a melting point below 100 °C, has become one of the most prolific areas of ionic liquids research to date, due to their unique properties, including low volatility, high polarity, good stability over a wide temperature range, and selective dissolving capacity by a proper selection of cation and anion [140]. Moreover, since ionic liquids are expensive it is desirable to minimize the amount of ionic liquid used in usual biphasic reaction systems. Dissolving organometallic complexes in supported films of ionic liquids has recently been introduced as a strategy (SILP) to immobilize molecular catalysts [141]. This allows fixing molecular catalysts in a widely tailorable environment. In the past few decades, the use of polyoxometalates (POMs) and POM-based compounds as catalysts has become a significant research area. Particularly, POMs have received much interest in the area of acid and oxidation catalysis because of their acidic and redox properties, which can be controlled at the molecular or atomic level [142].

Discriminating one site on a molecule from another and distinguishing among many similar molecules presents a difficult challenge to both industrial and biological

chemistry. The improvement of selective oxidation processes constitutes a dynamic area of academic as well as industrial research [143]. In view of their importance as intermediates in organic synthesis, several methods for oxidation of alcohols to aldehydes and ketones have been acknowledged in the literature [144]. Swern oxidation has been shown to be a good method for the oxidation of alcohols [145]. On the other hand; this method suffers from formation of dimethyl sulfide as a by-product and low chemo selectivity. Unfortunately, many of the most widespread methods suffer from the use of forcing conditions and/or toxic stoichiometric oxidants. From an economical and environmental point of view, catalytic oxidation processes are thus important, and those employing molecular oxygen or air are particularly attractive due to their lower cost, greater abundance and improved safety [146]. On the other hand, these protocols still suffer from low substrates conversion or high catalyst loadings, or require acidic media [147].

Herein, we report, an effective method for the aerobic oxidation of primary and secondary alcohols to the aldehydes and ketones under mild conditions with good to excellent conversions, using cation exchanged $H_5[PMo_{10}V_2O_{40}] \cdot 32.5H_2O$ (V) immobilized on 1-butyl-3-methylimidazoliumhexafluorophosphate ionic liquid-modified SBA-15 (V2ILSBA) catalyst. To the best of our knowledge, no report is available in the literature on aerobic oxidation of alcohols with air using a recyclable catalyst V2ILSBA. Our earlier studies along with some other research group show that the vanadium containing heteropoly acids are very effective for oxidation reaction and SBA-15 is a better support compared to other mesoporous supports due to high hydrothermal stability and substantially larger pore [148]. So, based on our earlier reports, we have chosen SBA-15 as mesoporous support for immobilization of ionic liquids and $H_5[PMo_{10}V_2O_{40}] \cdot 32.5H_2O$ as active catalyst species.

3.3.2. Catalyst Synthesis

3.3.2.1. Synthesis of ionic liquid modified $H_5[PMo_{10}V_2O_{40}] \cdot 32.5H_2O$ (1)

1-butyl-3-methylimidazolium bromide, $[C_4mim]Br$, was purchased from Fluka. $[C_4mim]^+$ salt of a $[PMo_{10}V_2O_{40}]^{5-}$ $[C_4mim]^+$ salt of a $[PMo_{10}V_2O_{40}]^{5-}$ were precipitated from acetone solutions of $[PMo_{10}V_2O_{40}]^{5-}$ by the addition of excess $[C_4mim]Br$. The

yellow waxy solid was collected, washed thoroughly with H₂O, and dried. ¹³C NMR δ (ppm) = 137, 124, 123 (Aromatic), 50 (CH₂N), 37 (NCH₃), 32 (CH₂), 19 (CH₂), 13 (CH₃). This compound is soluble in DMSO at room temperature.

3.3.2.2. Synthesis of 1-(3-Trimethoxysilylpropyl)-3-methylimidazoliumchloride (2)

A mixture of 1-methylimidazole (3.36 g, 40mmol) 3-chloropropyltrimethoxysilane (9.63 g, 40 mmol) was heated under an argon atmosphere at 95 °C for 24 h. After cooling viscous oil was formed. This viscous oil was used immediately in the next step. ¹H NMR (CDCl₃): δ (ppm) = 8.53 (s,1H), 8.34 (d,1H), 8.26 (d,1H), 4.49 (t, 2H), 4.11(s, 3H), 3.40-3.52 (m, 6H), 1.85-1.91(m, 2H), 1.25-1.33 (t, 9H), 0.71-0.78 (m, 2H); ¹³C NMR (CDCl₃): δ (ppm) = 136.1, 124.3, 122.8, 52.2 (CH₂N), 51.4 (CH₂O), 36.4 (NCH₃), 25.1 (CH₂), 11.2 (CH₃), 7.0 (SiCH₂) [149].

3.3.2.3. Synthesis of 1-(3-Trimethoxysilylpropyl)-3-methylimidazoliumhexa fluoro-phosphate (3)

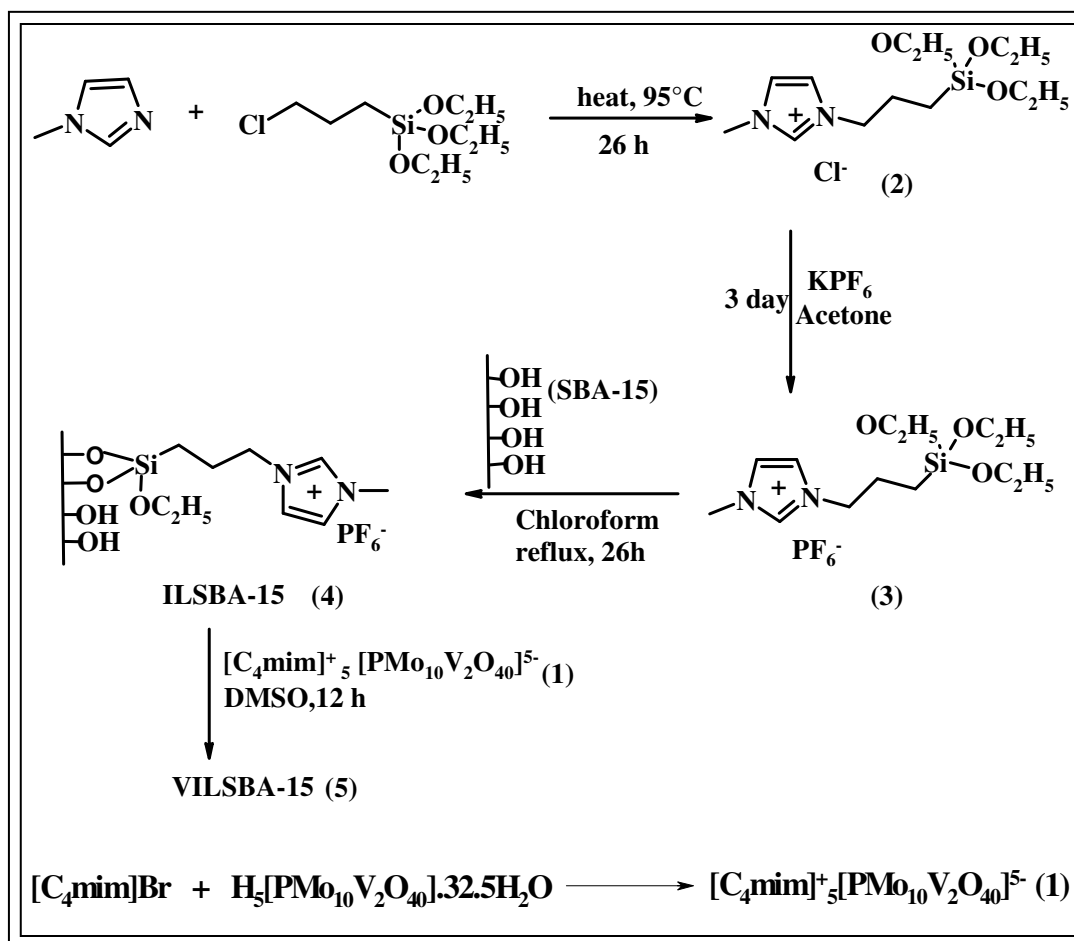
To a solution of the above salt (3.2 g, 10 mmol), in acetone (15 mL), potassium hexafluorophosphate (1.9, 10.5 mmol) was added in one portion. The mixture was stirred at room temperature for 3 days. After this time the mixture was filtered and the solvent evaporated under reduced pressure to give 2. ¹H NMR (CDCl₃), δ (ppm) = 8.90 (s, 1H), 7.58 (d, 1H), 7.55 (d, 1H), 4.39 (t, 2H), 4.15 (s, 3H), 3.59-3.71 (m, 6H), 1.88-1.94 (m, 2H), 1.27-1.35(t, 9H), 0.61-0.70 (m, 2H), ¹³C NMR (CDCl₃), δ (ppm) = 136.3, 124.0, 122.4, 51.5 (CH₂N), 51.3 (CH₂O), 36.0 (NCH₃), 24.9 (CH₂), 10.2 (CH₃), 6.9 (SiCH₂), ³¹P NMR (CDCl₃), δ (ppm) =143.6. [149]

3.3.2.4. Synthesis of ionic liquid modified SBA-15 (ILSBA-15) (4)

The ionic liquid 2 (2.81 g, 6.5 mmol) was dissolved in chloroform (50 mL) and treated with mesoporous silica (dried under vacuum and heated at 180 °C overnight, 4.00 g). The mixture was heated under reflux (65 °C) for 26 h. After cooling to room temperature, the solid was isolated by filtration and washed with chloroform (50 mL) and diethyl ether (50 mL).The solid was dried under reduced pressure to give a powder. ¹³C NMR δ (ppm) = 136.39, 124.0, 122.4 (Aromatic), 63 (CH₂N), 47-51 (CH₂O), 36.0 (NCH₃), 22 (CH₂), 14 (CH₃), 8.4 (SiCH₂), ²⁹Si MAS NMR: (59.7 MHz) δ (ppm) = -110 (Q⁴), -102 (Q³), -68 (T³), -60 (T²). (Fig. 3.3.5 (a)) [149].

3.3.2.6. Preparation of ionic liquid modified $H_5[PMo_{10}V_2O_{40}] \cdot 32.5H_2O$ catalyst supported on ionic liquid-modified SBA-15 (V2ILSBA) (5)

Ionic liquid modified SBA-15 (ILSBA-15) (1 g) was vigorously stirred with (0.4 g) of $[C_4mim]^+$ salt of a $[PMo_{10}V_2O_{40}]^{5-}$ in 50 mL of DMSO at room temperature for 12 h. The solid was then filtered off, washed with a large amount of DMSO, and dried in vacuum to afford V2ILSBA. ^{13}C NMR δ (ppm) = 136.3, 124.0, 122.1 (Aromatic), 63 (CH₂N), 47-51 (CH₂O), 36.0 (NCH₃), 22 (CH₂), 14 (CH₃), 8.4 (SiCH₂), ^{29}Si MAS NMR: (59.7 MHz) δ (ppm) = -110 (Q⁴), -102 (Q³), -68 (T³).



Scheme 3.3.1. Synthesis of V2ILSBA

3.3.3. Catalyst characterization

3.3.3.1. ICP/AES analysis

The molybdenum and vanadium content was 4.15 ppm and 21.5 ppm respectively estimated by inductively coupled plasma-optical emission spectroscopy (ICP-AES).

3.3.3.2. Low angle XRD

The low angle powder X-ray diffraction patterns of SBA-15 and V2ILSBA (40) are depicted in Fig. 3.3.1 (A). SBA-15 patterns showed an intense peak assigned to reflections at (100) and two low intensity peaks at (110) and (200), indicating a significant degree of long-range ordering in the structure and a well-formed hexagonal lattice. The V2ILSBA (40) sample showed a decrease in the intensities of all the above mentioned peaks with a marginal shift towards lower 2θ values demonstrating the occurrence of functionalisation inside the mesopores channels of SBA-15 and the induction of a relatively high number of polyoxometalate anions inside the SBA-15.

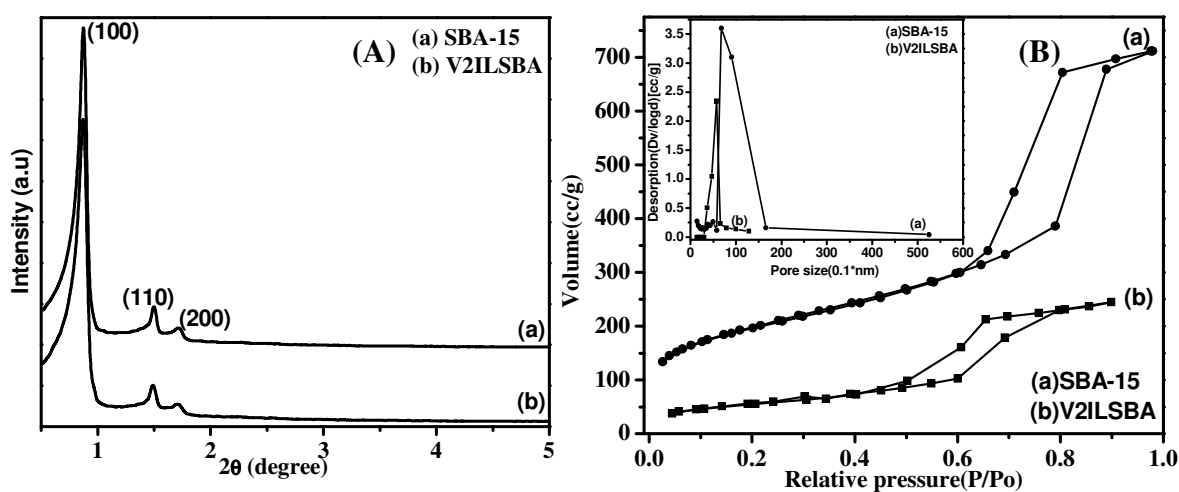


Fig. 3.3.1. (A) Small angle XRD of (a) SBA-15 and (b) V2ILSBA and (B) N_2 sorption isotherms of (a) SBA-15 and (b) V2ILSBA

However, the mesoporous structure of the support remained intact under the conditions used for functionalisation.

3.3.3.3. Surface area

The N_2 adsorption–desorption isotherms of SBA-15 and V2ILSBA (40) are depicted in Fig. 3.3.1.(B) BET surface areas and BJH distributions were calculated using

N_2 adsorption at 77 K. Functionalization and introduction of polyoxometalate anions affect the surface area and pore distribution of the modified samples significantly. The samples display a type IV isotherm with H1 hysteresis and a sharp increase in pore volume adsorbed above $P/P_0 \sim 0.7$ cm^3/g , which is a characteristic of highly ordered mesoporous materials. The textural properties of SBA-15 were substantially maintained over ionic liquid functionalisation and on subsequent anchoring of vanadium modified polyoxometalates. The parent SBA-15 sample shows a maximum pore diameter (6.8 nm) and surface area (714 m^2/g). Functionalization and introduction of polyoxometalate of mesoporous silica results in a shift of the pore maximum to lower diameter (5.7 nm) and a decrease in surface area (209 m^2/g). HRTEM pictures support the mesoporous structure of V2ILSBA (Fig 3.3.2)

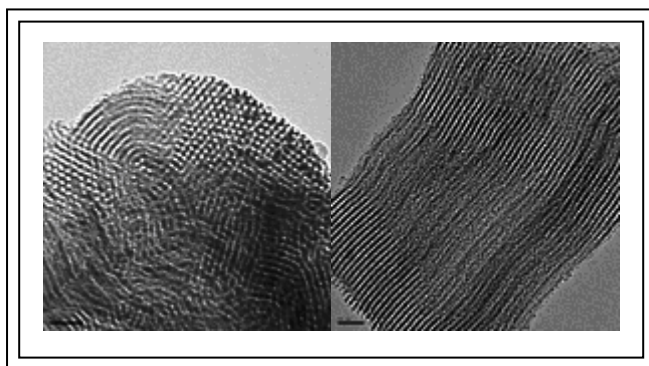


Fig. 3.3.2. HRTEM pictures of V2ILSBA

3.3.3.4. ^{31}P and ^{51}V CP-MAS NMR

Due to the nature of the compound, ionic liquid modified $H_5[PMo_{10}V_2O_{40}] \cdot 32.5H_2O$ (relatively viscous) we were not able to have a good rotation, so the ^{31}P one shows numerous spinning sidebands around 4.2 ppm (Fig. 3.3.3(a)). The ^{31}P NMR spectrum of ionic liquid modified SBA-15 shows only the resonance of PF_6^- corresponds to the formula $BMIM^+ \cdot PF_6^-$ as this anion gives a signal at ca. -150 ppm (Fig. 3.3.3 (b)). The phosphorus spectrum of ionic liquid modified $H_5[PMo_{10}V_2O_{40}] \cdot 32.5H_2O$ catalyst supported on ionic liquid-modified SBA-15 (V2ILSBA) shows the two signals at 4.2 and 150 ppm of the heteropolyanion and PF_6^- (the multiplet corresponds to the P-F couplings) (Fig. 3.3.3(c)).

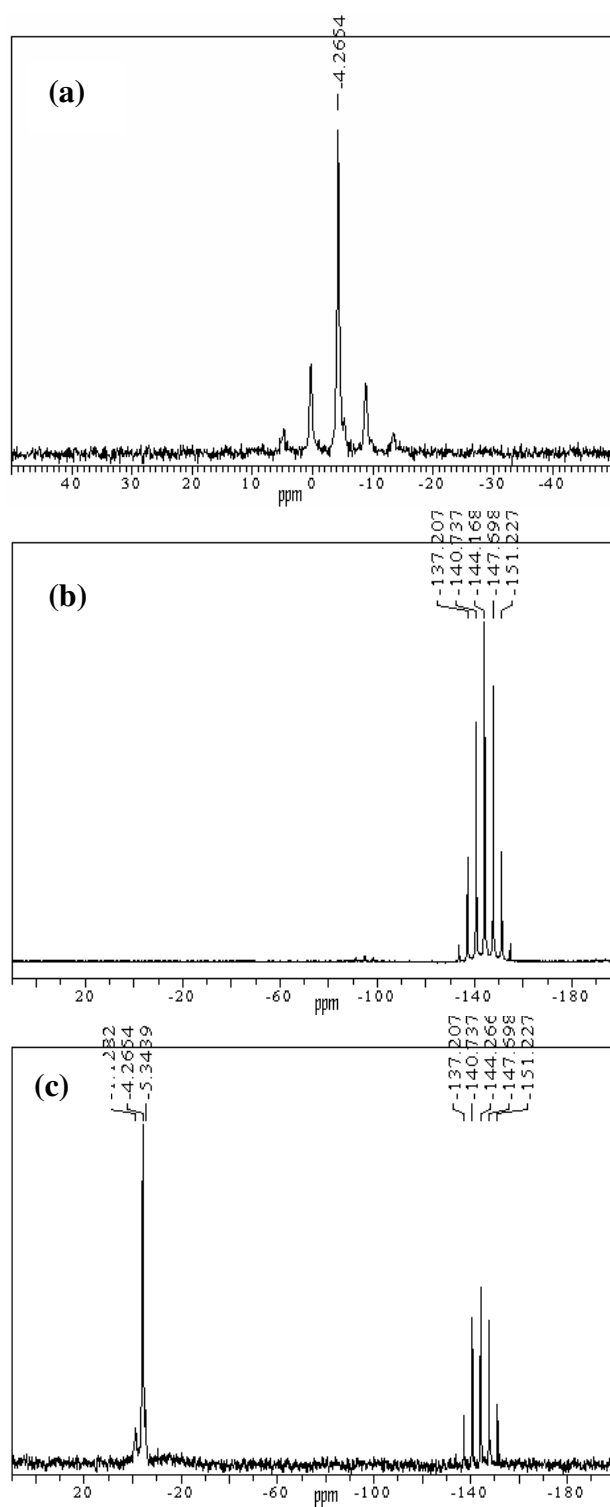


Fig. 3.3.3. ^{31}P CP MAS NMR of (a) $[\text{C}_4\text{mim}]^+$ salt of a $[\text{PMo}_{10}\text{V}_2\text{O}_{40}]^{5-}$ (b) ILSBA (c) V2ILSBA

Vanadium-51 spectra showed the presence of numerous spinning side band envelopes centered on -400 ppm, attributed to the various possible stereoisomers present (Fig. 3.3.4 (a)). In fact, from the ^{51}V NMR spectra, we could not make a clear distinction between different isomers, but could see that vanadium was octahedrally distorted.

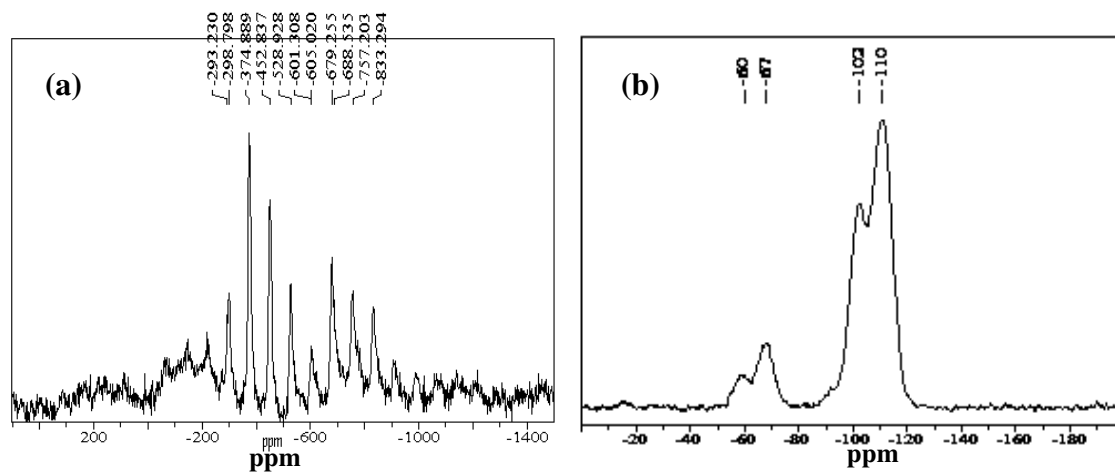


Fig. 3.3.4. (a) ^{51}V CP MAS NMR of V2ILSBA and (b) ^{29}Si MAS NMR of ILSBA-15

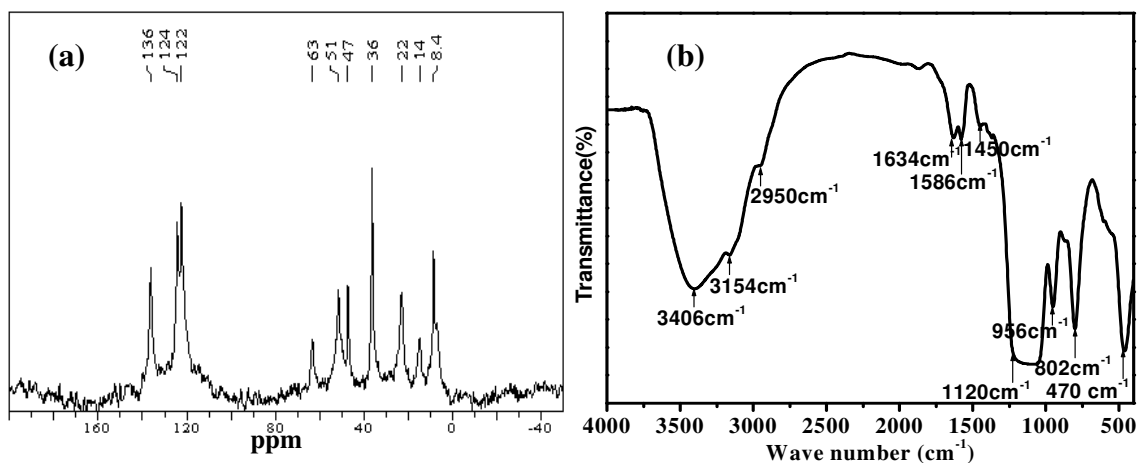


Fig. 3.3.5. (a) ^{13}C MAS NMR of ILSBA-15 and (b) FT-IR spectra of V2ILSBA

The ^{29}Si MAS NMR spectrum of ILSBA-15 showed two signals at -110 and -102 ppm corresponding to Q^4 and Q^3 species of the silica framework, respectively ($Q^m =$

$Si(OSi)_m(OH)_{4-m}$ (Fig. 3.3.4 (b)). Additional signals appeared at -68 and -60 ppm assignable to T^3 and T^2 organosilica species, respectively ($T^n = RSi(OSi)_n(OEt)_{3-n}$)

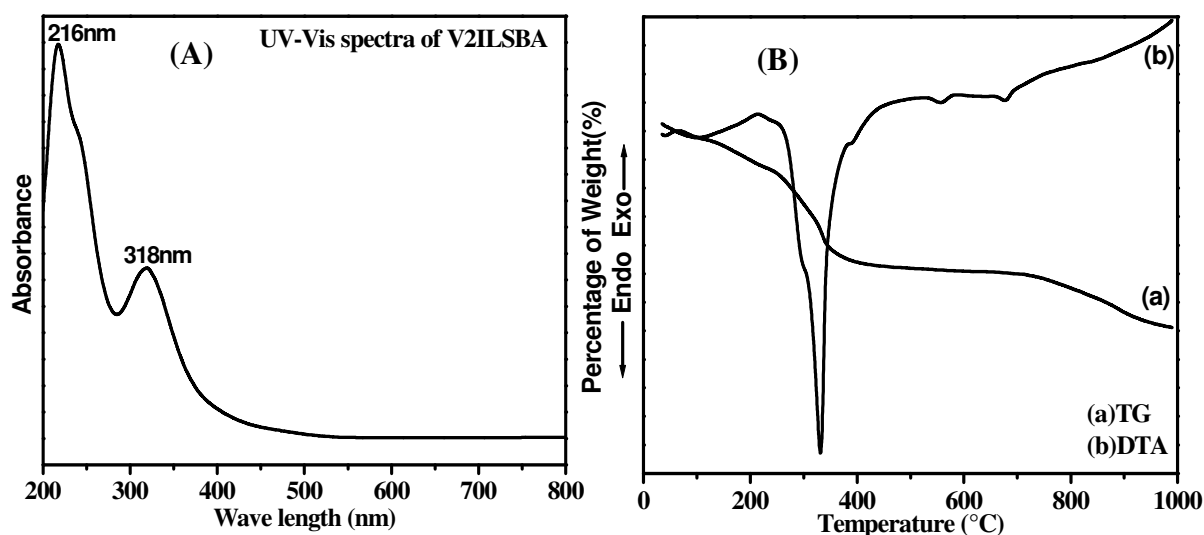


Fig. 3.3.6. (A) UV-Vis spectra of V2ILSBA and (B) TG and DTA of V2ILSBA

3.3.3.5. FT-IR

The typical FT-IR bands due to siliceous material Si–O–Si are observed for V2ILSBA (Fig. 3.3.5(b)): a main band at 1120 cm^{-1} , due to asymmetric Si–O–Si stretching modes and symmetric stretch at 960 , 802 and 470 cm^{-1} . A broad, asymmetric feature at 3400 cm^{-1} is observed due to O–H vibrations of silanols and water. Additional features at 2950 , 3154 cm^{-1} and 1450 cm^{-1} due to C–H stretching and deformation vibrations respectively confirming the functionalization of ionic liquid in the material. The bands at 1586 and 1634 cm^{-1} are due to C=N and C=C ring vibration of imidazole part of the ionic liquid. The characteristic features of V2, masked by the intense bands of the SBA-15 and ionic liquid due to its comparatively low concentration.

3.3.3.6. UV-Vis

UV-vis spectra of V2ILSBA are shown in Fig.3.3.6. (A). Because V2 exhibits characteristic absorption bands in UV-Vis region, diffuse-reflectance UV-Vis spectroscopy, often characterizes their structures. V2ILSBA exhibits certain features of LMCT; these characteristic bands were observed at around 216 and 318 nm

3.3.3.7. TG-DTA

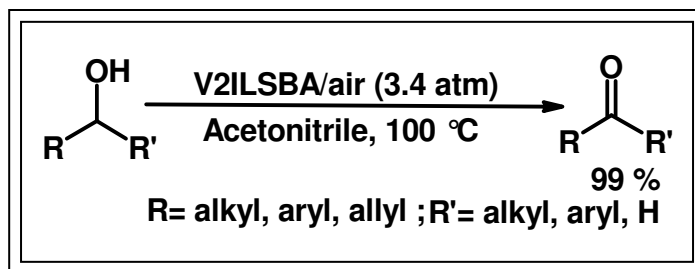
The thermal behavior of V2ILSBA was determined by TG-DTA. Fig. 3.3.6. (B) shows the TG-DTA curves of V2ILSBA from 25–100 °C. Evident loss of weight was observed at 300 °C. The sample showed endothermic peaks on heating. V2ILSBA was stable up to 295 °C and decomposed rapidly over 330 °C.

3.3.4. Catalysis

A couple of experiments were performed to optimize the reaction condition for this newly synthesized catalyst V2ILSBA. In the first experiment, the reaction was carried out at 1 atm air pressure at 100 °C in a Parr autoclave with the active catalyst in acetonitrile solvent, which gave only 40% yield. Product yield increased with the increasing of pressure 2 to 3.4 atm (60% to 100%). In the next experiment, we studied the effect of temperature, no reaction between alcohol and molecular oxygen of air was seen at 50 °C. Alcohol yield increased with increasing temperature to 80–100 °C (80-100 %). From the above observations, we can conclude that the maximum yield can be obtained at 100 °C and 3.4 atm. To investigate the effect of V2 loading on alcohol oxidation, immobilized catalysts were prepared with various V2 loadings (20–50 %) on SBA-15 and tested in alcohol oxidation; the results showed that with an increase in V2 loading, yield get increased. At higher V2PA loading (60%), alcohol conversion decreased, possibly due to changes in the morphology of the support (mesopore diameter and volume). Moreover, higher loadings might have acted as an inhibitor rather than as a catalyst by capturing active radicals. V2ILSBA (40%) exhibited the highest activity, because of the ease of diffusion constraints; thus, this was used for further studies.

3.3.4.1. Typical Procedure for the Oxidation

Alcohol (1 mmol) and catalyst (V2ILSBA) (100 mg, 0.02 mol % eq. V2) were stirred at *ca.* 100 °C in acetonitrile (20 mL) under air pressure (3.4 atm) in Parr autoclave (pressure reactor) for 12 h and α,α -azobisisobutyronitrile (AIBN) or *tert*-butylhydroperoxide (TBHP) as radical initiator being used (Scheme3.3.2). After filtering the catalyst, the filtrate was analyzed by GC and passed through a short pad of silica gel using ethyl acetate and hexane (1:19) as eluent or distilled to provide the 100 % analytically pure aldehydes and ketones.



Scheme 3.3.2. Oxidation of alcohols to aldehydes and ketones

The oxidation of 1-(Naphthyl-2-yl) ethanol, as a model substrate was first investigated using V2ILSBA under atmospheric oxygen (Table 3.3.1) in acetonitrile solvent, α,α -azobisisobutyronitrile (AIBN) or *tert*-butylhydroperoxide (TBHP) as radical initiator. We were pleased to find that the alcohol was completely oxidized to methylnaphthylketone in 99 % yields. To evaluate the scope of this protocol, the oxidation of other alcohols was further studied. As indicated in Table 3.3.1 (entries 2-6), secondary alcohols such as diphenylmethanol, cyclohexanol, phenylethanol, 2-hexanol and 2-phenylpropanol oxidized to the corresponding ketones in high yields. A similar reactivity was observed in the oxidation of substrates having electron-withdrawing and donating groups in the aromatic ring, i.e., 4-methoxy-, 4-methyl-, 4-chloro-, 4-bromo- and 4-nitrophenylethanol to corresponding ketones in good yields (entries 7-11). The oxidation proceeds well with some complicated alcohols also such as benzoin, menthol, [1,7,7] trimethylbicyclo[2,2,1]heptan-2-ol and 3,5,5-trimethylcyclohex-2-enol, in high yields (entries 12-15). Benzylalcohol was oxidized to benzaldehyde within 12 h with excellent yield (entry 16). The oxidation profile of a 1:1 mixture of benzyl alcohol and phenyl ethanol (Figure 3.3.7) was found that the rate of oxidation of the secondary alcohol (phenyl ethanol) is faster compared to primary alcohol (benzyl alcohol). In another experiment, we have taken 1, 3-butanediol as a substrate to check the reactivity (entry 17) and surprisingly found that 4-hydroxybutane-2-one was the only product after 8 h with 83 % product yield, resulting from the oxidation of secondary alcohol. Similarly, allylic alcohols such as geraniol and cinnamyl alcohol oxidized to aldehydes without cleavage of carbon-carbon double bonds (entries 18,19). Furthermore, pyridine-2-methanol was oxidized to corresponding aldehyde in high yields (entry 20). No oxidation was observed with heteroatom.

Table 3.3.1. Aerobic Oxidation of Alcohols to Aldehydes and ketones

Entry	Substrate	Product	t/h	Yield ^b (%)
1	1-(Naphthyl-2-yl) ethanol	2-Methylnaphthylketone	7	99
2	Diphenylmethanol	Benzophenone	7	99
3	Cyclohexanol	Cyclohexanone	6	99
4	Phenylethanol	Acetophenone	6	99
5	2-Hexanol	2-Hexanone	5	98
6	2- Phenyl propanol	Propiophenone	7	93
7	4-Methoxy phenylethanol	4- Methoxy acetophenone	6	98
8	4-Methyl phenylethanol	4-Methyl acetophenone	6	96
9	4-Chloro phenylethanol	4- Chloro acetophenone	6	98
10	4-Bromo phenylethanol	4-Bromo acetophenone	6	98
11	4-Nitro phenylethanol	4-Nitro acetophenone	6	94
12	Benzoin	Benzil	7	95
13	Menthol	Menthone	6	96
14	[1,7,7]Trimethylbicyclo [2,2,1]heptan-2-ol	Camphor	8	95
15	3,5,5-Trimethylcyclohex-2- enol	3,5,5-trimethylcyclohex-2- enone:	7	94
16	Benzyl alcohol	Benzaldehyde	12	98
17	1, 3-Butanediol	4-hydroxybutane-2-one	8	83
18	Geraniol	Geranial	10	97
19	Cinnamyl alcohol	Cinnamaldehyde	13	98
20	Pyridine-2-methanol	2-Pyridine carboxaldehyde	11	96

Reaction Conditions: Catalyst: V2ILSBA Substrate (1 mmol) and catalyst (V2ILSBA) (100 mg, 0.02 mol % of V2) were stirred at *ca.* 100 °C in acetonitrile (20 mL) under air pressure (3.4 atm) in Parr autoclave (pressure reactor) and α,α -azobisisobutyronitrile (AIBN) or *tert*-butylhydroperoxide (TBHP) as radical initiator being used, ^bGC yield.

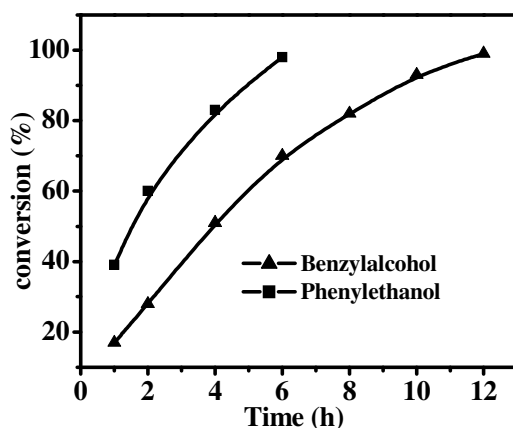
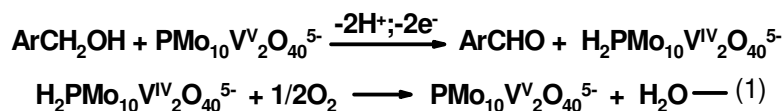


Fig 3.3.7. Progress of the oxidation of benzyl alcohol and phenylethanol

The selective oxidation of primary and secondary alcohols to aldehydes and ketones respectively, without overoxidation of the aldehydes to the carboxylic acids, found for heteropolyoxometalates are electrontransfer redox-type oxidations utilizing molybdenum-vanadium mixed-addenda Keggin anions[150].As per literature, such reactions are thought to proceed by the generalized mechanism, shown in eq.3.3.1.



Equation 3.3.1. Possible mechanism of oxidation of alcohols

3.3.5. Conclusion

In conclusion, a novel and efficient protocol is presented for a broad range of benzylic, allylic and aliphatic alcohols oxidation under mild conditions with a high degree of chemoselectivity using V2ILSBA as nanoreactor catalyst system. The benzylic and allylic alcohols were oxidized with excellent conversions, whereas aliphatic alcohols were less reactive. The method is environmentally friendly and a valid alternative to the classical Swern oxidation. Therefore, we can avoid the use of toxic reagents and conducting oxidation at very low temperature. The activities and product selectivities were comparable to those of the homogeneous analogue, showing that the homogeneous catalysis could be heterogenized successfully. The rate of oxidation of the secondary alcohols was found to be faster than that of the primary ones.

3.4. References

1. H. Song, R.M. Rioux, J.D. Hoefelmeyer, R. Komor, K. Niesz, M. Grass, P. Yang, G.A. Somorjai, *J. Am. Chem. Soc.* 128 (2006) 3027.
2. R. Ganesan, B. Viswanathan, *Bull. Catal. Soc. of India.* 10 (2000) 1.
3. A. Mazeaud, Y. Dromzee and R. Thouvenot, *Inorg. Chem.* 39 (2000) 4735.
4. Á. Kukovecz, Z. Kónya, I. Kiricsi, *J. Mol. Str.* 565 (2001) 121.
5. B.J.S. Johnson, A. Stein, *Inorg. Chem.* 40 (2001) 801.
6. W. Kaleta, K. Nowińska, *Chem. Commun.* (2001) 535.
7. A. Maldotti, A. Molinari, G. Varani, M. Lenarda, L. Storaro, F. Bigi, R. Maggi, A. Mazzacani, and G. Sartori, *J. Catal.* 209 (2002) 210.
8. H.L Li, N. Perkas, Q.L. Li, Y. Gofer, Y. Kolytyn, A. Gedanken, *Langmuir.* 19 (2003) 10409.
9. J. Wang, H. O. Zhu, *Catal. Lett.* 93 (2004) 209.
10. R.J. Errington, S.S. Petkar, B.R. Horrocks, A. Houlton, L.H. Lie, S.N. Patole, *Angew. Chem. Int. Ed.* 44 (2005) 1254.
11. N. Kato, A. Tanabe, S. Negishi, K. Goto, K. Nomiya, *Chem. Lett.* 34 (2005) 238.
12. Y. Izumi, K. Urabe, *Chem. Lett.* (1981) 663.
13. R. Neumann, M. Levin, *J. Org. Chem.* 56 (1991) 5707.
14. S. Fujibayashi, K. Nakayama, Y. Nishiyama, Y. Ishii. *Chem. Lett.* (1994) 1345.
15. G.I. Giles, R.P. Sharama. *J. Peptide Sci.* 11 (2005) 417.
16. Anthracycline Antibiotics, New Analogues, Methods of Delivery, and Mechanisms of Action. Priebe, W., Ed.; American Chemical Society Symposium Series. (1993) 574.
17. J.S. Driscoll, G.F. Hazard, H.B. Wood, A Goldin, *Cancer Chemother. Rep.* 2 (1974) 1.
18. D. Cairns, E. Michalitsi., T. C. Jenkins, S. P. Mackay, *Bioorg. Med. Chem.* 10 (2002) 803.
19. P. Krapcho, M. J. Maresch, M. P. Hacker; L Hazelhurst, E. Menta, A. Oliva, S. Spinelli, G. Beggiolin, F Giuliani, G. Pezzoni, S. Tognella, *Curr. Med. Chem.* 2 (1995) 803.

20. J.W. Lown, *Pharmacol. Ther.* 60 (1993) 185.
21. C. Cheng, R.K. Y Zee-Cheng, *Prog. Med. Chem.* 20 (1983) 83.
22. H.S. Huang, J.F. Chiou, Y Fong, C.C. Hou, Y.C. Lu, J.Y. Wang, J.W. Shih, Y.R Pan, J. J. Lin, *J. Med. Chem.* 46 (2003) 3300.
23. P. Ge, R.A. Russell, *Tetrahedron* 53 (1997) 17469.
24. C.P. Lee, KH. Singh, *J. Natural Products* 45 (1982) 206.
25. C. Monneret. *European J. Medicinal Chemistry.* 36 (2001) 483.
26. MN. Preobrazhenskaya, A.E. Shchekotikhim, A.A. Shtil, H.S. Huang. *J. Medical Sciences.* 26 (2006) 4.
27. Ullmann's Encyclopedia of Industrial Chemistry, VCH, Weinheim, 2 (1985) 347.
28. B.E. Butterworth, O.B. Mathre, K. Ballinger, *Mutagenesis*, 16 (2001) 169.
29. H. Zollinger. *Colour Chemistry: Synthesis, Properties and Application of Organic Dyes and Pigment.* John Wiley and Sons Canada Ltd.(1987)
30. *Anthraquinone pulping: A Tappi press anthology of published papers; Paper book* (1997).
31. E.H.V. Dijk, D.J.T. Myles, M.H.V. Veen, J. C. Hummelen, *Org. Lett.* 8 (2006) 2333.
32. P.K. Tandon, R. Baboo, A.K. Singh and Gayatri. *Appl. Organo. Chem.* 20 (2006) 20.
33. D.E. Dodor, H.M. Hwang, S.I.N. Ekunwe, *Enzyme and Microbial Tech.* 35 (2004) 210.
34. P. Baldrian, T.Cajthaml, V.Merhautova, J. Gabriel, F. Nerud, P. Stopka, M. Hruby, M.J. Benes, *App.Catal. B* 59 (2005) 267.
35. G. Maayan, B. Ganchegui, W. Leitner and R. Neumann, *Chem. Commun.* (2006) 2230.
36. A.S.M. Chong, X.S. Zhao, *J. Phys. Chem. B* 107 (2003) 12650.
37. K. Mukhopadhyay, A. Ghosh, R. Kumar, *Chem. Commun.* (2002) 2404.
38. D. Zhao, Q. Huo, J. Feng, B.F. Chmelka, G.D. Stucky, *J. Am. Chem. Soc.* 120 (1998) 6024.
39. G.A. Tsigdinos, C.J. Hallada, *Inorg. Chem.* 7 (1968) 437.
40. S.J. Gregg, K.S.W. Singh, *Adsorption, Surface Area and Porosity*, 1982 (2nd ed.

- Academic Press, London).
41. J. Horniakova, T. Raja, Y. Kubota, Y. Sugi, *J. Mol. Catal.* 217 (2004) 73.
 42. S.E. O'Donnell, M.T. Pope, *J. Chem. Soc. Dalton Trans.* 1976, 2290.
 43. M. Khenkin, R. Neumann, A.B. Sorokin, A. Tuel. *Catal. Lett.* 63 (1999) 189.
 44. D. Zhao, J. Feng, Q. Huo, N. Melosh, G.H. Fredrickson, B.F. Chmelka, G. D. Stucky, *Science* 279 (1998) 548.
 45. M.-C. Chao, H.-P. Lin, H.-S. Sheu, C.-Y. Mou, *Stud. Surf. Sci. Catal.* 141 (2002) 387.
 46. I.V. Kozhevnikov, A. Sinnema, R.J.J. Jansen, K. Pamin, H. van Bekkum, *Catal. Lett.* 34 (1994) 241.
 47. A.G. Siahkali, A. Philippou, J. Dwyer, M.W. Anderson, *Appl. Catal. A*: 192 (2000) 57.
 48. Y. Kanda, K.Y. Lee, S. Nakata, S. Asaoka, M. Misona, *Chem. Lett.* 1 (1988) 139.
 49. V.M. Mastikhin, S.M. Kulikov, A.V. Nosov, I.V. Kozhevnikov, I.L. Mudrakovsky, M. N. Timofeeva, *J. Mol. Catal.* 60 (1990) 65.
 50. W. Huang, L. Todaro, G.P.A. Yap, R. Beer, L.C. Francesconi, T. Polenova. *J. Am. Chem. Soc.* 126 (2004) 11564.
 51. J. Kasai, Y. Nakagawa, S. Uchida, K. Yamaguchi, N. Mizuno. *Chem. Eur. J.* 12 (2006) 4176.
 52. D. Casarini, G. Centi, P. Jiru, V. Lena, Z. Tvaruzkova, *J. Catal.* 143 (1993) 325.
 53. Z. Luan, J.A. Fournier, J.B. Wooten, D.E. Miser, *Micro. Meso.Mater.* 83 (2005) 150.
 54. K. Nowin'ska, R. Fo'rmaniak, W. Kaleta, A. Waclaw. *Appl. Catal. A*: 256 (2003) 115.
 55. M. Fournier, C. Feumi-Jantou, C. Rabia, G. Herve, S. Launay, *J. Mater. Chem.* 2 (1992) 971.
 56. I. Kozhevnikov, *Catalyst for Fine Chemical Synthesis: Catalysis by polyoxometalates*, Wiely, Vol 138.
 57. O.A. Kholdeeva, M.P. Vanina, M.N. Timofeeva, R.I. Maksimovskaya, T.A. Trubitsina, M.S. Melgunov, E.B. Burgina, J. Mrowiec-Bialon, A.B. Jarzebski, C.L. Hill, *J. Catal.* 226 (2004) 363.

58. R.A. Sheldon, J.K. Kochi, *Metal Catalyzed Oxidation of Organic Compounds*, Academic Press, New York, 1981.
59. C.L. Hill, in: A.L. Baumstark (Ed.), *Advances in Oxygenated Processes*, vol. 3, JAI Press, London, 1998, p. 1.
60. M. Hudlucky, *Oxidations in Organic Chemistry*, ACS Monograph Series, American Chemical Society, Washington, DC, 1990.
61. A.E. Shilov, G.B. Shul'pin, *Activation and Catalytic Reactions of Saturated Hydrocarbons in the Presence of Metal Complexes*, Kluwer Academic Publishers, Dordrecht, 2000.
62. A.E. Shilov, G.B. Shul'pin, *Chem. Rev.* 97 (1997) 2879.
63. D.H.R. Barton, *Chem. Soc. Rev.* (1996) 237.
64. M.J. Perkins, *Chem. Soc. Rev.* (1996) 229.
65. E. Gretz, T.F. Oliver, A. Sen, *J. Am. Chem. Soc.* 109 (1987) 8109.
66. X. Wan, M. Duncan, P. Nass, J.W. Harmon, *Anticancer Res.* 21 (2001) 2657.
67. T. Joseph, M. Hartmann, S. Ernst, S.B. Halligudi, *J. Mol. Catal. A* 207 (2004) 129–135.
68. S. Shinachi, M. Matsushita, K. Yamaguchi, N. Mizuno *J. Catal.* 233 (2005) 81–89.
69. N. Shida, T. Ushiroguchi, K. Asakawa, T. Okino, S. Saito, Y. Funaki, A. Takaragi, K. Tsutsumi, K. Inoue, T. Nakao, *J. Photopolym. Sci. Technol.* 13 (2000) 601.
70. N. Matsuzawa, S. Takechi, T. Ohfuji, K. Kuhara, S. Mori, M. Endo, K. Kamon, T. Morisawa, A. Yamaguchi, M. Sasago, *Jpn. J. Appl. Phys.* 37 (1998) 5781.
71. I. Tabushi, T. Nakajima, K. Seto, *Tetrahedron Lett.* 21 (1980) 2565.
72. A.E. Tapper, J.R. Long, R.J. Staples, P. Stavropoulos, *Angew. Chem. Int. Ed.* 39 (13th) (2000) 2343.
73. I.V. Kozhevnikov, *Chem. Rev.* 98 (1998) 171, and references therein.
74. M. Faraj, C. Hill, *J. Chem. Soc., Chem. Commun.* (1987) 1487.
75. J. M. Thomas, *Nature (London)*, 1985, 314, 669. (b) T. Ito, J. H. Lunsford, *Nature (London)*, 1985, 314, 721.
76. A. Mazeaud, Y. Dromzee and R. Thouvenot, *Inorg. Chem.* 39 (2000) 4735.
77. Â. Kukovecz, Z. KoÂnya, I. Kiricsi, *J. Mol. Str.* 565 (2001) 121.
78. B.J.S. Johnson, A. Stein, *Inorg. Chem.* 40 (2001) 801.

79. A. Maldotti, A. Molinari, G. Varani, M. Lenarda, L. Storaro, F. Bigi, R. Maggi, A. Mazzacani, G. Sartori, *J. Catal.* 209 (2002) 210.
80. H.L Li, N. Perkas, Q. L. Li, Y. Gofer, Y. Kolytyn, and A. Gedanken, *Langmuir*. 19 (2003) 10409.
81. J. Wang and H. O. Zhu, *Catal. Lett.* 93 (2004) 209.
82. R.J. Errington, S.S. Petkar, B.R. Horrocks, A. Houlton, L.H. Lie, S.N. Patole, *Angew. Chem. Int. Ed.* 44 (2005) 1254.
83. N. Kato, A. Tanabe, S. Negishi, K. Goto, K. Nomiya, *Chem. Lett.* 34 (2005) 238.
84. Y. Izumi and K. Urabe, *Chem. Lett.* (1981) 663.
85. R. Neumann, M. Levin, *J. Org. Chem.* 56 (1991) 5707.
86. S. Fujibayashi, K. Nakayama, Y. Nishiyama, Y. Ishii. *Chem. Lett.* (1994) 1345.
87. W. Kaleta, K. Nowińska, *Chem. Commun.* (2001) 535.
88. O.A. Kholdeeva, M.P. Vanina, M.N. Timofeeva, R.I. Maksimovskaya, T.A. Trubitsina, M.S. Melgunov, E.B. Burgina, J. Mrowiec-Bialon, A.B. Jarzebski, C.L. Hill, *J. Catal.* 226 (2004) 363.
89. H. Mimoun, L. Saussine, E. Daire, M. Postel, J. Fischer, R. Weiss, *J. Am. Chem. Soc.* 105 (1983) 3101.
90. N.A. Alekar, V. Indira, S.B. Halligudi, D. Srinivas, S.Gopinathan, C. Gopinathan, *J. Mol. Catal. A: Chem.* 164 (2000) 181.
91. P. Gomez-Romero *Adv.Mater.* 13 (2001) 163.
92. S.S. Park, C.S. Ha, *The Chemical record* 6 (2006) 32.
93. T. Okuhara, N. Mizuno, M. Misono, *Adv. Catal.* 41 (1996) 113.
94. A. Bordoloi, F. Lefebvre, S.B. Halligudi, *J. Catal.* 247 (2007) 166.
95. W. Kaleta, K. Nowińska, *Chem. Commun.* (2001) 535.
96. A. Maldotti, A. Molinari, G. Varani, M. Lenarda, L. Storaro, F. Bigi, R. Maggi, A. Mazzacani, G. Sartori, *J. Catal.* 209 (2002) 210.
97. A. Mazeaud, Y. Dromzee R. Thouvenot, *Inorg. Chem.* 39 (2000) 4735.
98. B.J.S. Johnson, A. Stein, *Inorg. Chem.* 40 (2001) 801.
99. H.L Li, N. Perkas, Q. L. Li, Y. Gofer, Y. Kolytyn, A. Gedanken, *Langmuir*. 19 (2003) 10409.
100. R.J. Errington, S.S. Petkar, B.R. Horrocks, A. Houlton, L. H. Lie, S.N. Patole,

- Angew. Chem. Int. Ed. 44 (2005) 1254.
101. L.F. Fieser, M. Tushler, W.L. Sampson, J. Biol. Chem. 137 (1941) 659.
 102. M. Periasamy, M.V. Bhatt, Tetrahedron Lett. 4 (1978) 4561.
 103. R.P. Kreh, R.M. Spotnitz, J.T. Lundquist, J. Org. Chem. 54(1989) 1526.
 104. J. Karzewski, Tetrahedron 40 (1984) 4997.
 105. S. Torri, H. Janaka, S. Nakane, Bull. Chem. Soc. Jpn. 55 (1982) 1673.
 106. H. Hiranuma, S.I. Miller, J. Org. Chem. 47 (1982) 5083.
 107. A.B. Sorokin, A. Tuel, New J. Chem. 23 (1999) 473.
 108. J. Kowalski, J. Ploszynska, A. Sobkowiak, J. Appl. Electrochem. 28 (1998) 1261.
 109. L.F. Fieser, J. Biol. Chem. 133 (1940) 391.
 110. R.A. Sheldon, Top. Curr. Chem. 164 (1993) 21.
 111. W. Adam, W.A. Herrmann, J. Lin, C.R. Saha-Moller, R.W.Fischer, J.D.G. Correia, Angew. Chem. 106 (1994) 25456.
 112. W.A. Herrmann, J.J. Haider, R.W. Fischer, J. Mol. Catal. A Chem. 138 (1999) 115.
 113. S. Yamaguchi, M. Inoue, S. Enomoto, Chem. Lett. (1985)827.
 114. W. Adam, W.A. Herrmann, J. Lin, C.R. Saha-Moller, J. Org.Chem. 59 (1994) 8281.
 115. R. Song, A. Sorokin, J. Bernadou, B. Meunier, J. Org. Chem.62 (1997) 673.
 116. O.A. Anunyiata, L.B. Pierella, A.R. Beltramone, J. Mol. Catal. A: Chem. 149 (1999) 255.
 117. A. Bohle, A. Schubert, Y. Sun, W.R. Thiel, Adv. Synth. Catal. 348(2006)1011.
 118. G.A. Tsigdinos, C.J. Hallada, Inorg. Chem. 7 (1968) 437.
 119. W.Guo, J.Y. Park, M.O. Oh, H.W. Jeong, W.J. Cho, I. Kim, C.S. Ha, Chem. Mater. 15 (2003) 2295.
 120. W.H. Zhang, B. Daly, J. O'Callaghan, L. Zhang, J.L. Shi, C. Li, M.A. Morris, J.D. Holmes, Chem. Mater. 17 (2005) 6407.
 121. Q. Hu, J. Pang, Z.Wu, Y. Lu, Carbon 44 (2006) 1298.
 122. B. Jarrais, A.R. Silva C. Freire, Eur. J. Inorg. Chem.(2005) 4582.
 123. A.M. Khenkin, R. Neumann, A.B. Sorokin, A. Tuel, Cat.Lett. 63 (1999) 189.
 124. S.E. O'Donnell, M.T. Pope, J. Chem. Soc. Dalton Trans. (1976) 2290.

125. M. Khenkin, R. Neumann, A.B. Sorokin, A. Tuel, *Catal. Lett.* 63 (1999) 189.
126. A.G. Siahkali, A. Philippou, J. Dwyer, M.W. Anderson, *Appl. Catal. A*: 192 (2000) 57.
127. Y. Kanda, K.Y. Lee, S. Nakata, S. Asaoka, M. Misona, *Chem. Lett.* 1 (1988)139.
128. V.M. Mastikhin, S.M. Kulikov, A.V. Nosov, I.V. Kozhevnikov, I.L. Mudrakovsky, M. N. Timofeeva, *J. Mol. Catal.* 60 (1990) 65.
129. W. Huang, L. Todaro, G. P. A. Yap, R. Beer, L.C. Francesconi, T. Polenova. *J. Am. Chem. Soc.* 126 (2004) 11564.
130. J. Kasai, Y. Nakagawa, S. Uchida, K. Yamaguchi, N. Mizuno. *Chem. Eur. J.* 12 (2006) 4176.
131. D. Casarini, G. Centi, P. Jiru, V. Lena, Z. Tvaruzkova, *J. Catal.* 143 (1993) 325.
132. Z. Luan, J.A. Fournier, J.B. Wooten, D.E. Miser, *Micro. Meso. Mater.* 83 (2005) 150.
133. O. Muth, C. Schellbach, M. Froba, *Chem. Commun.* (2001) 2032.
134. M. Dusi, T. Mallat, A. Baiker, *Catal. Rev.* 42 (2000) 213.
135. (a) M.V. Vasylev, R. Neumann, *J. Am. Chem. Soc.* 126 (2004) 884. (b) M. Musawir, P. N. Davey, G. Kelly, I.V. Kozhevnikov, *Chem. Commun.* (2003) 1414 (c) K. Yamaguchi, N. Mizuno, *New J. Chem.* 26 (2002) 972. (d) T. Okuhara, *Chem. Rev.* 102 (2002) 3641 and references cited therein.
136. (a) B.F. Sels, D.E. De Vos, M. Buntinx, F. Pierard, A.K.D. Mesmaeker, P.A. Jacobs, *Nature*, 400 (1999) 855. (b) B. F.Sels, D.E. De Vos, P.A. Jacobs, *J. Am. Chem. Soc.* 123 (2001) 8350. (c) T. Matsushita, K. Ebitani, K. Kaneda, *Chem. Commun.* (1999) 265. (d) K. Yamaguchi, K. Mori, T. Mizugaki, K. Ebitani, K. Kaneda, *J. Am. Chem. Soc.* 122 (2000) 7144. (e) K. Yamaguchi, K. Mori, T. Mizugaki, K. Ebitani, K. Kaneda, *J. Am. Chem. Soc.* 124 (2002)11572. (f) K.Yamaguchi, N. Mizuno, *Angew. Chem., Int. Ed.* 41 (2002) 4538. (g) C. Nozaki, C.G. Langmuir, A.T. Bell, T.D. Tilley, *J. Am. Chem. Soc.* 124 (2002) 13194. (h) K.L. Fajdala, I.J. Drake, A.T. Bell, T.D. Tilley, *J. Am. Chem. Soc.* 126(2004) 10864.
137. (a) Y. Uozumi, R. Nakao, *Angew. Chem., Int. Ed.* 42 (2003) 194. (b) N.E. Leadbeater, M. Marco, *Chem. Rev.* 102 (2002) 3215. (c) C.A. McNamara, M.J.

- Dixon, M. Bradley, *Chem. Rev.* 102 (2002) 3275. (d) D.E. Bergbreiter, *Chem. Rev.* 102 (2002) 3345 and references cited therein.
138. (a) A.L. Villa, B.F. Sels, D.E. De Vos, P.A. Jacobs, *J. Org. Chem.* 64 (1999) 7267. (b) D.Hoegaerts, B. F. Sels, D.E. De Vos, F. Verpoort, P.A. Jacobs, *Catal. Today* 60 (2000) 209. (c) R. Neumann, M. Cohen, *Angew. Chem., Int. Ed.* 36 (1997) 1738. (d) T. Sakamoto, C. Pac, *Tetrahedron Lett.* 41 (2000) 10009. (e) R. Neumann, H. Miller, *J. Chem. Soc., Chem. Commun.* (1995) 2277. (f) G. Gelbard, T. Gauducheau, E. Vidal, V. I. Parvulescu, A. Crosman, V.M. Pop, *J. Mol. Catal. A: Chem.* 182/183 (2002) 257. (g) J. Ichihara, S. Yamaguchi, T. Nomoto, H. Nakayama, K. Iteya, N. Naitoh, Y. Sasaki, *Tetrahedron Lett.* 43 (2002) 8231.
139. (a) N.M. Okun, T.M. Anderson, C.L. Hill, *J. Am. Chem. Soc.* 125 (2003) 3194. (b) N.M. Okun, T.M. Anderson, C.L. Hill, *J. Mol. Catal.* 197 (2003) 283.
140. (a) T. Welton, *Chem. Rev.* 99 (1999) 2071. (b) D. Zhao, M. Wu, Y. Kou, E. Min, *Catal. Today* 74 (2002) 157.
141. (a) A. Riisager, R. Fehrmann, S. Flicker, R. Van Hal, M. Haumann, P. Wassercheid, *Angew. Chem. Int. Ed.* 44 (2005) 815. (b) M. Gruttadauria, S. Riela, C. Aprile, P.L. Meo, F. D'Anna, R. Noto, *Adv. Synth. Catal.* 348 (2006) 82. (c) C.P. Mehnert, *Chem. Eur. J.* 1 (2004) 50.
142. (a) T. Okuhara, *Chem. Rev.* 102 (2002) 3641. (b) I.V. Kozhevnikov, *Chem. Rev.*, 98 (1998) 171. (c) T. Okuhara, N. Mizuno, M. Misono, *Adv. Catal.* 41 (1996) 113.
143. M.B. Smith, J. March, *March's Advanced Organic Chemistry: Reactions, Mechanisms, and Structure*, 5th ed.; Wiley-Interscience: New York (2001) 1514
144. (a) R.A. Sheldon, J.K. Kochi, *Metal-Catalyzed Oxidations of Organic Compounds*; Academic Press: New York (1984). (b) M. Hudlicky, *Oxidations in Organic Chemistry*; ACS Monograph 186 (1990).
145. A.J. Mancuso, D. Swern, *Synthesis* (1981) 165.
- 146 (a) G.W. Parshall, S.D. Ittel, *Homogeneous Catalysis: The Applications and Chemistry of Catalysis by Soluble Transition Metal Complexes*, 2nd ed.; Wiley-Interscience: New York, (1992). (b) C. Marchal, A. Davidson, R. Thouvenot, G.

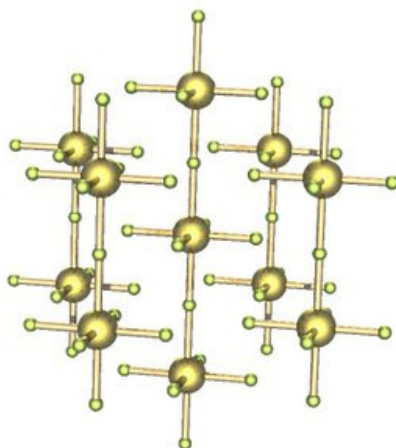
- Herve', J. Chem. Soc., Faraday Trans. 89 (1993) 3301. (c) M. Ai, E. Muneyama, A. Kunishige, K. Ohdan, Bull. Chem. Soc. Jpn. 67 (1994) 551. (d) W. Partenheimer, Catal. Today 23 (1995) 69. (e) K. Weissermal, H. Arpe, J. Industrial Organic Chemistry, 3rd ed.; VCH: Weinheim, (1997). (f) N. Mizuno, M. Misono, Chem. Rev. 98 (1998)199. (g) R.A. Sheldon, I.W.C.E. Arends, A. Dijksman, Catal. Today 57 (2000)157. (h) R. Ben-Daniel, P. Alsters, R. Neumann, J. Org. Chem. 66 (2001) 8650. (i) A. Dijksman, A. Marino-Gonzalez, A.M.I. Payeras, I.W.C.E. Arends, R.A. Sheldon, J. Am. Chem. Soc. 123 (2001), 6826. (j) G.T. Ten Brink, I.W.C.E. Arends, R.A. Sheldon, Science 287 (2000) 1636.
147. (a) J.A. Osborn, K.S. Coleman, C.Y. Lorber, Eur. J. Inorg. Chem. (1998) 1673. (b) S.V. Ley, R. Lenz, J. Chem. Soc., Perkin Trans. 1 (1997) 3291. (c) Cecchetto, F. Fontana, F. Minisci, F. Recupero, Tetrahedron Lett. 42 (2001) 6651.
148. (a) A. Bordoloi, F. Lefebvre, S.B. Halligudi, J. Catal. 247 (2007)166. (b) A. Bordoloi, A. Vinu, S.B. Halligudi, App.catal. A 308 (2007) 216.
149. K. Yamaguchi, C. Yoshida, S. Uchida, N. Mizuno, J. Am. Chem. Soc. 127 (2005) 530-531.
150. R. Newmann, M. Levin, J. Org Chem. 56 (1991) 5707.

CHAPTER IV

Inorganic-organic hybrid materials based on Coordination polymers

This chapter features the following sections:

- | | |
|---------------------------------------|-----|
| 4.1. <i>Oxidation of Monoterpenes</i> | 130 |
| 4.2. <i>Amine oxidation</i> | 143 |



4.1. Organotin-oxometalate coordination polymer catalyzed oxyfunctionalization of monoterpenes

4.1.1. Introduction

Selective oxyfunctionalization of monoterpenes is an interesting route to utilize these inexpensive natural products for number of applications. Limonene, a monoterpene is the major component of citrus oil and is obtained easily from the citrus fruit peel waste. Limonene epoxide is a key raw material for a wide variety of applications, such as pharmaceutical, flavor and perfumery industry as well as useful synthetic intermediates, food additives and chiral building blocks. Limonene oxyfunctionalisation could be done either by epoxidation or by allylic oxidation reactions. Epoxidation is carried out with peracid (RCO_3H) route wherein stoichiometric amount of catalyst is consumed and this process is becoming unacceptable because of the non-selective formation of mono- and di- epoxides monoterpenes as well as cleaved products of these [1,2]. Allylic oxidation takes place usually via a free radical chain reaction pathway and occurs when the intermediate metallic species are in low oxidation states [3,4].

During the past few years, catalysts such as $\text{PdCl}_2/\text{CuCl}_2/\text{O}_2$ and $\text{Pd}(\text{OAc})_2/\text{H}_2\text{O}_2$ systems have been used for efficient and selective oxidation of limonene [5-10]. Drawbacks of the above homogeneous catalyst systems are their corrosive natures and the contamination of the reaction products with the catalyst and the formation of undesired organochlorine compounds [11]. Heteropoly acids [12] and transition metal substituted heteropoly acids [13] have been used with and without support for the oxidation of monoterpenes. Synthetic metalloporphyrins [14] and transition metal Schiff base complexes of various metals (Co, Mn, etc) have also been used for the oxidation of monoterpenes. However, separation of the catalysts is usually troublesome and not economical for applications. Numerous attempts have been made to immobilize metal Schiff base complexes by anchoring onto polymeric matrix [15]. Encapsulation [16-18], entrapment [19] and anchoring of metal bases onto porous inorganic supports have also been reported for the oxidation of monoterpenes [20-23]. Incorporation of Titanium inside the framework of the hexagonal mesoporous silica MCM-41 was successfully

carried out by many researchers [24,25]. It was found that Ti ions leached out from the MCM-41 when the catalyst was used with hydrogen peroxide as an oxidant [26-28].

Recently, Abrantes et.al [29] reported that organotin-oxometalate coordination polymers formulated as $[(n\text{Bu}_3\text{Sn})_2\text{MO}_4]$ (M = Mo or W) exhibited good catalytic activities and product selectivities in the oxyfunctionalisation of olefins. Hence, these catalyst systems are interesting for the oxidation of monoterpenes. The purpose of our study is to investigate the performance of the organotin-oxometalate coordination polymer catalyst systems in the liquid phase oxidation of monoterpenes and to optimize reaction conditions for higher substrate conversions and desired epoxide selectivities. We are presenting here our results on the oxyfunctionalization of monoterpenes catalyzed by organotin-oxometalate coordination polymers using UHP as an oxidant.

4.1.2. Experimental

4.1.2.1. Materials

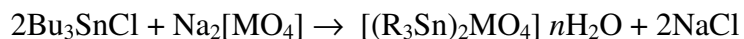
$\text{Na}_2\text{MoO}_4 \cdot 2\text{H}_2\text{O}$, H_2O_2 (30%), $\text{Na}_2\text{WO}_4 \cdot 2\text{H}_2\text{O}$ and $n\text{Bu}_3\text{SnCl}$ were procured from Merck India, Ltd., Mumbai. Limonene, α -pinene, β -pinene, 3-carene, camphene, geraniol and linalool were obtained from Aldrich. Tert-butyl hydrogen peroxide (TBHP) was purchased from Acros. Urea hydrogen peroxide (UHP) was freshly prepared in the laboratory following a standard procedure [30]. Solvents procured from Ranbaxy, were dried by standard methods, distilled under nitrogen and stored over molecular sieves prior to their use in the oxyfunctionalization reactions.

4.1.2.2. Catalyst preparation

$[(n\text{Bu}_3\text{Sn})_2\text{MoO}_4]$: $n\text{Bu}_3\text{SnCl}$ (3.25 g, 10 mmol) was dissolved in a mixture of water (6 ml) and acetone (27 ml). A saturated aqueous solution of $\text{Na}_2\text{MoO}_4 \cdot 2\text{H}_2\text{O}$ (1.21 g, 5 mmol in 8 ml H_2O) was added drop wise with magnetic stirring to $n\text{Bu}_3\text{SnCl}$ solution. A white precipitate was formed immediately and stirring was continued for 5 min. The precipitate was filtered, washed thoroughly with water, and dried in air at 100 °C for 6 h to give 90% yield of $(n\text{Bu}_3\text{Sn})_2\text{MoO}_4$. Calculated for $\text{C}_{24}\text{H}_{54}\text{O}_4\text{Sn}_2\text{Mo}$ (740.1): C 38.9%, H 7.3%. Analytically found: C 38.7%, H 7.2% [29].

$[(n\text{Bu}_3\text{Sn})_2\text{WO}_4]$: This material was prepared as described above using $\text{Na}_2\text{WO}_4 \cdot 2\text{H}_2\text{O}$ instead of $\text{Na}_2\text{MoO}_4 \cdot 2\text{H}_2\text{O}$. Calculated for $\text{C}_{24}\text{H}_{54}\text{O}_4\text{Sn}_2\text{W}$ (827.81): C 34.8%, H 6.6%.

Analytically found: C 34.7%, H 6.5% The general reaction for the preparation of organotin-oxometalate coordination polymer is shown below:



(Where M = Mo/or W, Bu = Butyl group-organic moiety)

Elemental analysis of the above materials confirmed that these are as per the stoichiometric composition of the coordination polymers $[(n\text{Bu}_3\text{Sn})_2\text{MoO}_4]$ and $[(n\text{Bu}_3\text{Sn})_2\text{WO}_4]$, respectively.

4.1.3.3. Catalytic activity measurements

The oxyfunctionalization of monoterpenes for example limonene was conducted in air atmosphere. In a typical experiment, reaction mixture containing known amounts of limonene (0.68 g), urea hydrogen peroxide, UHP (0.98 g), acetonitrile (10 ml) and 3 wt.% of catalyst (co-ordination polymers) were placed in a round bottom flask (batch reactor) fitted with reflux condenser, equipped with a magnetic stirrer and immersed in a thermostatic oil bath for maintaining the desired reaction temperature. The reactions was conducted at the desired temperature and the progress of the reaction was monitored by withdrawing reaction mixture samples periodically, centrifuged and analyzed for their compositions by Shimadzu 14B gas chromatograph, equipped with a flame ionization detector using HP-5 capillary column (cross linked 5% ME silicone, 30m×0.53×1.5 μm film thickness). The identity of the products was confirmed by GC-MS (Shimadzu GCMS QP 5000) and ^1H NMR. Conversion is defined as the percentage of oxyfunctionalization of monoterpenes into products and the selectivity to individual product is accounted for total 100%.

4.1.3. Results and discussion

4.1.3.1. Characterization

4.1.3.1.1. XRD

Powder XRD patterns of $[(n\text{Bu}_3\text{Sn})_2\text{MoO}_4]$, and $[(n\text{Bu}_3\text{Sn})_2\text{WO}_4]$ are depicted in Fig.4.1 1. The good crystallinity of $[(n\text{Bu}_3\text{Sn})_2\text{MoO}_4]$, and $[(n\text{Bu}_3\text{Sn})_2\text{WO}_4]$ can be seen by their XRD patterns. The XRD patterns of $[(n\text{Bu}_3\text{Sn})_2\text{MoO}_4]$, and $[(n\text{Bu}_3\text{Sn})_2\text{WO}_4]$ have shown characteristic peaks of MoO_4 and WO_4 of the materials at the range of 2θ , 22 and 28, which are similar to the one reported in literature [29]. The average crystallite

size is estimated from the full width at half maximum of the diffraction peak by following the Scherrer equation.

$$D_{hkl} = k\lambda/[\beta (2\theta) \cos \theta]$$

Where, $\beta (2\theta)$ is the width of the pure diffraction profile in radians, k is the constant, 0.89 , λ is the wavelength of the X-rays (0.154056 nm), θ is the diffraction angle, and D_{hkl} is the crystallite diameter in the $[h k l]$ direction. By fitting various peaks to the above formula and taking into account the instrumental broadening, the average crystallite size were found to be 200 nm.

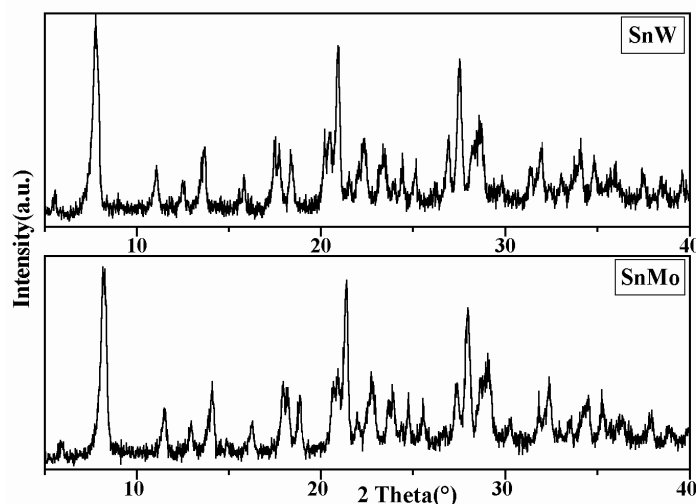


Fig.4.1.1. Powder XRD patterns of (SnMo) = $[(n\text{Bu}_3\text{Sn})_2\text{MoO}_4]$ and (SnW) = $[(n\text{Bu}_3\text{Sn})_2\text{WO}_4]$.

4.1.3.1.2. N_2 sorption study

The textural characteristics such as BET surface area, pore size distribution and pore volume of the catalyst powders are summarized in Table 4.1.1. It is found that the surface area and pore volume of the materials are quite low.

Table 4.1.1. Physicochemical properties of different catalysts

Compound	Surface area (m^2/g)	Pore volume (cc/g)	BJH average mesopore diameter (nm)
$[(n\text{Bu}_3\text{Sn})_2\text{MoO}_4]$	20	0.013	2.57
$[(n\text{Bu}_3\text{Sn})_2\text{WO}_4]$	19.4	0.012	2.46

4.1.3.1.3. FT-IR and FT-Raman

FT-IR spectra of $[(n\text{Bu}_3\text{Sn})_2\text{MoO}_4]$, and $[(n\text{Bu}_3\text{Sn})_2\text{WO}_4]$ are depicted in Fig.4.1.2. The $[\text{MoO}_4]^{2-}$ and $[\text{WO}_4]^{2-}$ units of catalyst $[(n\text{Bu}_3\text{Sn})_2\text{MoO}_4]$ and $[(n\text{Bu}_3\text{Sn})_2\text{WO}_4]$ give characteristic bands at 815 cm^{-1} . Broad bands observed in the range 2845 cm^{-1} to 2975 cm^{-1} are due to $\nu(\text{CC})$ and $\nu(\text{CH})$ stretching of the catalysts.

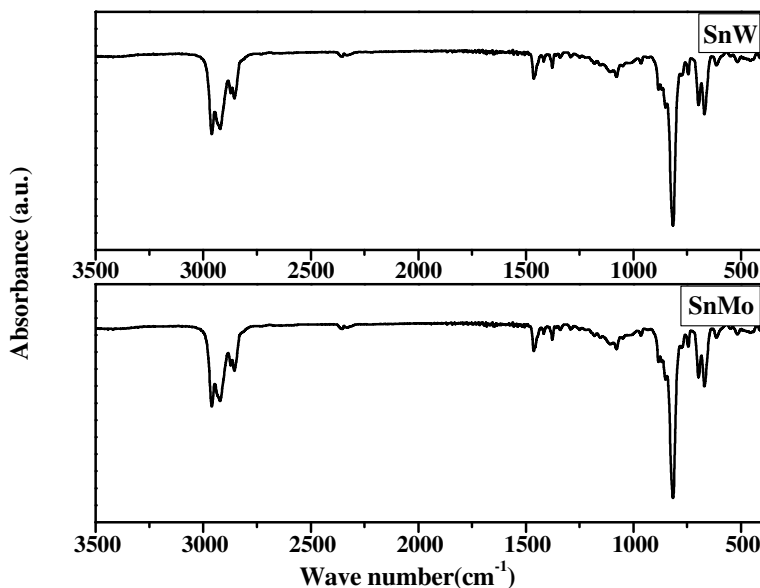


Fig. 4.1.2. FT-IR spectra of (SnMo) = $[(n\text{Bu}_3\text{Sn})_2\text{MoO}_4]$ and (SnW) = $[(n\text{Bu}_3\text{Sn})_2\text{WO}_4]$.

The other characteristic bands observed for $[(n\text{Bu}_3\text{Sn})_2\text{MoO}_4]$ and $[(n\text{Bu}_3\text{Sn})_2\text{WO}_4]$ catalyst are $1459\text{ cm}^{-1}(\text{s})$, $1376\text{ cm}^{-1}(\text{s})$, $1151\text{ cm}^{-1}(\text{w})$, $1068\text{ cm}^{-1}(\text{w})$, $963\text{ cm}^{-1}(\text{w})$, $723\text{ cm}^{-1}(\text{w})$, $663\text{ cm}^{-1}(\text{w})$ and $1460\text{ cm}^{-1}(\text{s})$, $1337\text{ cm}^{-1}(\text{s})$, 1307 cm^{-1} , $1149\text{ cm}^{-1}(\text{w})$, $1083\text{ cm}^{-1}(\text{w})$, $968\text{ cm}^{-1}(\text{w})$, $720\text{ cm}^{-1}(\text{w})$, $670\text{ cm}^{-1}(\text{w})$, respectively, which are due to various organic and metal organic functionalities.

FT-Raman spectra of $[(n\text{Bu}_3\text{Sn})_2\text{MoO}_4]$, and $[(n\text{Bu}_3\text{Sn})_2\text{WO}_4]$ are depicted in Fig.4.1.3. Since $[\text{MO}_4]^{2-}$ unit $[\text{M} = \text{W or Mo}]$ of the catalyst systems are in T_d symmetry, according to the mutual exclusion rule, the IR forbidden Raman active vibrational bands of these two units of $[\text{MoO}_4]^{2-}$ and $[\text{WO}_4]^{2-}$ of the catalysts are observed at 309 cm^{-1} , 860 cm^{-1} , 924 cm^{-1} and 312 cm^{-1} , 862 cm^{-1} , 962 cm^{-1} , respectively. Raman shift observed at 513 cm^{-1} in both the catalyst systems is due to the $\nu(\text{SnC})$ stretching [31].

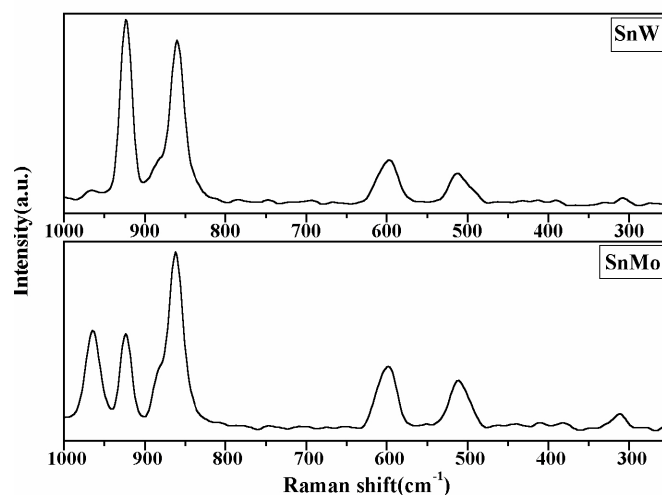


Fig. 4.1.3. FT Raman spectra of (SnMo) = $[(n\text{Bu}_3\text{Sn})_2\text{MoO}_4]$ and (SnW) = $[(n\text{Bu}_3\text{Sn})_2\text{WO}_4]$.

4.1.3.1.4. ^{119}Sn and ^{13}C MAS NMR

^{119}Sn and ^{13}C MAS NMR of $[(n\text{Bu}_3\text{Sn})_2\text{MoO}_4]$, are depicted in Fig.4.1.4(a) and 4.1.4(b) respectively. ^{119}Sn MAS NMR spectra of $[(\text{Bu}_3\text{Sn})_2\text{MoO}_4]$ shows a tetrameric structure in which each Sn atom has trigonal bipyramidal coordination geometry [32]. The material $[(\text{Bu}_3\text{Sn})_2\text{MoO}_4]$ gives rise to a complicated ^{13}C CP MAS NMR spectra at room temperature. Four main signals are observed for the four-methyl groups, two peaks each for the beta and gamma carbons, however, for alpha carbon; the signal is clearly the sum of two components. The two small broad signals at ca. 24 and 17 ppm are probably related to the coupling between ^{13}C and ^{117}Sn .

4.1.3.1.5. TG/DTA

Thermo gravimetric and differential thermal analysis of $[(n\text{Bu}_3\text{Sn})_2\text{MoO}_4]$ and $[(n\text{Bu}_3\text{Sn})_2\text{WO}_4]$ are shown in Fig.4.1.5(A) and Fig.4.1.5(B), respectively. The endothermic peaks around 240 °C and 269 °C, respectively for $[(n\text{Bu}_3\text{Sn})_2\text{WO}_4]$ and $[(n\text{Bu}_3\text{Sn})_2\text{MoO}_4]$ in the DTA curve indicates the decomposition of the coordination polymers. The loss in weight (50% of the total wt.) in the temperature range 269 °C to 309 °C for both the catalyst indicates the complete decomposition of the compounds (losing organic moiety).

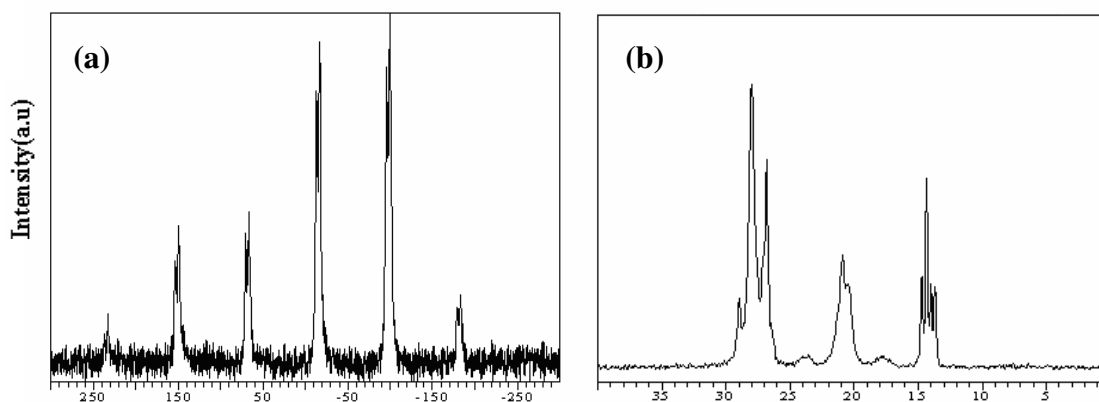


Fig.4.1.4: (a) ^{119}Sn MAS & (b) ^{13}C MAS NMR profile of $[(n\text{Bu}_3\text{Sn})_2\text{MoO}_4]$

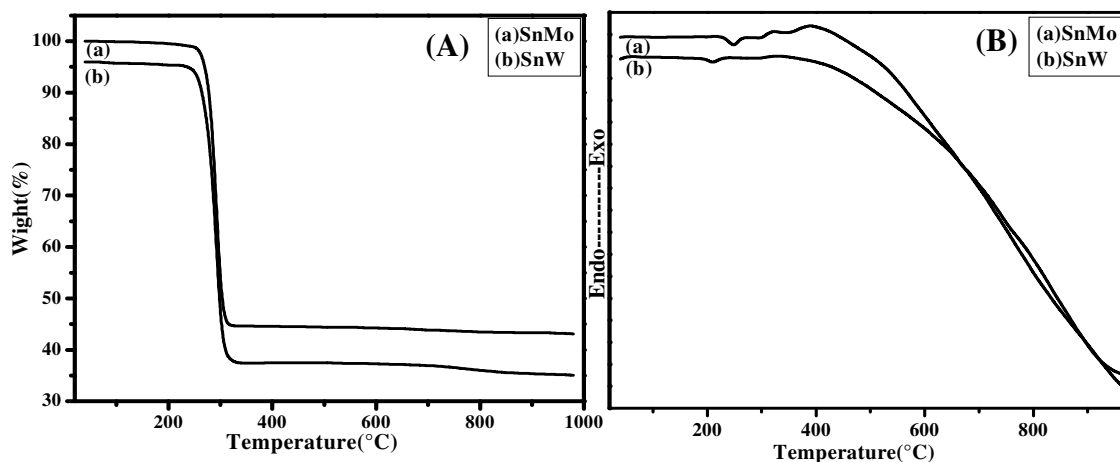


Fig.4.1.5. (A) TG profiles of (SnMo) = $[(n\text{Bu}_3\text{Sn})_2\text{MoO}_4]$ and (SnW) = $[(n\text{Bu}_3\text{Sn})_2\text{WO}_4]$.,

(B) DTA profiles of (SnMo) = $[(n\text{Bu}_3\text{Sn})_2\text{MoO}_4]$ and (SnW) = $[(n\text{Bu}_3\text{Sn})_2\text{WO}_4]$.

4.1.3.1.6. SEM

The SEM photographs of $[(n\text{Bu}_3\text{Sn})_2\text{MoO}_4]$ and $[(n\text{Bu}_3\text{Sn})_2\text{WO}_4]$ are shown in Fig. 4.1.6 (a) and Fig. 4.1.6 (b). The typical average particle size estimated by SEM or the both the catalysts is around 500 nm.

4.1.3.2. Catalytic activity

Oxidation of limonene by UHP gave Limoneneoxide (Epoxide), Carvone, Carveol and Carvacrol is shown in Scheme 4.1.1. The catalytic activities of $[(n\text{Bu}_3\text{Sn})_2\text{MoO}_4]$ and $[(n\text{Bu}_3\text{Sn})_2\text{WO}_4]$ are expressed in terms of limonene conversion (Fig 7). It is found that under selected reaction conditions, the catalyst $[(n\text{Bu}_3\text{Sn})_2\text{MoO}_4]$

showed slightly higher activity (54% limonene conversion) than $[(n\text{Bu}_3\text{Sn})_2\text{WO}_4]$ (49% limonene conversion). This could be due to difference in acidity of the materials or the difference between decomposition rates of the oxidant. The reason for higher activity of $[(n\text{Bu}_3\text{Sn})_2\text{MoO}_4]$ is concomitant with the earlier reports [29, 33].

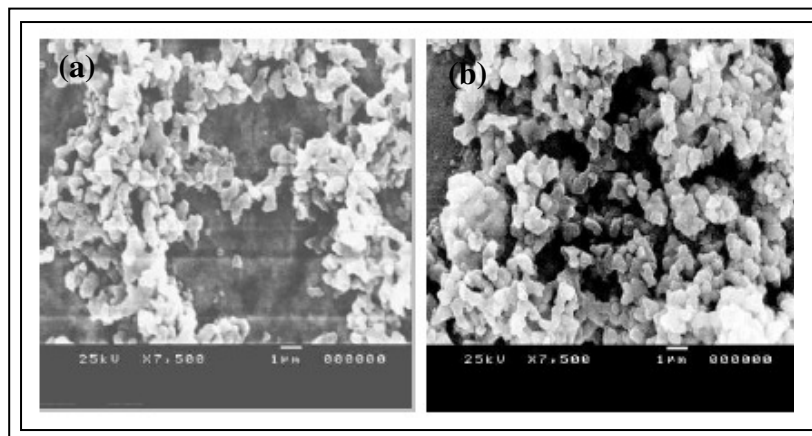
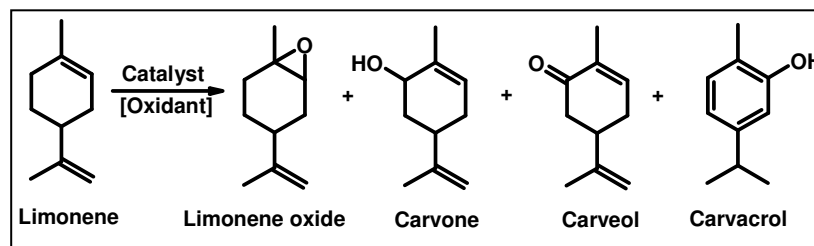


Fig.4.1.6. SEM photographs of (a) $[(n\text{Bu}_3\text{Sn})_2\text{WO}_4]$ and (b) $[(n\text{Bu}_3\text{Sn})_2\text{MoO}_4]$



Scheme 4.1.1. Oxyfunctionalisation of Limonene

4.1.3.3. Spectral characteristics of the oxidation products of limonene

The products of oxidation of limonene by UHP are separated by column chromatography by following a standard procedure and analyzed by ^1H NMR. The details of the spectral characteristics of the limonene oxidation products are given below:

Limonene oxide: 1.11(3H, s), 1.24-1.59(6H, m), 1.61 (3H, s), 2.11 (1H, m), 2.68 (1H, t), 4.57 (2H, s); **Carveol:** 1.51 (6H, s), 1.54-2.13 (5H, m), 3.59 (1H, m), 4.04 (1H, s), 4.53 (1H, s), 4.78 (1H, s), 5.27 (1H, m); **Carvone:** 1.51-1.7 (8, m), 1.49 (3H, s), 1.72 (3H, s), 1.9-3(5H, m), 2.43 (1H, m), 4.49 (1H, s), 4.69 (1H, s), 6.15 (1H, m) and **Carvacrol:** 1.18 (6H, s), 2.15 (3H, s), 3.02 (1H, s), 6.39 (1H, s), 6.59 (2H, m), 9.53 (1H, s).

4.1.3.4. The performance of [(nBu₃Sn)₂MoO₄] catalyst in the oxidation of monoterpenes

In order to delineate the scope and limitations of the catalyst system, based on their performances in limonene oxidation, the best catalyst is used for the oxidation of different monoterpenes to know its catalytic performance and products selectivities. Monoterpenes, like limonene, α -pinene, β -pinene, carene, camphene and gerniol have been considered to evaluate the catalytic activity of [(nBu₃Sn)₂MoO₄] under selected reaction conditions with UHP as an oxidant. UHP has been employed as an oxidant for limonene oxidation with an aim of controlled release of H₂O₂ into the solution, to get better activity and desired epoxide selectivity in the oxidation. Gradual increase in conversion with UHP is due to the slow release of H₂O₂ during the reaction in a controlled manner, which allows the formation of the epoxide more selectively. The data on the activities (conversion of substrates), product selectivities along with the reaction conditions used for the above study are presented in Table 4.1.2.

The differences in the conversions of substrates has been considered as the measure of the efficiency of the catalyst [(nBu₃Sn)₂MoO₄] under identical conditions. It is seen from the results (Table 4.1.2) that the activity (conversion of substrate) is dependent on the nature of monoterpenes and the position of the olefinic bond and its ability to hold to metal centre in a metal-oxo mediated oxyfunctionalization of terpenes and allowing oxygen transfer before reductive elimination forming corresponding oxygenated products, while regenerating the active catalyst in a catalytic cycle.

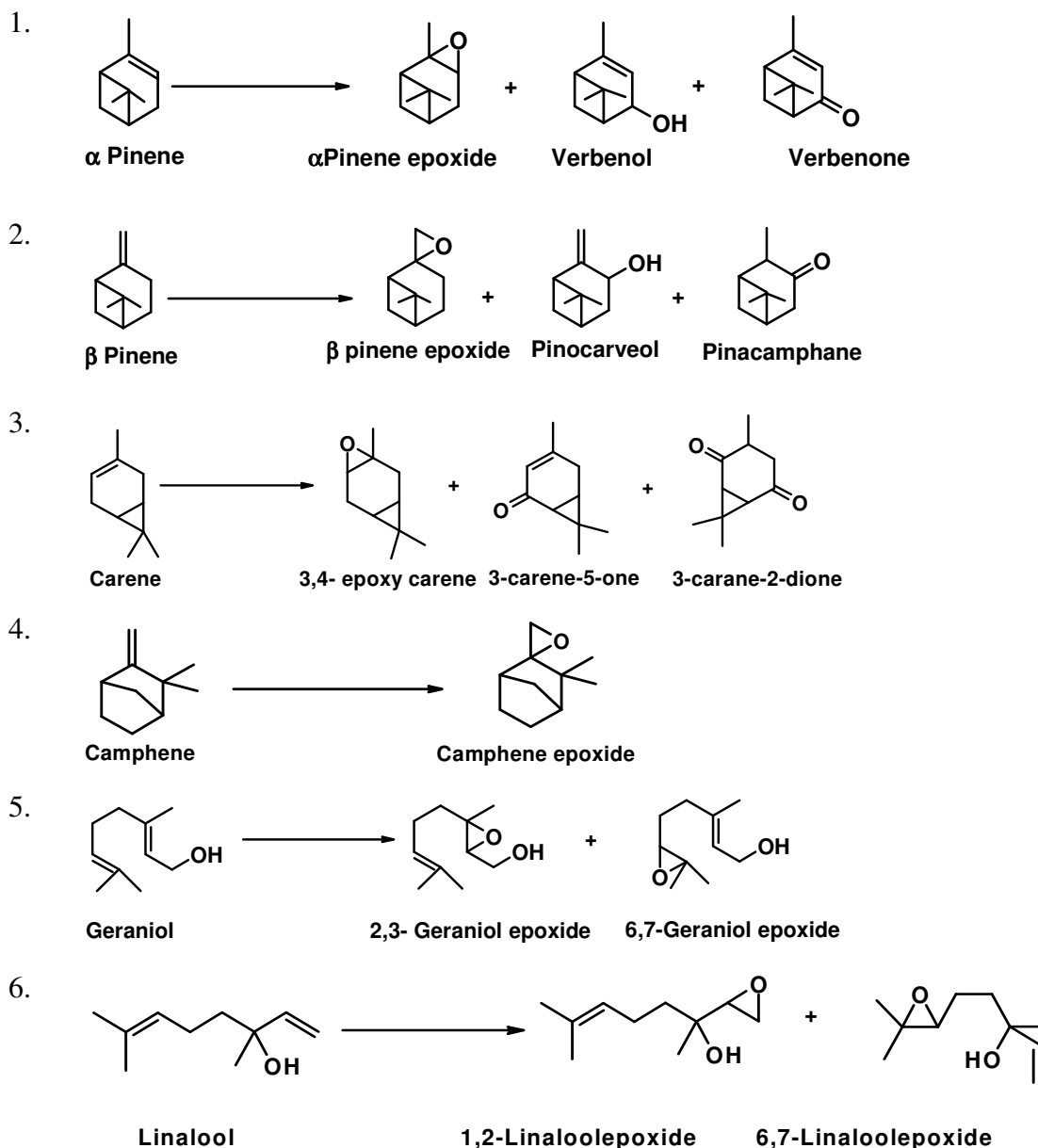
The oxidation of α -pinene produces α -pinene epoxide, verbenol and verbenone (used as a building block of taxol) as shown in Scheme 4.1.2. At α -pinene conversion 66%, the selectivity towards α -pinene epoxide is 60% and the selectivity for other products verbenol (19%) and verbenone (13%), camphene, campholenic aldehyde and low molecular weight oligo/polymerization products are also formed in the reaction (8% not analyzed). Similarly, β -pinene gave β -pinene epoxide, pinocamphone and pinocarveol (Scheme 4.1.2) as its products. Some unidentified products were also obtained in the oxidation β -pinene, which are myrtemal, pinocarvone, etc. At β -pinene conversion, 40%, the highest selectivity is for its epoxide β -pinene epoxide (70%), pinocamphone (11%), pinocarveol (9%) and the remaining others.

Table 4.1.2. Activity of [(nBu₃Sn)₂MoO₄] in oxyfunctionalisation of monoterpenes

Mono- terpenes	Conv. (mol %)	Product selectivity (%)		
Limonene	54	Epoxide(76)	Carvone (7)	Carveol(3) & Carvacrol (3)
α -Pinene	66	Epoxide(60)	Verbenol(19)	Verbenol(13)
β -Pinene	40	Epoxide(70)	Pinocarveol(11)	Pinocarveol(9)
Carene	60	Epoxide (40)	3-Carene-5-one (27)	3-Carene-2- dione(22)
Camphene	20	Epoxide (70)	-	-
Geraniol	100	2,3 epoxide (60)	6,7 epoxide (24)	-
Linalool	70	2,3 epoxide (67)	6,7 epoxide (24)	

Conditions: temperature = 50 °C; solvent acetonitrile = 10 ml; time = 10 h; substrate: UHP molar ratio = 1:2; catalyst wt.: 0.030 g, n.a = not analyzed

The main product of oxidation of 3-carene is 3,4-epoxycarene and minor products are 3-carene-5-one and 3-carene-2,5-dione (Scheme 4.1.2). At 60% carene conversion, the product selectivities are 3,4-epoxycarene (40%), 3-carene-5-one (27%) and 3-carene-2,5-dione (22%) and the remaining others. Geraniol shows interesting properties, as it has two double bonds: one in allylic position with respect to the –OH group, while the other (6–7 double bond) is isolated double bond. It is found that in the oxidation of Geraniol, the catalyst is very active and gave 99% geraniol conversion. In principle, two different epoxidation products can be observed, but with the present catalyst system, only 2,3-epoxide is predominantly formed (Scheme 4.1.2). Oxyfunctionalisation of camphene is shown in Scheme 4.1.2 and it gives very low conversion (20%) and with a high selectivity for camphene epoxide (70%). Oxidation of linalool (Scheme 4.1.2) which contains two double bonds and hydroxy group gives rise to the predominant formation of the 1,2-epoxide (67%) whereas 6,7-isomer is formed in much lower concentration.



Scheme 4.1.2. Oxyfunctionalisation of monoterpenes

Since, α -pinene molecule is rigid in structure in which the four-membered ring is puckered and five carbons of the six-membered ring are approximately in the same plane but β -pinene prefers a pseudo-chair conformation. Due to which a strong preference exhibited by α -pinene compared to β -pinene for oxidation. The carene conversion increases with the amount of UHP added but this was accompanied by a decrease in selectivity for the epoxide. The bicyclic monoterpene, camphene has an exocyclic disubstituted double bond, like β -pinene, but the only allylic hydrogen is at a bridgehead

position and not easily abstractable. Therefore, we are unable to get the allylic derivatives. As for geraniol, the epoxidation is preferentially occurs at the 2,3 double bond, which has lower HOMO coefficients than 6,7 double bond, affording 6,7-epoxygeraniol as the major products. The result shows that no allylic assisted epoxidation of linalool occurs under our reaction conditions. This may be due to the steric situation around the hydroxyl group. We further studied $[(n\text{Bu}_3\text{Sn})_2\text{MoO}_4]$ catalyzed oxyfunctionalization of limonene using UHP as an oxidant and acetonitrile solvent to know the effects of reaction parameters. The discussion is continued in further text.

4.1.3.5. Effect of reaction parameters

The effect of reaction parameters such as mole ratio of limonene:UHP, catalyst concentration, substrate and time on stream data concentration on the limonene conversions and epoxide selectivities were collected. The data along with the reaction conditions are listed in Table 4.1.3. It is generally found that the limonene conversion increased with increase in the concentrations of the parameters. The maximum limonene conversion of (39 mol %) was obtained at 50 °C, acetonitrile (10 mL), cat. wt. (0.030g) and limonene : UHP mole ratio (1:2) to give highest epoxide selectivity (90 mol %) in 2 h. However, in some cases epoxide selectivity is affected as seen from the results presented in Table.4.1.3.

4.1.3.6. Catalyst recycling and leaching

In order to study the recyclability of the catalyst, the reaction was studied at 50 °C with 3 wt.% catalyst using UHP/ limonene molar ratio 2. After 2 h, the limonene conversion was found to be 38%. Then catalyst is separated by filtration and was washed with dichloromethane and dried at 50 °C for 5 h and used again with fresh reaction mixture. The conversion of limonene after 2 h in a second cycle was almost the same as that of the first cycle. Few more cycles were repeated and it was found that the conversions of limonene and product selectivity are not changed much and hence confirmed the recyclability of the catalyst in oxidation reaction. Catalyst leaching was studied by following the standard procedure, which did not show the presence of leached catalyst in the reaction mixture after several hours of its use and the catalyst system is truly heterogeneous.

Table 4.1.3. Effect of reaction parameters on limonene conversion and epoxide selectivity

No.	Parameter	Convsn. (mol %)	*Products selectivities (%)
			Oxide and (*Others)
A) Effect of mole ratio of limonene:UHP (conditions: temp = 50 °C, time = 2 h, acetonitrile = 10 mL , Cat. Wt. = 0.030g)			
	1:1	16	94 (6)
	1:2	39	90(10)
	1:3	42	80 (20)
B) Effect of catalyst weight (wt.% of total wt. of reaction mixture) (conditions:temp = 50 °C, time = 2 h, acetonitrile = 10 ml , limonene : UHP mole ratio = 1:2)			
	0.01	25	90 (10)
	0.03	39	90 (10)
	0.05	46	78 (22)
C) Effect of substrate (limonene) concentration (M) (conditions: temp = 50 °C, Time = 2 h, acetonitrile = 10 mL , cat. wt. = 0.030 g)			
	0.0025	22	90 (10)
	0.0045	39	90 (10)
	0.0100	42	80 (20)
D) Effect of time on stream (Minutes) (conditions: temp = 50 °C, acetonitrile = 10 mL , limonene : UHP mole ratio = 1:2, Cat. Wt. = 0.03 g)			
	60	26	90 (10)
	120	39	90 (10)
	240	45	82 (18)
	480	48	80 (20)
	600	54	79 (21)

*Other products include Carvone, Carveol and Carvacrol, which are identified by GC-MS and ¹H NMR and are present in the range 5 –8% of the product mixture.

4.1.4. Conclusions

Coordination polymers [(nBu₃Sn)₂MO₄] (M= Mo, W) are used as a catalyst for the oxidation of monoterpenes. The interesting feature of these catalysts is their heterogeneity and selectivity. The molybdenum containing catalyst showed good activity in terpene oxidation. [(nBu₃Sn)₂MoO₄] is very active and chemo-selective catalyst system and could be used for further applications in oxidation reactions.

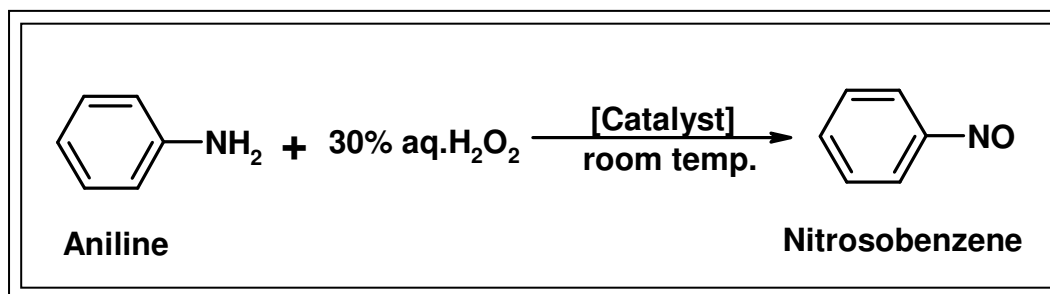
4.2. Tungsten and molybdenum based coordination polymers catalyzed *N*-oxidation of primary aromatic amines with aqueous hydrogen peroxide

4.2.1. Introduction

Oxidative biotransformation is amongst the most useful of all the identified biologically mediated conversions. Environmentally friendly technologies acceptable with efficient formation of the desired products and with negligible waste and recyclability of the catalyst systems are the major aspects which must be considered when designing a new catalyst for selective oxidation reactions. One of the most attractive approaches is the catalytic oxidation reaction by heterogeneous means. [34–36] Oxidation of amines is widespread in the area of biological science, reflecting the diverse roles for amine compounds. Amine compounds play important roles in neurotransmission [37], cell growth, differentiation [38], and neoplastic cell proliferation [39,40]. On the other hand, the oxidation of amines is a fundamentally important reaction for industrial applications, particularly for the synthesis of oxygenated derivatives such as hydroxylamine, nitroso, nitro, oxime, azo and azoxy compounds. Among these, the preparations of nitro, oxime and azoxy compounds have assumed special importance as synthetically useful intermediates. Nitroso derivatives hold a key position in the chemistry of heterocycles offering functional group manipulation and structural modification possibilities that are not accessible by any other methods.[41] Aromatic nitroso compounds are used in the vulcanization of rubber, stabilization of halogenated materials and as antioxidants in lubricating oil [42].

Few homogeneous metal-catalyzed methods reported in the literature are able to yield aromatic nitroso compounds [43]. These include the use of Caro's acid, 3-chloroperoxybenzoic acid (MCPBA), potassium permanganate, peracetic acid, peroxyformic acid, peroxybenzoic acid, oxaziridinium salts, oxygen difluoride, nitrous acid, trifluoroperacetic acid and, more recently, molybdic peroxo complexes. Catalytic methods using H₂O₂ or *tert*-butyl hydroperoxide as oxidant and sodium tungstate, oxomolybdate complexes, phosphotungstate, phosphomolybdate and zirconate salts were published later. Dimeric products due to condensation reactions such as azo or azoxy

derivatives as well as over-oxidation to the nitro compounds are often observed as by-products or sometimes as main products. Some methods for the direct oxidation of aromatic amines to nitro derivatives with peracids were described and, more recently dioxirane, tert-butyl hydroperoxide and H_2O_2 have been used as oxidants whereas metal peroxo complexes, FeCl_3 , $\text{Pb}(\text{OAc})_4$ and chromium silicalite have been employed as catalysts [44]. Nitroso compounds can also be produced by the direct reduction of nitro compounds with Mn_3O_4 [45]. But organic synthetic methods have not yet provided an easy and mild path to obtain the aromatic nitroso compounds. Our earlier report shows that $[(n\text{-Bu}_3\text{Sn})_2\text{MO}_4]$, ($\text{M}=\text{Mo}$ and W) is able to transfer one peroxidic oxygen atom to an olefin to yield epoxides.[46] Hence, to the best of our knowledge we present here for the first time a heterogeneous catalytic system based on tungsten and molybdenum coordination polymers $[(n\text{-Bu}_3\text{Sn})_2\text{MO}_4]$ for the selective oxidation of primary aromatic amines to the corresponding nitroso derivatives with 30% aqueous H_2O_2 as oxidant at ambient conditions such as room temperature and under an air atmosphere (Scheme 4.2. 1). This is a simple and clean process where the desired compounds are formed free from any contamination with by-products.



Scheme 4.2.1. Oxidation of aniline

4.2.2. Catalytic activity measurements

Amine (4 mmol), catalyst (0.4 mmol) and 30% aqueous H_2O_2 (8 mmol) were stirred in acetone (7 mL) at room temperature for the appropriate time (Table 4.2. 1). After the completion of the reaction, the catalyst was filtered and the filtrate was subjected to reduced pressure to remove the solvent. Then 10 mL of CH_2Cl_2 were added and the mixture was washed with 10 mL of distilled water and brine. The organic layer was separated and dried over anhydrous Na_2SO_4 . The mixture was again filtered and

concentrated under reduced pressure to afford a residue, which was purified by flash chromatography over silica (*n*-hexane:CH₂Cl₂, 4:6). The catalyst could be recycled without a loss of activity. All compounds were analyzed by GC, GCMS, IR and ¹H NMR.

4.2.3. Results and Discussion

The catalysts [(*n*-Bu₃Sn)₂MO₄], (M=Mo and W) were then investigated for the oxidation of aniline in the presence of 30% aqueous H₂O₂. We were pleased to find that the oxidation occurred to afford nitrosobenzene in quantitative yield when the reaction mixture (4 mmol of aniline and 8 mmol of 30% aqueous H₂O₂) was allowed to stir in the presence of 0.4 mmol of catalyst, at room temperature and under atmospheric air for 1 h in acetone. A blank experiment showed that no oxidation occurred in the absence of catalyst and the amine remained unchanged. The catalytic activity of [(*n*-Bu₃Sn)₂WO₄] and [(*n*-Bu₃Sn)₂MoO₄] catalysts in the oxidation of aniline shows that both the catalysts have almost similar activity (Table 4.2.1) However, Na₂WO₄ and Na₂MoO₄ catalysts show approximately half the activity compared to their corresponding polymers while Bu₃SnCl does not show any activity in the oxidation of aniline. Hence, we can conclude that the reaction was promoted mainly by tungsten and molybdenum species, and that tin enhances the activity.

Table 4.2.1. Oxidation of aniline with different catalysts^[a]

Entry	Catalyst	Substrate	Product	Yield (%)
1.	Na ₂ WO ₄	Aniline	Nitrosobenzene	38
2.	Na ₂ MoO ₄	Aniline	Nitrosobenzene	31
3.	[(<i>n</i> Bu ₃ Sn) ₂ WO ₄	Aniline	Nitrosobenzene	82
4.	[(<i>n</i> Bu ₃ Sn) ₂ MoO ₄	Aniline	Nitrosobenzene	79
5.	Bu ₃ SnCl	Aniline	Nitrosobenzene	No reaction

^[a] **Reaction conditions:** amine (4 mmol), catalyst: [(*n*- Bu₃Sn)₂WO₄] (0.4 mmol) and 30% aqueous H₂O₂ (8 mmol) were stirred in acetone (7 mL) at room temperature; reaction time=1 h., ^[b] Yield [%]=actual yield/expected yield X 100 %

To study the scope of the above catalysts for general applications, the oxidation of other amines were studied with [(*n*-Bu₃Sn)₂WO₄] catalysts (Table 4.2.2). Aniline was

oxidized to the corresponding nitrosobenzene in high yield. Similarly, 4-methylaniline, 2,4-dimethylaniline, 2,4,6-trimethylaniline, 4-ethylaniline, 2-ethyl-6-methylaniline, isopropylaniline, 4-*tert*-butylaniline, 4-methoxyaniline, 1-naphthylamine could be oxidized to the respective nitroso compounds.

Table 4.2.2. Oxidation of primary amines using 30% aq H₂O₂ catalyzed by [(*n*-Bu₃Sn)₂WO₄]^[a]

Entry	Substrates	Product	Yield (%) ^[b]
1.	Aniline	Nitrosobenzene	82
2.	4- Methyl aniline	4- Methyl nitrosobenzene	86
3.	2,4-Dimethylaniline	2,4-Dimethyl nitrosobenzene	90
4.	2,4,6-Trimethylaniline	2,4,6-Trimethyl nitrosobenzene	94
5.	4-Ethylaniline	4-Ethyl nitrosobenzene	89
6.	2-Ethyl,6-methylaniline	2-Ethyl,6-methyl nitrosobenzene	83
7.	Isopropylaniline	Isopropyl nitrosobenzene	81
8.	4- <i>tert</i> Butylaniline	4- <i>tert</i> Butyl nitrosobenzene	85
9.	4-Methoxyaniline	4-Methoxy nitrosobenzene	87
10.	2-Bromoaniline	2-Bromo nitrosobenzene	70
11.	2-Chloroaniline	2-Bromo nitrosobenzene	74
12.	4-Bromoaniline	4-Chloro nitrosobenzene	68
13.	4-Chloroaniline	4-Chloro nitrosobenzene	63
14.	2-Nitro aniline	2-Nitro nitrosoaniline	35
15.	4-Nitro aniline	4-Nitro nitrosoaniline	20
16.	1-Naphthylamine	1-Naphthyl nitrosobenzene	72

^[a] **Reaction conditions:** amine (4 mmol), catalyst: [(*n*- Bu₃Sn)₂WO₄] (0.4 mmol) and 30% aqueous H₂O₂ (8 mmol) were stirred in acetone (7 mL) at room temperature; reaction time=1 h.

^[b] Yield [%]=actual yield/expected yield X 100%

Amines containing electron-withdrawing ring substituents, such as 2-bromoaniline, 4-bromoaniline, 2-chloroaniline, 4-chloroaniline, 2-nitro aniline, 4-nitroaniline are less reactive. These results clearly reveal that the present method could be applied for the oxidation of a variety of aromatic primary amines with 30% aqueous H₂O₂ by heterogeneous means. The products were detected by gas chromatography-mass

spectrometry and quantified with FT-IR and ^1H NMR after work-up of the solutions and separation by flash chromatography.

In order to obtain the highest yields of the nitroso derivatives, it is necessary to avoid the possible subsequent oxidation to the corresponding nitro derivatives, by frequent checking of the reaction profile, and by stopping the reaction immediately after the complete consumption of amine. The results given in the Table 4.2.2 represent the conditions for obtaining the best yields. The nitroso derivatives obtained in this way are monomeric and the FT-IR spectra in KBr showed a weak band close to 1500 cm^{-1} , attributable to the stretching mode of the $\text{N}=\text{O}$ bond of the monomer. These assignments are in good agreement with reported values. The oxidation path of this reaction could follow the steps from amine to hydroxylamine and then to nitrosoamine. The oxygenation of the nitrogen atom of the substrate is accomplished by the formation of an oxo-tungsten complex, originating from nucleophilic attack of the amine onto peroxidic oxygen or SET processes [47]. Earlier literature reports and a recent communication on this subject support this hypothesis [48].

The catalyst could be filtered and recycled without a loss of activity. After completion of the reaction, the catalyst was filtered, washed with acetone, dried at $100\text{ }^\circ\text{C}$ and reused in the oxidation of aniline with fresh 30% aq. H_2O_2 for four runs. No loss of activity was observed and the corresponding nitrosobenzene was obtained in high yield. In another experiment, the filtrate was used for the oxidation of aniline in the presence of 8 mmol of 30% aqueous H_2O_2 and no reaction was observed. This indicates that the active ingredient has not leached out of the solid catalyst during the reaction

4.2.4. Conclusion

In conclusion, the N-oxidation of primary aromatic amines is described using tungsten- and molybdenum based coordination polymers (heterogeneous catalyst) in the presence of 30% aqueous H_2O_2 at room temperature and atmospheric air to give the corresponding nitroso derivatives in high yield. It is a clean process and the catalyst is recyclable without any loss of activity.

4.3. References

1. D.H. Pybus, C.S. Sell (Eds.), *The Chemistry of Fragrances*, RSC Paperbacks, Cambridge, 1999.
2. W.E. Erman, *Chemistry of the Limonene. An Encyclopedic Handbook*, Marcel Dekker, New York, 1985.
3. H. Mimoun, *Chimia* 50 (1996) 620.
4. C. Chapuis, D. Jacoby, *App. Catal. A: General* 221 (2001) 93.
5. D. Silva, M.L. Patitucci, H. R. Bizzo, E. D'Elia, O.A.C. Antunes, *Catal. Comm.* 3 (2002) 435.
6. L.E. Firdoussi, A. Baqqa, S. Allaoud, B.A. Allal, A. Karim, Y. Castanet, A. Mortreux, *J. Mol. Catal A: Chemical*, 135 (1998)11.
7. M.J. da Silva, E.V. Gusevskaya, *J. Mol. Catal. A: Chemical*, 176 (2001) 23.
8. E.V. Gusevskaya, J.A. Goncalves, *J. Mol. Catal. A* 121 (1997) 131.
9. E.V. Gusevskaya, V.S. Ferreira, P.A. Robles-Dutenhefner, *Appl. Catal. A* 174 (1998) 177.
10. J.A. Goncalves, E.V. Gusevskaya, *Appl. Catal. A: General* 258 (2004) 93.
11. A. Kishi, T. Higashini, S. Sakaguchi, Y. Ishii, *Tet. Lett.* 41 (2000) 99.
12. S. Casuscelli, E. Herrero, M. Crivello, C. Pe´rez, M.G. Egusquiza, C.I. Cabello, I. L. Botto, *Catal. Today* 107 (2005) 230.
13. N.K. Kala Raj, V.G. Puranik, C. Gopinathan, A.V. Ramaswamy, *App. Catal. A: General* 256 (2003) 265.
14. C. Schuster, W.F. Hölderich, *Catal. Today* 60 (2000) 193.
15. A. Valente, J. Vital, *J. Mol. Catal. Chem. A* 156 (2000) 163.
16. J. Pires, J. Francisco, A. Carvalho, M. Brotas de Carvalho, A. Silva, C. Freire, B. de Castro, M.M.A. Freitas, *Langmuir* 20 (2004) 2861.
17. Corma, V. Fornes, F.R.A. Cervilla, E. Liopis, A. Ribera, *J. Catal.*152 (1995) 237.
18. A.R. Silva, C. Freire, B. De Castro, M.M.A. Freitas, J.L. Figuirodo, *Micropor. Mesopor. Mater.* 46 (2001) 211.
19. C. Baleizaõo, B. Gigante, D. Das, M. A ´lvvaro, H. Garcia, A. Corma, *J.Catal.*223 (2004)106.

22. P. Oliveira, A.M. Ramos, I. Fonseca, A. Botelho do Rego, J. Vital, *Catal. Today* 102 (2005) 67.
23. T. Joseph, S.B. Halligudi, *J. Mol. Catal. A: Chemical* 229 (2005) 241.
24. M. V. Cagnoli, S.G. Casuscelli, A.M. Alvarez, J.F. Bengoa, N.G. Gallegos, M. E. Crivello, E.R. Herrero, S.G. Marchetti, *Catal. Today* 107 (2005) 397.
25. M.V. Cagnoli, S.G. Casuscelli, A.M. Alvarez, J.F. Bengoa, N.G. Gallegos, N.M. Samaniego, M.E. Crivello, G.E. Ghione, C.F. Pe´rez, E.R. Herrero, S.G. Marchetti *App. Catal. A: General* 287 (2005) 227.
26. L.Y. Chen, G.K. Chuah, S. Jaenicke, *Catal. Lett.* 50 (1998) 107.
27. L.S. Davies, P. Mc Morn, D. Bethell, P.C. Bulman Page, F. King, F.E. Hancock, G.J. Hutchings, *J. Mol. Catal. A: Chem.* 165 (2001) 243.
28. L.S. Davies, P. Mc Morn, D. Bethell, P.C. Bulman Page, F. King, F.E. Hancock, G.J. Hutchings, *J. Catal.* 198 (2001) 319.
29. M. Abrantes, A. Valente, M. Pillinger, I. S. Gon¸calves, J. Rocha, C. C. Romo Jr, *J. Catal.* 209 (2002) 237
30. G.S. Patil, G. Nagendrappa, *Syn. Comm.* 32 (2002)2677
31. K. Nakamoto, *Infrared and Raman spectra on Inorganic and Coordination compounds; Fifth Ed.* John Wiley and Sons, Inc.
32. *NMR: Basic Principles and progress, Solid-state NMR 11: Inorganic Matter* Edited by P. Diehl, E. Fluck, H. Gunther, R. Kosfeld, J. Seelig 125 (1993) Springer-Verlag.
33. W.A. Herrmann, J.J. Haidar, F.J. Lobmaier, G.M. Spiegler, *J. Oganomet. Chem.* 603 (2000) 69.
34. R. A. Sheldon, J. K. Kochi, *Metal Catalyzed Oxidation of Organic Compounds*, Academic Press, New York, (1981).
35. M. Hudlicky, *Oxidations in Organic Chemistry*, American Chemical Society, Washington DC, (1990).
36. S.I. Murahashi, *Angew.Chem. Int. Ed. Engl.* 34 (1995) 2443.
37. D.E. Edmondson, A. Mattevi, C. Binda, M. Li, F. Hubalek, *Curr. Med. Chem.*, 11(2004) 1983.
38. T. Thomas, T.J. Thomas, *Cell. Mol. Life Sci.* 58 (2001) 244.

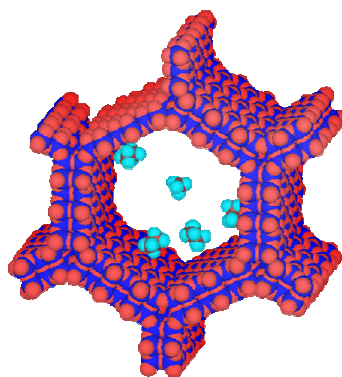
39. A. Pegg, *Cancer Res.* 48 (1988) 759.
40. N. Seiler, C.L. Atanassov, F. Raul, *Int. J. Oncol.*, 13 (1998) 993.
41. M. Mure, S.A. Mills, J.P. Klinman, *Biochemistry* 41 (2002) 9269.
42. (a) T.L Gilchrist, *Comprehensive OrganicSynthesis*, Pergamon, Oxford 7 (1991) 735. (b) D.H. Rosenblatt, E.P Burrows; *The Chemistry of Amino, Nitroso and Nitro Compounds and Their Derivatives*, Wiley, Chichester, (1982) 1085.
43. (a) S. Sakaue, Y. Sakata, Y. Nishiyama , Y. Ishii, *Chem. Lett.* (1992) 289. (b) P. Burckard, J. P. Fleury, F. Weiss, *Bull. Soc. Chim. Fr.* (1965) 2730.
44. (a) G. Gowenlock, *Rev. Chem. Soc.*, 12 (1958) 321. (b) H. G. Zengel, *Chem. - Ing.-Tech.* 55(1983) 962.
45. R.R. Holmes, R.P. Bayer, *J. Am. Chem. Soc.* 82 (1960) 3454.
46. S. Sakaue, Y. Sakata, Y. Nishiyama, Y. Ishii, *Chem. Lett.* (1992) 289.
47. D. Entwistle, T. Gilkerson, R. A. W. Johnstone R. P. Telford, *Tetrahedron* 34 (1978) 213.
48. (a) T. L.F. Favre, P. J. Seijsener, P.J. Kooyman, A. Maltha, A.P. Zuur, V. Ponec, *Catal. Lett.* (1988) 1457. (b) W. Weimin, Y. Yongnian, Z. Jiayu, *Appl. Catal. A* 133 (1995) 81.

CHAPTER V

Inorganic- organic hybrid materials based on Metal complex

This chapter features the following sections:

- | | |
|-----------------------------------|-----|
| 5.1. <i>Epoxides ring opening</i> | 151 |
| 5.2. <i>Hydrogenation</i> | 163 |



Section A.

5.1. Immobilized CobpbH₂Cl₂·2H₂O complex as heterogeneous catalyst for epoxides ring opening by amines under ambient conditions

5.1.1. Introduction

β -Amino alcohols are versatile synthons for a wide range of biologically active natural and synthetic products [1-7], unnatural amino acids [8,9] and chiral auxiliaries [10]. The most practical and widely used route for synthesizing β -Amino alcohols is by direct aminolysis of epoxides in presence of surplus amine at elevated temperature. However, this methodology suffers from one or more disadvantages such as high toxicity and corrosiveness of the acids employed, moisture sensitivity of catalyst systems, the requirement to use high temperature, hazardous organic solvent, extended time and use of the catalyst in a stoichiometric amount or inconvenient handling procedures [11-19]. Therefore, continuous efforts have been made to develop various catalysts such as sulfamic acid [20], metal triflates [21,22], metal alkoxides [23], metal halides [24–28], transition metal salts [29–31], heteropolymolybdate or tungstate [32,33], for the synthesis of β -Amino alcohols under milder conditions using stoichiometric amount of the amine reagent.

The use of heterogeneous catalysts provides a perfect solution to overcome the above limitations. The use of solid acid catalysts such as amberlyst-15 [34], monodispersed silica nanoparticles [35], zeolites [36], montmorillonite K10 under microwave irradiation [37] and ionic liquids [38, 39], functionalized alumina or silica and polymer supported ferric chloride or copper sulfate, Yb(OTf)₃ in supercritical CO₂ under high pressure at 328 K [40] and TS-1 [41] has revealed great promise in this area. Therefore, the introduction of new methods for ring opening of epoxides that work under milder conditions is of immense significance.

The coordination chemistry of bispyridylamides with the general structure LH₂ (where, L = pyridine amide ligand) has been extensively studied by Ojima et al [42]. The deprotonated amide is a strong σ -donor capable of stabilizing early as well as late

transition metal ions in high oxidation states, making high-valent metal complexes of the ligands suitable as Lewis acid catalysts. The recent introduction of the hybrid materials (metal complex anchored in porous materials) has a substantial impact in the area of heterogeneous catalysis, and they have been shown to promote a wide range of synthetic transformations [43]. Cobalt complexes of various ligand systems have been specifically used for the ring opening reactions in literature [44] and hence we have thought cobalt could be better option for making metal complex with pyridine amide ligand system for development of an immobilized catalyst system for ring opening reaction. Keeping in view of the above facts, we have immobilized cobalt pyridine amide complex on to sulfonic acid-modified mesoporous silica (SBA-15-SO₃-CobpbH₂Cl₂2H₂O) for application in the ring opening of epoxide reactions. We report here results on the catalytic performance studies of immobilized catalyst (SBA-15-SO₃-CobpbH₂Cl₂2H₂O) as an efficient and reusable catalyst system in the facile conversion of epoxides into β-Amino alcohols through ring opening at ambient conditions.

5.1.2. Experimental section

5.1.2.1. Materials

TEOS, P123 block copolymer (poly(ethyleneglycol)-poly(propylene glycol)-poly(ethylene glycol), average molecular mass 5800) (3-Mercaptopropyl) trimethoxysilane, 2-pyridinecarboxylic acid, 1,2-diaminobenzene, triphenyl phosphate, epoxides and amines were purchased from Aldrich, USA. All the chemicals were of research grade and were used without any further purification.

5.1.2.2. Catalysts preparation

5.1.2.2.1. Preparation of ligand (1,2-Bis(pyridine-2-carboxamido)benzene (H2bpb))

1,2-Bis(pyridine-2-carboxamido)benzene(H2bpb) shortly pyridine amide ligand was prepared by following standard literature method reported elsewhere [45]. To a solution of 2-pyridinecarboxylic acid (73.8 g, 0.6 mol) in pyridine (240 mL) 1,2-diaminobenzene (32.4 g, 0.3 mol) in pyridine (60 mL) was added. After the addition of triphenyl phosphite (186 g, 0.6 mol), the reaction solution was heated on a steam bath for 4 h and allowed to stand at room temperature overnight. A pale brown crystalline solid

was resulted, 87 g (92%). The sample was recrystallized twice from chloroform to give long white needles. Molecular formula $C_{18}H_{14}N_4O_2$, melting pt. 448 K, 1H NMR ($CDCl_3$, 200 MHz): $\delta = 10.1-10.3$ (2H), 8.1 (m, 4H), 7.6 (m, 4H), 7.1 (m, 4H).

5.1.2.2.2. Preparation of Cobalt complex (CobpbH₂Cl₂2H₂O)

CobpbH₂Cl₂2H₂O (Cobalt pyridine amide complex) was prepared by following standard literature method reported elsewhere [46]. The 1:1 complex was prepared by mixing hot solution of cobalt chloride and the ligand in 95% ethanol. The complex formed immediately, was filtered and washed with ethanol and dried under vacuum. Physical appearance: pink powder. Chem. comp. (wt %) C (44.7), H (3.4), N (11.7). Cl (14.3); Anal. Calcd. C (44.5), H (3.4), N (11.3), Cl (14.2).

5.1.2.2.3. Preparation of SBA-15-SH

Thiol-functionalized SBA-15 (SBA-15-SH) was prepared [49-54] by treating (3-Mercaptopropyl) trimethoxysilane with SBA-15. The thiol loading estimated by sulfur analysis was 1.62 mmol/g. Chem. comp. (wt %) C (6.2), H (1.5), S (4.8); Anal. Calcd C (6.1), H (1.5), S (4.7).

5.1.2.2.4. Preparation of SBA-15-SO₃H

Sulfonic acid functionalized SBA-15 (hereafter referred as SBA-15-SO₃H) was prepared [54-57] from SBA-15-SH and 30% aq. H₂O₂. Sulfonation was accomplished by oxidizing the thiol-groups with H₂O₂. The content of -SO₃H functional group = 0.57 mmol/g SBA-15 (estimate based on sulfur analysis); Chem. Comp. (wt %) C (4.7), H (1.4), S (1.7); Anal. Calcd C (4.6), H (1.5), S (1.7).

5.1.2.2.5. Preparation of immobilized CobpbH₂Cl₂2H₂O complex

The sulfonic acid-functionalized SBA-15 material (SBA-15-SO₃H; 3 g) was first dried at 353 K, under vacuum, for 3 h and then dispersed in 50 ml of dry-toluene. CobpbH₂Cl₂2H₂O (0.5 g) was added and the contents of the flask were refluxed, under nitrogen atmosphere, for 24 h. The solid was filtered, dried at 333 K and Soxhlet-

extracted, initially with toluene for 12 h and then, with dichloromethane for another 12 h. As the SBA-15-SO₃H possess ion-exchange capacity [58-61], Co (Pyridine amide)⁺ ions could be readily immobilized on the functionalized SBA-15 surface. The immobilization process has been depicted in scheme 5.1.1. The solid catalyst material (SBA-15-SO₃-CobpbH₂Cl₂2H₂O), thus prepared, was dried (353 K, 12 h) and used further in characterization and catalytic activity studies and designed as SBA-15/Co. Sulfonic acid functional group = 0.40 mmol/g silica (estimate based on sulfur analysis). Co (pyridine amide)⁺ (estimated by ICP-AES) = (0.17mmol/g). Chem. comp. (wt %) C (8.8), H (2.5), S (1.0), N (1.7); Anal. Calcd C (8.9), H (2.6), S (0.9), N (1.8).

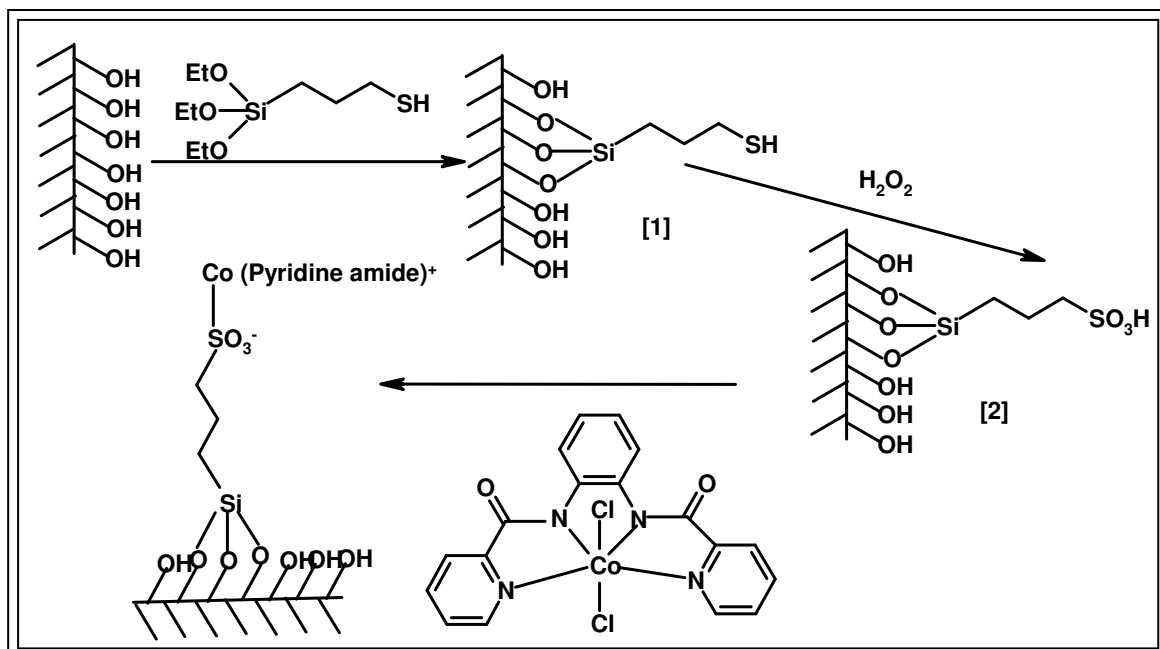
5.1.2.3. Typical procedure for epoxide ring opening

In a typical reaction, known amounts of catalyst and epoxide and an equimolar amounts of amine were placed in a double necked round-bottomed flask (50 mL) kept in a temperature controlled oil bath and fitted with a water-cooled condenser. The reaction was conducted for a specified period. The progress of the reaction was monitored by obtaining an aliquot of the sample, diluting it with a known quantity of dichloromethane, separating the catalyst by centrifugation, and subjecting the diluted liquid to gas chromatography (GC Shimadzu 14B) with a capillary column (cross-linked 5% diphenyl-95% dimethylpolysiloxane capillary column, 30 m × 0.53 × 1.5 μm film thickness), coupled with flame ionization detector. In most cases, the products were confirmed without any chromatographic purification by GC-Mass spectroscopy (Shimadzu GC-17A & QP-5000) with identical columns. GC-MS studies of some products are as follows:

1-phenyl-2-(phenyl amino) ethanol: GC-MS (m/e): 214.8, 213.7, and 182.0.

2-Phenylamino-cyclohexanol: GC-MS (m/e): 193.0, 192.2, 191.3, and 132.2.

1-Chloro-3-phenylamino propan-2-ol: GC-MS (m/e): 188, 187, 186.2, 183.5, and 106.2.



Scheme 5.1.1. Immobilization of CobpbH₂Cl₂·2H₂O complex into SBA-15

5.1.3. Results and discussion

5.1.3.1. Catalyst characterization

Small angle XRD patterns of the samples SBA-15, SBA-SO₃H, and SBA-15/Co were compared in Fig.5.1.1. The X-ray diffraction patterns for SBA-15 sample showed a well resolved pattern with a prominent peak at 2θ (0.9) ° and three weak peaks at 2θ (1.5), (1.7) and (2.3) ° for all the crystallized samples indexed to (100), (110), (200) and (210) reflections, respectively, indicating that significant long range ordering of the hexagonal arrayed pore structure, which match well with the pattern reported for SBA-15. The only reflection of (210) of samples SBA-SO₃H, and SBA-15/Co was diminished, which indicates that functionalization did not damage the ordered hexagonal structure of SBA-15. The slight decrease in intensity of the diffraction peaks was owing to the introduction of functionalizing moiety and loading of metal complex, which indicated that functionalization, has some interference on the assembly of the mesophase. This observation is further reinforced by transmission electron microscopy (Fig.5.1.2).

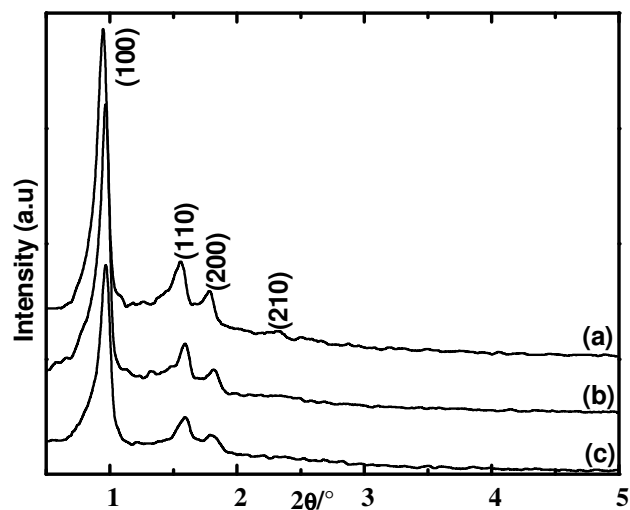


Fig.5.1.1. Low angle XRD patterns of (a) SBA-15-, (b) SBA-15-SO₃H, (c) SBA-15/Co

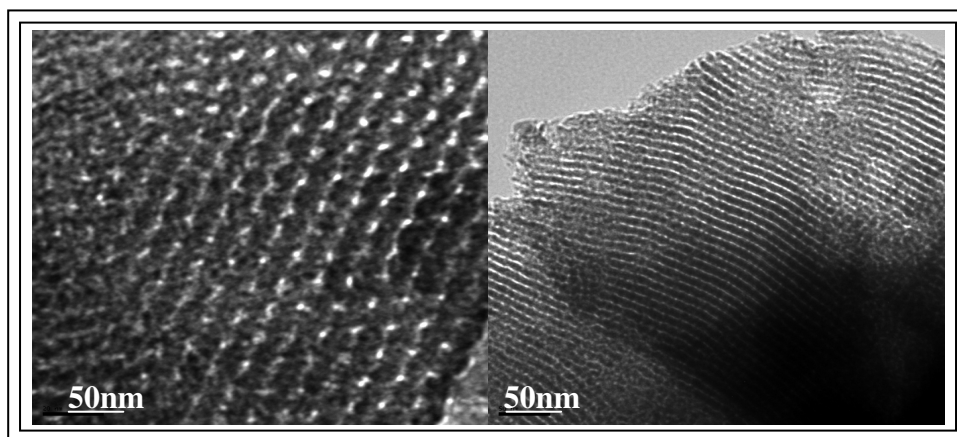


Fig.5.1.2. HRTEM pictures of SBA-15/Co

N₂ sorption isotherms of the samples SBA-15, SBA-SO₃H, and SBA-15/Co are depicted in Fig.5.1.3 (A). All samples yielded type IV isotherms with a H1 hysteresis loop, with steep increases in adsorption at P/P₀ ~ 0.6–0.8, due to capillary condensation of nitrogen in the mesoporous, which are typical for mesoporous materials with two-dimensional structures. Pore volume, pore size, and Brunauer–Emmett–Teller (BET) surface area data are summarized in Table 5.1.1.

Table 5.1.1. Physicochemical properties of catalyst systems

Catalyst	Surface area (m ² /g)	Pore volume (cm ³ /g)	Pore diameter (nm)	Conv ⁿ . ^a (mol %)	Isomers Selectivity (%)	
					I	II
					CobpbH ₂ Cl ₂ 2H ₂ O	-
SBA-15	600	1.1	7.8	-	-	-
SBA-SO ₃	421	0.92	6.6	43	94	6
SBA-15/Co	243	0.59	6.6	96	97	3

Reaction conditions: 0.1 M of styrene oxide, 0.1 M of aniline, catalyst (200 mg), 300 K and 12 h.^a GC conversion.

Compared with SBA-15, the surface area of the sample SBA–SO₃H, was reduce from 600 to 421 m²g⁻¹, attributing to the functionalization of sulphonic acid. The pore volume of SBA–SO₃H decreased from 1.1 to 0.92 cm³g⁻¹ further confirmed the previous conclusion. The introduction of metal complex led to a further decrease in surface area (421 to 243 m²g⁻¹) and pore volume (0.92 to 0.59 cm³g⁻¹). The BJH pore-size distribution (PSD) analysis shows very narrow PSD values in the diameter range of 7.8–6.6 nm.

The UV–vis DRS spectra of immobilized CobpbH₂Cl₂2H₂O complex exhibited several bands in the spectral region 200–800 nm (Fig.5.1.3 (B)). The bands of SBA-15/Co observed at 224, 270 and 320 nm were due to ligand. The band at 515 nm due to ligand-to-metal charge transfer transition (LMCT) [45] undergoes a red shift to 520 nm upon immobilization. In addition, weak d–d transition bands were observed at 625, 670 and 705 nm, respectively.

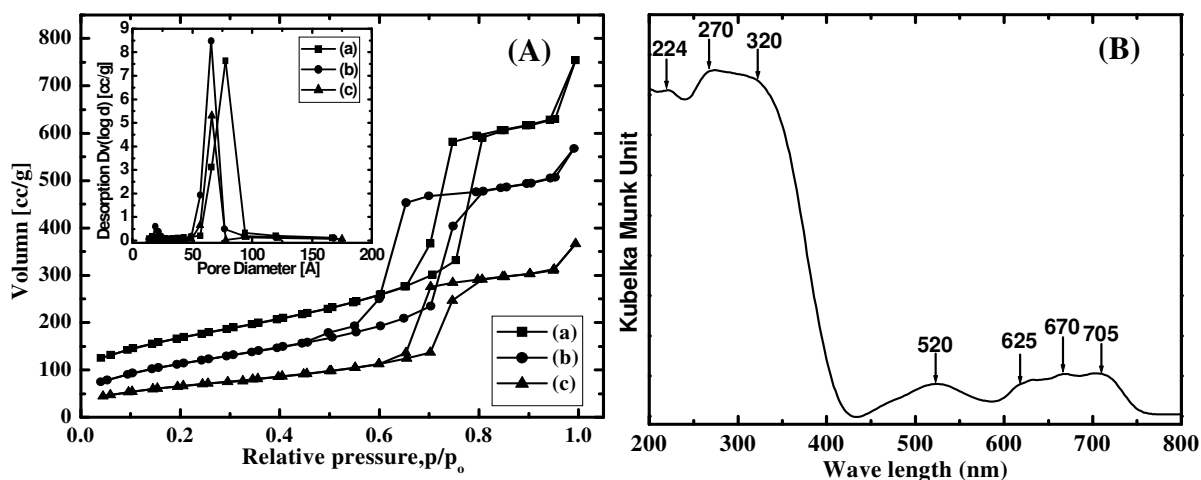


Fig 5.1.3. (A) Nitrogen adsorption-desorption isotherms and BJH adsorption pore size distributions of (a) SBA-15, (b) SBA-15-SO₃H, (c) SBA-15/Co
(B) DRUV-Vis spectra for SBA-15/Co

“Neat” CobpbH₂Cl₂2H₂O showed characteristic IR bands 3200, 3045 (N-H) 645, 1020, 1055, 1100, 1180, 1270, 1550, 1640 cm⁻¹ (amide) 690, 755, 815, 930 cm⁻¹ (C-H deformation) 1315, 1360, 1385 cm⁻¹ (C-H vibration) 1475 cm⁻¹ (aromatic ring) 1455 cm⁻¹ (skeletal vibrations) 1595 cm⁻¹ (aromatic ring) 1570 cm⁻¹ (skeletal vibrations) as shown in Fig.5.1.4. Sulfonic acid-functionalized SBA-15 showed characteristic FT-IR peaks at 2800 – 3700, 1040–1250, 805 and 460 cm⁻¹ due to O–H of the silanols, adsorbed water molecules and Si–O–Si stretching vibrations, respectively. The sulfonic acid-functionalized SBA-15 showed typical peaks at 980 and 600 cm⁻¹ due to the –SO₃H moiety (Fig. 5.1.4). The bands at 2945 and 2865 cm⁻¹ were due to C–H stretching modes of the propyl spacer. The characteristics bands of neat complex masked by the intense bands of the support, were only weakly visible in the supported materials due to the low concentration of CobpbH₂Cl₂2H₂O upon immobilization on SBA-15, the band at 1545, 1640 cm⁻¹ due to (amide) [45] and the bands at 1305, 1340, 1385 cm⁻¹ corresponding (C–H vibration) were observed [45]. The band at 1595 cm⁻¹ could be due to ring vibrations. Some shifting of bands was observed in between neat and immobilized complex, which is attributed to geometrical constraints of the mesoporous support and changes in conformation geometry of the pyridine amide ligand.

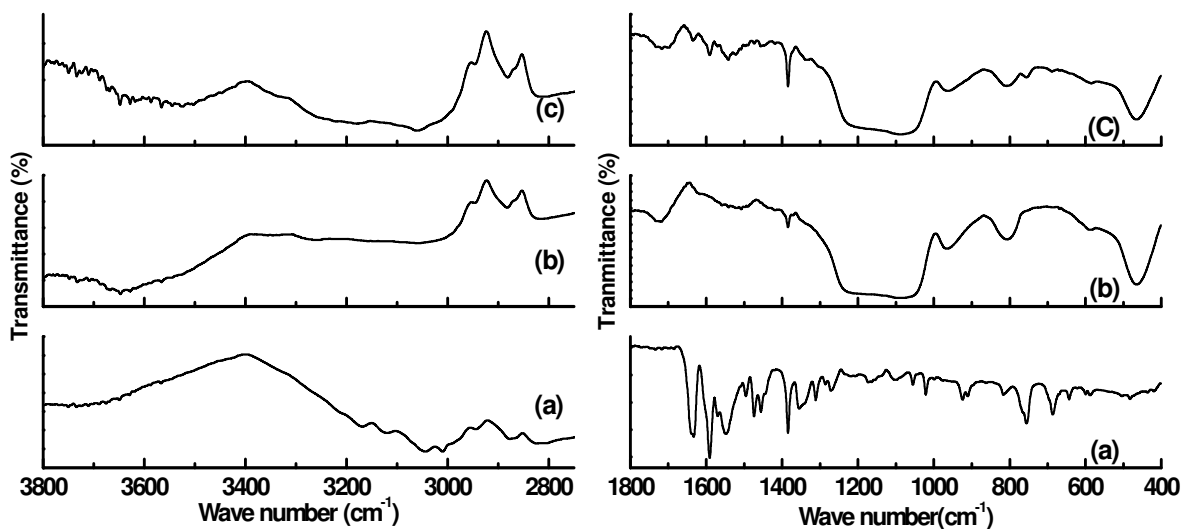
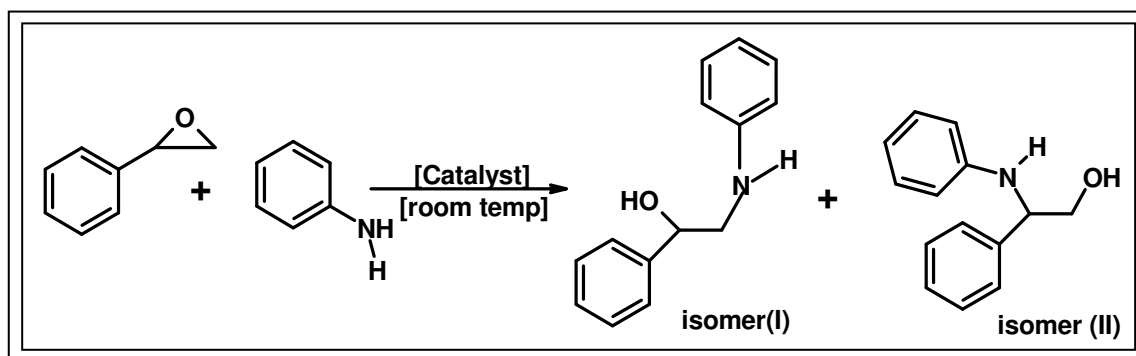


Fig 5.1.4. FT-IR spectrum of (a) $\text{CobpbH}_2\text{Cl}_2 \cdot 2\text{H}_2\text{O}$, (b) SBA-15- SO_3H and (c) SBA-15/Co

5.1.3.2. Catalytic epoxide ring opening studies

β -Amino alcohols were synthesized by the ring opening of epoxides with amines over (SBA-15/Co) catalyst at ambient temperatures and under solvent free conditions (Table 5.1.2). The pyridine amide ligand system is capable of stabilizing early as well as late transition metal ions in high oxidation states, making high-valent metal complexes of the ligands suitable as Lewis acid catalysts. Therefore we have chosen this ligand system for this particular reaction. In a typical experiment, a reaction mixture containing 0.1 mol of styrene oxide, 0.1 mol of aniline and catalyst 200 mg was kept for 12 h with constant stirring. The reaction of styrene oxide with aniline yielded two types of isomers: I and II (Scheme 5.1.2.). Selectivity for the isomer I was found to be always higher (Table 5.1.2). A comparison of the activities of both homogeneous (neat metal complex, amount: 0.025 mmol) and immobilized catalysts in aminolysis of epoxide has been made under similar reaction conditions. The TOF (turn over frequency) of immobilized catalyst system (235) was quite comparable with the homogeneous one ($\text{CobpbH}_2\text{Cl}_2 \cdot 2\text{H}_2\text{O}$) showed TOF 256. The high selectivity of product I in heterogeneous catalyst system could be due to the reason that in constrained environments, the active metal complexes lose some of the degrees of freedom that they had in the bulk state, adopt a particular geometry, hook onto

the functional groups available on the support surfaces, change their coordination sphere geometry, and relax or restrict their sphere of influence, depending on whether or not they reside inside the channels of the mesoporous supports. Thus, they exhibit improved reactivity so as to promote the reaction in sterically controlled pathways. To evaluate the scope of this catalyst, the reaction of other amines and epoxides were further studied. As indicated in Table 5.1.2 (entries 2-6) substituted anilines such as 4-methylaniline, 2-chloroaniline, 2-bromoaniline, 2-nitroaniline and 4-methoxyaniline gave corresponding β -Amino alcohols in good yields. A similar reactivity was observed with a secondary amine like piperidine (entry 7). Furthermore, epichlorohydrin and cyclohexane epoxide were aminolyzed to corresponding β -Amino alcohols in high yields (entries 8, 9). In spite of the fact that epichlorohydrin has many reactive positions and can in principle lead to some other products. Anilines containing electron-withdrawing ring substituent were showed less conversion compared with aniline but they were not following any trend. A negligible conversion was observed in the absence of catalyst.

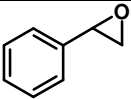
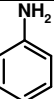
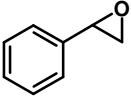
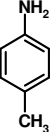
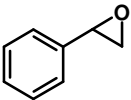
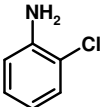
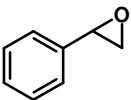
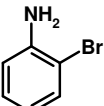
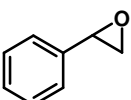
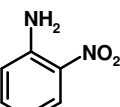
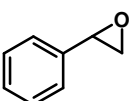
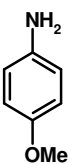
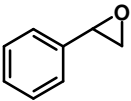
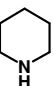
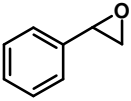
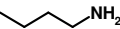
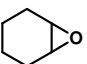
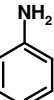
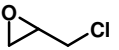
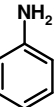


Scheme 5.1.2 Aminolysis of epoxides over SBA-15/Co

5.1.3.3. Catalyst stability and recyclability

One of the main advantages of using solid catalysts in the liquid phase reaction is the ease of separation and reuse in catalytic cycles. After completion of the reaction, the catalyst was separated by filtration, washed with dichloromethane and butyronitrile, dried under vacuum for 4 h, and then reused for another cycle with a fresh reaction mixture. This procedure was repeated in four cycles (Table 5.1.3).

Table 5.1.2. Aminolysis of epoxides catalysed by SBA-15/Co

Entry no	Epoxide	Amine	Epoxide conversion ^a (mol %)	Product selectivity (%)	
				Isomer (I)	Isomer (II)
1			96	98	2
2			87	98	2
3			91	97	3
4			90	97	3
5			74	94	6
6			79	96	4
7			91	95	5
8			4	100	0
9			91	100	0
10			90	96	4

Reaction conditions: 0.1M of styrene oxide, 0.1 M of aniline, catalyst 200mg , 300 K and 12 h. ^a GC conversion

The results show that the conversions were nearly the same in all four cycles indicating that the catalyst could be used in repeated cycles without loss in its activity. The marginal decrease in conversion observed after each cycle could be due to mechanical or handling loss of the catalyst during reaction/regenerations. We confirmed

the absence of leaching of CobpbH₂Cl₂·2H₂O complex from the immobilized system into the reaction medium during the reaction. The confirming reaction was carried out at 300 K for 3 h (conditions same as used in recycling study) and then the catalyst was removed by filtration under hot condition. The conversion of styrene oxide was 38%. The reaction was continued for another 3 h with the filtrate only and the conversion of styrene oxide remained the same after 3 h. Again, we have performed ICP-AES analysis with the filtrate and there was no trace amount of cobalt has been observed. Hence, we can conclude that our catalyst system is stable towards leaching under applied oxidizing conditions.

Table 5.1.3. Recyclability of Catalyst SBA-15/Co

Run	1	2	3	4
Conversion ^a (mol %)	96	95	92	90

Reaction conditions: 0.1M of styrene oxide, 0.1 M of aniline, catalyst 200mg,

300 K and 12 h.^a GC conversion

5.1.4. Conclusions

In conclusion, the results summarized in this report constitute the first example of a highly efficient and simple protocol for the ring opening of epoxides catalyzed by CobpbH₂Cl₂·2H₂O complex immobilized on to SBA-15 and thereby expanding the chemistry of these catalyst systems to an important reaction class. The facile synthesis of catalysts, their benign nature, the ease of handling and the simplified reaction and isolation procedures make them an attractive alternative to current methodologies. Thus the present method is “environmentally friendly” and potentially useful for industrial applications.

Section B

5.2. [Ru (salen) (NO)] complex encapsulated in mesoporous SBA-16 as catalyst for hydrogenation of ketones to alcohols

5.2.1. Introduction

The most studied method to prepare heterogeneous catalysts is probably the immobilization of their homogeneous counterparts on solid supports [62]. SBA-16 is a material with a 3D cubic arrangement of mesopores corresponding to the *Im3m* space group, and is a good candidate for trapping metal complex catalyst with large molecular size into the nanopores or cavities of mesoporous materials, due to its multidirectional pore systems and tunable pore entrances that are likely to be more resistant to local pore blockage than channel-like pores [63]. The large cages of these mesoporous materials can accommodate metal complexes of large molecular size, whereas the smaller pore entrances may prevent leaching of the metal complex confined in the mesoporous cage. In addition, the existence of plentiful hydroxyl groups in the mesoporous silica provides the possibility of tailoring the pore entrance size by a simple silylation reaction.

Transition metal-catalyzed procedures for transfer hydrogen to a wide variety of functional groups by different hydrogen donors are an interesting alternative to conventional catalytic hydrogenation [64-67]. Hydrogenation of C=O double bonds using molecular hydrogen is very important process not only of academic interest, but also in industrial organic syntheses, due to its simplicity, environmental friendliness, economic viability and complete atom efficiency [68-70]. There has been a massive research effort aimed at developing catalysts that can carry out this goal with high efficiency and chemo selectivity. The ability of transition metal catalysts to add or remove hydrogen from organic substrates by either direct or transfer hydrogen processes is a valuable synthetic tool. Salen and its derivatives are well known to be very versatile ligands and readily form coordination compounds with various transition metal ions [71-74]. The potential of second-row transition metallosalen complexes have not been sufficiently explored. Among second-row transition metal ions, ruthenium has currently gained a growing utility in catalytic process due to its characteristic feature showing a wide range of

accessible oxidation states. Bosnich et al. earlier demonstrated that a cationic [Ru(salen)(NO)] complex served as Lewis acid to catalyze various carbon-carbon bond-forming reactions such as Mukaiyama aldol condensation [75,76]. Ruthenium complexes have a long pedigree as catalysts for hydrogen transfer reactions. In the present study, we have synthesized a heterogeneous catalyst system by encapsulating [Ru(salen)(NO)(Cl)] complex into mesoporous silica SBA-16 that behaves as very efficient catalyst system in the hydrogenation of a series of ketones to alcohols.

5.2.2. Experimental

5.2.2.1 Chemicals

All the solvents procured from Merck, India (A R grade) were distilled and dried prior to their use. The other chemicals purchased from Aldrich were used as received.

5.2.2.2 Catalyst preparation

5.2.2.2.1. Preparation of the complex $Ru(NO)Cl_3 \cdot 5H_2O$

$Ru(NO)Cl_3 \cdot 5H_2O$ complex was synthesized by modification of literature procedure [75]. $RuCl_3 \cdot 3H_2O$ 2.5 g (9.6 mmol) was added to 10 mL of degassed 1 M HCl and the mixture heated to reflux, and then 1.97 g of $NaNO_2$, (28.5 mmol) dissolved in 5 mL of H_2O was added drop wise over a period of 30 min. The resulting brown solution was refluxed for another 2.5 h to give dark red solution, which was then dried under reduced pressure to get a red colored solid. This solid was then treated repeatedly in successive steps with 10 mL ethanol, 5 mL of 6 M HCl, and 2 mL of H_2O and dried under reduced pressure in each step to get finally a red colored residue, which was stored in a desiccator ($CaSO_4$) for 12 h, yielding (2.6 g) 83% of the desired $Ru(NO)Cl_3 \cdot 5H_2O$ complex.

5.2.2.2.2. Preparation of the [Ru(salen)(NO)(Cl)] complex

[Ru(salen)(NO)(Cl)] was prepared under inert argon atmosphere. NaH (80% dispersion in mineral oil, 260 mg, 8.68 mmol) was weighed into a 200-mL Schlenk flask and washed with dry hexane (3 X 10 mL) prior to its use in the preparation. To this, degassed DMF (30 mL) was added, followed by salenH (1,2-phenylenebis(azan-1-yl-1-ylidene))bis(methan-1-yl-1-ylidene)diphenol, (1.05 g, 3.92 mmol), while the NaH suspension was rapidly stirred. The mixture was then transformed into a clear yellow solution after the release of H_2 gas. To this, $Ru(NO)(Cl)_3 \cdot 5H_2O$ (1.00 g, 3.92 mmol) was

added, followed by another lot of DMF (10 mL). The mixture was then stirred at 110 °C for 24 h, which resulted in opaque red-brown color, from which the DMF was removed under high vacuum (0.2 mm) to give red colored residue. Henceforth, all subsequent work was done in air. Dichloromethane (80 mL) and H₂O (90 mL) were added to the residue obtained as above and the mixture was filtered through Celite. The filtrate was transferred into 500 mL separating funnel, and allowed to stand for some time resulting in the separation of two layers. The dark red dichloromethane layer was washed with H₂O (3 X 80 mL). The dichloromethane layer was then stirred with anhydrous MgSO₄ (18 g) for few min and filtered, and the filtrate volume was reduced under vacuum to 200 mL. The same procedure was followed one more time. The volume of the final solution was reduced under vacuum to 30 mL, giving very fine dark red-maroon crystals. Slow addition of Et₂O precipitated more solid from the solution as well as a flocculent green side product. The mixture was then allowed to stand at 5 °C for 12 h and the crystals obtained were filtered off and washed with Et₂O (30 mL), CH₂Cl₂ : Et₂O (1:1, 25 mL), and finally cold CH₂Cl₂ (10 mL). Finally, the crystals were recrystallized twice with CH₂Cl₂ : Et₂O (1:1) and were washed each time with it. The crystals of [Ru (salen)(NO)(C1)] : 0.6 CH₂Cl₂ composition (940 mg, 49% yield) obtained were air stable and stored in a vacuum desiccator. The presence of dichloromethane in the crystal was confirmed by ¹H NMR. Heating a pulverized sample at 60 °C under high vacuum (0.2 mm) for 28 h resulted in the lowering of this ratio to 0.1 CH₂Cl₂ per unit of the complex [76].

5.2.2.2.3. Preparation of SBA-16

SBA-16 silicas were synthesized using poly-(ethylene oxide)-poly(propylene oxide)-poly(ethylene oxide) triblock copolymers as supramolecular templates in a way modified with respect to that originally reported by Zhao et. al [77,78]. Pluronic F127 copolymer (EO106PO70EO106) and its mixtures with Pluronic P123 copolymer (EO20PO70EO20) were used to attain average molar composition EO70PO70EO70 in a way similar to that reported by Kim et al. Tetraethyl orthosilicate (TEOS) was used as the silica source under acidic synthesis conditions. Briefly, an aqueous solution of copolymers was prepared by dissolving in a solution of hydrochloric acid in distilled water. TEOS was then added with magnetic stirring at 308 K. The starting molar composition was 0.0025P123 : 0.0034F127 : 1.0TEOS : 4.6HCl : 151H₂O for

EO70PO70EO70. The mixture was magnetically stirred for about 15 min until TEOS was completely dissolved. The mixture was placed in an oven for 24 h under static condition at 308 K for precipitation of the product. The mixture was further maintained at 373 K for hydrothermal treatment, whose time was varied from 1 h to 7 days, depending on the particular sample. The white solid precipitate was isolated by filtration without washing and dried at 373 K. Subsequently, the product was calcined under air at 823 K after washing with ethanol in order to remove the copolymer template.

5.2.2.2.4. Preparation of [Ru (salen)(NO)(Cl)] encapsulated SBA-16

A typical synthetic procedure is as follows: 1.0 g of SBA-16 (evacuated at 398 K for 6 h) was dispersed in 6 mL of dichloromethane (DCM) (containing 0.2 g of [Ru (salen)(NO)(Cl)]) [63]. After stirring the mixture at refluxing temperature for 24 h under argon atmosphere, DCM was removed by evaporation. The resulting solid was added to a solution containing 1 mL of dry toluene, 1.25 mL of anhydrous pyridine and 5 mmol of diphenyldichlorosilane. After refluxing for 24 h under argon atmosphere, the resulting solid was isolated by filtration and washed thoroughly with toluene, DCM and THF. The prepared catalyst was denoted as Ru(salen)/SBA-16 (0.012 mmol /g of Ru ,ICP analysis)

5.2.2.3. Catalytic experiments

General procedure for the hydrogenation of ketone

Synthesis of 1-(naphthalen-2-yl) ethanol (entry 1, Table 5.2.2): To a test tube, the precatalyst, Ru(salen)/SBA-16 (0.2 g, 0.002 mmol of Ru) and 1M *t*BuOK (potassium *tert*-butoxide) in isopropyl alcohol (0.3 mL, 0.02 mmol) was added under nitrogen and stirred at room temperature for 30 min before 2-methylnaphthyl ketone (6mmol, 1.02 g) and isopropyl alcohol (40 mL) was introduced. The contents of the test tube was transferred to 300 mL autoclave and then sealed. After purging with hydrogen for five times, the final H₂ pressure was adjusted to 20 atm. After stirring at 373 K for 12 h, the reaction was stopped. The conversion was determined by GC to be 90%. The reaction mixture was filtered and washed several times with isopropyl alcohol. The filtrate was removed under reduced pressure and purified by column chromatography on silica as the stationary phase (pet ether:ethyl acetate, 85:15) to give 1-(naphthalene-2-yl) ethanol white solid, ¹H NMR (CDCl₃, 200 MHz): $\delta = 7.73\text{--}7.78$ (m, 4H), 7.37–7.46 (3H, m),

4.95–5.05 (1H, q), 1.49–1.53 (3H, d), ^{13}C NMR (CDCl_3): $\delta = 133.5$ (C), 131.2 (C), 128.0 (CH), 127.6 (CH), 127.5 (CH), 127.3 (CH), 126.9 (CH), 126.1 (CH), 124.9 (CH), 123 (C), 76.1 (CH), 22.6 (CH_3).

5.2.3. Results and discussion

Fig. 5.2.1 (A) shows the XRD patterns of SBA-16 material. SBA-16 material exhibits two diffraction (110) and (200) peaks, characteristic of mesoporous materials with the cubic $Im\bar{3}m$ structure. The diffraction peaks gradually decreased in intensities for sample, Ru(salen)/SBA-16 demonstrating occurrence of silylation and entrapment of metal complex inside mesopores of SBA-16.

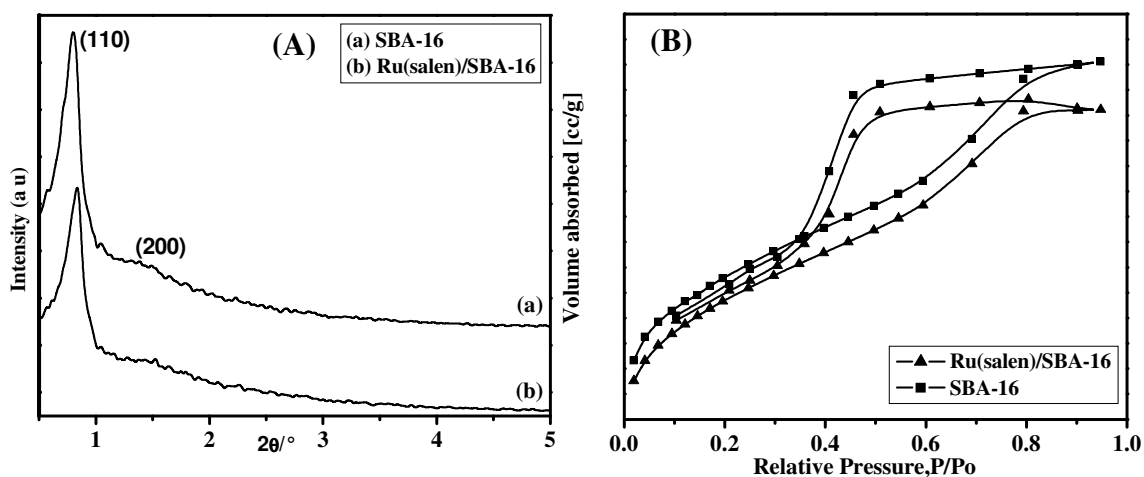


Fig.5.2.1. (A) Low angle Powder XRD patterns of (a) SBA-16 and (b) Ru(salen)/SBA-16, (B) N_2 sorption isotherms of samples of (a) $[\text{Ru}(\text{salen})(\text{NO})(\text{Cl})]$ and (b) Ru(salen)/SBA-16

The N_2 sorption isotherms of SBA-16 and SBA-16 (silylated with diphenyldichlorosilane and metal complex encapsulated) exhibit type IV isotherm patterns with H2 hysteresis loops (Fig.5.2.1. (B)), confirming that the cage-like structure of SBA-16 was maintained after the encapsulations. For cage-like mesopores materials, the capillary condensation pressure is an increasing function of the pore cage diameter (analogous to the case of cylindrical pores) [79,80]. However, the capillary evaporation pressure tends to reflect either the size of the largest entrance to the given mesopore (if evaporation takes place above the lower limit of hysteresis) or the upper limit of possible

entrance sizes (if evaporation takes place at the lower limit of hysteresis) [80]. This is because the emptying of interiors of cage-like mesopores cannot take place when these interiors do not have a direct access to the surrounding gas phase through a continuous pathway of gas phase. The exception is the case where the lower limit of hysteresis is reached, at which point the capillary evaporation from the interiors of mesopores takes place even if the connecting pores are still filled with the liquid-like adsorbate phase. After encapsulation, the surface area and pore volume of SBA-16 apparently decreased from 870 to 780 m²/g and from 0.7 to 0.59 cc/g respectively. This confirms that the diphenyldichlorosilane was grafted on the surface of SBA-16.

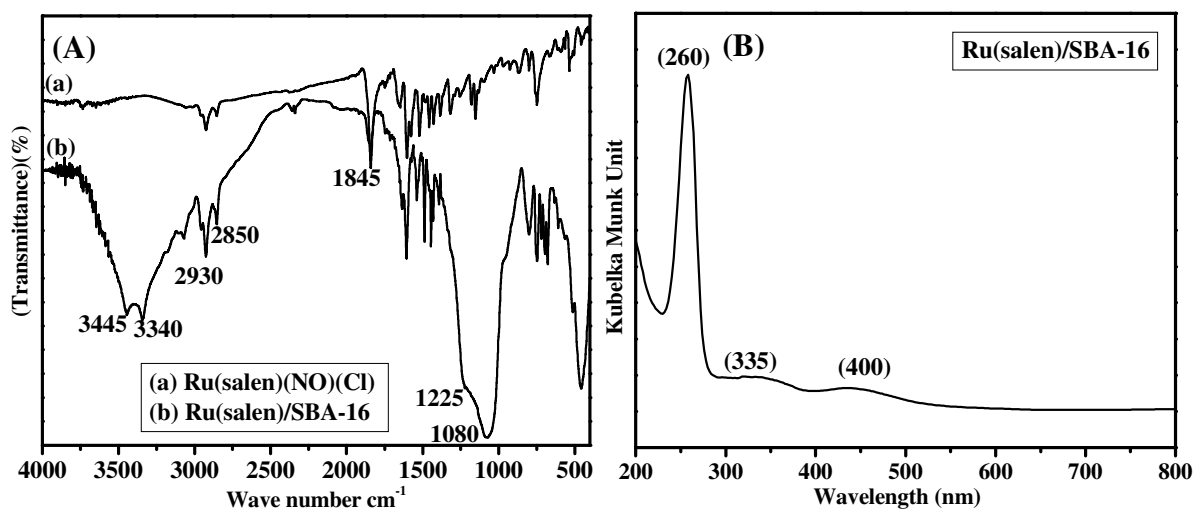


Fig.5.2.2. (A) FT-IR spectra of (a) [Ru(salen)(NO)(Cl)] and (b) Ru(salen)/SBA-16
(B) UV-Vis DRS spectra UV-Vis spectra of Ru(salen)/SBA-16

“Neat” [Ru(salen)(NO)(Cl)] showed characteristic IR bands 3445, 3340 (N-H) 695, 745, 800 cm⁻¹ (C-H deformation) 1300 and 1380 cm⁻¹ (C-H Vibration), 1495 cm⁻¹ (aromatic ring), 1430 cm⁻¹ (skeletal vibrations), 1605 cm⁻¹ (aromatic ring) as seen in Fig. 5.2.2 (A). Characteristic FT-IR peaks at 2930, 2850, 1080–1225 and 460 cm⁻¹ were due to O–H of the silanols, adsorbed water molecules and Si–O–Si stretching vibrations, respectively. The band at 1845 cm⁻¹ was due to NO stretching of the ligand system. The characteristics bands of neat complex masked by the intense bands of the support, were

only weakly visible in the supported materials due to the low concentration of [Ru(salen)(NO)(Cl)] upon encapsulation in SBA-16, the band at 1845, due to NO stretching and the bands at 1300 and 1380 cm^{-1} (C-H Vibration) 1495 cm^{-1} (aromatic ring) 1430 cm^{-1} (skeletal vibrations) 1605 cm^{-1} (aromatic ring). There are some shifting of bands were observed in between neat and immobilized complex which is attributed to geometrical constrains of the mesoporous support and changes in conformation geometry of the ligand.

The UV-vis DRS spectra of immobilized [Ru(salen)(NO)(Cl)] complex exhibited several bands in the spectral region 200–800 nm (Fig. 5.2.2.(B)). The bands of Ru(salen)/SBA-16 observed at 260 and 335 nm were due to ligand. The band at 400 nm was due to ligand-to-metal charge transfers transition (LMCT). The weak d-d transition bands were unable to observe in the spectra. Hydrogenation of 1-(naphthalene-2-yl)ethanone has been carried out by applying above-mentioned procedure. A comparison of the activities of both homogeneous (neat) and immobilized catalysts in hydrogenation of 1-(naphthalene-2-yl)ethanone has been made under similar reaction conditions. The homogeneous catalyst showed 99% conversion of methynaphthylketone in 12 h, while with immobilized catalyst, the conversion was found to be 98%. A couple of experiments were performed to optimize the reaction condition for this newly synthesized catalyst Ru(salen)/SBA-16. In the first experiment, the reaction was carried out at 20 atm H_2 pressure at 373 K in a Parr autoclave with the active catalyst in isopropanol solvent, which gave only 98 % conversion. Product yield decreased with the decreasing of pressure 27-7 atm (98-18 %). The reaction does not proceed below 7 atm pressures. In the next experiment, we studied the effect of temperature; little conversion of ketone has been observed at 80 °C. Alcohol yield increased with increasing temperature 80–100 °C (16-98 %). There was no further increase in conversion with the increase of temperature (Table 5.2.1). The activity of the Ru(salen)/SBA-16 catalyst was studied as a function of time (Fig.5.2.3) in the synthesis of 1-(naphthalen-2-yl) ethanol. From the above observations, we can conclude that the maximum yield can be obtained at 100 °C and 20 atm. in 12 h.

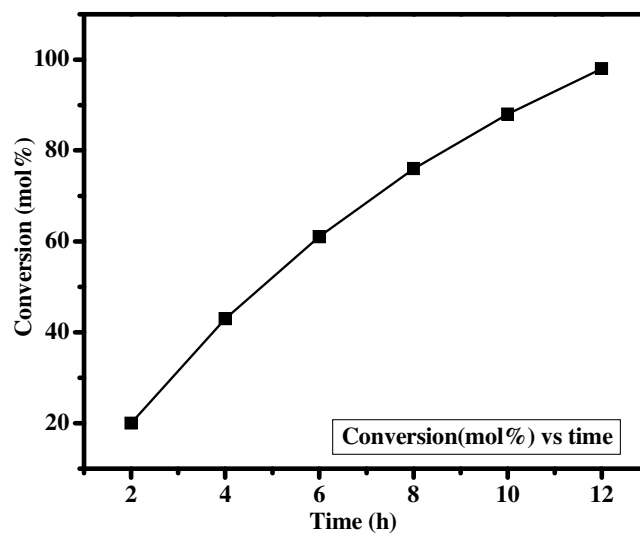


Fig.5.2.3. The activity of the Ru(salen)/SBA-16 catalyst as a function of time

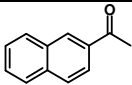
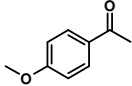
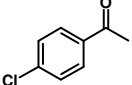
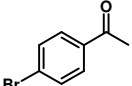
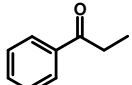
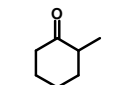
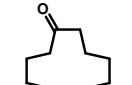
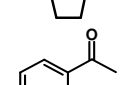
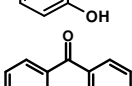
Table 5.2.1. Catalytic parameters of hydrogenation of ketones using catalyst Ru(salen)/SBA-16

Entry	Catalyst wt (g)	Temp (K)	Pressure (atm)	Time (h)	Conversion (mol%)
1	0.2	373	27	12	98
2	0.2	373	20	12	98
3	0.2	373	14	12	92
4	0.2	373	7	12	18
5	0.2	353	20	12	16
6	0.2	363	20	12	35
7	0.2	383	20	12	97
8	0.1	373	20	12	20
9	0.3	383	20	12	98

Reaction condition: Substrate (6 mmol), solvent isopropanol (40 mL)

To investigate the effect of catalyst amount on hydrogenation of ketones, the results showed that the conversion is very low with 0.1 g of catalyst and with the increase in catalyst amount, the conversion get increased (Table 1). The reaction attained its maximum methyl 2-naphthyl ketone (conversion 98%) after 12h. A negligible conversion was observed in the absence of catalyst.

Table.5.2.2. Hydrogenation of ketones using catalyst Ru(salen)/SBA-16

Entry	Substrate	Time (h)	Conversion (mol%)
1		12	98
2		12	79
3		12	84
4		12	80
5		12	67
6		12	98
7		12	60
8		12	20
9		12	20

Reaction condition: Substrate (6 mmol) and catalyst (Ru(salen)/SBA-16) (200 mg, 0.002 mmol of Ru) were stirred at *ca.* 100 °C in isopropanol (40 mL) under H₂ pressure (20 atm) in Parr autoclave

To evaluate the scope of this catalyst, the reaction of other ketones was further studied with optimized condition. As indicated in Table 2, (entries 2-5) various substrates such as 1-(4-methoxyphenyl)ethanone, 1-(4-chlorophenyl)ethanone, 1-(4-

bromophenyl)ethanone and propiophenone gave corresponding alcohols in good yields. A similar reactivity was observed with the cyclic ketones like 2-methyl cyclohexanone (entry 6) and cyclododecanone (entry 7). While substrate like (2-hydroxyphenyl)ethanone (entry 8) and (2-hydroxyphenyl)(phenyl)methanone (entry 9) showed comparatively very less conversion, which could be due to the presence of hydroxyl group in ortho position, that is prone to strong intramolecular hydrogen bonding of the molecules.

One of the main advantages of using solid catalysts in the liquid phase reaction is the ease of separation and reuse in catalytic cycles. The repeated use of the catalyst Ru(salen)/SBA-16 was carried out [conditions: substrate (6 mmol) and catalyst (Ru(salen)/SBA-16) 200 mg, 0.002 mmol of Ru were stirred at *ca.* 373 K in isopropanol (40 mL) under H₂ pressure (20 atm) for 12 h]; the first cycle gave 98% conversion of methyl 2-naphthyl ketone. The catalyst was separated by filtration, washed with isopropanol, dried under vacuum for 4 h, and then reused in the second cycle with a fresh reaction mixture and the conversion was found to be 87%. This procedure was repeated and conversion was found to be 84% and 80% for third and fourth recycle, respectively. The decreases in conversions after first cycle could be due to partial leaching of physisorbed active species of the catalyst during reaction/regenerations. But after first regeneration there is a very marginal decrease in conversion after each cycle, which could be due to mechanical loss.

5.2.4. Conclusions

SBA-16 silica of *Im3m* structure is a robust copolymer templated ordered mesoporous material, whose mesopore cage diameter and pore entrance size can be tailored using several synthetic strategies. The [Ru(salen)(NO)] complex was encapsulated in the cage-like mesoporous material SBA-16. Fine-tuning of the pore entrance size of the mesoporous cage-like silica was found to be the key factor for successful trapping of complex in the cage of the mesoporous materials. The catalyst was found to be an active encapsulated catalyst system for the hydrogenation of ketones. The activities are comparable with that of homogeneous analogues in all the reactions studied. This strategy could be a promising method for preparing efficient heterogeneous catalyst system.

5.3. References

1. I. Erden, in: A. Padwa (Ed.), *Comprehensive Heterocyclic Chemistry*, Second Ed. Pergamon Press: Oxford, 1996 (Chapter 1.03).
2. M Bartok, K.L Lang, in: A. Weissberger, E.C. Taylor (Eds.), *The Chemistry of Heterocyclic Compounds*, Wiley: New York, 1985, Vol. 42; part 3.1.
3. A.S. Rao, S.K Paknikar, J.G. Kirtane, *Tetrahedron* 39 (1983) 2323.
4. D.R. Gehlert, D.J. Goldstein, P.A. Hipskind, *Ann. Rep. Med. Chem.* (1999) 201.
5. E.J. Corey, F. Zhang, *Angew. Chem. Int. Ed.* 38 (1999)1931.
6. J. De Cree, H. Geukens, J. Leempoels, H. Verhaegen, *Drug Dev. Res.* 8 (1986) 109.
7. J.G. Smith, *Synthesis* (1984) 629.
8. P.O. Brien, *Angew. Chem. Int. Ed.* 38 (1999) 326.
9. G. Li, H.-T. Chang, K.B. Sharpless, *Angew. Chem. Int. Ed. Engl.* 35 (1996) 451.
10. D.J. Ager, I. Prakash, D.R. Schaad, *Chem. Rev.* 96 (1996) 835.
11. S.C. Bergmeier, *Tetrahedron* 56 (2000) 2561.
12. D.M. Hodgson, A.R. Gibbs, G.P. Lee, *Tetrahedron.* 52 (1996) 14361.
13. M. Hanson, *Chem. Rev.* 91(1991) 437.
14. O. Mitsunobu, in: E. Winterfeldt (Ed.), *Comprehensive Organic Synthesis*, Pergamon Press, New York, 1996, Vol. 6, part 1.3.4.1
15. P.A. Crooks, R. Szyudler, *Chem. Ind. (London)* (1973) 1111.
16. J.A. Deyrup, C.L. Moyer, *J. Org. Chem.* 34 (1969) 175.
17. M. Freifelder, G.R. Stone, *J. Org. Chem.* 26 (1961) 1477.
18. M. Mousseron, J. Jullien, Y. Jolchine, *Bull. Soc. Chim. Fr.* (1952) 757.
19. R.E. Lutz, J.A. Freek, R.S. Murphy, *J. Am. Chem. Soc.* 70 (1948) 2015.
20. A. Kamal, B. Rajendra Prasad, A. Malla Reddy, M. Naseer, A. Khan, *Catal. Commun.* 8 (2007) 1876.
21. A.T. Placzek, J.L. Donelson, R. Trivedi, R.A. Gibbs, S.K. De, *Tetrahedron Lett.* 46 (2005) 9029.
22. T. Ollevier, G. Lavie-Campin, *Tetrahedron Lett.* 45 (2004) 49.
23. S. Sagawa, H. Abe, Y. Hase, T. Inaba, *J. Org. Chem.* 64 (1999) 4962.

24. A.V. Narsaiah, D. Sreenu, K. Nagaiah, *Syn. Commun.* 36 (2006) 3183.
25. S.K. De, R.A. Gibbs, *Syn. Commun.* 35 (2005) 2675.
26. L.D. Pachón, P. Gamez, J.J.M. van Brussel, J. Reedjik, *Tetrahedron Lett.* 44 (2003) 6025.
27. J. Iqbal, A. Pandey, *Tetrahedron Lett.* 31 (1990) 575.
28. A.K. Chakraborti, A. Kondaskar, *Tetrahedron Lett.* 44 (2003) 8315.
29. M. Chini, P. Crotti, F. Macchia, *Tetrahedron Lett.* 31 (1990) 4661.
30. F. Carre´e, R. Gil, J. Collin, *Org. Lett.* 7 (2005) 1023.
31. A. Kamal, R. Ramu, M.A. Azhar, G.B.R. Khanna, *Tetrahedron Lett.* 46 (2005) 2675.
32. N. Azizi, M.R. Saidi, *Tetrahedron* 63 (2007) 888.
33. S. Ramesh Kumar, P. Leelavathi, *J. Mol. Catal. A: Chem.* 266 (2007) 65.
34. M. Vijender, P. Kishore, P. Narender, B. Satyanarayana, *J. Mol. Catal. A: Chem.* 266 (2007) 290.
35. B. Sreedhar, P. Radhika, B. Neelima, N. Hebalkar, *J. Mol. Catal. A: Chem.* 272 (2007) 159.
36. R.I. Kureshy, S. Singh, N.H. Khan, S.H.R. Abdi, E. Suresh, R.V. Jasra, *J. Mol. Catal. A: Chem.* 264 (2007) 162.
37. A.K. Chakraborti, A. Kondaskar, S. Rudrawar, *Tetrahedron* 60 (2004) 9085.
38. J.S. Yadav, B.V.S. Reddy, A.K. Basak, A.V. Narasaiah, *Tetrahedron Lett.* 44 (2003) 1047.
39. A. Harva´th, R. Skoda-Fo´ldes, S. Maho´, Z. Berente, L. Kolla´r, *Steroids* 71 (2006) 706.
40. M. Shi, Y. Chen, *J. Fluorine Chem.* 122 (2003) 219.
41. J.K. Satyarthi, L. Saikia, D. Srinivas, P. Ratnasamy, *Appl. Catal. A: Chem.* 330 (2007) 145.
42. H. Ojima, *Nippon Kagaku Zasshi* 88 (1967) 333.
43. O. Belda, C. Moberg, *Coord. Chem. Rev.* 249 (2005) 727.
44. K. Maruyama, T. Nakamura, S. Nakamura, A. Ogino, A. Nishinaga, *React. Kinet. Catal. Lett.* 45 (1991) 165.
45. D.J. Barnes, R.L. Chapman, R.S. Vagg, E.C. Watton, *J. Chem. Eng. Data* 23

- (1978) 349.
46. R. Chapman, R. Vagg, *Inorganica Chimica Acta* 33 (1919) 221.
 47. F. Feng, G.E. Fryxell, L.-Q. Wang, A.Y. Kim, K.M. Kemner, *Science* 276 (1997) 923.
 48. L. Mercier, T.J. Pinnavaia, *Adv. Mater.* 9 (1997) 500.
 49. A. Stein, B.J. Melde, R.C. Schroden, *Adv. Mater.* 12 (2000) 1403.
 50. T. Kang, Y. Park, J.C. Park, Y.S. Cho, J. Yi, *Stud. Surf. Sci. Catal.* 146 (2003) 527.
 51. T. Kang, Y. Park, J. Yi, *Ind. Eng. Chem. Res.* 43 (2004) 1478.
 52. C.M. Crudden, M. Sateesh, R. Lewis, *J. Am. Chem. Soc.* 127 (2005) 10045.
 53. W.M. Van Rhijn, D.E. De Vos, B.F. Sels, W.D. Bossaert, P.A. Jacobs, *Chem. Commun.* (1998) 317.
 54. D. Das, J.-F. Lee, S. Cheng, *Chem. Commun.* (2001) 2178.
 55. E. Cano-Serrano, J.M. Campos-Martin, J.L.G. Fierro, *Chem. Commun.* (2003) 246.
 56. B.C. Wilson, C.W. Jones, *Macromolecules* 37 (2004) 9709.
 57. D.E. De Vos, M. Dams, B. F. Sels, P. A. Jacobs, *Chem. Rev.* 102 (2002) 3615.
 58. W.M. Van Rhijn, D.E. De Vos, B.F. Sels, W.D. Bossaert, P.A. Jacobs, *Chem. Commun.* (1998) 317.
 59. D. Das, J.-F. Lee, S. Cheng, *Chem. Commun.* (2001) 2178.
 60. E. Cano-Serrano, J.M. Campos-Martin, J.L.G. Fierro, *Chem. Commun.* (2003) 246.
 61. B.C. Wilson, C.W. Jones, *Macromolecules* 37 (2004) 9709.
 62. D.E. De Vos, M. Dams, B. F. Sels, P. A. Jacobs, *Chem. Rev.* 102 (2002) 3615
 63. H. Yang, J. Li, J. Yang, Z. Liu, Q. Yang, C. Li, *Chem. Commun.* (2007) 1086.
 64. R. Noyori, S. Hashiguchi, *Acc. Chem. Res.* 30 (1997) 97.
 65. H. Doucet, T. Ohkuma, K. Murata, T. Yokozawa, M. Kozawa, E. Katayama, F. A. England, T. Ikariya, R. Noyori, *Angew. Chem., Int. Ed.* 37 (1998) 1703.
 66. H. Jiang, Q.D. Qiao, H. Gong, *React. Kinet. Catal. Lett.* 65 (1998) 193.
 67. G. Venkatachalam, R. Ramesh, *Tetrahedron Lett.* 46 (2005) 5215.
 68. H. Blaser, C. Malan, B. Pugin, F. Spindler, H. Steiner, M. Studer, *Adv. Synth.*

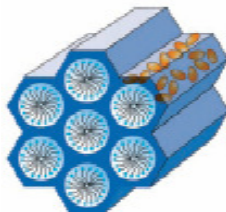
- Catal. 345 (2003) 103.
69. I. C Lennon, G. Casy, N. B. Johnson, Chem. Today (2003) 63.
 70. E. P. Kelson, P. P. Phengsy, J. Chem. Soc., Dalton Trans. (2000) 129.
 71. M. Albrecht, H. Crabtree, J. Mata, E. Peris, Chem. Commun. (2002) 32.
 72. J.-E. Backvall, J. Organomet. Chem. 652 (2002) 105.
 73. J.-Q. Yu, H.-C. Wu, C. Ramarao, J. B. Spencer, S. V. Ley, Chem. Commun. (2003) 678.
 74. J. Hannedouche, G.J. Clarkson, M. Wills, J. Am. Chem. Soc. 126 (2004) 986.
 75. J.G. Muller, K.J. Takeuchi, Inorg. Chem. 29 (1990) 2185.
 76. W. Odenkirk, A.L. Rheingold, B. Bosnich, J. Am. Chem. Soc. 114 (1992) 6392.
 77. D. Zhao, Q. Huo, J. Feng, B.F. Chmelka, G.D. Stucky, J. Am. Chem. Soc. 120 (1998) 6024.
 78. T.W. Kim, R. Ryoo, M. Kruk, P.G. Kamil, M. Jaroniec, S. Kamiya, O. Terasaki, J. Phys. Chem. B 108 (2004) 11480.
 79. P.I. Ravikovitch, A.V. Neimark, Langmuir 18 (2002) 1550.
 80. M. Kruk, M. Jaroniec, Chem. Mater. 15 (2003) 2942.

CHAPTER VI

Nanocomposites

This chapter features the following sections:

6.1. *WO_x/SBA-15 Nanocomposites* 177



6. Studies in structural characterization and correlation with the catalytic activity of an efficient and stable WO_x/SBA-15 nanocomposite catalyst

6.1. Introduction

Nanocomposite materials are created by introducing nanocrystals into a macroscopic matrix, which is one of the growing fields of interest in catalysis. The functionality of nanocomposite has been attributed to their different surface properties, such as surface-to-bulk atomic ratio, the polyhedral surface morphology and the concentration of surface defects (coordinatively unsaturated ions, which are due to planes, edges, corners, anion/cation vacancies, electron excess centers), and shape selectivity [1,2]. Immobilization of nano-scopic materials in high surface area supports with improved catalytic activity and product selectivity is a task of great economic and environmental importance in chemical as well as pharmaceutical industries [3]. There are few reports describing the use of mesoporous silica as support for the immobilization of tungsten oxide species [4,5]. Zhang et al. described the synthesis of tungsten containing MCM-41 with good dispersion, but segregated crystalline WO_x was detected after mild thermal treatment [6]. The crystalline phases of WO_x that form at low pH in the presence of H₂O₂ were prevented by the use of oxoperoxometalate precursors and its stability was poor, which was evident from the extensive leaching of the tungsten species [7]. Currently atomic layer deposition (ALD) method has been applied for grafting tungsten oxide species onto mesoporous silica (SBA-15) [8,9].

The oxygen transfer reaction is one of the most elementary transformations in organic chemistry and several metal-catalyzed oxidation reactions have been investigated till date [10,11]. Among these, oxidation of sulfur compounds to sulfoxides is an interesting and attractive method [12,13]. Sulfoxide is one of the useful building blocks as chiral auxiliaries in organic synthesis [14-18] and plays a key role in enzyme activation [19-22]. However, conventional transformations have limiting success, due to over oxidation and generation of toxic wastes [23-25]. The efficacy of heterogeneous tungstate systems have been dynamically examined due to the fact that a variety of

tungsten-based homogeneous catalysts are known to exhibit high activities in practical oxidation procedures including epoxidation of alkenes [26, 27], alcohol oxidation [27, 28], oxidative cleavage or halogenation of olefins [28], or oxidative desulfurization [29-32]. As a result, some promising heterogeneous systems such as insoluble polyoxotungstates [33-34], immobilized peroxotungstates, triphasic phosphotungstate [35], and pseudo-heterogeneous systems [36] have been recently reported. Inorganic polymers are effective mediators for organizing tungsten oxide species into higher order composite structures [19-22]. Here, we report the synthesis of tungsten oxide and SBA-15 nanocomposite (hereafter WO_x/SBA-15) with large pore diameters and its catalytic activity in the selective oxidation of sulfur compounds to the corresponding sulfoxides under ambient reaction conditions.

6.2. Experimental section

6.2.1. Materials

Sodium Tungstate was purchased from Sisco Research Laboratory Pvt. Ltd., India. TEOS, P123 block copolymer (poly (ethyleneglycol)-poly (propylene glycol)-poly(ethylene glycol), average molecular mass 5800) and all the sulfides were purchased from Aldrich Chemicals and used as received. 70% aq. TBHP was procured from Acros Organics. All the solvents procured from Merck (AR grade), India were distilled and dried prior to their use. Titanium silicates (TS-1 and TS-2) were collected from Catalysis Pilot Plant (CPP), National Chemical Laboratory, Pune (INDIA).

6.2.2. Catalyst preparation

Hexagonally ordered mesoporous WO_x/SBA-15 nanocomposite materials were synthesized by using tetraethylorthosilicate (TEOS) as a silica source and (poly ethylene oxide)-*block*-poly(propylene oxide)-*block*-poly(ethylene oxide) triblock copolymer (Aldrich, *MW* avg. 5800, EO₂₀PO₇₀EO₂₀, P123) as a structure-directing agent. In a typical synthesis, 4.0 g of P123 block copolymer was dissolved with stirring in a solution of 30.0 g of water and the required amounts (20, 10, 5 and 2.5 mL) of aqueous sodium tungstate solution (NaWO₄·2H₂O, 0.5 M) were simultaneously and quickly added into the mixture under vigorous stirring. After one hour, 120 g of HCl (2 M), and 9.1 g of TEOS were added with stirring at 313 K. After 24 h of constant stirring, the gel composition was

kept at 373 K under static condition for 48 h. After being cooled to room temperature, the solid product was recovered by filtering, washing, drying and calcining at 823 K. The nanocomposite samples were denoted as WO_x/SBA-15(x), where x denotes the volume of sodium tungstate solution.

6.2.3. Typical procedure for the oxidation sulfides to sulfoxides

The liquid-phase catalytic oxidation of sulfides was conducted under atmospheric pressure at room temperature in 50 ml reaction vessel equipped with a magnetic stirrer. In a typical experiment, substrate (2 mmol) was oxidized using 70% TBHP (3 equiv) and catalyst (0.05 g) in CH₃OH: CH₂Cl₂ (1:1) (10 mL) at room temperature. The progress of the reaction was monitored by TLC and GC Shimadzu 14B gas chromatography (GC) with a capillary column (cross-linked 5% diphenyl–95% dimethylpolysiloxane capillary column, 30 m × 0.53 × 1.5 μm film thickness), coupled with flame ionization detector. In most cases, the products were analyzed without any chromatographic purification by GC (Shimadzu 14B) and GC-Mass spectroscopy (Shimadzu (GC-17A & QP-5000) with identical columns. All known reaction products gave satisfactory GC mass and GCIR (Perkin Elmer system 2000) spectra as compared to those obtained from authentic samples.

After completion of the reaction, the reaction mixture was filtered off and the catalyst was washed with dichloromethane (25-30 mL). The excess of solvent was removed under reduced pressure. The mixture was filtered to remove the catalyst and the solvent was removed under reduced pressure. It was then dried in vacuum and purified by column chromatography on silica gel (60-120 mesh) as the stationary phase (petroleum ether/ethyl acetate, 50/50). Yield: 99%. Methylphenylsulfoxide: Colorless liquid
¹H NMR (CDCl₃, 200 MHz): δ = 7.47–7.53 (m, 3H), 7.60–7.65 (m, 2H), 2.69 (s, 3H),
¹³C NMR (CDCl₃, 200 MHz): δ = 131.1 (C), 129.3 (CH), 128 (CH), 127.3 (CH), 125.3 (CH), 123.5 (CH), 44 (CH₃), GCMS: m/z 140 (M⁺), 125, 112, 97, 91, 77, 65, 51.

6.3. Results and discussion

6.3.1. Catalyst characterization

The wide and low angle XRD patterns of the WO_x/SBA-15 nanocomposites with different loading of WO_x are shown in Figs. 6.1.A and 6.1.B, respectively. All diffraction peaks could be indexed to monoclinic WO₃ which are in good agreement with those of bulk monoclinic crystal (JCPDS Card No. 83-0951). Low angle XRD measurements showed that WO_x/SBA-15 materials exhibit three peaks at a 2θ in the range 0.5-5°, which can be indexed to (100), (110), and (200) reflections of the hexagonal $p6mm$ space group. The observation is in quite agreement with the XRD pattern of pure hexagonally ordered SBA-15 material reported in the literature [37-39], indicating that the WO_x/SBA-15 materials possess a well-ordered two-dimensional mesoporous structure with a hexagonal porous network. Fig. 6.1.A clearly displays the peaks at higher angle and the intensities of the peaks increases with increasing WO_x loading, which confirms the presence of WO_x nanoclusters in the mesochannels of SBA-15. The size of the WO_x crystallites in the SBA-15 porous matrix is calculated using the Scherrer equation to be in the range 2-5 nm. The nitrogen adsorption-desorption isotherms of SBA-15 and WO_x/SBA-15 nanocomposites are found to be type IV isotherms and a sharp increase in the adsorbed amount of nitrogen at a relative pressure (P/P_0) of 0.6-0.9, features typical curves of mesoporous structures, which are still maintained in WO_x/SBA-15 (Fig. 6.2 A&B) [40, 41]. The amount of nitrogen adsorbed is found to decrease with increasing the loading of WO_x nanoclusters. Surface areas and pore volumes are lower for WO_x/SBA-15 samples compared to SBA-15 (Table 6.1). Interestingly, the pore diameters of the WO_x/SBA-15 material are larger than pure SBA-15. The catalyst was characterized by XPS (Fig. 6.2 C), elemental mapping (Fig. 6.4) and energy-dispersive X-ray analysis (EDAX) for the evaluation of their elemental composition and purity. No peak of any metallic tungstate was observed in XPS spectra of as-prepared WO_x nanoclusters, indicating high purity of the material. The EDAX analysis of the materials (Table 6.1) shows the presence of W, Si and O peaks.

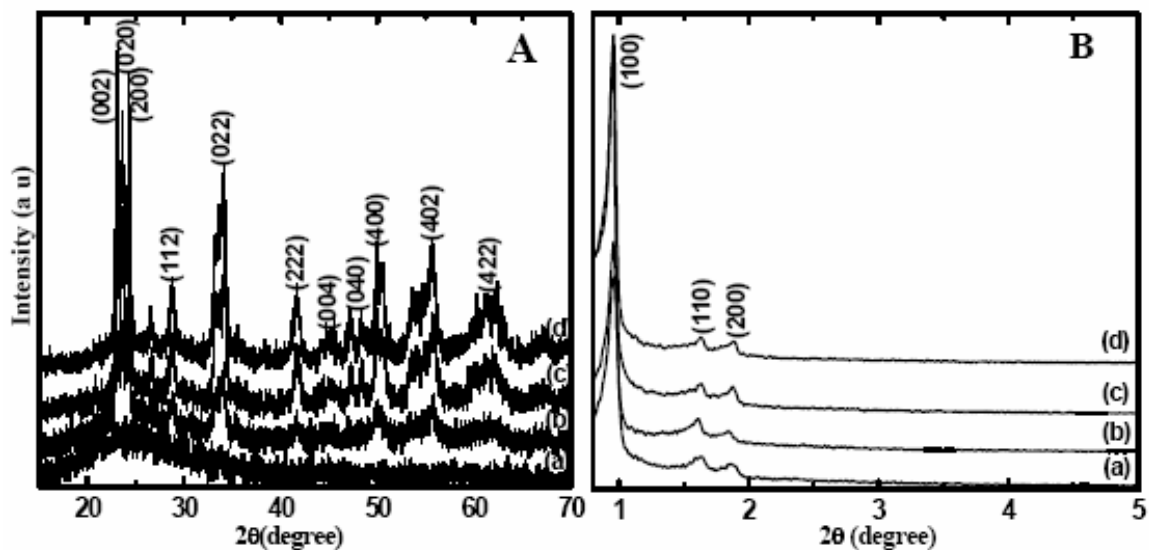


Fig. 6.1. (A) Wide and (B) Low angle XRD patterns of $\text{WO}_x/\text{SBA-15}$ with different concentration of WO_x : (a) $\text{WO}_x/\text{SBA-15}(2.5)$, (b) $\text{WO}_x/\text{SBA-15}(5)$, (c) $\text{WO}_x/\text{SBA-15}(10)$, (d) $\text{WO}_x/\text{SBA-15}(20)$.

Table 6.1. Physicochemical properties of catalyst systems

No	Materials	Surface area (m^2/g)	Pore volume (cm^3/g)	Pore diameter (nm)	EDAX analysis (%)					
					W		Si		O	
					Wt.	At.	Wt.	At.	Wt.	At.
					wt.		wt.		wt.	
1	SBA-15	910	1.25	9.2	0	0	38.1	26.0	61.9	74.0
2	$\text{WO}_x/\text{SBA-15}(2.5)$	632	1.02	9.3	2.5	0.3	40.0	28.3	57.5	71.4
3	$\text{WO}_x/\text{SBA-15}(5)$	562	0.98	10.0	8.1	0.9	34.7	25.5	57.2	73.6
4	$\text{WO}_x/\text{SBA-15}(10)$	464	0.88	10.0	20.5	2.6	30.3	25.3	49.2	72.1
5	$\text{WO}_x/\text{SBA-15}(20)$	321	0.69	10.0	36.9	5.8	26.6	27.6	36.5	66.6

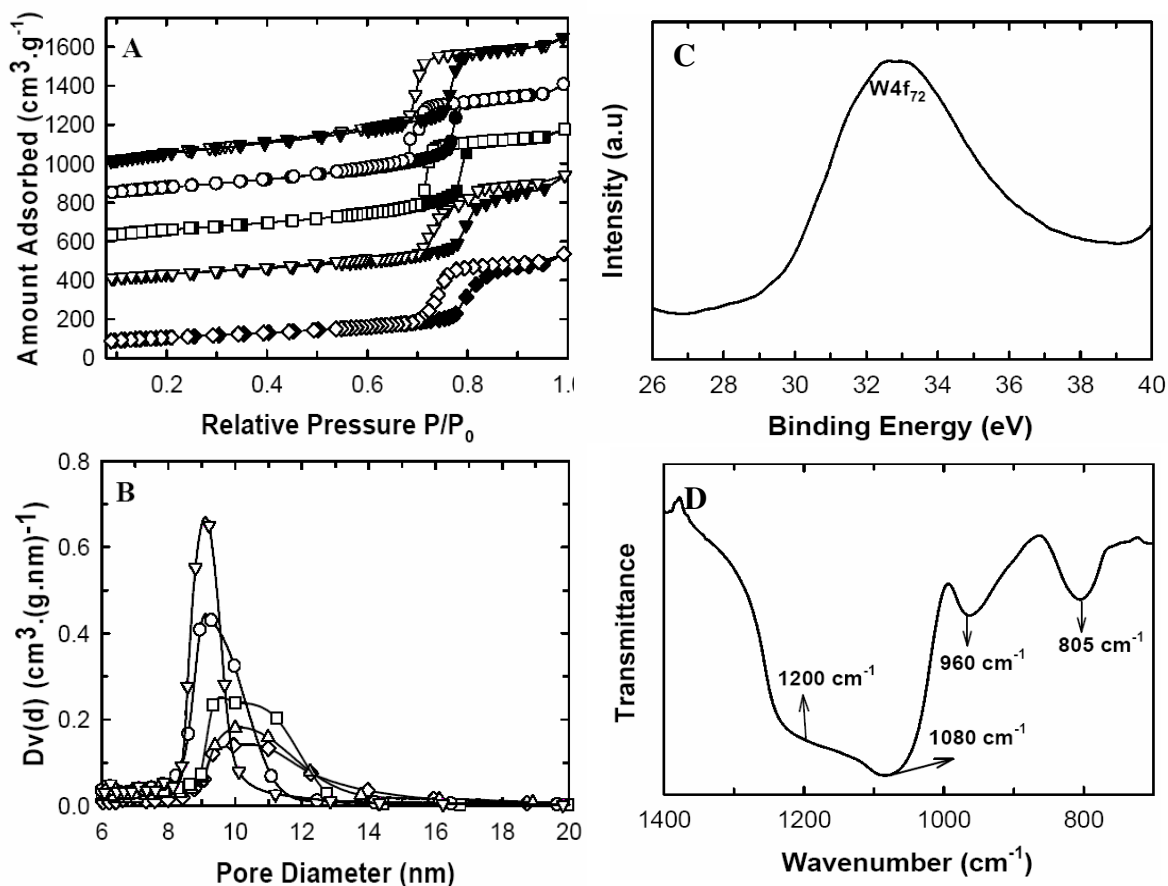


Fig. 6.2. (A) Nitrogen adsorption-desorption isotherms and (B) BJH adsorption pore size distributions of SBA-15 and $\text{WO}_x/\text{SBA-15}$: (∇) SBA-15, (\circ) $\text{WO}_x/\text{SBA-15}(2.5)$, (\square) $\text{WO}_x/\text{SBA-15}(5)$, (∇) $\text{WO}_x/\text{SBA-15}(10)$, and (\diamond) $\text{WO}_x/\text{SBA-15}(20)$. (C) XPS spectra of W(4f) of $\text{WO}_x/\text{SBA-15}(20)$. (D) FT-IR spectrum of $\text{WO}_x/\text{SBA-15}(20)$

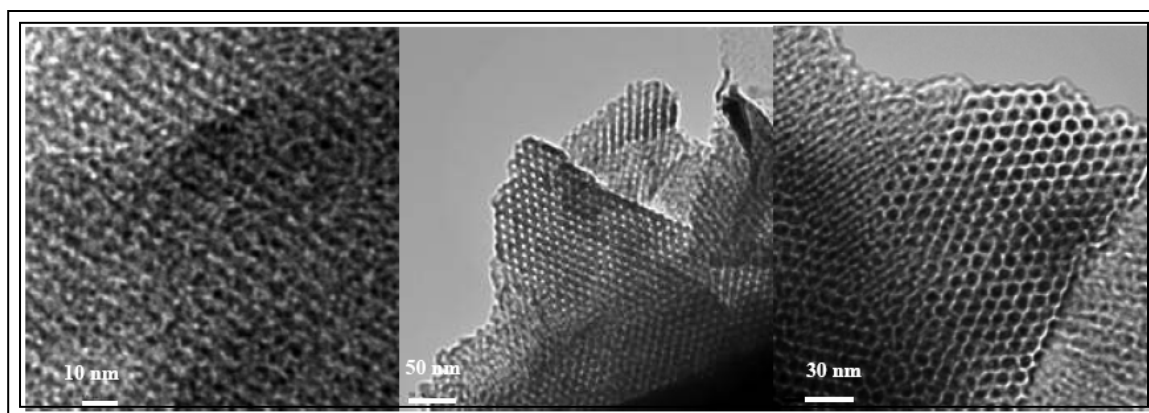


Fig. 6.3. HRTEM pictures of $\text{WO}_x/\text{SBA-15}(20)$

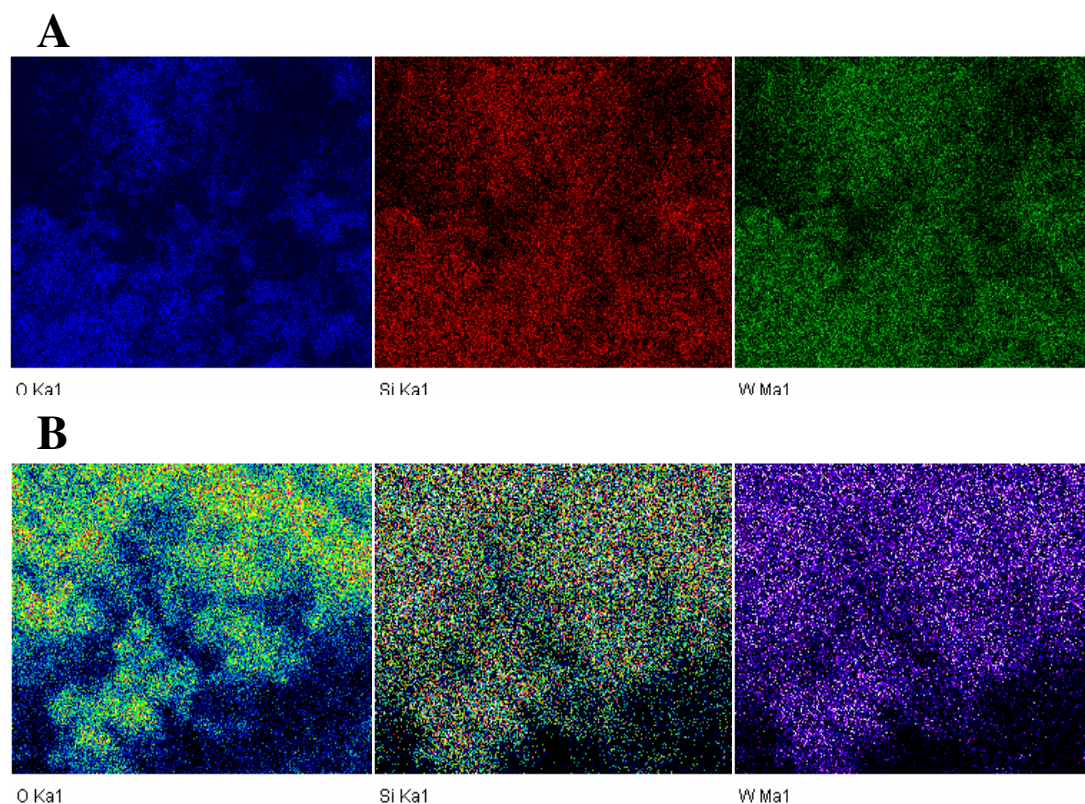


Fig. 6.4. (A) Elemental mapping of WO_x/SBA-15(20). (B) WO_x/SBA-15(5)

HRTEM images of WO_x/SBA-15(20) nanocomposite (Fig. 6.3) show that the materials retain the hexagonally ordered porous structure even after the formation of WO_x nanoclusters in the mesochannels. However, the WO_x nanoclusters are not seen in the HRTEM images, which confirm that the WO_x nanoclusters are not deposited on the external surface but indeed, present inside the mesochannels of SBA-15 [42]. SEM images show that the morphology of WO_x/SBA-15(20) nanocomposite remains the same as that of parent SBA-15 (Fig. 6.5).

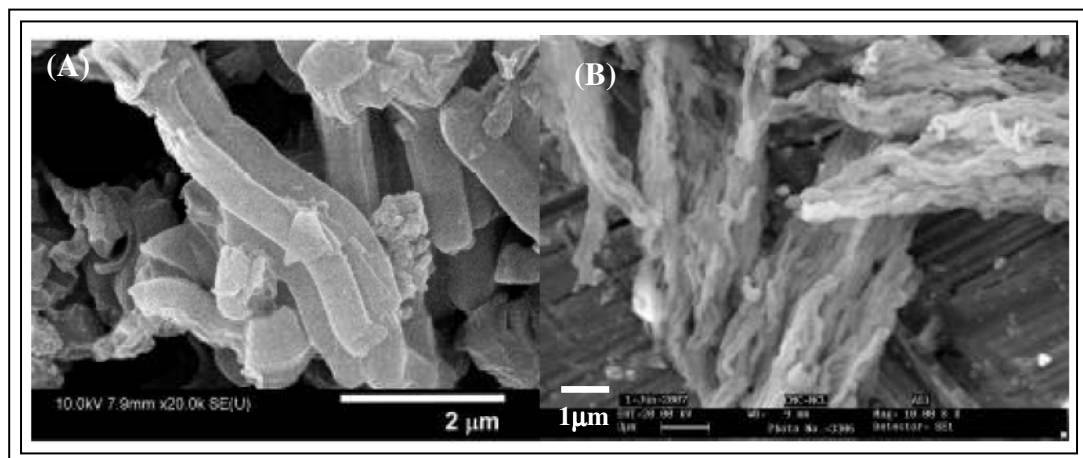


Fig. 6.5. HRSEM images of (a) SBA-15 and (b) WO_x/SBA-15(20)

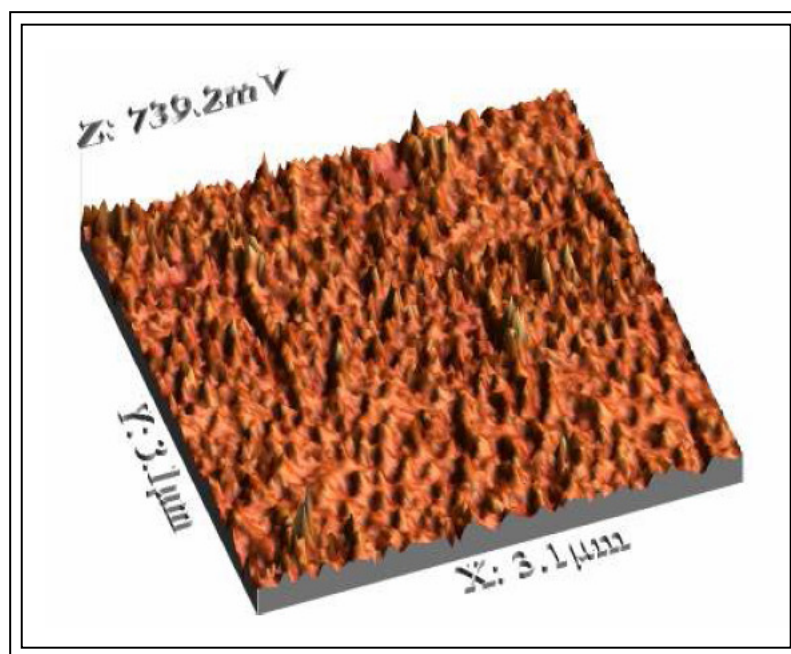


Fig. 6.6. AFM image of WO_x/SBA-15 (20)

The AFM image of WO_x/SBA-15(20) revealed clearly that well organized mesostructure was maintained upon calcination, along with elimination of the organic template from the pore voids. Upon calcination, the template was removed accompanying with the crystallization of WO_x, which decreased the long-range order and resulted in marginal collapse of mesopores (Fig. 6.6).

MAS NMR is an incredibly attractive technique for characterizing surface protons in high-surface area materials. ^1H NMR–MAS spectra of WO_x/SBA samples are shown in Fig. 6.7(a) and 6.7(b). Fig. 6.7 shows spectra for (a) “as synthesized” WO_x/SBA and (b) for the latter after calcined in air at 773 K. The “as synthesized” NMR spectrum of WO_x/SBA shows two ^1H NMR line centered at 2.5 and -0.56 ppm. The line at 2.5 ppm Fig. 6.7(a) is assigned to protons in H_2O and Si-OH interacting with each other via hydrogen bonding and, the latter (-0.56 ppm) reflecting the presence of isolated silanols (Si-OH).

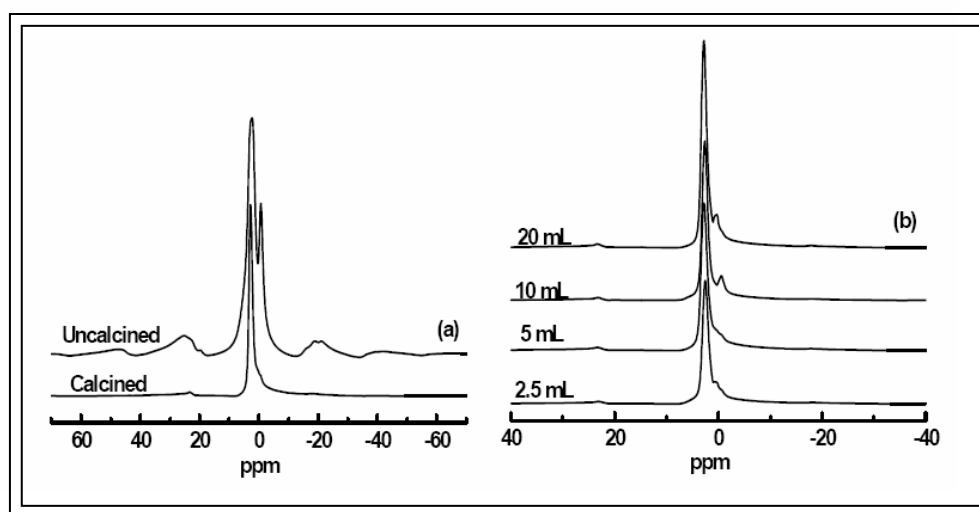


Fig. 6.7. (a) CP-MAS NMR profile of calcined and uncalcined $\text{WO}_x/\text{SBA-15(20)}$
 (b) CP-MAS NMR profile of $\text{WO}_x/\text{SBA-15}$ with different concentration of WO_x

The line at 2.8 ppm observed in calcined sample $\text{WO}_x/\text{SBA-15}$ is due to hydrogen-bonded hydroxyl groups and/or physisorbed water. ^1H NMR–MAS spectrum of $\text{WO}_x/\text{SBA-15}$ nanocomposite samples calcined at 773 K are presented in Fig. (6.7 (b)). A sharp line observed at 2.8 ppm is due to hydrogen-bonded hydroxyl groups and/or physisorbed water, while a small hump observed at 0.28 ppm for the $\text{WO}_x/\text{SBA-15}$ samples could be due to water molecules that are hydrogen-bonded to W-OH protons [43, 44].

FT-IR spectroscopy in the skeletal region ranging between $1400\text{-}700\text{ cm}^{-1}$ was employed to follow the variation of the structure of $\text{WO}_x/\text{SBA-15(20)}$. The typical bands due to siliceous material Si-O-Si are observed for both the parent and the $\text{WO}_x/\text{SBA-15}$

(20) (Fig. 6.2 (D)): a main band at 1080 cm^{-1} , with a shoulder at 1200 cm^{-1} due to asymmetric Si–O–Si stretching modes and symmetric stretch at 805 cm^{-1} . Furthermore, an additional band at ca. 960 cm^{-1} was observed, which is widely used to characterize the presence of transition metal atoms near the silica framework as the stretching Si–O vibration mode perturbed by the neighboring metal ions. Thus, the presence of such an infrared band due to perturbed silica vibrations can be attributed to the formation of WO_x nanoclusters in SBA-15.

The optical absorption edge energies of $\text{WO}_x/\text{SBA-15}$ nanocomposite samples were obtained from DRUV-vis absorption spectra. The optical absorption edge energy is defined as the minimum photon energy required to excite an electron from the highest occupied molecular orbital (HOMO, at the top of the valence band in semiconductor domains) to the lowest unoccupied molecular orbital (LUMO, at the bottom of the conduction band). There are two basic types of electronic transitions, direct and indirect. Direct transitions require only the photons excited electrons, while indirect transitions require concerted vibrations and energy from the crystal lattice (phonons). For dispersed WO_x domains, Barton et al. used the square root of the Kubelka–Munk function multiplied by the photon energy, which allows the edge energy to be obtained by extrapolation to zero absorbance for amorphous semiconductors. The values thus obtained carry information about the average domain size of the oxide nanoparticles, although the values depend on local symmetry and support electronegativity. DRUV-vis spectra are shown in Fig. 6.8 (a) for the $\text{WO}_x/\text{SBA-15}$ samples. All the $\text{WO}_x/\text{SBA-15}$ catalysts display main absorption features at energies ranging from 3.5 to 2.6 eV due to ligand-to-metal charge transfers in tungsten species existing on the SiO_2 surface as reported by Herrera et al [8] and Barton et al [43].

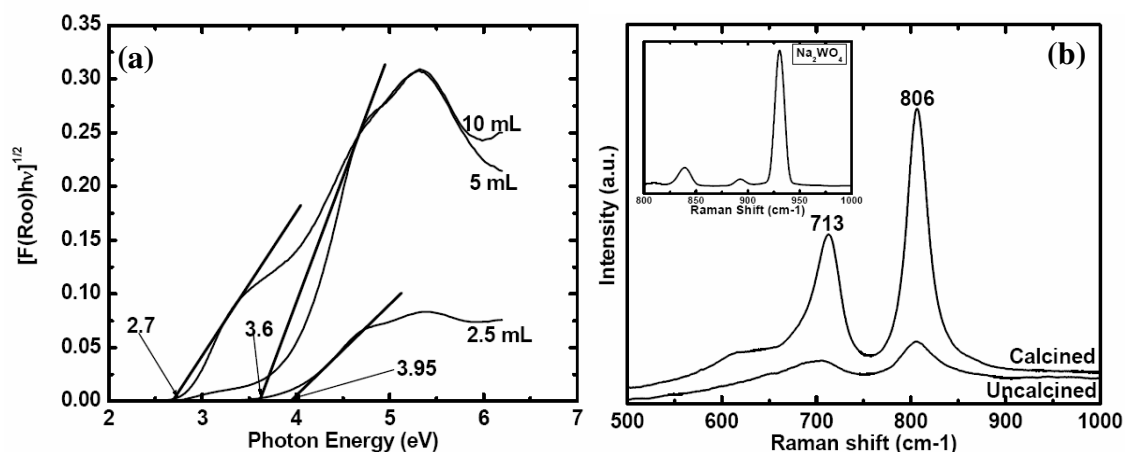


Fig. 6.8. (a): DRUV–Vis spectra for three $\text{WO}_x/\text{SBA-15}$ samples with different tungsten loadings. $[F(R_\infty)/h\nu]$ represents the Kubelka–Munk function multiplied by the photon energy. (b) Raman spectra of calcined and uncalcined samples of $\text{WO}_x/\text{SBA-15}(20)$.

Inset: Raman spectra of $\text{Na}_2\text{WO}_4 \cdot 2\text{H}_2\text{O}$

Raman experiment has been performed to know in which step of synthesis ($\text{WO}_x/\text{SBA-15}$), the WO_x nanoclusters have been formed. Raman bands corresponding to crystalline WO_3 (Fig. 6.8 (b)) appear at 806 and 713 cm^{-1} ; these bands correspond to W–O stretching and bending modes, respectively in both calcined and uncalcined material [43]. It has been found that the intensities of Raman bands of uncalcined material are comparatively lower than the calcined one. However, in inset fig., the Raman bands of the cubic Na_2WO_4 phase were observed at 932 and 840 cm^{-1} correspond to internal vibrations of WO_4 . These results showed that the formation of WO_x nanoclusters started in the ageing step of synthesis. A weight loss found in thermo gravimetric analysis (TGA) of calcined $\text{WO}_x/\text{SBA-15}(20)$ sample below 373 K was due to the desorbed water (Fig. 6.9 (a)).

Temperature resolved PXRD patterns of $\text{WO}_x/\text{SBA-15}(20)$ sample collected over the temperature range 298 – 1173 K at 100 K intervals and again at room temperature are shown in Fig. 6.9 (b).

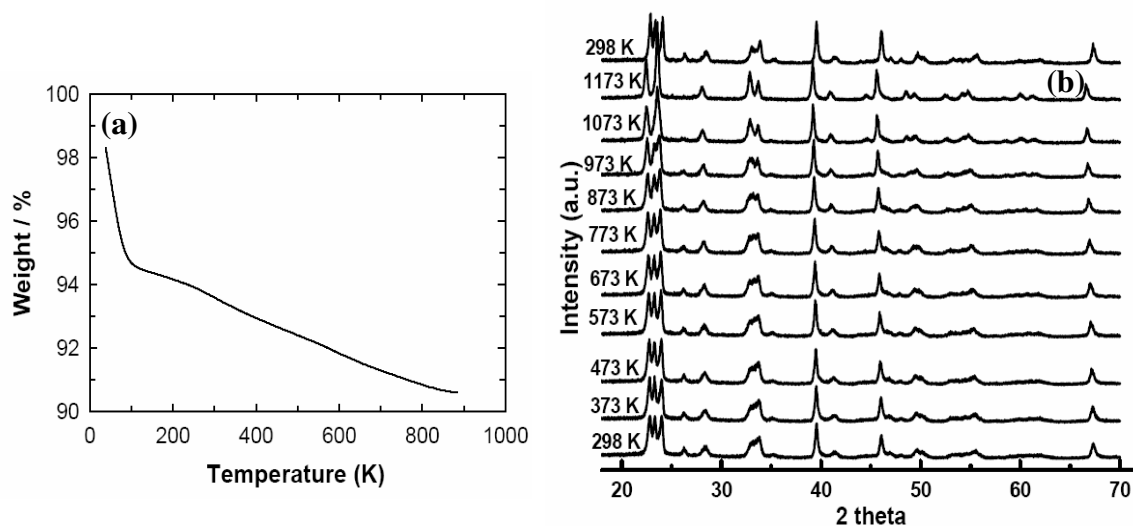


Fig. 6.9. (a) TGA plot of $\text{WO}_x/\text{SBA-15 (20)}$. (b) X-Ray diffraction patterns of $\text{WO}_x/\text{SBA-15 (20)}$. The diffractograms were obtained in situ during thermal treatment at the indicated temperatures.

It is clear from Fig. 6.9 (b) that $\text{WO}_x/\text{SBA-15(20)}$ material under examination showed monoclinic phase in the temperature range studied concomitant with the literature data. The data quality of the scan is comparatively good due to the X'celerator detector, which uses the RTMS (real time multiple strip) technology enhancing both the resolution and intensity of the reflections. The multiple plots of the powder patterns measured in static air indicated the stability of the monoclinic phase of WO_x at temperature as high as 1123 K. At temperatures higher than 1023 K, the expected anatase to rutile phase transformation is observed. The powder pattern of the sample obtained when cooled to room temperature is similar to the pattern at high temperature (298 K), indicating reversible anatase to rutile phase transformation.

Temperature programmed reduction (TPR) with hydrogen is a widely used technique for the characterization of reducible solids and catalysts. In TPR, a reducible catalyst or catalyst precursor is exposed to a flow of a reducing gas mixture (typically a few vol. % of hydrogen in an inert gas) while the temperature is linearly increased.

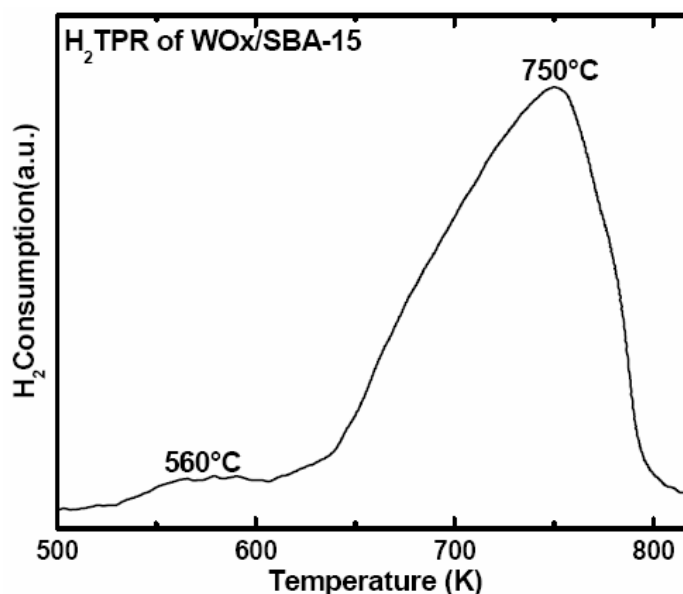


Fig. 6.10. Temperature programmed reduction profile of catalyst: WO_x/SBA-15 (20)

According to the literature [44], pure WO₃ exhibits three reduction peaks, namely a shoulder at 833 K (WO₃ → W₂₀O₅₈), a sharp peak at 1023 K (W₂₀O₅₈ → WO₂) and a peak at higher temperature (WO₂ → W). Pure SiO₂ does not show any detectable TPR peak at temperature below 1273 K. So, the reduction peaks observed (Fig. 6.10) can be attributed to the reduction of WO_x only.

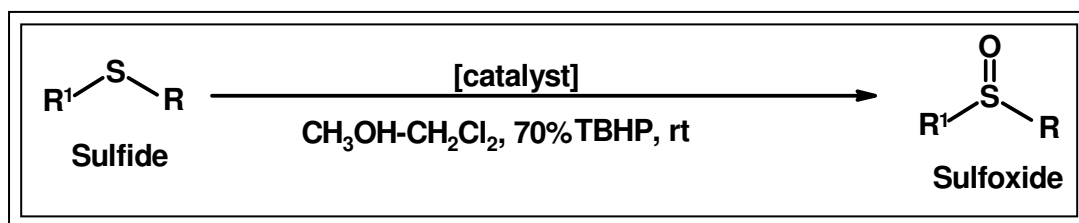
6.3.2. Catalytic oxidation of sulfides

To test the catalytic activity, we selected the oxidation of methylphenylsulfide using 70% TBHP as a model reaction at room temperature (Scheme 6.1.).

Excellent yield (99%) of corresponding the sulfoxide was obtained in 10 h (Table 6.2, entry 1) and there was no overoxidation of sulfoxides to sulfones. The efficiency of TBHP for the above mentioned reaction was evaluated from the amount of the oxidative products produced from methylphenylsulfide divided by the amount of TBHP consumed. It was found that, there was 99% conversion of TBHP, which indicates the 100% efficiency of TBHP. In the absence of the catalyst, no significant oxidation was observed under similar reaction conditions.

In a similar way, various types of structurally diverged aryl alkyl sulfides underwent smooth oxidation to afford the corresponding sulfoxides selectively in

excellent yields (Table 6.2, entries 2-6). Another useful feature of the present protocol can be seen in the selective oxidation of allyl phenyl sulfide to corresponding sulfoxide; neither over-oxidation to the sulfone nor epoxidation of the double bond was observed (Table 6.2, entry 7). Interestingly, under the described reaction conditions, even hindered diaryl sulfides furnished the corresponding sulfoxides in excellent yields (Table 6.2, entry 8). The compounds, which have electron-withdrawing ring substituent, such as bromo and chloro are less reactive (Table 6.2, entries 9-11). It is also worth mentioning that the strong electron withdrawing NO_2 group on the phenyl ring does not affect much the synthesis efficiency (Table 6.2, entry 12). The catalyst was found to be active in the oxidation of dialkyl sulfides also. We found that under the similar reaction conditions, diethyl sulfide converted into diethyl sulfoxide in excellent yield. (Table 6.2, entry 13). In the same way, dibenzyl sulfide furnished the corresponding sulfoxide in high yields (Table 6.2, entry 14). The oxidation of methylphenylsulfide with 70% TBHP was studied using TS-1 and TS-2 under similar reaction conditions and the results are presented in Table 6.3. TS-1 showed negligible activity, while the activity TS-2 was comparable with that of $\text{WO}_x/\text{SBA-15}(20)$ but sulfoxide selectivity was found to be lower [45,46]. Undoubtedly, the proposed catalyst system is very active in the oxidation of methylphenylsulfide to give sulfoxides selectively at room temperature.



Scheme 6.1. Oxidation of Sulfide to Sulfoxide

Table 6.2. WO_x/SBA-15 (20) catalyzed oxidation of sulfides to sulfoxides

Entry	R	R ¹	Yield(%) ^{a, b}
1	Me	Ph	99
	1 st		97 ^c
	2 nd		95 ^c
	3 rd		91 ^c
	4 th		90 ^c
2	Et	Ph	99
3	<i>i</i> -Pr	Ph	99
4	-CH ₂ -C ₆ H ₅	Ph	95
5	-CH ₂ - <i>p</i> -Tol	4-Me-C ₆ H ₄	99
6	Me	4-MeO-C ₆ H ₄	99
7	-CH ₂ - CH ₂ CH ₂	Ph	92 ^d
8	Ph	Ph	95
9	Me	2-Cl-C ₆ H ₄	68
10	Me	4-Cl-C ₆ H ₄	65
11	Me	4-Br-C ₆ H ₄	68
12	Me	4-NO ₂ -C ₆ H ₄	49
13	Et	Et	99
14	-CH ₂ -C ₆ H ₅	-CH ₂ -C ₆ H ₅	92

Reaction conditions: substrate (2 mmol), 70% TBHP (3 equiv.) and catalyst (0.05 g) in CH₃OH : CH₂Cl₂ (1:1) (10 mL) at room temperature.

^a Isolated yields, ^b GC conversion unless otherwise stated, ^c Recycling experiment.

^d No epoxidation product was detected

Table 6.3. Comparison of different catalysts in the oxidation of methylphenylsulfide

Entry	Catalyst	Conversion (mol %)	Selectivity of sulfoxide (mol %)
1	WO _x /SBA-15 (20)	100	99
2	TS-1	10	100
3	TS-2	90	80

Reaction conditions: substrate (2 mmol) using 70% TBHP (3 equiv.) and catalyst (0.05 g) in CH₃OH: CH₂Cl₂ (1:1) (10 mL) at room temperature

6.3.2. Catalyst stability and recyclability

WO_x/SBA-15(20) has been used for establishing the stability of the catalyst in recycling experiments. A couple of XRD and EDAX experiments were performed to establish the stability of the catalyst system after recycling. The wide angle and small XRD patterns of first, third and seventh recycled catalysts are depicted in the Fig. 6.11. The wide angle XRD patterns are comparable with results obtained for the fresh catalyst (Fig. 6.1). In small angle XRD pattern, we have observed a decrease in the intensities of the peaks, which could be due to marginal loss in the orderness of the material after recycling. But the presence of three well-resolved peaks in XRD patterns of seventh recycled catalyst indicates the retainment of well-ordered structure of WO_x/SBA-15 (20). The EDAX data (Table 6.4) also supports the structural integrity of the material after recycling. To investigate the stability of WO_x/SBA-15 (20) system towards a strong oxidant such as TBHP, two additional experiments were carried out. To check the leaching of WO_x species from the catalytic system into the reaction medium, a fresh WO_x/SBA-15 (20) sample was treated with a freshly prepared reaction mixture and the reaction was carried at room temperature for 24 h. The reaction mixture was then filtered to separate catalyst and the filtrate was analyzed for the presence of tungsten. The catalyst separated as above after 1st cycle is again treated in another fresh reaction mixture and the filtrate was analyzed for tungsten. Like this the catalyst was recycled in 7 cycles. ICP-AES analysis of all the recycle experiments showed the complete absence of tungsten in the reaction

mixture. The above results confirmed that $\text{WO}_x/\text{SBA-15}$ (20) system was stable and there was no leaching of active species WO_x even after 7th recycle. These results demonstrate the practical reuse of the reported catalyst system under described reaction conditions.

Table 6.4. EDAX analysis data of recycled catalyst $\text{WO}_x/\text{SBA-15}$ (20)

Recycles	EDAX analysis (%)					
	W		Si		O	
	Wt.	At. wt.	Wt.	At. wt.	Wt.	At. wt.
1st	36.9	5.8	26.6	27.6	36.5	66.6
3rd	36.8	5.7	26.6	27.6	36.7	66.7
7th	36.8	5.7	26.5	27.5	36.8	66.8

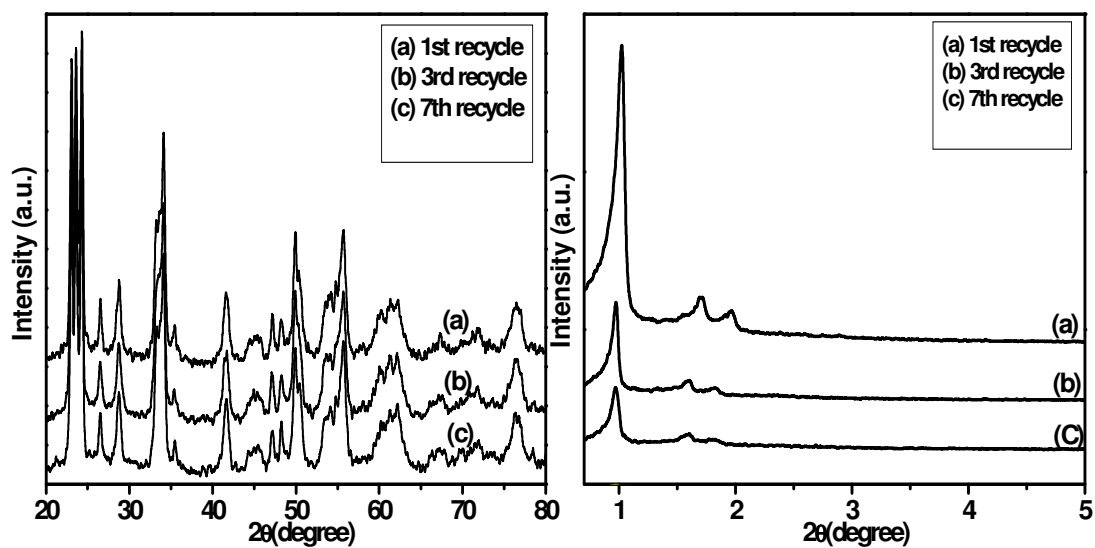


Fig.6.11. Wide and Low angle XRD patterns of recycled $\text{WO}_x/\text{SBA-15}$ (20) (a) 1st recycle (b) 3rd recycle and (c) 7th recycle.

6.4. Conclusions

In conclusion, we have successfully demonstrated that highly dispersed WO_x nanoclusters in the mesochannels of SBA-15 could be prepared by in-situ hydrothermal method in a highly acidic medium. The catalyst exhibits high catalytic activities for oxidation of sulfur compounds due to highly dispersed tungsten oxide species present in the SBA-15 mesochannels. The enhanced chemoselectivities at higher substrate conversions achieved over this catalyst are attributed to the unique large pore diameters and low surface acidity of WO_x /SBA-15, which allow the facile discharge of the desired products from the channels of the catalyst at ambient conditions. In addition to this, the catalyst is recyclable without loss in its activity. This strategy could be used for similar chemical transformations to use in a eco-friendly manner.

6.5. References

1. M.D. Hughes, Y.-J. Xu, P. Jenkins, P. McMorn, P. Landon, D.I. Enache, A.F. Carley, G.A. Attard, G.J. Hutchings, F. King, E.H. Stitt, P. Johnston, K. Griffin, C.J. Kiely, *Nature* 437 (2005) 1132.
2. B. Vishwanathan, S. Sivasanker, A. V. Ramaswamy (Ed.s), *Catalysis: Principles and Application*; Narosa Publishing House: New Delhi, India, 2007, p. 147.
3. D.J. Cole-Hamilton, *Science* 299 (2003) 1702.
4. X.-L. Yang, W.-L. Dai, H. Chen, Y. Cao, H. Li, H. He, K. Fan, *J. Catal.* 229 (2005) 259.
5. J. Jarupatrakorn, M.P. Coles, T.D. Tilley, *Chem. Mater.* 17 (2005) 1818.
6. Z. Zhang, J. Suo, X. Zhang, S. Li, *Appl. Catal. A: Gen.* 179 (1999) 11.
7. E. Briot, J.-Y. Piquemal, M. Vennat, J.-M. Bregeault, G. Chottard, J.-M. Manoli, *J. Mater. Chem.* 10 (2000) 953.
8. J.E. Herrera, J.H. Kwak, J.Z. Hua, Y. Wang, C.H.F. Peden, J. Macht, E. Iglesia, *J. Catal.* 239 (2006) 200.
9. R.A. Sheldon, J.K. Kochi (Ed.s), *Metal Catalyzed Oxidation of Organic Compounds*; Academic Press: New York 1981, p. 5.
10. J.-E. Backvall (Ed.), *Modern Oxidation Methods*, Wiley-VCH, Weinheim, 2004, p. 4.
11. G. Soladie, *Synthesis* 3 (1981) 185.
12. M.C. Carreno, *Chem. Rev.* 95 (1995) 1917.
13. J. Fuhrhop, G. Penzlin (Eds.), *Organic Synthesis, Concepts, Methods, Starting Materials*, 2nd ed., Wiley-VCH, Weinheim, 1994, p. 26.
14. E. Block (Ed.), *Reaction of Organosulfur Compounds*, Academic Press, New York, 1978, p. 15.
15. C.G. Venier, T.G. Squires, Y.Y. Chen, G.P. Hussmann, J.C. Shei, B.F. Smith, *J. Org. Chem.* 47 (1982) 3773.
16. R.W. Murray, R. Jeyaraman, *J. Org. Chem.* 50 (1985) 2847.
17. S.W. Kaldor, M. Hammond, *Tetrahedron Lett.* 32 (1991) 5043.
18. W. Adam, L. Hadjiarapoglou, *Tetrahedron Lett.* 33 (1992) 469.

19. G.W. Breton, J.D. Fields, P.J. Kropp, *Tetrahedron Lett.* 36 (1995) 3825.
20. D.H.R. Barton, W. Li, J.A. Smith, *Tetrahedron Lett.* 39 (1998) 7055.
21. M. Hirano, S. Yakabe, J.H. Clark, T. Morimoto, *J. Chem. Soc., Perkin Trans. 1* (1996) 2693.
22. R.A. Sheldon, M. Wallau, I.W.C.E. Arends, U. Schuchardt, *Acc. Chem. Res.* 31 (1998) 485.
23. A. Corma, H. Garcia, *Chem. Rev.* 103 (2003) 4307.
24. C. Venturello, R. D'Aloisio, J.C.J. Bart, M. Ricci, *J. Mol. Catal.* 32 (1985) 107.
25. W.A. Herrmann, J. Fridgen, G.M. Lobmaier, M. Spiegler, *New. J. Chem.* 23 (1999) 5.
26. D. Sloboda-Rozner, P.L. Alsters, R. Neumann, *J. Am. Chem. Soc.* 125 (2003) 5280.
27. K. Sato, M. Aoki, R. Noyori, *Science* 281 (1998) 1646.
28. B.F. Sels, D.E. De Vos, P.A. Jacobs, *J. Am. Chem. Soc.* 123 (2001) 8350.
29. F.M. Collins, A.R. Lucy, C. Sharp, *J. Mol. Catal. A: Chem.* 117 (1997) 397.
30. C. Venturello, R. D'Aloisio, *J. Org. Chem.* 53 (1988) 1553.
31. K. Kamata, K. Yonehara, Y. Sumida, K. Yamaguchi, S. Hikichi, N. Mizuno, *Science* 300 (2003) 964.
32. M.V. Vasylyev, R. Neumann, *J. Am. Chem. Soc.* 126 (2004) 884.
33. B. Karimi, M. Ghoreishi-Nezhad, J.H. Clark, *Org. Lett.* 7 (2005) 625.
34. K. Yamaguchi, C. Yoshida, S. Uchida, N. Mizuno, *J. Am. Chem. Soc.* 127 (2005) 530.
35. Y.M.A Yamada, M. Ichinohe, H. Takahashi, S. Ikegami, *Org. Lett.* 3 (2001) 1837.
36. X. Zuwei, Z. Ning, S. Yu, L. Kunlan, *Science* 292 (2001) 1139.
37. D. Zhao, J. Feng, Q. Huo, N. Melosh, G.H. Fredrickson, B.F. Chmelka, G.D. Stucky, *Science* 279 (1998) 548.
38. D. Zhao, Q. Huo, J. Feng, B.F. Chmelka, G.D. Stucky, *J. Am. Chem. Soc.* 120 (1998) 6024.
39. H. Song, R.M. Rioux, J.D. Hoefelmeyer, R. Komor, K. Niesz, M. Grass, P. Yang, G.A. Somorjai, *J. Am. Chem. Soc.* 128 (2006) 3027.
40. Y. J. Han, J.M. Kim, G.D. Stucky, *Chem. Mater.* 12 (2000) 2068.
41. (a) X.L. Yang, W.L. Dai, H. Chen, J.H. Xu, Y. Cao, H.X. Li, K.N. Fan, *Appl.*

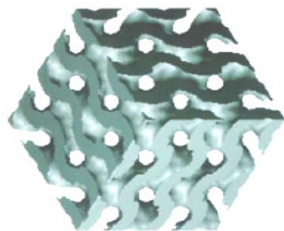
- Catal. A 283 (2005) 1.
42. P. Kuśtrowski, L. Chmielarz, R. Dziembaj, P. Cool, E.F. Vansant, J. Phys. Chem. B 109 (2005) 11552.
 43. D.G. Barton, M. Shtein, R.D. Wilson, S.L. Soled, E. Iglesia, J. Phys. Chem. B 103 (1999) 630.
 44. M.G. Falco, S.A. Canavese, N.S. Fi'goli, Catal. Today 107 (2005) 778.
 45. R.S. Reddy, J.S. Reddy, R. Kumar, P. Kumar, J. Chem. Soc., Chem. Commun. (1992) 84.
 46. S.V.N. Raju, T.T. Upadhya, S. Ponrathnam, T. Danie, A. Sudalai, Chem. Commun. (1996) 1969.

CHAPTER VII

Summary and Conclusions

This chapter features the following sections:

7.1. <i>Summary</i>	198
7.2. <i>Conclusions</i>	201
7.3. <i>Future directions</i>	203



7. Summary and Conclusions

7.1. Summary

This thesis describes synthesis of various inorganic – organic hybrid materials based on heteropoly acids and transition metal complexes, coordination polymers and nanocomposites. It also describes catalytic application of these synthesized materials in various academic as well as industrially important organic transformations. This chapter presents a brief summary of the work described in previous chapters and general conclusions arrived from the work.

Chapter 1 gives a brief introduction of inorganic organic hybrid materials and their importance. It also gives an introduction to both industrially and synthetically important various oxidative organic transformations. It further gives an introduction to the catalysts used for oxidative transformations viz. inorganic organic hybrid materials based on heteropoly acids and metal complexes, coordination polymers and nanocomposites. A review of the literature to date in these areas is included. Finally, the aim of the thesis is outlined briefly.

Chapter 2 presents a brief discussion of theory and experimental procedures of all characterization techniques such as N₂ sorption, AAS, EDAX, XRD, TEM, SEM, FT-IR, FT-Raman and MAS NMR, H₂-TPR and EPR for all materials (inorganic-organic hybrid materials based on heteropoly acids and metal complexes, coordination polymers and nanocomposites) used for catalyst screening whichever applicable to particular catalyst system.

Chapter 3 Section (A) describes the preparation of inorganic – organic hybrid materials by immobilization of Molybdovanadophosphoric acids onto Mesoporous silica such as MCM-41, MCM-48 and SBA-15. All catalyst materials were characterized by elemental analysis, FT-IR, N₂ sorption measurements, SAXS, UV/Vis, XPS, MAS-NMR, SEM and TEM for their structural integrity and physico-chemical properties. These inorganic-organic hybrid materials were applied for the liquid-phase oxidation of anthracene with 70% aqueous *tert*-butylhydroperoxide (TBHP) oxidant in benzene.

It also describes the further screening of this catalyst system for C-H activation (oxidation of adamantane). Catalysts with different isopoly and heteropoly ions immobilized on SBA-15 were prepared and well characterized. Detailed kinetics and mechanisms were discussed for oxidation of adamantane.

Section B describes the synthesis of inorganic–organic hybrid materials based on functionalized silica and carbon by anchoring $\text{H}_5[\text{PMo}_{10}\text{V}_2\text{O}_{40}]\cdot 32.5\text{H}_2\text{O}$ onto ethane bridged SBA-15 and mesoporous carbon. Small angle X-ray diffraction, N_2 sorption analysis, HRTEM, SEM, FT-IR, CP-MAS NMR were used to diagnose the structural integrity of the materials. These materials were applied in the environmentally friendly oxidation of 2-methylnaphthalene (2MN) with 30% aqueous hydrogen peroxide.

Section C describes synthesis of a simple cation exchanged form of $\text{H}_5[\text{PMo}_{10}\text{V}_2\text{O}_{40}]\cdot 32.5\text{H}_2\text{O}$ supported on to ionic liquid-modified SBA-15 (V2ILSBA) and its application in catalyzed aerobic oxidation of primary and secondary alcohols to corresponding aldehydes and ketones with no trace of over oxidation.

Chapter 4 describes the preparation, characterization and catalytic activities of organotin-oxometalate coordination polymers $[(\text{nBu}_3\text{Sn})_2\text{MO}_4]\cdot \text{nH}_2\text{O}$ (where, M= Mo or W) and its catalytic assessment in the oxyfunctionalization of monoterpenes with urea hydroperoxide (UHP) as an oxidizing agent. The oxyfunctionalization of monoterpenes gave commercially important products such as epoxides, ketones and hydroxyl derivatives. The integrity of the organotin–oxometalates polymers were confirmed by X-ray diffraction, Surface analysis, FT-IR, FT-Raman, SEM, TG/DTA and MAS NMR (^{13}C , ^{119}Sn) analysis. The effects of reaction parameters on limonene conversions and product selectivities have been studied in detail using $[(\text{nBu}_3\text{Sn})_2\text{MoO}_4]$ catalyst.

It also describes the further use of this catalyst system for developing a green protocol for N-oxidation of primary aromatic amines in the presence of 30% aq. H_2O_2 in high yield with good recyclability.

Chapter 5, Section A deals with the synthesis of $\text{CobpbH}_2\text{Cl}_2\cdot 2\text{H}_2\text{O}$ [where, $\text{bpbH}_2 = 1,2\text{-Bis(Pyridine-2-carboxamido)benzene}$] complex immobilized on sulfonic acid-functionalized SBA-15 molecular sieve (SBA-15- $\text{SO}_3\text{-CobpbH}_2\text{Cl}_2\cdot 2\text{H}_2\text{O}$). The

catalyst was characterized by elemental analysis, FT-IR, N₂ sorption measurements, small angle XRD, UV-vis, and HRTEM for their structural integrity and physicochemical properties. This catalyst system has been applied for the opening of epoxide rings by amines, and this provided an environmentally friendly method for the synthesis of β -amino alcohols under solvent free conditions.

Section B describes the synthesis of [Ru(salen)(NO)Cl] complex, its immobilization on mesoporous SBA-16 by ship in a bottle method and detailed characterization of the catalyst material. This well characterized material has been applied for hydrogenation of ketones.

Chapter 6 describes the synthesis and detailed characterizations of nanocomposite material composed of tungston oxide nanoclustur and nanoporous SBA-15. This catalyst system has been applied for the selective oxidation of sulfur compounds giving excellent yields at room temperature with exceptional recyclability.

Chapter 7 summarizes the conclusions reached in this thesis.

7.2. Conclusions

- ❖ Structural integrity of mesoporous supports as well as heteropoly acids has been well preserved after immobilization of heteropoly acids to the mesoporous network. It has been proven with the help of various characterization techniques. Our investigation demonstrates that molybdovanadophosphoric acid immobilized on mesoporous silica can be used for selective oxidation of AN to AQ under milder liquid phase oxidation conditions.
- ❖ C-H activation by IOHM was primarily promoted by vanadium species and rest of the keggion enhances the activity. Evidence of presence of V(4+)-superoxo species in the reaction mechanism has been demonstrated by EPR spectroscopy.
- ❖ Compared to the conventional preparation of vitamin K3 by oxidation of 2-methylnaphthalene, IOHM catalyst system could be economical and environmentally benign.
- ❖ An efficient protocol has been developed for a broad range of benzylic, allylic and aliphatic alcohols oxidation under mild conditions with a high degree of chemoselectivity using V2ILSBA as nanoreactor catalyst system. The benzylic and allylic alcohols were oxidized with excellent conversions, whereas aliphatic alcohols were less reactive. The method is environmentally friendly and a valid alternative to the classical Swern oxidation. Therefore, we can avoid the use of toxic reagents and conducting oxidation at very low temperature. The activities and product selectivities were comparable to those of the homogeneous analogue, showing that the homogeneous catalysis could be heterogenized successfully. The rate of oxidation of the secondary alcohols was found to be faster than that of the primary ones

- ❖ Tungsten containing coordination polymer has been applied successfully as a selective catalyst for the oxidation of monoterpenes.
- ❖ The N-oxidation of primary aromatic amines is described using tungsten- and molybdenum based coordination polymers (heterogeneous catalyst) in the presence of 30% aqueous H₂O₂ at room temperature and atmospheric air to give the corresponding nitroso derivatives in high yield. It is a clean process and the catalyst is recyclable without any loss of activity.
- ❖ A highly efficient and simple protocol for the ring opening of epoxides catalyzed by CobpbH₂Cl₂·2H₂O complex immobilized onto SBA-15 has been demonstrated and thereby expanding the chemistry of these catalyst systems to an important reaction class. The facile synthesis of catalysts, their benign nature, the ease of handling and the simplified reaction and isolation procedures make them an attractive alternative to current methodologies. Thus the present method is “environmentally friendly” and potentially useful for industrial applications.
- ❖ [Ru(salen)(NO)] complex was encapsulated in the cage-like mesoporous material SBA-16. Fine-tuning of the pore entrance size of the mesoporous cage-like silica was found to be the key factor for successful trapping of complex in the cage of the mesoporous materials. The catalyst was found to be an active encapsulated catalyst system for the hydrogenation of ketones.
- ❖ We have successfully demonstrated the highly dispersed WO_x nanoclusters in the mesochannels of SBA-15 prepared by in-situ hydrothermal method in a highly acidic medium. The catalyst exhibits high catalytic activities for oxidation of sulfur compounds due to highly dispersed tungsten oxide species present in the SBA-15 mesochannels. In addition to this, the catalyst is recyclable without loss in its activity.

7.3. Future directions of inorganic-organic hybrid materials

Inorganic-organic hybrid materials represent one of the most fascinating developments in materials chemistry in recent years. The tremendous possibilities of combination of different properties in one material initiated an explosion of ideas about potential materials and applications. However, the basic science is sometimes still not understood, therefore investigations in this field in particular to understand the structure–property relationships are crucial. There are numerous inorganic-organic hybrid materials that have been prepared and characterized but not yet tested as catalysts. Additionally, very few of the materials that have been exposed to reaction conditions have been rigorously tested for reuse. Thus, there are many opportunities for investigation with currently available materials. Since much is known about how organic moieties, metal complexes and polyoxometalates can serve as catalysts for homogeneous reactions, many elements of “design” can be used in future developments of inorganic-organic hybrid materials for use as recyclable catalysts.

Papers published (Refereed Journals):

1. Impact of LimeSludge Waste of Jagiroad Paper Mill on Growth and Development of Plantons

Eco. Env. &Cons.11 (2005) 201-206

Shabeena Yasmin, **Ankur Bordoloi** and S.Deka*

2. Liquid-phase veratrole acylation and toluene alkylation over WO_x/ZrO_2 solid acid catalysts

J. Mol. Catal. A 247(2006) 58-64

Ankur Bordoloi, Nevin T. Mathew, Biju M. Devassy, S.P. Mirajkar and S.B. Halligudi*

3. Shape selective synthesis of long-chain linear alkyl benzene (LAB) with AIMCM-41/Beta zeolite composite catalyst

J. Mol. Catal. A. 253, (2006), 239-244

Ankur Bordoloi, Biju M. Devassy, P.S. Niphadkar, P.N. Joshi and S.B. Halligudi*

4. Selective oxidation of anthracene using inorganic–organic hybrid materials based on molybdovanadophosphoric acids

J. Catal. 247(2007)166-175

Ankur Bordoloi, F. Lefebvre and S.B. Halligudi*

5. Organotin-oxometalate coordination polymer catalyzed oxyfunctionalization of monoterpenes

J. Mol. Catal. A 270(2007)177-184,

Ankur Bordoloi, F. Lefebvre and S.B. Halligudi*

6. Tungsten and Molybdenum based Coordination Polymers - Catalyzed N-Oxidation of Primary Aromatic Amines with Aqueous Hydrogen Peroxide

Adv. Syn. and Catal. 348(2007)2085-2088

Ankur Bordoloi and S.B. Halligudi*

7. One-step synthesis of SBA-15 containing tungsten oxide nanoclusters: a chemoselective catalyst for oxidation of sulfides to sulfoxides at ambient conditions

Chem. Commun.(2007)4806-4808

Ankur Bordoloi , Ajayan Vinu and S. B. Halligudi*

8. Oxyfunctionalisation of adamantane using inorganic - organic hybrid materials based on isopoly and heteropoly anions: kinetics and mechanistic study

App.catal. A 308(2007) 216-222

Ankur Bordoloi, Ajayan Vinu and S.B. Halligudi*

9. Inorganic–organic hybrid materials based on functionalized silica and carbon: A comprehensive understanding toward the structural property and catalytic activity difference over mesoporous silica and carbon supports

Microp. Mesop. Mater. Article in press

Ankur Bordoloi, Nevin T. Mathew, F. Lefebvre and S.B. Halligudi*

10. Studies in structural characterization and correlation with the catalytic activity of an efficient and stable WO_x/SBA-15 nanocomposite catalyst

Ankur Bordoloi, and S.B. Halligudi *

Manuscript accepted in J. Catal.

11. Heteropoly Acid Based SILP Catalyst for Selective Aerobic Oxidation of Alcohols

Ankur Bordoloi, Suman Sahoo, F. Lefebvre, S. B. Halligudi*

Manuscript submitted to the journal.

12. Immobilized CobpbH₂Cl₂H₂O complex as heterogeneous catalyst for epoxides ring opening by aromatic amines under ambient conditions

Ankur Bordoloi and S.B. Halligudi *

Manuscript submitted to the Journal.

13. Mesoporous SBA-16 encapsulated [Ru (salen)(NO)] complex as catalyst for hydrogenation of ketones

Ankur Bordoloi, Amol P. Amrute and S.B. Halligudi *

Manuscript submitted to the Journal.